

**Copyright**  
**By**  
**Jason Clarence Stith**  
**2010**

The Dissertation Committee for Jason Clarence Stith certifies that this is the approved version of the following dissertation:

**PREDICTING THE BEHAVIOR OF HORIZONTALLY CURVED  
I-GIRDERS DURING CONSTRUCTION**

Committee:

---

Todd A. Helwig, Co-Supervisor

---

Eric B. Williamson, Co-Supervisor

---

Karl H. Frank

---

Michael D. Engelhardt

---

Kenneth M. Liechti

**PREDICTING THE BEHAVIOR OF HORIZONTALLY CURVED  
I-GIRDERS DURING CONSTRUCTION**

by

**Jason Clarence Stith, B.S.; M.S.; M.B.A.**

**Dissertation**

Presented to the Faculty of the Graduate School of  
The University of Texas at Austin  
in Partial Fulfillment  
of the Requirements  
for the Degree of  
**Doctor of Philosophy**

**The University of Texas at Austin**

**August 2010**

## **Dedication**

To my beautiful, loving, and supportive wife  
She is the source of so much of my life's joy and inspiration.



## **Acknowledgements**

The following dissertation benefited from the insight, direction, and assistance of numerous people. First and foremost, I would like to thank my co-supervisors, Todd Helwig and Eric Williamson. Dr. Helwig, I appreciate your knowledge of field studies, all things ANSYS, and dry sense of humor. Dr. Williamson, I appreciate your knowledge of the finite element method, computer programming, and intense competitive nature. To the other members of our weekly project meeting, Karl Frank and Michael Engelhardt, the project greatly benefitted from your wisdom, experience, and insight. Dr. Liechti, I appreciate your time and comments on this dissertation as well as the well taught class on elasticity. To the other professors who have taught me at UT, I thank each of you: Sharon Wood, Richard Klingner, John Tassoulas, Loukas Kallivokas, David Fowler, and John Breen.

My return to graduate school would not have occurred without the funding made available by the Texas Department of Transportation, and I would like to recognize the members of our project monitoring committee for their assistance and direction on the project. The field tests were successfully completed due to the coordination and assistance from a number of folks from the following companies: HDR Inc., Lone Star Infrastructures, Chowtaw Erectors Inc., and Hirschfeld Industries. Several students from the Ferguson Lab gave freely of their time to help complete various stages of the field study and became true friends during my time in Austin including: Jeremiah Fasl, Seong Yeong Yang, Rangsan Wonjeeraphat, Anthony Battistini, and Craig Quadrato. Quan Chen was instrumental in my learning of ANSYS. Sezgin Kucukcoban provided the necessary intellectual groundwork so that I could develop both a FORTRAN based program and also an object-oriented program written in Visual Basic. The following friends should be mentioned as they each contributed to my enjoyment of Austin both academically and socially: Daniel Williamson for politics and poker nights, Catherine Hovell for Sonic runs, Kim Talley for weekends at the river, Gun Up Kwon for a smile and dinners with spouses, Isamu Ikeda for Brazilian barbeques, Carrie Davis for soccer

teams to play on, Jason Varney and James Foreman for redneck weekends, and Steven Foster for men's weekends. I would also like to acknowledge the staff at the Ferguson Lab; the lab would not function without these dedicated persons.

I feel that a special thanks should be said to each of my project team members, without their tireless contribution of time and talent the numerous developments made through our project would not have occurred. Andrew Schuh was there in the beginning. His enthusiasm for taking on the unknown expectations of the project and flying through the air in man-lifts was only matched by his enthusiasm for catfish and coleslaw dinners. Jamie Farris brought experience and a practical approach to the project. I could always rely on her for sound advice on bridge design practices and game winning softball hits. Brian Petruzzi's willingness to learn object-oriented programming and put in the long hours needed to complete UT Bridge is most graciously acknowledged. His drive to make a mark on our project and willingness to drive on an awesome road trip to Phoenix and back will provide lasting memories. Dr. Hyeong Jun Kim developed the post-processor to UT Bridge and provided the slick body to the engine I developed. His late night advice and contributions to this project will not be forgotten.

In addition to the assistance mentioned above, I also received the necessary support from my family to complete this journey. My wife, Samantha Stith, provided consummate companionship during this sometime difficult process. I appreciated her tireless love and support throughout this research and dissertation writing process, because it would not have been completed without her. I could not ask for a better partner to travel through life with or around Khövsgöl nuur (lake), Mongolia. My parent's, Richard and Veronica Stith, encouragement was unwavering during my entire 23 years of formal educational development. The assistance of these individuals and my entire family has been invaluable.

Jason Stith

August 2010

# **PREDICTING THE BEHAVIOR OF HORIZONTALLY CURVED I-GIRDERS DURING CONSTRUCTION**

Jason Clarence Stith, Ph.D.

The University of Texas at Austin, 2010

Supervisors: Todd A. Helwig and Eric B. Williamson

The majority of a bridge designer's time is spent ensuring strength and serviceability limit states are satisfied for the completed structure under various dead and live loads. Anecdotally, the profession has done an admirable job designing safe bridges, but engineering the construction process by which bridges get built plays a lesser role in the design offices. The result of this oversight is the complete collapse of a few large bridges as well as numerous other serviceability failures during construction. According to the available literature there have been only a few attempts to monitor a full-scale bridge in the field during the entire construction process. Another challenge for engineers is the lack of analysis tools available which predict the behavior of the bridge during the intermediate construction phases. During construction, partial bracing is present and the boundary conditions can vary significantly from the final bridge configuration. The challenge is magnified for complex bridge geometries such as curved bridges or bridges with skewed supports.

To address some of the concerns facing engineers a three span curved steel I-girder bridge was monitored throughout the entire construction process. Field studies collected data on the girder lifting behavior, partially constructed behavior, and concrete deck placement behavior. Additional analytical studies followed using the field measurements to verify the finite element models. Finally, conclusions drawn from the physical and analytical testing were utilized to derive equations that predicted behavior,

and analysis tools were developed to provide engineers with solutions to a wide range of construction related problems. This dissertation describes the development of two design tools, UT Lift and UT Bridge. UT Lift is a macro-enabled Excel spreadsheet that predicts the behavior of curved I-girders during lifting. The derivation of the equations necessary to accomplish these calculations and the implementation are described in this dissertation. UT Bridge is a PC-based, user-friendly, 3-D finite element program for I-girder bridges. The basic design philosophy of UT Bridge aims to allow an engineer to take the information readily available in a set of bridge drawings and easily input the necessary information into the program. A straight or curved I-girder bridge with any number of girders or spans can then be analyzed with a robust finite element analysis for either the erection sequence or the concrete deck placement. The development of UT Bridge as well as the necessary element formulations is provided in this dissertation.

# TABLE OF CONTENTS

|   |      |
|---|------|
| Table of Contents .....   | ix   |
| List of Tables .....  | xiii |
| List of Figures .....   | xiv  |
| Chapter 1: Introduction .....   | 1    |
| 1.1 Introduction .....  | 1    |
| 1.2 Background .....  | 7    |
| 1.2.1 Horizontally Curved I-girder Bridges .....  | 7    |
| 1.2.2 Bridge Building .....   | 8    |
| 1.2.3 Curved I-girder Analysis Methods .....  | 18   |
| 1.3 Scope .....   | 21   |
| 1.4 Organization .....  | 22   |
| Chapter 2: Literature Review and Recent Work .....  | 24   |
| 2.1 Introduction: .....   | 24   |
| 2.2 Development of Guide Specifications for Horizontally Curved Highway<br>Bridges: .....   | 24   |
| 2.2.1 Consortium of University Research Teams (CURT): .....                                 | 24   |
| 2.2.2 Curved Steel Bridge Research Project (CSBRP): .....                                   | 25   |
| 2.3 Curved Girders During Lifting: .....  | 26   |
| 2.4 Full-Scale Tests and Field Tests .....  | 28   |
| 2.5 Computational Modeling of Curved I-girder Bridges .....                                 | 36   |
| 2.5.1 Synthesis of Computational Modeling Choices .....                                     | 36   |
| 2.5.2 V-Load Method .....   | 37   |
| 2.5.3 Refined Methods Compared to Monitored Bridge .....                                    | 40   |
| 2.5.4 Level of Analysis Comparisons .....   | 42   |
| 2.5.5 M/R-Method for Curved Box Girders .....   | 43   |
| 2.6 State of Practice (Code Requirements): .....  | 43   |
| 2.6.1 AASHTO LRFD Bridge Design Specifications .....  | 43   |
| 2.6.2 AASHTO LRFD Bridge Construction Specifications .....                                  | 46   |
| 2.6.3 AASHTO/NSBA Steel Bridge Erection Guide Specification .....                           | 46   |
| 2.6.4 TxDOT Preferred Practices for Steel Bridge Design, Fabrication, and<br>Erection ..... | 47   |
| 2.6.5 NCHRP Synthesis 345 Report .....  | 48   |
| 2.7 Recent Work: .....  | 49   |
| 2.7.1 Field Study in Austin, Texas – Bridge 88: .....                                       | 49   |
| 2.7.2 Field Study San Angelo, Texas – Hirschfeld Lift Test: .....                           | 56   |
| 2.7.3 Computational Parametric Studies .....  | 61   |
| 2.7.3.1 Introduction .....  | 61   |
| 2.7.4 Parametric Finite Element Model .....   | 63   |
| 2.7.5 Eigenvalue Buckling .....   | 67   |
| 2.7.5.1 Prismatic Girders .....   | 68   |

|  |     |
|--|-----|
| 2.7.5.2 Non-prismatic Girders .....  | 70  |
| 2.7.5.3 Eigenvalue Buckling Analysis Conclusions .....   | 76  |
| 2.7.6 Geometric Nonlinear Buckling .....   | 77  |
| 2.8 Conclusions .....  | 82  |
| Chapter 3: Behavior of Curved I-girders during Lifting .....   | 83  |
| 3.1 Introduction .....   | 83  |
| 3.2 Rigid Body Rotation .....  | 84  |
| 3.3 Cross-Sectional Twist .....  | 95  |
| 3.3.1 Torque on an Open Cross Section .....  | 95  |
| 3.3.2 Calculating the Torsional Moment Diagram .....   | 98  |
| 3.4 Calculation of Displacements and Longitudinal Stresses .....                                       | 111 |
| 3.5 UT Lift Spreadsheet .....  | 114 |
| 3.5.1 Introduction and Purpose .....   | 114 |
| 3.5.2 Girder Input Sheet .....   | 116 |
| 3.5.3 C.G. & Ideal Lift Sheet .....  | 121 |
| 3.5.4 Calculated Behavior Sheet .....  | 122 |
| 3.5.5 Girder Deformations and Torsional Diagrams .....   | 126 |
| 3.5.6 Verification of UT Lift .....  | 128 |
| 3.5.7 UT Lift Example .....  | 131 |
| 3.6 Conclusion .....   | 133 |
| Chapter 4: UT Bridge: A 3-D Finite Element Analysis Program for I-girders<br>during Construction ..... | 135 |
| 4.1 Introduction .....   | 135 |
| 4.2 General Information: .....   | 135 |
| 4.2.1 Finite Element Analysis .....  | 136 |
| 4.2.2 Pre-processor: .....   | 138 |
| 4.2.3 Processor: .....   | 139 |
| 4.2.4 Post-Processor: .....  | 140 |
| 4.3 UT Bridge Pre-processor .....  | 140 |
| 4.4 UT Bridge Processor .....  | 152 |
| 4.4.1 Node Numbering .....   | 152 |
| 4.4.2 Aspect Ratio Parametric Study: .....   | 155 |
| 4.4.2.1 Rectangular Element Parametric Study: .....  | 155 |
| 4.4.2.2 Parallelogram Element Parametric Study: .....  | 158 |
| 4.4.2.3 Girder Flange Parallelogram Parametric Study: .....  | 159 |
| 4.4.3 Activation of Nodes .....  | 161 |
| 4.4.4 Element Elastic Stiffness Formulations: .....  | 161 |
| 4.4.4.1 Shell Element Elastic Stiffness Formulations: .....  | 162 |
| 4.4.4.2 Truss Element Elastic Stiffness Formulations: .....  | 171 |
| 4.4.4.3 Beam Element Elastic Stiffness Formulations: .....   | 172 |
| 4.4.4.4 Shear Stud Beam Element Elastic Stiffness Formulation: .....                                   | 175 |
| 4.4.5 Eigenvalue Buckling Analysis: .....  | 178 |
| 4.4.5.1 Mathematical Introduction .....  | 178 |

|  |     |
|--|-----|
| 4.4.5.2 Eigenproblem in UT Bridge .....                                | 179 |
| 4.4.6 Element Geometric Stiffness Formulations: .....                  | 180 |
| 4.4.6.1 Shell Element Geometric Stiffness Formulations: .....          | 180 |
| 4.4.6.2 Truss Element Geometric Stiffness Formulations:.....           | 184 |
| 4.4.6.3 Beam Element Geometric Stiffness Formulations: .....           | 186 |
| 4.4.7 Boundary Conditions and Loading Options .....                    | 187 |
| 4.4.8 Solvers:.....  | 190 |
| 4.4.8.1 Linear Elastic Solver: .....                                   | 190 |
| 4.4.8.2 Eigenvalue Solution Method: .....                              | 190 |
| 4.4.8.3 Inverse Reciprocal Approach: .....                             | 191 |
| 4.4.8.4 Eigenvalue Solver:.....  | 192 |
| 4.5 Post-Processing within UT Bridge.....                              | 192 |
| 4.5.1 Nodal Stress Recovery: .....                                     | 192 |
| 4.5.2 Inter-element Averaging: .....                                   | 196 |
| 4.5.3 Calculating Reactions:.....                                      | 198 |
| 4.6 Post –Processor, UT Viewer .....                                   | 198 |
| 4.7 Verification .....   | 202 |
| 4.8 The Effect of Utilizing Composite Action in UT Bridge.....         | 213 |
| 4.9 UT Bridge Conclusions.....   | 216 |
| Chapter 5: Conclusions and Recommendations .....                       | 217 |
| 5.1 Introduction .....   | 217 |
| 5.2 Literature Review Summary .....                                    | 217 |
| 5.3 Results from Field Tests .....                                     | 218 |
| 5.4 Three Dimensional Finite Element Modeling.....                     | 219 |
| 5.5 Design Tool Development .....                                      | 220 |
| 5.6 Future Research.....   | 222 |
| Appendix A: UT Bridge Processor Flow Chart.....                        | 224 |
| Appendix B: Bridge 88 Bridge Plans.....                                | 226 |
| Appendix C: Wichita Falls Alignment “T” Bridge Plans.....              | 265 |
| Appendix D: UT Bridge Verification: TxDOT Direct Connector 2-Span 469' |     |
| Direct Connector.....  | 288 |
| D.1 Introduction .....   | 289 |
| D.2 2-Span 469' Direct Connector Bridge Plans.....                     | 289 |
| D.3 Comparison of Vertical Deflections.....                            | 294 |
| D.4 Conclusion from Model Comparison.....                              | 297 |
| D.5 Alternate 1: Concrete Placement Variation.....                     | 297 |
| D.6 Alternate 2: Increase Girder Depth .....                           | 299 |
| D.7 Alternate 3: Torsional Stiffening Truss.....                       | 299 |
| D.8 Conclusions .....  | 301 |
| Appendix E: UT Bridge Verification: TxDOT Direct Connector 2-Span 428' |     |
| Direct Connector.....  | 303 |
| E.1 Introduction .....   | 304 |

|  |     |
|--|-----|
| E.2 2-Span 469' Direct Connector Bridge Plans .....                      | 304 |
| E.3 Comparison of Vertical Deflections .....                             | 309 |
| E.4 Conclusion from Model Comparison .....                               | 311 |
| Appendix F: UT Bridge Verification: Spur 366 Extension Connector F ..... | 312 |
| F.1 Comparison of Vertical Deflections .....                             | 320 |
| References.....  | 321 |
| Vita .....   | 330 |



## LIST OF TABLES

---

|  |     |
|--|-----|
| Table 2.1: Plate Girder Dimension for Erection Test (Linzell et al. 2004) .....  | 32  |
| Table 2.2: Girder Plate Dimension Range (Bell 2004).....   | 35  |
| Table 2.3: Geometric Summary (Bell 2004).....  | 35  |
| Table 2.4: Eigenvalue Parametric Study Variables .....   | 63  |
| Table 4.1: Push-out Test Results (Topkaya 2002).....   | 149 |
| Table 4.2: Constant ( $\alpha$ ) Depending on Ratio of the Rectangle's Side Lengths<br>(Timoshenko and Woinowsky-Krieger 1959) ..... | 156 |
| Table 4.3: Constant ( $\alpha$ ) Depending on Ratio of the Rectangle's Side Lengths<br>(Timoshenko and Woinowsky-Krieger 1959) ..... | 156 |
| Table 4.4: Plate Bending Aspect Ratio Parametric Summary .....   | 157 |
| Table 4.5: Plate Bending Parallelogram Parametric Summary .....  | 158 |
| Table 4.6: Girder Flange Parallelogram Parametric Summary.....   | 160 |
| Table 4.7: Girder Flange Parallelogram Parametric Summary.....   | 160 |
| Table 4.8: Eigensolver Mode Comparison (Popp 2004) .....   | 191 |
| Table 4.9: Natural Coordinates of 9-Node Shell Element .....   | 194 |
| Table 4.10: Gauss Element Coordinates of 9-Node Shell Element .....  | 195 |
| Table 4.11: 1 <sup>st</sup> Eigenvalue Buckling Check Results.....   | 211 |
| Table 4.12: 2 <sup>nd</sup> Eigenvalue Buckling Check Results .....  | 212 |
| Table 4.13: 3 <sup>rd</sup> Eigenvalue Buckling Check Results .....  | 213 |
| Table E.1: UT Bridge Specified Substructure Skew .....   | 309 |

## LIST OF FIGURES

---

|  |    |
|--|----|
| Figure 1.1: Curved Steel I-girder Bridge during Girder Erection.....   | 2  |
| Figure 1.2: Colorado I-girder Bridge Widening Collapse during Construction<br>(NTSB 2006).....                                     | 4  |
| Figure 1.3: Illinios I-girder Bridge Collapse during Construction (Photo Courtesy<br>of ILDOT).....                                | 4  |
| Figure 1.4: Curved I-girder Direct Connector Bridge in Austin, Texas during<br>Construction.....                                   | 5  |
| Figure 1.5: Wichita Falls Bridge Serviceability Camber Error (Photo Courtesy of<br>TxDOT).....                                     | 6  |
| Figure 1.6: Basics of Horizontal Alignment.....  | 8  |
| Figure 1.7: Pictures from I-girder Fabrication.....  | 9  |
| Figure 1.8: I-girder Transported by Truck to the Jobsite.....  | 10 |
| Figure 1.9: Curved I-girder Lifted with a Single Crane using a Spreader Beam.....  | 12 |
| Figure 1.10: Ground Splicing of I-girders (Farris 2008) .....  | 13 |
| Figure 1.11: Aerial Splicing of I-girders ((a)Farris 2008) .....   | 13 |
| Figure 1.12: Curved I-girders during Girder Erection.....  | 14 |
| Figure 1.13: Curved I-girder Bridge during Erection.....   | 15 |
| Figure 1.14: Temporary Support used for Stability Girder and Controlling<br>Deflections.....                                       | 16 |
| Figure 1.15: Concrete Deck Placement of Curved I-girder Bridge .....   | 17 |
| Figure 1.16: Concrete Deck Placement Utilizes a Screed and a Pump Truck.....   | 17 |
| Figure 1.17: Curved I-girder System to Analyze.....  | 20 |
| Figure 1.18: P- $\Delta$ Graph Demonstrating the Effect of Different Levels of Analysis<br>(Adopted from McGuire et al. 2000)..... | 21 |
| Figure 2.1: Mast’s Equilibrium of Beam in Tilted Position (1989).....  | 28 |
| Figure 2.2: Plan View of Test Frame at FHWA Turner-Fairbanks Structures<br>Laboratory (Linzell et al. 2004).....                   | 32 |
| Figure 2.3: Test Frame at FHWA Turner-Fairbanks Structures Laboratory<br>(Hartmann 2005).....                                      | 33 |
| Figure 2.4: Plan View of Bridge Studied by Bell (2004) .....   | 35 |
| Figure 2.5: Cross Section of Bridge Showing Cross Frame, Girders, and Internal<br>Forces (Adapted from Fiechtl et al. 1987).....   | 38 |

|  |    |
|--|----|
| Figure 2.6: Plan and Isometric Bridge Modeled by Chavel (2008).....                                | 41 |
| Figure 2.7: Unit 6 Bridge Layout & Girder Elevations w/ Gage Locations (Schuh 2008).....           | 50 |
| Figure 2.8: Instrumented Girder Cross Section with Data Acquisition System.....                    | 51 |
| Figure 2.9: Instrumentation Locations on Bridge 88 Span 14.....                                    | 51 |
| Figure 2.10: Curved I-girder Flange Stress Distribution (Schuh 2008).....                          | 52 |
| Figure 2.11: Bending and Warping Stress Isolation (Schuh 2008).....                                | 52 |
| Figure 2.12: Girder 4 at Section C Bottom Flange Stress Changes (Schuh 2008).....                  | 53 |
| Figure 2.13: Girder 4 at Section C Top Flange Stress Changes (Schuh 2008).....                     | 53 |
| Figure 2.14: Large Wooden Support Timbers.....   | 54 |
| Figure 2.15: Bridge 88 Concrete Placement Girder Deflection Readings (inches).....                 | 55 |
| Figure 2.16: Fabricated Wood Supports for Girder Lift.....   | 57 |
| Figure 2.17: Prismatic Girder Rotational Change for the S1 Support (Adapted from Schuh 2008).....  | 59 |
| Figure 2.18: Prismatic Girder Stress Change for the S1 Support (Adapted from Schuh 2008).....      | 59 |
| Figure 2.19: Prismatic Girder Rotational Change for the S2 Support (Adapted from Schuh 2008).....  | 60 |
| Figure 2.20: Prismatic Girder Stress Change for the S2 Support (Adapted from Schuh 2008).....      | 60 |
| Figure 2.21: Girder Parameter Definitions (Adapted from Farris 2008).....                          | 64 |
| Figure 2.22: ANSYS Model of a Curved I-girder during Lifting.....                                  | 65 |
| Figure 2.23: Close-up of the ANSYS Model of a Curved I-girder during Lifting.....                  | 66 |
| Figure 2.24: Actual I-girder Lifted during Field Test.....   | 66 |
| Figure 2.25: Buckled Shape of I-girder during Lifting (Schuh 2008).....                            | 67 |
| Figure 2.26: Effect of Lift Location and $b_f/D$ on the Eigenvalue (Adapted from Schuh 2008).....  | 69 |
| Figure 2.27 $Cb$ vs. $a/L$ for Given Radius of Curvatures (Adapted from Schuh 2008).....           | 70 |
| Figure 2.28: Effect of Lift Location and $b_f/D$ on the Eigenvalue (Adapted from Farris 2008)..... | 71 |
| Figure 2.29: $\lambda$ vs. $L_{Lift}$ (Section 1=Section 2 = 60') (Adapted from Farris 2008).....  | 72 |

|   |     |
|---|-----|
| Figure 2.30: $\lambda$ vs. Average $a/L$ (Section 1=Section 2 = 60') (Adapted from Farris 2008).....  | 73  |
| Figure 2.31: $C_b$ vs. $a/L$ for Given Radius of Curvatures (Symmetric Lift) (Farris 2008).....       | 75  |
| Figure 2.32: $C_b$ vs. $a/L$ for Given Radius of Curvatures (Unsymmetric Lift) (Farris 2008).....     | 75  |
| Figure 2.33: Effect of Radius of Curvature on the Eigenvalue (Schuh 2008).....                        | 77  |
| Figure 2.34: Flange Lateral Displacement for Girder with $a/L = 0.2$ $b_f/D = 0.25$ $R = Str$ .....   | 79  |
| Figure 2.35: Flange Lateral Displacement for Girder with $a/L = 0.25$ $b_f/D = 0.25$ $R = Str$ .....  | 80  |
| Figure 2.36: Flange Lateral Displacement for Girder with $a/L = 0.2$ $b_f/D = 0.25$ $R = 500'$ .....  | 80  |
| Figure 2.37: Flange Lateral Displacement for Girder with $a/L = 0.25$ $b_f/D = 0.25$ $R = 500'$ ..... | 81  |
| Figure 3.1: Plan View Schematic of Curved and Straight Girder Center of Gravity (Schuh 2008).....     | 84  |
| Figure 3.2: Lifting of a Horizontally Curved Steel I-Girder with 1 Crane & 2 Lift Clamps.....         | 85  |
| Figure 3.3: Variable Definition for C.G.....  | 86  |
| Figure 3.4: C.G. Location.....  | 87  |
| Figure 3.5: Schematic of Method used to Obtain Radial Distance to C.G.....                            | 88  |
| Figure 3.6: Possible Lines of Support that Intersect the C.G.....                                     | 90  |
| Figure 3.7: Zero Rotation/Equal Force Lift Location.....  | 90  |
| Figure 3.8: Spreader Bar used by a Single Crane Lifting a Girder.....                                 | 91  |
| Figure 3.9: Predicted Rotation and Lift Reactions.....  | 92  |
| Figure 3.10: Approximating the Height of the Axis of Rotation (Schuh 2008).....                       | 93  |
| Figure 3.11: Schematic of the Rigid Body Rotation.....  | 94  |
| Figure 3.12: Torsion Induced Stresses (Schuh 2008).....   | 95  |
| Figure 3.13: Basic Idea for Calculating Torsion Diagram.....  | 99  |
| Figure 3.14: Shear Center of a Plate Girder.....  | 100 |
| Figure 3.15: Center of Gravity Eccentricity and Shear Center Eccentricity.....                        | 101 |
| Figure 3.16: Schematic 1 <sup>st</sup> Step in Calculating Torque Applied by Lift Clamps.....         | 102 |

|  |     |
|--|-----|
| Figure 3.17: Schematic 2 <sup>nd</sup> Step in Calculating Torque Applied by Lift Clamps .....     | 103 |
| Figure 3.18: Schematic 3 <sup>rd</sup> Step in Calculating Torque Applied by Lift Clamps.....      | 104 |
| Figure 3.19: Schematic of Unsymmetrical Non-prismatic Girder Self Weight<br>Torque.....            | 105 |
| Figure 3.20: Schematic of Unsymmetrical Non-prismatic Girder Self Weight<br>Torque.....            | 106 |
| Figure 3.21: Torsion Diagram for $L_{Lift}/L = 0.2$ .....  | 108 |
| Figure 3.22: Torsion Diagram for $L_{Lift}/L = 0.211$ .....  | 109 |
| Figure 3.23: Torsion Diagram for $L_{Lift}/L = 0.238$ .....  | 109 |
| Figure 3.24: Torsion Diagram for $L_{Lift}/L = 0.25$ .....   | 109 |
| Figure 3.25: Discretized Girder 1-D Beam Element Degrees of Freedom .....                          | 112 |
| Figure 3.26: Longitudinal Stress Components .....  | 113 |
| Figure 3.27: Lifting of a Horizontally Curved Steel I-Girder with 1 Crane & 2<br>Lift Clamps ..... | 115 |
| Figure 3.28: Screen Shot of UT Lift Girder Geometric Input .....                                   | 117 |
| Figure 3.29: Screen Shot of UT Lift Girder Cross Frame Input.....                                  | 118 |
| Figure 3.30: Plate Dimensions.....   | 119 |
| Figure 3.31: Options of Cross Frame Location .....   | 120 |
| Figure 3.32: Screen Shot of UT Lift C.G. & Ideal Lift Output .....                                 | 122 |
| Figure 3.33: Definition of the Height to Axis of Rotation (Schuh 2008).....                        | 123 |
| Figure 3.34: Screen Shot of UT Lift Calculated Behavior Input.....                                 | 125 |
| Figure 3.35: Screen Shot of UT Lift Calculated Behavior Output .....                               | 126 |
| Figure 3.36: Screen Shot of UT Lift Graphical Output .....   | 127 |
| Figure 3.37: UT Lift Validation Graph 1 .....  | 128 |
| Figure 3.38: UT Lift Validation Graph 2.....   | 129 |
| Figure 3.39: UT Lift Validation Graph 3 .....  | 129 |
| Figure 3.40: UT Lift Validation Graph 4.....   | 130 |
| Figure 3.41: Plan View of a 2 Span Bridge with Skewed Supports .....                               | 131 |
| Figure 3.42: Elevation View of a Girders.....  | 131 |
| Figure 3.43: Out-of-Plane Displacements of the Girder.....   | 132 |
| Figure 3.44: Total Rotations of the Girders .....  | 132 |
| Figure 3.45: Torsion Diagram of the Girder.....  | 133 |

|  |     |
|--|-----|
| Figure 4.1: Finite Element Idealization .....  | 137 |
| Figure 4.2: UT Bridge Basic Program Architecture .....                                   | 138 |
| Figure 4.3: Flow Chart of UT Bridge .....  | 139 |
| Figure 4.4: Screen Shot of a UT Bridge Form.....   | 141 |
| Figure 4.5: Typical Bridge Cross-Section Looking Ahead Station .....                     | 142 |
| Figure 4.6: Sign Convention for Curved Bridges .....                                     | 142 |
| Figure 4.7: Skew Angle Sign Convention .....   | 143 |
| Figure 4.8: Typical X-Type Cross-Frame.....  | 144 |
| Figure 4.9: Bridge Erection Sequence with Associated UT Bridge Model.....                | 145 |
| Figure 4.10: Bridge Erection Sequence with Associated UT Bridge Model.....               | 146 |
| Figure 4.11: Bridge Erection Sequence with Associated UT Bridge Model.....               | 146 |
| Figure 4.12: Deformation Pattern for Shear Studs in Concrete Deck (Topkaya<br>2002)..... | 147 |
| Figure 4.13: Schematic View of Push-out Test (Topkaya 2002).....                         | 148 |
| Figure 4.14: Picture of Push-out Test Setup (Topkaya 2002) .....                         | 148 |
| Figure 4.15: Typical Load Displacement Graph (4 hr Concrete) (Topkaya 2002) .....        | 148 |
| Figure 4.16: Coarse Mesh Density.....  | 150 |
| Figure 4.17: Normal Mesh Density .....   | 151 |
| Figure 4.18: Fine Mesh Density.....  | 151 |
| Figure 4.19: Schematic of the Node Numbering Used in UT Bridge.....                      | 153 |
| Figure 4.20: Skewed Bridge Nodal Cross-Section Schematic.....                            | 154 |
| Figure 4.21: ANSYS Screen Shot of Plate Bending Problem .....                            | 157 |
| Figure 4.22: ANSYS Screen Shots of Girder Flange Parallelogram Parametric<br>Study ..... | 160 |
| Figure 4.23: Nine-Node Shell Element Schematic .....                                     | 163 |
| Figure 4.24: Schematic of Bridge Shell Elements .....                                    | 164 |
| Figure 4.25: Natural Coordinate System and Lagrangian Shape Functions.....               | 164 |
| Figure 4.26: Cross-Frame Schematic.....  | 171 |
| Figure 4.27: Web Stiffener Schematic.....  | 174 |
| Figure 4.28: Schematic Effect of Composite Action .....                                  | 176 |
| Figure 4.29: Tributary Area of Shear Stud Stiffness .....                                | 178 |

|  |     |
|--|-----|
| Figure 4.30: Picture of Holding Crane and Shore Tower .....  | 188 |
| Figure 4.31: Extrapolation from $3 \times 3$ "Gauss Element" (e) to 9-Noded Shell<br>Element ..... | 194 |
| Figure 4.32: 18 Gauss Points of the $3 \times 3 \times 2$ Integration .....                        | 196 |
| Figure 4.33: Through Thickness Stress Variation .....  | 197 |
| Figure 4.34: UT Viewer Screen Shot of a Bridge.....  | 199 |
| Figure 4.35: UT Viewer Screen Shot of a Buckled Shape .....  | 200 |
| Figure 4.36: UT Viewer Screen Shot of Stress Plot .....  | 201 |
| Figure 4.37: Screen Shot of UT Bridge XY Plot for Concrete Placed in Span 1 .....                  | 202 |
| Figure 4.38: UT Bridge Field Data Comparison for Girder 3 (a) and Girder 4 (b) .....               | 203 |
| Figure 4.39: UT Bridge Field Data Comparison for Girder 3 (a) and Girder 4 (b) .....               | 204 |
| Figure 4.40: Girder 3 UT Bridge Comparison to Field Data and Commercial<br>Programs .....          | 204 |
| Figure 4.41: Girder 4 UT Bridge Comparison to Field Data and Commercial<br>Programs .....          | 205 |
| Figure 4.42: Girder 1 Comparison for Steel Dead Load Only.....                                     | 206 |
| Figure 4.43: Girder 2 Comparison for Steel Dead Load Only.....                                     | 206 |
| Figure 4.44: Girder 3 Comparison for Steel Dead Load Only.....                                     | 207 |
| Figure 4.45: Girder 4 Comparison for Steel Dead Load Only.....                                     | 207 |
| Figure 4.46: Girder 5 Comparison for Steel Dead Load Only.....                                     | 208 |
| Figure 4.47: Girder 1 Comparison for Steel and Concrete Slab Loading.....                          | 208 |
| Figure 4.48: Girder 2 Comparison for Steel and Concrete Slab Loading.....                          | 209 |
| Figure 4.49: Girder 3 Comparison for Steel and Concrete Slab Loading.....                          | 209 |
| Figure 4.50: Girder 4 Comparison for Steel and Concrete Slab Loading.....                          | 210 |
| Figure 4.51: Girder 5 Comparison for Steel and Concrete Slab Loading.....                          | 210 |
| Figure 4.52: Schematic of 1 <sup>st</sup> Eigenvalue Buckling Check Constant Axial Load .....      | 211 |
| Figure 4.53: Schematic of 2 <sup>nd</sup> Eigenvalue Buckling Check Constant Moment.....           | 212 |
| Figure 4.54: Schematic of 2 <sup>nd</sup> Eigenvalue Buckling Check Point Load at Midspan .....    | 212 |
| Figure 4.55: Placement of Positive Moment Region of Span 1 .....                                   | 213 |
| Figure 4.56: Placement of Positive Moment Region of Span 2.....                                    | 213 |
| Figure 4.57: Placement of Negative Moment Region of the Bridge .....                               | 214 |

|   |     |
|---|-----|
| Figure 4.58: Effect of Accounting for Composite Action in Deck Placement Analysis.....  | 215 |
| Figure D.1: UT Bridge Screen Shot of Plan View of 469' Bridge.....                      | 289 |
| Figure D.2: UT Bridge Screen Shot of 469' Bridge.....                                   | 289 |
| Figure D.3: UT Bridge, ANSYS1 Screen Shot of 469' Direct Connector.....                 | 295 |
| Figure D.4: ANSYS2 Screen Shot of 469' Direct Connector.....                            | 295 |
| Figure D.5: Steel Dead Load Program Comparison for Girder 1 and 2.....                  | 295 |
| Figure D.6: Steel Dead Load Program Comparison for Girder 3 and 4.....                  | 296 |
| Figure D.7: Steel & Concrete Deck Dead Load Program Comparison for Girder 1 & 2.....    | 296 |
| Figure D.8: Steel & Concrete Deck Dead Load Program Comparison for Girder 3 & 4.....    | 296 |
| Figure D.9: Step 1 Composite Deck Stiffening.....                                       | 297 |
| Figure D.10: Step 2 Composite Deck Stiffening.....                                      | 297 |
| Figure D.11: Step 3 Composite Deck Stiffening.....                                      | 298 |
| Figure D.12: Step 4 Composite Deck Stiffening.....                                      | 298 |
| Figure D.13: Total Deflected with Varied Deck Placement Sequence for Girders 1 & 2..... | 298 |
| Figure D.14: Total Deflected with Varied Deck Placement Sequence for Girders 3 & 4..... | 299 |
| Figure D.15: ANSYS Plan View of Span 2 with Bottom Chord Truss.....                     | 300 |
| Figure D.16: ANSYS Plan View of Bent 18 with Bottom Chord Truss.....                    | 300 |
| Figure D.17: Total Dead Load Deflections Including Model with Bottom Chord Truss.....   | 301 |
| Figure D.18: Total Dead Load Deflections Including Model with Bottom Chord Truss.....   | 301 |
| Figure E.1: UT Bridge Screen Shot of Plan View of 428' Bridge.....                      | 304 |
| Figure E.2: UT Bridge Screen Shot of 428' Bridge.....                                   | 304 |
| Figure E.3: Steel Dead Load Program Comparison for Girder 1 and 2.....                  | 310 |
| Figure E.4: Steel Dead Load Program Comparison for Girder 3 and 4.....                  | 310 |
| Figure E.5: Steel & Concrete Deck Dead Load Program Comparison for Girder 1 & 2.....    | 310 |



|  |     |
|--|-----|
| Figure E.6: Steel & Concrete Deck Dead Load Program Comparison for Girder 3<br>& 4 ..... | 311 |
| Figure F.1: Steel & Concrete Deck Dead Load Program Comparison for Girder 1<br>& 2 ..... | 320 |
| Figure F.2 Steel & Concrete Deck Dead Load Program Comparison for Girder 3<br>& 4 .....  | 320 |

# CHAPTER 1:

## INTRODUCTION

---

*The more you know the more you realize that you don't know is an oft cited quote, but is a resounding truth during one's pursuit of knowledge. It can be imagined that the breadth of human knowledge is defined by a boundary at which beyond lies the unknown. As a researcher one focuses on a small sliver of that boundary which if probed and pushed can be expanded ever so slightly and human progress is made. That has been the philosophy behind the current pursuit of knowledge. With funding from the Texas Department of Transportation the research team from the University of Texas at Austin pushed this limits of knowledge on the behavior of horizontally curved steel I-girder bridges during construction. The following dissertation is a documentation of a portion of that work related to the development of two design tools that predict their behavior.*

### 1.1 INTRODUCTION

Horizontally curved I-girder bridges are commonly used by structural engineers when transportation engineers specify roadway layouts that incorporate long spans and complex geometries. These curved bridges are composed of girders connected by cross frames or diaphragms. Although the terms cross frames and diaphragms are often used interchangeably in practice, for the purposes of discussion in this dissertation, the term cross frame will be used to discuss the bracing. From a structural perspective, the behavior of girders braced by plate or channel diaphragms will not be substantially different. For straight girders, the primary purpose of the cross frames is to provide bracing of the girders against lateral torsional buckling. As a result, cross frames are often referred to as secondary members in straight bridges. For curved girders, the cross frames are primary structural members that link the girders together and create an efficient structural system for resisting the torsional loads. The cross frames transfer load from the interior girders to the girder on the exterior of the curve. During the erection

and early stages of construction, however, braces may not be present or attached, which significantly alters the behavior of the system when compared to the fully constructed bridge. Another aspect of the erection process that makes it different from the final bridge configuration is the lack of composite behavior between the girders and the concrete deck. Once the concrete deck is in place and hardened, the combined strength of the steel girder acting compositely with the concrete deck system efficiently resist applied loads. Prior to the placement and hardening of the deck, however, the steel girders alone must support both dead loads and construction live loads without the benefit of a composite section. It is during this pre-composite phase that the top flange, which is often designed to be smaller than the bottom flange to maximize structural efficiency, may experience its maximum stresses. Figure 1.1 shows a picture of an I-girder bridge during the erection process with piers, girders, and cross frames labeled.

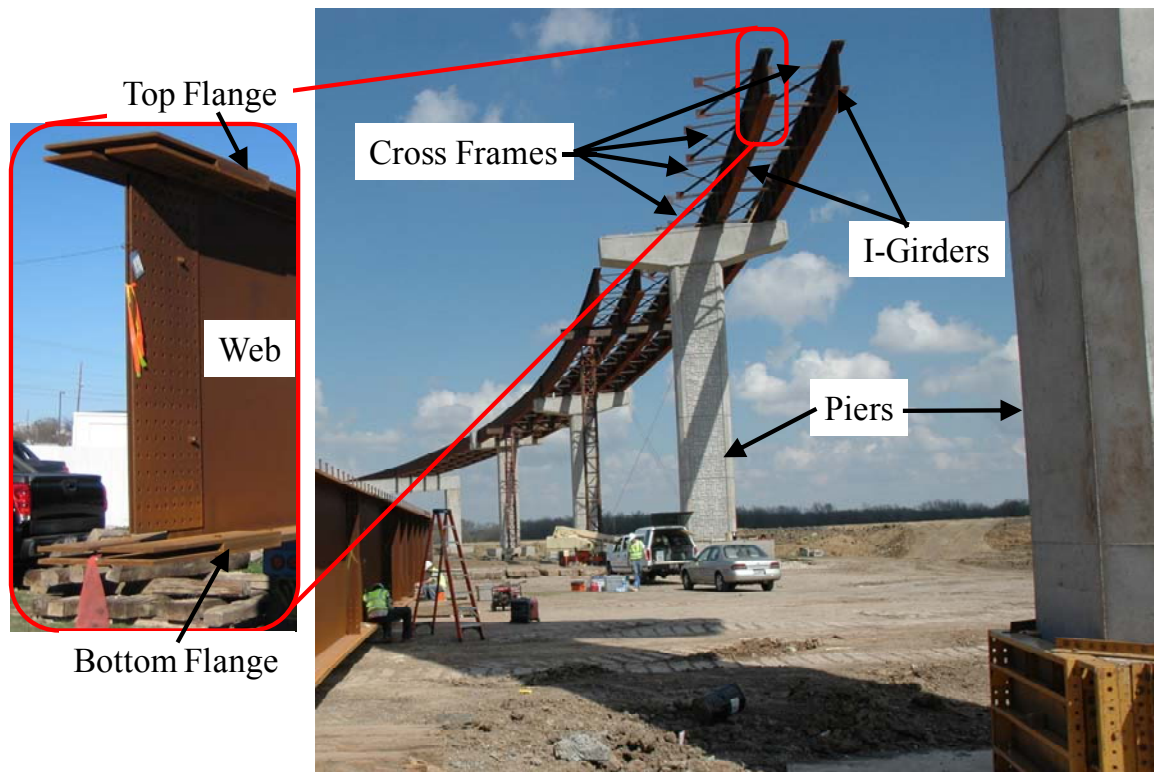


**Figure 1.1: Curved Steel I-girder Bridge during Girder Erection**

Methods for analyzing and designing curved bridges are given by the American Association for State Highway and Transportation Officials (AASHTO), which specify

minimum loads and the performance criteria that different bridge components must satisfy. Additional guidance is provided by supplemental sources such as the Texas Preferred Practices (2007), which provide recommendations based upon common practices and lessons learned from past experience. Although these sources of documents provide performance criteria and guidance, they do not engineer the final design of a bridge. In order to optimize the use of material and labor, an engineer must study every detail of the bridge plans for possible load conditions throughout the life of a bridge. Several commercially available computer programs exist to design steel I-girder bridges such as DESCUS (2008) and MDX (2009). These programs allow engineers to create two-dimensional (2-D) computer models of the bridge they are designing and track hundreds of load cases in order to develop shear and moment envelopes critical to the design of the bridge under consideration. These models, however, are created to evaluate the performance of a bridge in its final erected stage and not during the construction process. Additionally, complex system behavior typical of curved bridges and as well as diaphragm forces are not always analyzed accurately with these programs. The accurate evaluation of a bridge's behavior at every stage of the bridge's life is imperative to the safety of the public and the construction workers whose job it is to erect the bridge. Figure 1.2 shows the collapse of a bridge girder that occurred during the construction process, which involved the widening of an existing bridge in Colorado. The girder buckled under its own self weight when temporary bracing failed and tragically fell into the lanes of an active interstate road, killing a family. Figure 1.3 is another example of an I-girder bridge that collapsed during the construction process. This bridge, which was built in Illinois, did not have an adequate number of cross frames connected to provide the necessary stability during girder erection. The bridge collapsed when the contractor was removing a screw jack at a shore tower. While numerous bridges are safely erected, failures such as those described above understandably get significant exposure. Figure 1.4 is a construction photo of a direct connector in Austin, Texas that was constructed safely.



*(a) Buckled I-girder*

*(b) Aerial View of Collapse*

**Figure 1.2: Colorado I-girder Bridge Widening Collapse during Construction (NTSB 2006)**



**Figure 1.3: Illinois I-girder Bridge Collapse during Construction (Photo Courtesy of ILDOT)**





***Figure 1.4: Curved I-girder Direct Connector Bridge in Austin, Texas during Construction***

It is important to recognize that it is not just those cases of complete structural collapse, such as those shown previously, that are problematic. While the collapse of these bridges resulted in the loss of life and the loss of a bridge structure, such failures are extremely rare in the bridge industry. A much more common type of failure is that associated with a loss of serviceability. Serviceability failures do not result in complete structural collapse, but rather result in deficiencies that complicate the construction schedule or quality of the bridge. Examples include alignment errors, fit-up problems during erection, camber miscalculations, and cross frame buckling. These errors may not result in total loss, but the time and money required to fix these problems can be enormous. An example of a bridge that was structurally sound but had a serviceability failure was one that was constructed on Alignment “T” over US 281/287 in Wichita

Falls, Texas (Turco 2009). This bridge system consisted of a pair of three-span, continuous, curved steel I-girder units. The final superelevation was specified to be 6%; however, due to the unexpected global torsional flexibility in the system, the final superelevation was 0% on some spans and 9% on others. The 2-D grillage computer model used by the engineers that designed the bridge failed to accurately predict the global torsional stiffness and the entire structure twisted more than expected. The problem resulted in the eventual removal of part of the deck and a torsional stiffening retrofit that required significant added expense to the bridge owner and delayed the opening of the bridge by more than one year. Figure 1.5 shows the bridge in Wichita Falls with two straight lines to show the “sagging” of the exterior girder that resulted from miscalculations of the camber.

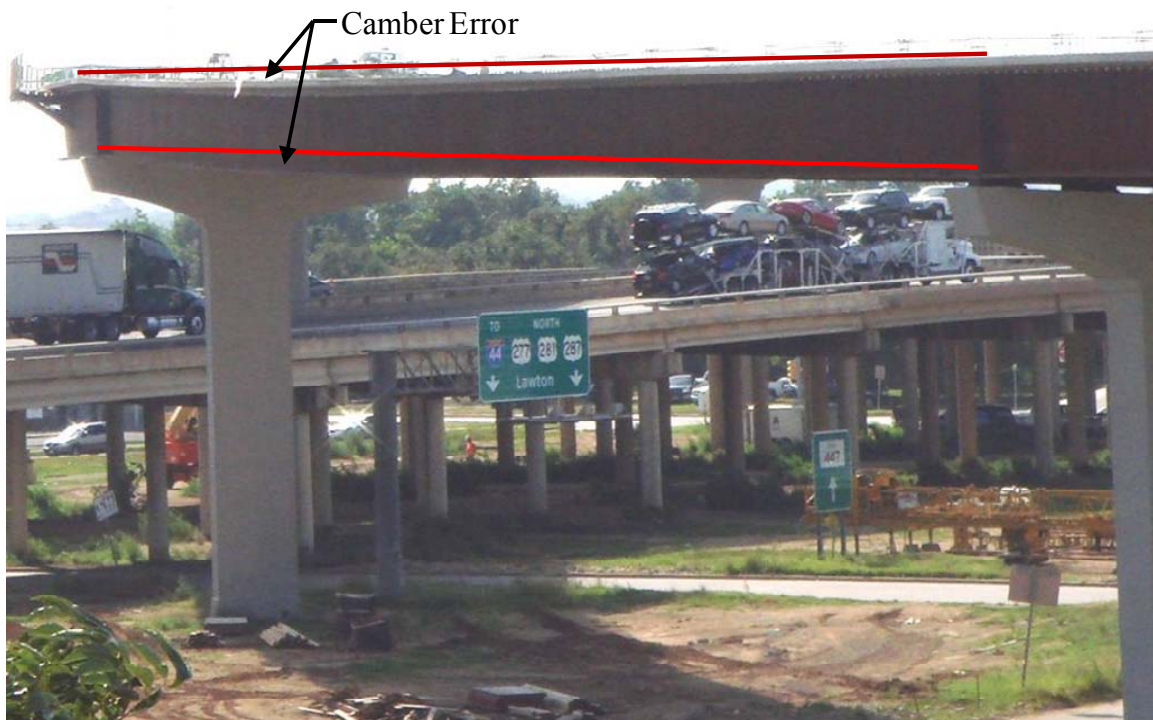


***Figure 1.5: Wichita Falls Bridge Serviceability Camber Error  
(Photo Courtesy of TxDOT)***

As a result of past serviceability failures and due to an interest in designing safe and efficient bridges, the Texas Department of Transportation (TxDOT) funded a research project at the University of Texas to study the behavior of curved I-girder

bridges during construction. The research included a detailed literature review, surveys of construction stakeholders (engineers, contractors, and inspectors), field studies of bridges during construction, parametric finite element modeling, and the development of design tools capable of capturing the behavior of these complicated structures. Each of these tasks built on knowledge acquired throughout the study, with the literature review and surveys providing necessary background knowledge and scope to the project. The field studies provided experience and data for validation of the finite element models and computational design tools developed as part of the investigation. The parametric finite element study allowed for the behavior of a wide variety of geometries and loads to be studied, and the design tools encapsulated all of the recently developed knowledge into useful PC-based software that assist engineers in safely and economically construct curved I-girder bridges.

## **1.2 BACKGROUND**

### **1.2.1 Horizontally Curved I-girder Bridges**

The alignment of roadways are typically developed by a transportation engineer. When the need arises for a roadway to travel over an obstacle, whether manmade (e.g., another roadway, railway, or channel) or natural (e.g., river or valley), a structural engineer is tasked with designing the bridge that will span the road over the obstruction. Thus, a bridge designer normally does not have control over the horizontal and vertical alignment of a bridge, but they must ensure that the bridge they are designing is aligned correctly at the approaches. In general, the vertical alignment does not affect the structural system; however, the horizontal alignment can drastically influence the behavior of the bridge. Horizontal alignments typically consist of circular arcs in the roadway curves and tangent sections for straight segments. Figure 1.6 shows a schematic diagram of a horizontal alignment, including the point of curvature (PC) and point of tangency (PT), which define the transitions from a straight segment to a curved segment. The curve is defined by the arc length ( $L$ ), the radius of curvature ( $R$ ) and the subtended angle ( $\Delta$ ).



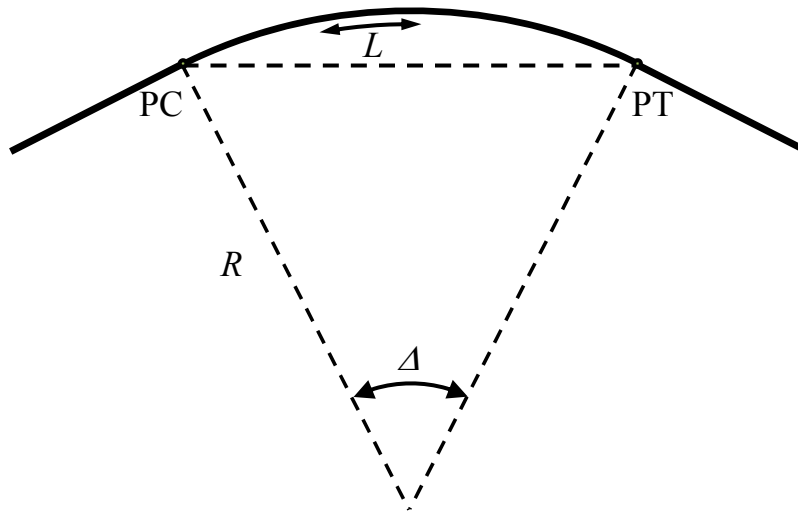


**Figure 1.6: Basics of Horizontal Alignment**

### **1.2.2 Bridge Building**

Humans have been building bridges since the first logs were placed across a stream to allow easier passage. The process has become more complicated as bridges have become larger and longer. The following section is not meant to provide the reader with a comprehensive review of bridge building technology, but rather provide a summary of typical methodologies and terms that are used throughout this dissertation.

Curved I-girder bridges are fabricated from three steel plates that can vary in size. The plate sizes are selected by engineers to optimize the cross section. The fabrication process consists of cutting steel plates to the proper size and welding them together. If the bridge being designed is curved in plan, two major techniques are used to achieve the curved girder geometry. The first method, heat curving, is utilized for girders that have a radius of curvature greater than approximately 1000 ft according to the AASHTO/AWS (2008) limits. With this process, the completed girder is turned on its side, and then the flanges are heated, allowing gravity to curve the girder until it reaches the desired profile. The second method is used for highly curved bridges (i.e., those that have a radius of curvature less than approximately 1000 ft.). For this method, the flanges are cut to the appropriate curvature from a large rectangular plate, and then the web is flexed to match the flange and welded into place. This method results in significant waste from the left over flange material. Figure 1.7 shows a set of pictures from the Hirschfeld Fabrication

plant in San Angelo, Texas. The pictures show various fabrication stages including the submerged arc welding of two plates for the girder flanges (a), the tack welding of the flange to the webs (b), the welding of the flange to the web (c), and the layout of the two girders to be curved (d). The girders are then transported to the job site by trucks. Figure 1.8 shows a picture of a girder on a truck being transported to the bridge construction site.



*(a) Submerged Arc Weld of Flange Plates*



*(b) Tack Welding of Flanges to Web*



*(c) Welding of Flange to Web*



*(d) Layout of Two Segments to be Curved*

*Figure 1.7: Pictures from I-girder Fabrication*



***Figure 1.8: I-girder Transported by Truck to the Jobsite***

Once at the job site, the girders are lifted into place. This process is completed in a variety of methods depending on a range of factors including: girder weight and length, construction crane availability, and site access. There are several options available to contractors when deciding how to lift I-girders into position. They include:

- A) Single crane with a single lift point (only practical for very short segments)
- B) Single crane with two lift points and spreader bar
- C) Two cranes with two lift points
- D) Two cranes with two spreader bars and four lift points
- E) Three or more cranes (complicated due to indeterminate force distribution)

The least desirable of the above options is Case A with the single lift point as there is little control of the girder movements, and it is only used for very short girder segments. The scenarios in Cases B and C that use either a single crane with a lifting beam (spreader bar) or two cranes with two lift points is a reasonable option and was the focus of much of the research presented in this dissertation. The research also included a survey of erectors to determine commonly used lifting practices, and Case B was the most widely used method for lifting girders (Farris 2008). Although the geometry of

curved girders results in torsional loads on the girder system, the two points of support can be positioned to provide a stable system during lifting. However, because an erector does not generally have a spreader beam with the “ideal length” to prevent rigid body rotation of the girder segment being lifted, the effects of rotations due to both rigid body motion and torsional deformations should be considered when evaluating the lifting behavior. Lifting the girders with the Case D scenario that makes use of two cranes and four lift points generally results in improved stability compared to Cases B and C due to the larger number of lift points as well as a more favorable distribution of bending moment. The four lift points provide better resistance to girder twist compared two lift points, and the four lifting reactions also lead to a reduction in the maximum bending moment. While the use of two lifting cranes can improve girder stability, this option is often reserved for relatively long girder segments due to the cost of the extra crane, but the cost can sometimes be overcome if two cranes can complete the work more efficiently than one. Similarly, the use of three or more cranes is uncommon due to the added equipment costs, difficulty in coordinating crane movement, and controlling variations of crane forces during lifting. The source of the variable lifting force when using more than 2 cranes results from the lifted girder being an indeterminate system. With all lifting options, two limit states should be checked to ensure safety of the girders and the workers during the lifting process: a strength limit state and a serviceability limit state, both of which are discussed in Chapter 3 of this dissertation. Figure 1.9 shows a picture of the Case B lifting scenario, which is a single crane lifting a girder using a spreader beam and two lift clamps.



***Figure 1.9: Curved I-girder Lifted with a Single Crane using a Spreader Beam***

For typical bridges, the girders are usually lifted individually; however in some cases they are also lifted in pairs to improve the stability of the girders both during lifting and in the partially erected state. Regardless of the method of girder lifting, many components of the bridge must be assembled in the air. When possible, erectors will often complete splices on the ground to minimize the amount of time the crane is required during girder lifting, but this procedure depends on the crane availability and site access. Figure 1.10 shows an I-girder being spliced on the ground. Nonetheless, even in cases where girders are first spliced on the ground, it will inevitably be required that the girders be spliced with other girders previously erected. Thus, an aerial splice will have to be made. This process requires the girders to fit together reasonably well, including vertical, horizontal, and rotational alignment, so that the splice plates on each side of the flanges and web match each other and so that the bolts can be installed. One proposal that resulted from the current research and will be discussed in this dissertation includes adding a serviceability limit on girder rotation during lifting to ensure aerial splices can



be completed with minimal difficulty. Typically, 50% of the bolts are installed prior to releasing the segment from the crane and continuing with the erection of the next girder segment. Figure 1.11 includes a pair of pictures showing aerial splices.



*(a) Bolting Web Splice Plates*

*(b) Bolting Flange Splice Plates*

**Figure 1.10: Ground Splicing of I-girders (Farris 2008)**



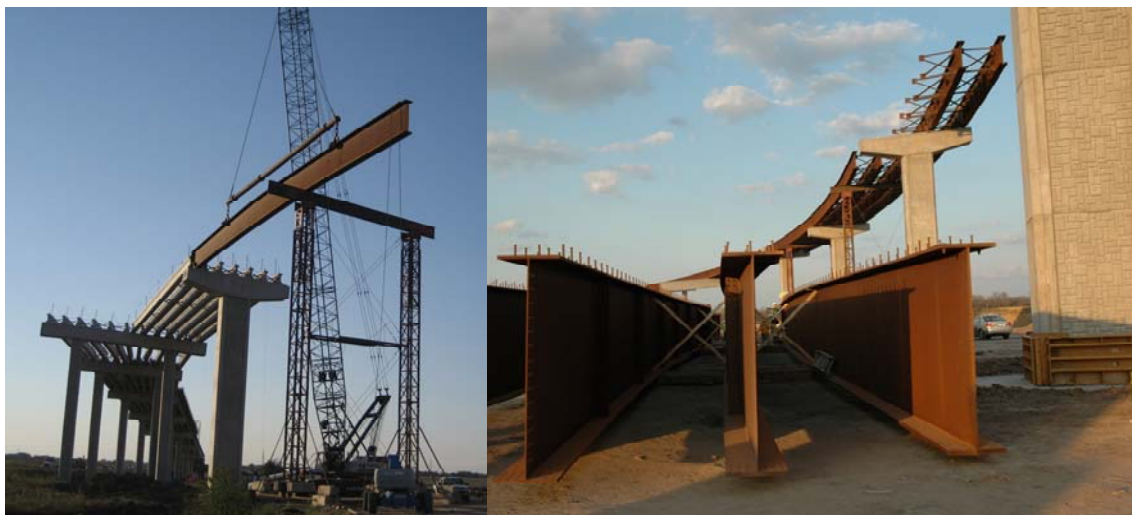
*(a)*

*(b)*

**Figure 1.11: Aerial Splicing of I-girders ((a)Farris 2008)**

The lifted girder segments are set on either the temporary or permanent supports, depending on the bridge geometry and site access. The most difficult girder segment to construct is the first girder to be lifted at any given cross section. The stability of the first girder is often one of the most critical segments from a stability perspective since there is minimal vertical and rotation support as well as no adjacent girder for bracing. Figure 1.12(a) shows an example of a single girder lifted onto a permanent support and a temporary support. The girder usually must be tied down to the supports to ensure the girder does not topple over. Another option available to contractors is to lift two girders

at a time, allowing the attached cross frames to assist in bracing the system and to improve the stability of the partially erected system. However, lifting girders in pairs essentially doubles the lifting weight and often requires two cranes. Figure 1.12(b) shows two girders extended over a pier, which helps provide stability against lateral-torsional buckling, because in order for the girder to buckle in a lateral-torsional mode the girder must be able to displace both laterally and torsionally. Preventing either type displacement (cross frames prevent relative rotation of the girder) braces the individual girder and thus increases the stability of the system.



*(a) First Girder Erected*

*(b) Girder Prepared for Lifting*

***Figure 1.12: Curved I-girders during Girder Erection***

As shown in Figure 1.12, it is often difficult to provide the necessary stability utilizing only the permanent supports. Therefore, temporary supports are often necessary. These temporary support perform three functions: 1) control deformations, 2) minimize stresses, and 3) provide stability to the girder system. The two most common temporary supports are holding cranes and shore towers. Holding cranes are smaller cranes that support girders at a point by providing a prescribed vertical load. Alternatively, shore towers can be built to support the girder from the underside. From a stability perspective, the location of the support point on the cross section can result in improved girder stability. As part of this study Petruzzi (2010) showed that the girders gain a substantial benefit when the crane connects to the top flange of the girder as

opposed to support from the bottom flange. However, while lifting cranes do not usually provide lateral stability, shore towers allow the erector to provide bracing from both lateral movement and twist as well as control vertical deformations. The vertical location of an applied load or support relative to a systems center of gravity can result in either a disturbing moment or restoring moment. This is known as the effect of load height and can have either a beneficial or detrimental effect on the stability of a structural system. Petruzzi (2010) provides a discussion of the behavior of curved I-girder systems in the partially constructed phase, with details of the effect of temporary supports. Figure 1.13 and Figure 1.14 shows a curved I-girder bridge during girder erection. The lifting crane, holding crane, and shore towers are identified for clarity.



***Figure 1.13: Curved I-girder Bridge during Erection***





***Figure 1.14: Temporary Support used for Stability Girder and Controlling Deflections***

The final stage of the construction process is the placement of the concrete deck. This stage is completed once permanent metal deck forms are set between girders to provide formwork for casting the deck. Overhangs are built on the exterior girders, and the deck reinforcing steel is installed. Concrete placement must have temperature and moisture controls to provide the highest quality concrete deck. Often in warm environments like Texas, the bulk of the cast will occur at night to ensure the workability of the concrete and prevent the formation of delayed ettringite formation (DEF), a detrimental expansive chemical process associated with high curing temperatures. Additionally, a curing compound can be sprayed on the deck, and burlap sacks or some other heavy cloth can be placed on top and saturated to ensure the concrete has sufficient water for hydration. The concrete is brought to the job site in concrete mixing trucks and dumped in to a pump truck that pumps the concrete onto the bridge. The screed is fixed to a metal rail supported by the overhangs and provides the finished surface at the proper elevation. Figure 1.15 shows a curved I-girder bridge with the permanent metal deck forms (a), concrete being placed and vibrated (b), curing compound added to the deck (c), and burlap sacks placed to hold moisture (d). Figure 1.16 shows both the screed and the concrete pump truck used in the construction of a curved I-girder bridge.



***(a) Permanent Metal Deck Forms***



***(b) Concrete being Placed and Vibrated***



***(c) Curing Compound Added to the Deck***



***(d) Burlap Sacks Placed on Deck***

***Figure 1.15: Concrete Deck Placement of Curved I-girder Bridge***



***(a) Screed Leveling Concrete***



***(b) Concrete Pump Truck***

***Figure 1.16: Concrete Deck Placement Utilizes a Screed and a Pump Truck***

### 1.2.3 Curved I-girder Analysis Methods

Prior to the construction of a bridge, it is necessary to analyze each stage of its expected service life. The level of analysis necessary to capture the behavior of a structural system varies depending on the loading, boundary conditions, and the general complexity of the system. The simplest type of analysis is a *linear elastic analysis* in which all material properties are assumed to remain elastic and the displacements are assumed to be small. A linear elastic analysis approach generally works well for service level loads ( $P_S$ ) because the response of typical bridge structures are designed to remain elastic and not undergo permanent deformations under these types of loads. However, engineers need to understand the behavior of structures at their limits, and detailed analyses that account for possible nonlinear effects are often necessary. A good reference that includes a thorough discussion of the topic of nonlinear analysis can be found in McGuire et al. (2000). There are many sources of nonlinearity that exist in the behavior of actual structures. Engineers typically use simplified models that are based on rational assumptions. The sources of nonlinearity can be divided into two major types: geometric nonlinearity and material nonlinearity. Geometric nonlinearity results from accounting for the change in structural response based on the changing geometry of the system by accounting for deformations and finite displacements in equations of equilibrium. Examples of geometric nonlinearity include: 1) initial imperfections or girders being out-of-plumb, 2)  $P$ - $\Delta$  effects, which are an amplification of bending moments in members caused by external loads acting through large displacements, and 3)  $P$ - $\delta$  effects, which also amplify bending moments but are due to the eccentricity of axial loads relative to the deformed axis of an individual member. Material nonlinearity results from changes in the material properties of members as load is applied. Examples of material nonlinearity include: 1) plastic deformation in steel or concrete, 2) creep in concrete, and 3) nonlinear load-deformation behavior in materials such as that which occurs in the deformation of elastomeric bearings. Both types of nonlinearity may exist in the same structure, and they can be accounted for in a computational model.

As mentioned previously, a linear elastic analysis assumes no nonlinearity. For buckling analyses, it is common to perform an *elastic eigenvalue buckling analysis* to determine the linear elastic eigenvalue ( $P_\lambda$ ) at which an alternate deformed shape is mathematically possible. The eigenvalue represents an amplifier on the applied load that causes buckling, while the buckled shape corresponds to the particular eigenvector. Elastic eigenvalue analyses are performed on the original geometry assuming small deformations and elastic material properties. Alternatively, an *inelastic eigenvalue buckling analysis* can account for material inelasticity prior to the buckling load and determine an inelastic eigenvalue ( $P_{\lambda}$ ). Both analyses result in a bifurcation of the  $P$ - $\Delta$  graph. Regardless of whether or not the problem under consideration assumes elastic response or accounts for material nonlinearity, an eigenvalue analysis will produce the buckling mode shape, but it will not indicate the magnitude of the displacements in the structure at the onset of buckling.

A *second-order elastic analysis* accounts for finite displacements in formulating the equations of equilibrium and can account for both types of  $P$ - $\Delta$  effects. Such an analysis is often completed computationally as an iterative process that corrects for residual forces in the equilibrium equations. A second-order elastic analysis can lead to two possible modes of response depending on the geometry of the problem and the loading applied. If the final geometry of the structure results in a stable system, the structure can continue to sustain load and the material stresses can continue to increase limitlessly. If, however, the geometry of the structure being analyzed becomes unstable, the structure will reach an elastic stability limit ( $P_{ES}$ ) load, which is the largest magnitude load the system can support without experiencing excessively large displacements. A second-order elastic analysis is necessary to determine the effects of imperfections on a structural system as the magnitude of the amplification of the  $P$ - $\Delta$  effects is most apparent with an iterative analysis approach.

A *linear inelastic analysis* accounts for only material nonlinearities. Such an analysis may be completed incrementally in a manner that is similar to the second-order elastic analysis described previously; however, for this case, the stresses or strains are

evaluated at each iteration for compliance with the specified constitutive model. As members experience inelastic response and eventually yield completely, plastic hinges form, which will ultimately result in the formation of a collapse mechanism. When a mechanism forms, the load the structure is capable of resisting is defined as the plastic limit ( $P_P$ ) load. A *second-order inelastic analysis* accounts for both material nonlinearities and geometric nonlinearities. The analysis allows for the actual behavior to be modeled, and an inelastic stability limit ( $P_{IS}$ ) load can be calculated. As the level of analysis increases, the computational effort will also increase and may become cost prohibitive for typical bridge designs. Figure 1.17 is a schematic showing a pair of curved girders during construction that is typically analyzed with various loads ( $P$ ) and monitored displacements ( $\Delta$ ). Figure 1.18 is a  $P$ - $\Delta$  (i.e., load-deformation) graph that demonstrates the differences in load path predicted by various types of analyses. For the purposes of the current study, inelastic response of materials during the construction phase (e.g., yielding of steel girders) and other forms of permanent deformations are undesirable; thus, material nonlinearities are not permitted and are therefore not considered in the analyses conducted for this research. Linear elastic analyses, elastic eigenvalue buckling analyses, and second-order elastic analyses are utilized as part of this research to determine the behavior of curved I-girders during construction.

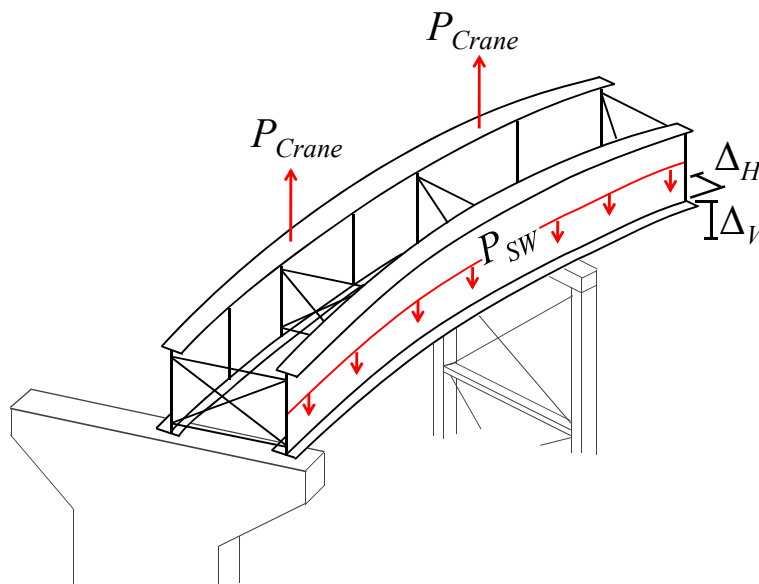


**Figure 1.17: Curved I-girder System to Analyze**

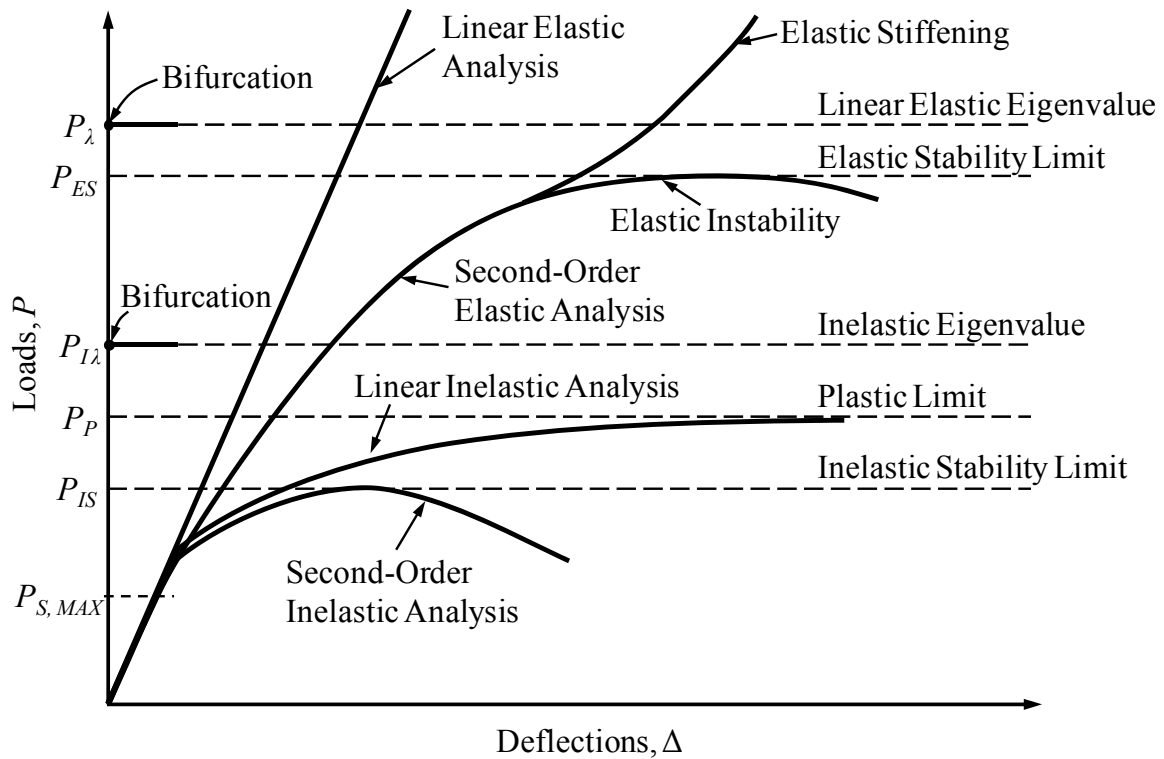


**Figure 1.18: *P-Δ Graph Demonstrating the Effect of Different Levels of Analysis***  
*(Adopted from McGuire et al. 2000)*

### 1.3 SCOPE

This dissertation is one part of a larger project funded by the Texas Department of Transportation (Project 0-5574 - Curved Plate Girder Design for Safe and Economical Construction). The research includes a literature review, field tests, parametric finite element studies, program development, and design recommendations. While many of these topics are touched on within this document, complete discussions are not included. Detailed descriptions of various portions of the investigation are available in Schuh (2008), Farris (2008), and Petruzzi (2010). Additional information regarding the project in its entirety is available in the project report (Stith et al. 2009).

The literature review conducted for this research focused on major research efforts related to curved I-girder bridge systems, full-scale laboratory tests, field tests, computational modeling efforts, and current code standards. The field tests conducted during this research project included monitoring curved steel girders on a bridge during

erection and construction as well as girder lift tests at a fabrication yard. The bridge that was monitored during construction consisted of a horizontally curved direct connector bridge located east of Austin, Texas with four steel bridge segments. The additional girder lift tests were conducted at both Hirshfeld Industries in San Angelo, Texas as well as at the construction site. The parametric finite element analyses were completed using the ANSYS computational software package. The behavior of curved I-girder bridges during girder lifting and the partially constructed phases were studied. The result of the studies allowed for the knowledge to create two design tools, UT Lift and UT Bridge.

The research and necessary derivations that led the creation of these two programs is the focus of this dissertation. UT Lift is the culmination of the understanding of curved I-girders during lifting and includes calculations of the center of gravity, the optimum location to lift a horizontally curved girder, and girder deformation behavior during the lifting process. This dissertation provides the equations derived to calculate each of these girder properties and the approach used to implement these equations in UT Lift. UT Bridge is a user-friendly 3-D finite element analysis program that calculates the behavior of steel I-girder bridges during the erection and the concrete deck placement phases of construction. The program has an intuitive pre-processor that prompts the user to input the necessary information that would be readily available from a set of bridge plans. The post-processor provides both 3-D visualization of the bridge and 2-D 10<sup>th</sup> point graphs of displacements, stresses, and rotations. The finite element formulations and other programming features are discussed in this dissertation.

#### **1.4 ORGANIZATION**

Following this introductory chapter, a literature review is provided in Chapter 2. Additionally, a review of the recent work conducted during this research project and reported by others is also included in Chapter 2. This recent work includes field test data that are used to verify the computational models and parametric finite element studies conducted for this research.

In Chapter 3, the behavior of curved I-girders during lifting is presented. The response is dominated by girder deformations and rotations—primarily the rigid body rotation and the cross-sectional twist. The rigid body rotation is calculated from the line of support defined by the lift apparatus and the center of gravity. Chapter 3 includes the derivation of the equations for the center of gravity of any curved girder with or without cross frames attached. The cross sectional twist cannot be determined exactly from a closed form solution, but the implementation of a 1-D finite element to approximate the twist is presented. This theory was implemented in UT Lift and verified by a 3-D finite element models in ANSYS using nonlinear geometry. Finally, an example problem is provided to demonstrate the results provided.

Chapter 4 begins with a brief introduction to the history and the basic concepts of finite element analyses. It then includes a description of the three basic aspects of a finite element program: pre-processor, processor, and post-processor. The pre-processor provides the user interface that allows for the input of the variables needed to define the bridge being analyzed. A discussion of all assumptions used in the program is also included in this chapter. The processor performs the structural analysis of the bridge input using the pre-processor, and the formulation of all necessary element types is provided in this chapter. The post-processor performs the necessary calculations to obtain the stresses from the displacements computed during the processor step. The visualization and output options for the results in the UT Bridge post-processor are also presented. Verification of UT Bridge is discussed by comparing the program output results to commercially available grillage software, 3-D ANSYS analyses, and field data.

The final chapter presents the conclusions from this research project including the recommended calculations and submittal information for curved I-girder bridges. As with most research projects, the list of potential work is longer than the time and resources available to complete the full scope of research on the topic and thus recommendations for future research topics within this field are also offered.



## **CHAPTER 2:**

### **LITERATURE REVIEW AND RECENT WORK**

---

#### **2.1 INTRODUCTION:**

This chapter provides an overview of past research on the behavior of curved girders. The first investigation into the behavior of curved beams was published by Barre De Saint Venant (1843). Numerous other studies and works have been conducted since then, but interest in the United States did not begin in earnest until 1969 when the Consortium of University Research Teams (CURT) was formed by the Federal Highway Administration (FHWA). Besides the investigations performed under the CURT study, there have been a number of smaller studies performed over the last few decades. The discussion of past studies described in this chapter focuses on work that is relevant to the current investigation. A comprehensive synthesis of past research on curved steel girders can be found in the works by McManus et al. (1969), Zureick et al. (1994), which considered research prior to 1993, and Yoo and Choi (2000), which focused on research from 1993 through 2000.

#### **2.2 DEVELOPMENT OF GUIDE SPECIFICATIONS FOR HORIZONTALLY CURVED HIGHWAY BRIDGES:**

##### **2.2.1 Consortium of University Research Teams (CURT):**

The FHWA was responsible for initiating the first major investigation of curved girder systems with the formation of the Consortium of University Research Teams (CURT) in 1969. The study, which was funded by 25 states, included Carnegie Mellon University, the University of Pennsylvania, the University of Rhode Island, and Syracuse University.

The CURT project focused on small-scale tests conducted primarily at Carnegie Mellon University, as well as theoretical and analytical work conducted at the other three universities. The results of I-girder bridge small-scale tests ( $\approx 15'$  long and  $\approx 50'$  radius

of curvature) were documented by Mozer and Culver (1970) and Mozer et al. (1971, 1973). Some of the first analytical models for curved bridges were validated with tests that examined the interaction between bracing members and adjacent girder lines by Brennan (1970, 1971, and 1974). McManus utilized some of the test results to validate the theoretical work to predict the behavior of doubly symmetric curved I-girders in bending (1971). Nasir studied the local buckling behavior of curved girder flanges (1970). A few studies on the stability of web panels were also conducted (Brogan 1974; Culver et al. 1972, 1973). Another study that focused on stability issues concentrated on the local buckling of the compression flange of curved I-girders in both the elastic and inelastic range (Culver and Frampton 1970; Culver and Nasir 1971). The CURT project did not explicitly address the erection behavior of curved steel bridge girders, but it did investigate the behavior before and after the deck was placed (Brennan 1970).

The major result of the CURT project was the development of recommendations for an allowable stress design (ASD) specification for curved bridges (Culver 1972; CURT 1975). These specifications were reviewed by the AASHTO Committee on Flexural Members, and the committee also evaluated scaled tests conducted at the University of Maryland (Kuo and Heins 1971)(Heins 1972) and analytical work conducted at the University of California Berkley (Mondkar and Powell 1974). The committee proposed a guide specification that was approved in 1976. Later, the American Iron and Steel Institute (AISI) sponsored a research project to add load factor design (LFD) to the guide specification recommendations by converting the CURT ASD format to LFD (Stegmann and Galambos 1976). The project resulted in the first edition of the *Guide Specifications for Horizontally Curved Highway Bridges* (AASHTO 1980). After eight interim revisions, the second edition of the Guide Specifications came out (AASHTO 1993).

### **2.2.2 Curved Steel Bridge Research Project (CSBRP):**

Research in the area of curved girders continued in the US through the 1980s (Yoo and Carbine 1985; Yoo and Littrell 1986; Schelling et al. 1989) and a number of

studies were also conducted in Japan. The Japanese conducted tests to support the Hanshin Expressway Corporation's *Guidelines for the Design of Horizontally Curved Girder Bridges*. The documents are written in Japanese, but have been reviewed by Zureick et al. (1994) and address many design concerns such as the effects of transverse stiffeners (Nakai et al. 1985) and longitudinal stiffeners (Nakai et al. 1986) among others. The understanding of curved girders was not significantly advanced again, however, until the early 1990s when the Structural Stability Research Council (SSRC) recommended areas of need for further research (SSRC 1991). These recommendations prompted the FHWA to fund the Curved Steel Bridge Research Project (CSBRP) in 1992. The project's goals included compiling a synthesis of all the previous research on the topic (Zureick et al. 1994) and addressing weaknesses in the CURT research project, specifically the lack of full-scale and field tests with realistic boundary conditions. This work lasted over ten years and greatly improved the understanding of curved bridge behavior. The results were formulated into the first Load and Resistance Factor Design (LRFD) provisions, which were later incorporated into the subsequent editions of the AASHTO bridge specifications. The provisions included in the *Guide Specifications for Horizontally Curved Steel Girder Highway Bridges 2003* (AASHTO 2003) have been incorporated into the *AASHTO LRFD Bridge Design Specifications 4<sup>th</sup> Edition 2007* (AASHTO 2007). Many of the projects and findings referenced in the following sections are a product of the CSBRP—either directly or indirectly.

### **2.3 CURVED GIRDERS DURING LIFTING:**

Limited research on the lifting of horizontally curved I-girders has been reported in the literature. Although the topic of stability during lifting has been identified as important (NCHRP 2005), little guidance is available. Robert Mast (1989) worked on the lateral stability of long prestressed concrete beams during lifting. Mast defined the *roll angle* as the rotation of a girder about the *roll axis* which is the line defined by connecting the lifting points as shown in the top of Figure 2.1, which was taken from Mast. Due to initial imperfections and the misplacement of lifting loops, the “straight” prestressed concrete beam has an imperfection geometry that results in the location of the

girder center of gravity at an eccentricity to the roll axis. This eccentricity results in the girder rotating to a new roll angle that produces weak-axis bending due to the girder self weight, which then increases the eccentricity of the center of gravity relative to the roll axis. The deformed geometry results in the girder either finding equilibrium or a failure from bending about the weak axis due to inadequate lateral stiffness. The other identified failure mode was a roll angle that exceeded a maximum permissible angle. Both failure modes are undesirable according to Mast, and he provided two equations for determining the factor of safety for each possibility.

$$FS = \frac{y_r}{\bar{z}_o} \left( 1 - \frac{\theta_i}{\theta_{max}} \right) \quad \text{Equation 2.1}$$

$$FS = \frac{\theta_{max}}{\theta_i} \left( 1 - \frac{\bar{z}_o}{y_r} \right) \quad \text{Equation 2.2}$$

where:

- $y_r$  = Height of the roll axis above the center of gravity of the beam
- $\bar{z}_o$  = Theoretical lateral deflection of the center of gravity of the beam, computed with the full dead weight applied laterally
- $\theta_{max}$  = Maximum permissible tilt angle of the beam
- $\theta_i$  = Initial roll angle of a laterally rigid beam  $\{e_i/y_r \text{ or exactly } \tan(e_i/y_r)\}$
- $e_i$  = Initial lateral eccentricity of the center of gravity of the beam with respect to the roll axis

Figure 2.1 shows a schematic diagram of the equilibrium of a beam in the tilted position provided by Mast (1989), which shows both the roll axis and the roll angle. This idea is very important for the lifting of curved girders, and this research project extends this concept to curved girders. The current research also accounts for the potential of cross-sectional twist in addition to lateral deformation and rigid body rotation. The behavior of girders during lifting is described in more detail in Chapter 3.

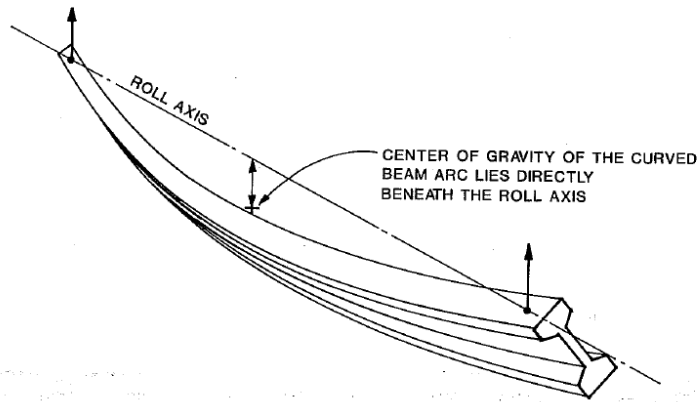


Fig. 1a. PERSPECTIVE OF A BEAM FREE TO ROLL AND DEFLECT LATERALLY

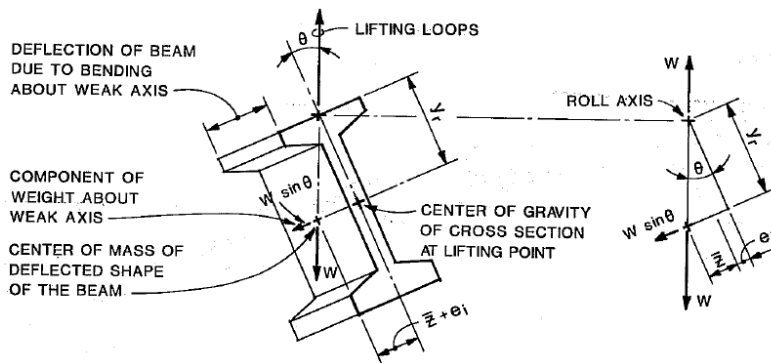


Fig. 1b. END VIEW

Fig. 1c. EQUILIBRIUM DIAGRAM

**Figure 2.1: Mast's Equilibrium of Beam in Tilted Position (1989)**

## 2.4 FULL-SCALE TESTS AND FIELD TESTS

Full-scale laboratory tests and field monitoring have played an important role in improving the understanding of the behavior of curved I-girders. However the size and cost of these studies have resulted in a limited amount of data available in the literature. This lack of information on the response of full-scale curved I-girders has been identified as an area of weakness within the research field according to SSRC (1991). The main studies consisted of field monitoring by Beal and Kissane in the 1970's, field monitoring in Minnesota in the late 1990's, field monitoring of a bridge in Pennsylvania in the early 2000's, and full scale laboratory tests at the FHWA Turner-Fairbanks Structures Laboratory, each of which are discussed in this section. One of the first attempts to monitor curved I-girders during the early stages of construction was by Beal and Kissane (1971(a)) when the Hulls Falls Bridge in New York was instrumented. This bridge was a

4-girder, 123-ft. simple span bridge with a radius of curvature equal to 477.9 ft. Dead load and static live load measurements were taken to determine the stress and deflection in the girders. To ensure that the instrumentation was not damaged, measurements were not recorded until after the erection. Measurements were taken during the deck placement and subsequent live load testing. Even with the precautions that were taken, the collected data were sparse due to damaged or malfunctioning instrumentation. The problems included strain gages damaged from the construction process, inadequate waterproofing, poor bonding of the gage cement, and high humidity. The diaphragm gages suffered from the same problems, with many damaged during construction; some recorded only sporadic data. The results determined from the limited data were that the stresses were less than the computed values, but the measured deflections exceeded the computed values, thereby suggesting the analysis results to be unconservative.

Shortly after this initial study, Beal and Kissane attempted a second instrumentation (1971b) of the Huyck Stream Bridge. This time, another 4-girder simple span bridge with a span length of 95 ft. and a 162-ft. radius of curvature was instrumented with 132 strain gages. While many of the strain gages were damaged or failed to work properly, the number was significantly less than their first attempt. They were able to conclude that the planar grid method of analysis available at that time was sufficient for predicting the vertical bending response and the deflections. However, the model did not have the ability to predict the lateral bending stresses in the flange, and several of the flange gages recorded values above the allowable stress. It was recommended that methods should be developed that could account for these stresses.

In their third attempt, Beal and Kissane (1972) instrumented an exit ramp bridge that consisted of a 5-girder, symmetric, two-span system with centerline span lengths of 100 ft. each and a 266-ft. radius of curvature. A planar grid method was used to analyze the bridge system, and instrumentation of one of the two spans was completed with 160 gages. As with the first two bridges, several gages malfunctioned, but the instrumentation showed a large absolute value difference in the stresses between the inside and the outside edge of the bottom flanges, representing significant lateral bending

and/or warping torsion. Many of the diaphragm gages worked for this test, and the ones that did not were averaged with the remaining data. It was shown that, during the static live load tests, the diaphragms experienced no significant stresses. The conclusions of this test were similar to the second test and showed that lateral bending played a significant role in the stress distribution of the girder. These stresses were not captured with the planar grid analysis method. The researchers also concluded that the negative moment region of the bridge appeared to have the highest stresses and should control the bridge design.

In 1996 Galambos et al. instrumented a two-span, curved I-girder bridge with a skewed substructure in Minnesota. The MNDOT Bridge No. 27998 had a centerline radius of curvature of 286 ft. and span lengths of approximately 146 ft. and 150 ft. The bridge had different depth girders ranging from 50 in. for the interior (inside of curve) girder to 72 in. for the exterior (outside of curve) girder. Sixty vibrating wire strain gages were used on both the girders and diaphragms of the superstructure. The gages were installed in the fabrication plant where a baseline reading could be recorded. Another baseline reading was taken in the field before the girders were lifted off the ground with the baseline readings differing by only 2-3%. Readings were taken throughout the erection process and concrete placement. Static tests with live loads were then conducted on the completed structure. Deflection readings were taken with a survey level. Additionally, a planar grid method computer program was developed and compared to the measured results. Conclusions from the comparison between the field data and the computational output showed a qualitative match with some quantitative matches. The computational predictions had similar trends to the field data, but only a few points matched quantitatively. During the first construction stage, the measured data showed little correlation with the model. This difference was attributed to the low level of girder self weight stress and the relatively large fit-up stresses. Once the concrete deck was placed, the measured data correlated better with the analysis model than it did during the first stage because the fit-up stresses became less significant. It was concluded that the

stresses were below yield throughout construction and that once composite action was achieved, significant correlation was possible (Galambos et al. 2000).

The computer program used by Galambos et al. was called the University of Minnesota Steel Curved Girder Bridge System Analysis Program (UM) and detailed by Huang (1996). The program utilized a grillage method, which is a stiffness-based finite element formulation. The elements were 3-dimensional, 2-node curved beam elements on a 2-dimensional planar grid. The beams had 4 degrees of freedom per node including out-of-plane displacement and rotations as well as a warping degree of freedom, but the two translational displacements and the rotation about an axis perpendicular to the plane of the curve were neglected and deemed insignificant. The program modeled cross frames as truss elements and added additional degrees of freedom at the supports to account for the translational displacements of these nodes (Galambos et al. 2000).

A full-scale laboratory test was conducted at the FHWA Turner-Fairbanks Structures Laboratory using a 90-ft. simple-span bridge with 3-girders and a radius of curvature of 200 ft. A plan view of the test setup is shown in Figure 2.2. To ensure the girders remained elastic throughout the multiple tests, the girders were fabricated with AASHTO M270 Grade 70W steel, and additional cross frames were placed between girder lines 1 and 2. Electrical resistance gages were used on the cross frames and bracing members, while vibrating wire strain gages were used on the girder. Select locations utilized displacement and rotation transducers to measure displacements, while a total station was used to measure global deformations (Linzell et al. 2004). The  $b_f/D$  ratio of the girders ranged from 1/3 for the inside girder to 1/2 for the exterior girder, which are significantly wider flanges than the AASHTO LRFD limit of 1/6. The dimensions of the girders that were tested are provided in Table 2.1.



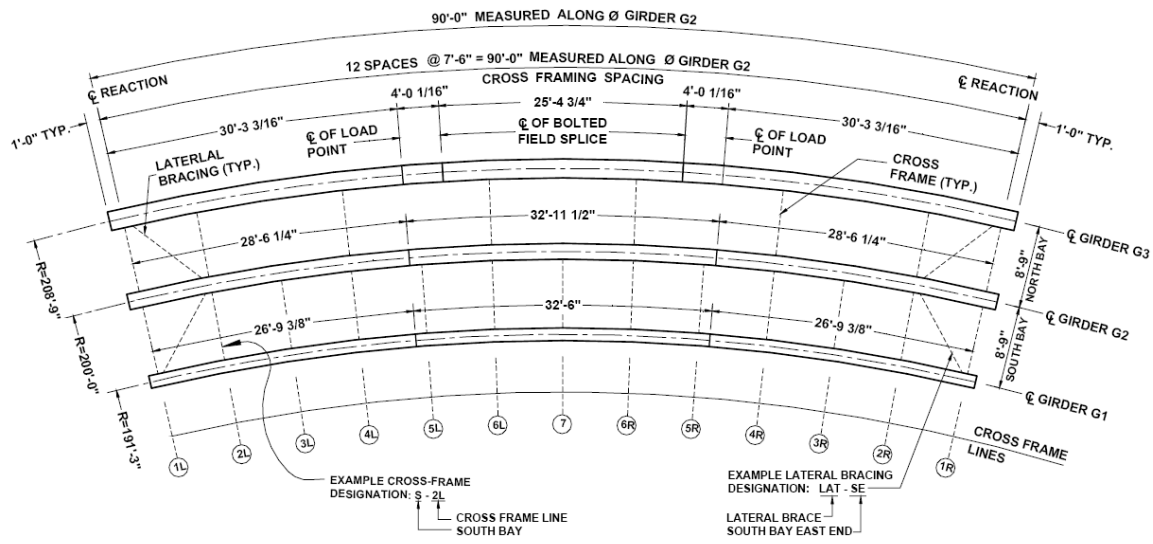


Figure 2-1: Plan View of Test Frame

**Figure 2.2: Plan View of Test Frame at FHWA Turner-Fairbanks Structures Laboratory (Linzell et al. 2004)**

**Table 2.1: Plate Girder Dimension for Erection Test (Linzell et al. 2004)**

| Girder Plate Dimensions |                                     |                                 |                |                        |
|-------------------------|-------------------------------------|---------------------------------|----------------|------------------------|
| Locations               | Flanges<br>$b_f \times t_f$<br>(in) | Web<br>$h_w \times t_w$<br>(in) | Span<br>Length | Radius<br>of Curvature |
| G1                      | 16 × 1-1/16                         | 48 × 7/16                       | 86'-1"         | 191'-3"                |
| G2                      | 20 × 1-3/16                         | 48 × 1/2                        | 90'-0"         | 200'-0"                |
| G3                      | 24 × 2-1/4                          | 48 × 1/2                        | 93'-11"        | 208'-0"                |

Six single-girder erection tests were conducted to examine the response of an individual girder to a variety of lateral support conditions. Two twin-girder erection tests were conducted, and one three-girder erection test was also conducted. Each test consisted of shoring the girder to the shop specified camber—designated the “no-load” situation—and then removing the shoring so that the system fully deflected under the self weight. The shoring was then reinstalled to bring the specimen back to the “no-load” condition. The tests were not intended to reproduce actual construction conditions, but rather to gain data for cases in which falsework was used to stabilize curved girders during construction. The conclusion from the erection test showed that the V-Load method gives conservative predictions for the bending moments of the exterior girder and

unconservative predictions for the bending moments for the interior girder (Linzell et al. 2004).

The bridge was modeled by Linzell using the ABAQUS finite element software (1999). The two interior girders had five plate elements through the depth of the web and beam elements to represent the flanges. The cross frames and bottom braces were modeled with truss elements. The exterior girder utilized plate elements for the web and the flange with a denser mesh closer to the center of the girder. The test indicated that it is beneficial to minimize radial restraint when constructing curved I-girders. It also showed that a detailed shell-element-based finite element analysis model could provide an acceptable level of accuracy in predicting erection behavior. Additionally, simplifying analytical representations of the cross frame connection detail, rigid connection of the cross frame beam element to the girder shell elements rather than explicit modeling of the gusset plate connection, may lead to discrepancies between the predicted and measured behavior in the radial load distributions. Linzell concluded that the exclusion of the gusset plates resulted in the mode of response of the model being less stiff than the measured data indicated (Linzell 1999).

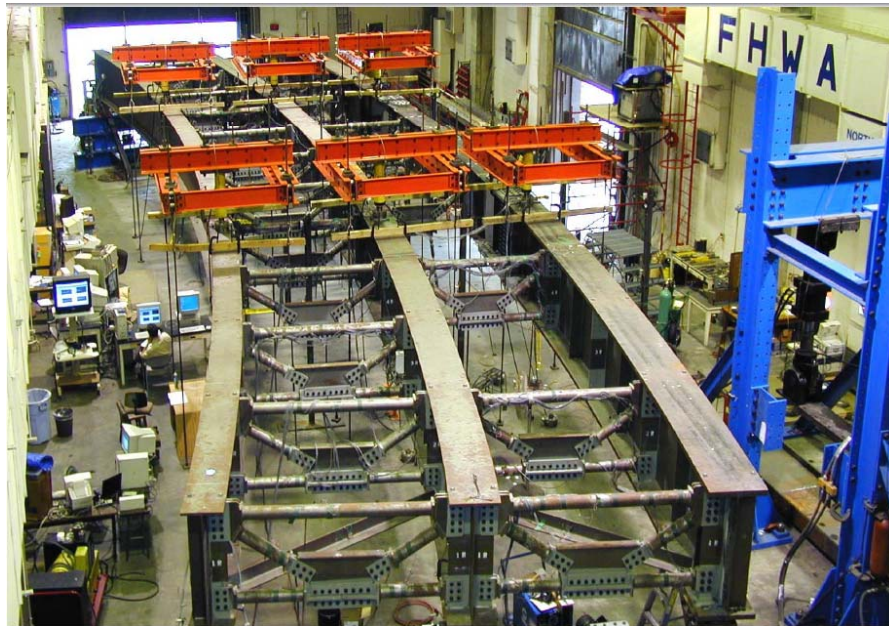


***Figure 2.3: Test Frame at FHWA Turner-Fairbanks Structures Laboratory  
(Hartmann 2005)***

Beyond the initial testing phase at the FHWA Turner-Fairbanks Laboratory, several additional component tests were conducted to determine the effects of web slenderness, flange slenderness, and stiffener spacing on vertical bending capacity. The results showed that the web slenderness and stiffener spacing had a negligible effect on the vertical bending capacity (Hartmann, 2005). Increases in the compression flange slenderness tended to decrease the bending capacity of the girder system.

A recent test on a full-scale bridge that experienced unexpected deflections and rotation during the girder erection process was documented by Bell (2004). The bridge was one of two side-by-side horizontally curved steel I-girder bridges built for an I-99 Interchange in State College, Pennsylvania. The bridge consisted of five 10.5-ft. deep singly symmetric steel plate girders spaced at 9.75 ft. with radii of curvature varying from 1920 ft. to 1959 ft. The structure was a 6-span bridge with two 3-span continuous units. The focus of the research was on the second unit, which included spans 4, 5, and 6. Sixteen removable strain transducers and twelve vibrating wire strain gages were used to monitor the strain at different locations, including the girder flange tips and cross-frame members. Additionally, surveying data were collected and utilized to calibrate an analysis model in SAP2000. With the calibrated model, Bell was able to conclude that for erection procedures involving lifting single girder lines, it is best to begin with the outer girder (largest radius) and construct the bridge toward the inside of the curve. Conversely, for bridges erected with pairs of girders, the erection sequence should be reversed, and the inner girders should be lifted first. The use of top lateral bracing stiffens the girders and reduces the deflections. Temporary supports can reduce the deflections when compared to erection sequences that do not use temporary supports. Table 2.2 and Table 2.3 provide a summary of the girder dimensions and girder geometry used in the research reported by Bell (2004). Figure 2.4 shows a plan view of the bridge unit that was studied, with the girder line, field splice, and support tower locations indicated.

**Table 2.2: Girder Plate Dimension Range (Bell 2004)**

| Girder | Top Flange Plate |                | Web Plate  |                | Bottom Flange Plate |                |
|--------|------------------|----------------|------------|----------------|---------------------|----------------|
|        | Width (in)       | Thickness (in) | Depth (in) | Thickness (in) | Width (in)          | Thickness (in) |
| G1     | 20 – 35          | 1.5 – 4        | 126        | 0.8125         | 26 - 43             | 1.75 – 3       |
| G2     | 17 – 34          | 1 – 3          | 126        | 0.8125         | 18 – 40             | 1.5 – 3        |
| G3     | 16 – 28          | 1 – 3          | 126        | 0.8125         | 18 – 34             | 1.25 – 3       |
| G4     | 16 – 28          | 1 – 3          | 126        | 0.8125         | 18 – 34             | 1.25 – 3       |
| G5     | 17 – 34          | 1 – 3          | 126        | 0.8125         | 22 – 40             | 1.25 – 3       |

**Table 2.3: Geometric Summary (Bell 2004)**

| Girder | Radius  | Span 4 | Span 5 | Span 6 |
|--------|---------|--------|--------|--------|
|        | (ft)    | (ft)   | (ft)   | (ft)   |
| G1     | 1959.36 | 298.84 | 336.5  | 268.79 |
| G2     | 1949.61 | 297.35 | 334.83 | 267.45 |
| G3     | 1939.86 | 295.85 | 333.16 | 266.11 |
| G4     | 1930.11 | 294.36 | 331.48 | 264.78 |
| G5     | 1920.36 | 292.86 | 329.8  | 263.44 |

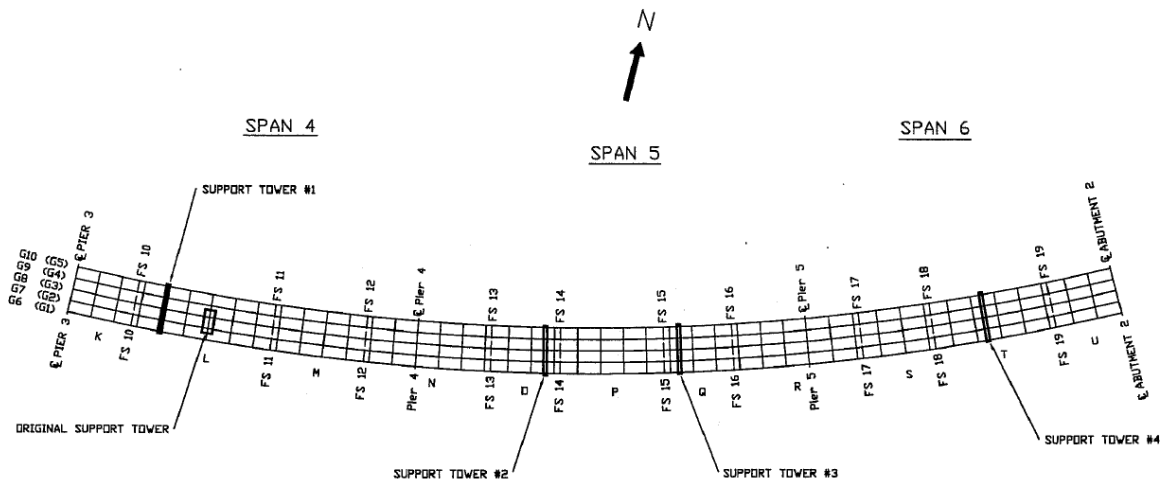


**Figure 2.4: Plan View of Bridge Studied by Bell (2004)**

## **2.5 COMPUTATIONAL MODELING OF CURVED I-GIRDER BRIDGES**

Currently there are several commercially available software programs capable of analyzing horizontally curved I-girder bridges. Many of these programs consist of 2-D grillage models that are useful for design calculations of various load cases of the completed structure. Two of the most widely used grillage programs are MDX (2009) and DESCUS (2008). These design software packages are intended to assist the design process and increase the efficiency of the engineer by accounting for various load cases, force envelopes, and code checks. The 2-D models used by these programs, however, are not capable of analyzing the girders during construction, and they can miss critical information of the actual girder behavior. Better predictions of the girder behavior are possible with a 3-D analysis. Alternatively, there are several general purpose 3-D finite element programs available including ANSYS (2007), ABAQUS (2010), LUSAS (2010), ADINA (2010), and BSDI (2010). These programs have capabilities to model complex structural problems, but they lack the bridge-specific, easy-to-use interface necessary for widespread use by design engineers. These 3-D packages also do not include pre-defined load cases or check the computer results against allowable limits set by the AASHTO specifications.

### **2.5.1 Synthesis of Computational Modeling Choices**

The difficult structural analysis problems present in the design of highway bridges have utilized many techniques over the years. Zureick and Naqib (1999) synthesized the available analysis methods and evaluated the strengths and limitations of each technique. The authors divided the methods into approximate methods and refined methods. Approximate methods include the plane-grid method that models a bridge as an assemblage of two-dimensional (2-D) grid members, with one translational and two rotational degrees of freedom at each end of the 2D members. The space-frame method models a bridge using idealized three-dimensional (3-D) straight members, with the effect of warping not usually included. The V-load method models a curved bridge using equivalent straight girders with span lengths equal to the arc length and adds self-

equilibrating vertical shear forces at the diaphragm locations to take bridge curvature into account.

Zureick and Naquib (1999) also discussed the refined methods, including the finite element method that models a bridge by discretizing the structure into small, well-defined structural components (i.e., elements) that are defined by specifically numbered nodes. The behavior of the elements and the entire structure are a function of the nodal quantities, which serve as the primary unknowns. The authors recognize that the finite element method is one of the most general and accurate methods, but it requires significant implementation time. The finite-strip method divides a bridge into narrow strips with radial supports and provides some simplicity over the finite element method, but it does not offer the same level of flexibility as the finite element method. The finite-difference method superimposes a grid on a structure, and the governing differential equations are replaced by algebraic difference equations that are solved at the grid points. The slope-deflection method establishes partial differential equations in terms of the slope-deflection equations, and these equations are solved using a Fourier series solution technique. Zureick and Naquib conclude that the approximate methods are suitable for preliminary design and that the finite element method, though it is the most difficult to implement, is also the most flexible with respect to representing complex structural configurations and boundary conditions. It was noted that the development of commercial finite element codes with graphical user interfaces are likely to expedite modeling and allow users to conveniently view results.

### **2.5.2 V-Load Method**

One of the first analytical methods used to design curved girders was introduced by U.S. Steel (Richardson 1963) and is referred to as the V-load method. Fiechtl et al. (1987) examined the applications of the V-load method to a variety of problems, and they presented a report on the development and evaluation of the method. The V-load method accounts for the curvature of a girder by applying self-equilibrating vertical loads on the girder being analyzed. Fiechtl's report compares these results with refined finite element

analyses for a variety of bridge configurations. Figure 2.5 shows a schematic adapted from Fiechtl et al. that shows the internal forces present in a curved girder pair with a cross frame. The flange forces ( $M_i/h$ ) resulting from the applied moments and the curvature result in the horizontal load transfer ( $H_i$ ) in the cross frames. To provide moment equilibrium, the cross frames must transfer a vertical shearing force ( $V$ ) between the girders.

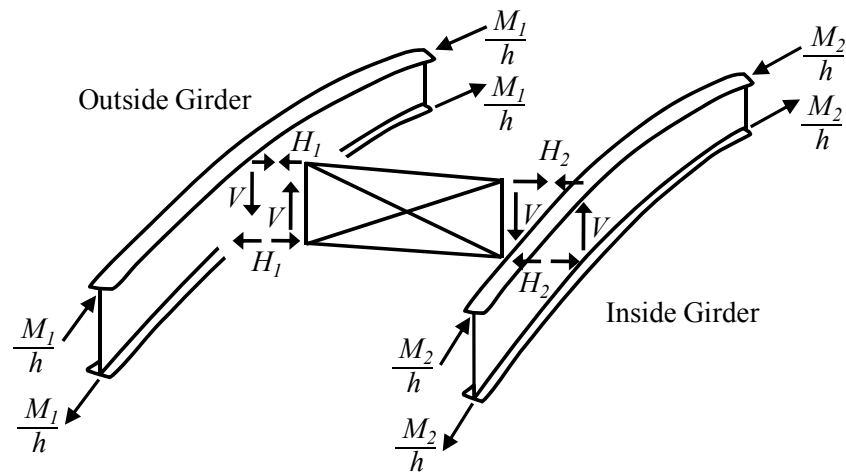


**Figure 2.5: Cross Section of Bridge Showing Cross Frame, Girders, and Internal Forces (Adapted from Fiechtl et al. 1987)**

The following steps are presented to summarize the V-load method, which is widely used as a preliminary analysis technique.

- 1) Apply the loads acting on a curved girder to an approximated straight girder with a length equal to the arc length of the curved girder (known as P-Loads).
- 2) Determine the moments and shears along the girder length from a linear analysis.
- 3) Determine the moments in the girder at each diaphragm line.
- 4) Use Equation 2.3 or Equation 2.4 to find the V-Loads at each diaphragm location.
- 5) Apply the V-Loads as point loads at the diaphragm locations.
  - For a 2-girder system, the V-Load is downward for the outer girder and upward for the inner girder.

- For multiple girders, the V-Load is assumed to be linearly distributed between the outer and inner girders;
  - Therefore, the V-Load is proportional to the distance from the centerline of the bridge.
- 6) Determine the moments and shears from a linear analysis with the applied V-Loads.
  - 7) Sum the moments and shears from steps 2 and 6 to determine the final moments and shears for the girder.

For Two Girders:

$$V = \frac{M_{p1} + M_{p2}}{RD/d} \quad \text{Equation 2.3}$$

For Multiple Girders

$$V = \frac{\sum_{i=1}^{N_g} M_{pi}}{C(RD/d)} \quad \text{Equation 2.4}$$

where:

- $M_{pi}$  = Moment for each diaphragm line due to the P-Load of the  $i^{\text{th}}$  girder
- $R$  = Radius of the girder
- $D$  = Spacing between girders
- $d$  = Arc Length between diaphragms
- $C$  = Constant distribution factor for multi-girder bridges

$$C = \frac{1 N_g(N_g + 1)}{6 (N_g - 1)} \quad \text{Equation 2.5}$$

$N_g$  = Number of girders

Note: In Equation 2.3 and Equation 2.4  $d$  should be measured along the radius line of  $R$ . The internal angle is the important aspect  $\phi = d/R$ . Therefore any girder radius  $R$  will work if the  $d$  is measured along that same girder.

The conclusion from the study showed that the V-load method was accurate for non-composite sections, but it did not perform well for girders that acted compositely with the deck due to the shear transfer by the deck. For two-girder systems, the analysis



was slightly conservative for the outer girder, while the solution was slightly unconservative for the inner girder when compared to the finite element models. The V-load method has greater error for bridges with skewed supports compared to normal supports.

### **2.5.3 Refined Methods Compared to Monitored Bridge**

Refined methods are becoming an oft used solution for complicated structures, however, these computational models are difficult to validate without pertinent field data from bridge systems. Chavel and Earls (2006a) analyzed the Ford City Veterans Bridge PA State Route 128 over the Allegheny River. The bridge consisted of a three-span system with a curved end span. The end span lengths were 322 ft and the center span length is 417 ft. The bridge consisted of four 14-ft deep girders spaced at 13.5 ft. Unfortunately, there was very little data recorded during the bridge erection. To validate the geometric nonlinear finite element analysis using ABAQUS, the data from Linzell's test (1999) were used. The authors were unable to predict several alignment problems experienced during construction with the results from the model. This difficulty was attributed to inconsistent detailing of the girder, which was discussed more fully in a subsequent article by Chavel and Earls (2006b). This second article highlighted the problems experienced with the erection of the Ford City Veterans Bridge. The erection problems were attributed to detailing inconsistencies. The girders were normally detailed to be plumb in the no-load condition or in computational models before the girders experience the deflections and rotations associated with self weight. The issue of inconsistent detailing becomes important as girders become larger, stiffer, or more highly curved (i.e., have smaller radii of curvature).

As part of his dissertation, Chavel (2008) utilized ABAQUS 6.3 to model a curved, skewed bridge in King of Prussia, Pennsylvania and to perform a series of parametric geometrically nonlinear analyses. The single-span bridge had a radial abutment and a second abutment at a 38.8 degree skew. The model utilized four-node shell elements with a maximum aspect ratio of 2:1 to model the girders, and the cross

frames were modeled with 3-D beam elements. The research focused on two aspects of the construction: the erection sequence and the cross frame detailing. With respect to the erection sequence, Chavel recommended that bridge engineers investigate each stage of steel erection for horizontally curved steel I-girder bridges in order to limit the problems that may develop in the field during construction and to highlight more difficult portions of the procedure for the erection. Figure 2.6 shows a plan view and an isometric view of the bridge modeled by Chavel in ABAQUS.

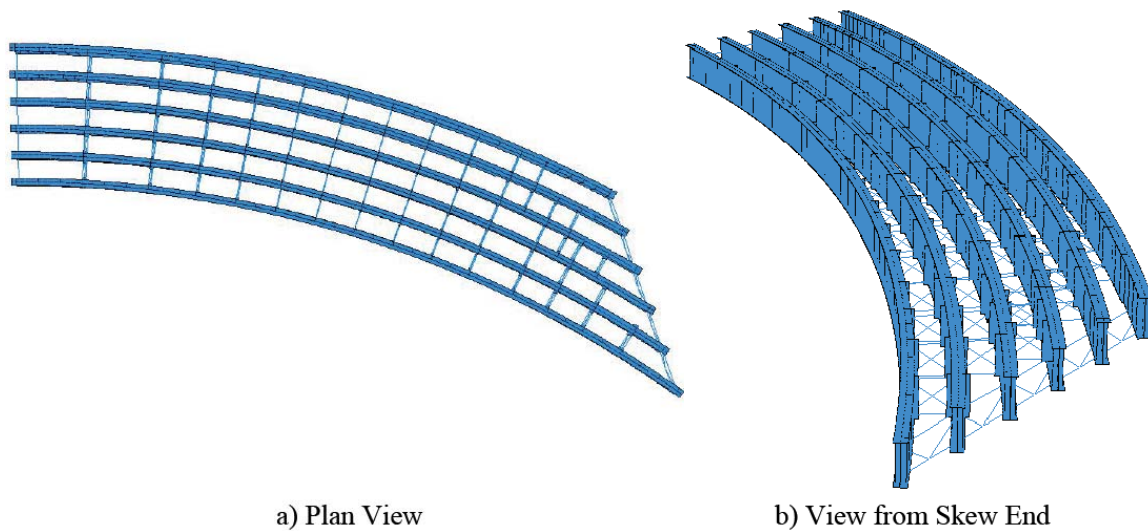


**Figure 2.6: Plan and Isometric Bridge Modeled by Chavel (2008)**

Another recent publication discussing modeling issues associated with steel bridges during construction was published by Ozgur et al. (2009). In this paper, the authors focus much of their attention on the material featured in Chavel (2008), including the King of Prussia, PA bridge. Additionally, the author describes an approximate method to determine uplift of the bearings during construction by utilizing Equation 2.6.

$$\xi = \frac{s_c}{w \cos(L_{as}/2R)} \quad \text{Equation 2.6}$$

where:

- $w$  = Width of the bridge
- $L_{as}$  = Arc length of the bridge
- $R$  = Radius of curvature
- $s_c$  = Distance from the centroid of the bridge to a chord line through the inner most bearings of the bridge.

The author recommends a limit of 0.8 for  $\xi$ , which is accurate for simple-span singularly curved bridges.

#### **2.5.4 Level of Analysis Comparisons**

With such a wide variety of computational methods available it is important for designers to determine the level of analysis necessary for the complexity of the bridge being designed. Nevling et al. (2006) utilized the results from a field study on a three-span curved bridge with five girders to compare different analysis programs. The goal of the project was to assess the accuracy of different levels of analysis. The authors established three levels of analysis to compare to the field data: manual, 2-D grillage, and 3-D finite element method (FEM). For the manual analysis, a line girder procedure from the AASHTO (1993) *Guide Specification for Horizontally Curved Highway Bridges* and the V-load method were used. Three commercially available 2-D grillage software programs were compared including SAP2000, MDX, and DESCUS. The 3-D FEM models were created in SAP2000 and independently by Bridge Software Development International (BSDI). The authors reported that the 3-D mesh was coarse due to BSDI requirements. Based on the results of their work, the authors concluded that both the 2-D and 3-D models produced girder vertical bending moment distributions that generally correlated well with the field test distributions and provided improved accuracy over the manual methods. Thus, it was recommended that 2-D analyses provide a reasonable approach when compared to a coarse 3-D mesh.

Coletti and Yadlosky (2008) authored a paper discussing challenges and proper usage of computer models for steel bridges. They specifically addressed the importance of properly understanding the fundamental assumptions and analytical implications of boundary conditions for different levels of analysis, the effect of representing a complex structure in a simple model, and the influence of span length, curvature, and skew on the construction tolerances and fit-up. Several examples were presented to highlight the importance of each issue. Admittedly the authors state that the purpose of the paper is to bring awareness to issues in need of further research investigation rather than providing a

litany of solution. The article highlights the need for additional research in the field of steel bridge analysis.

### **2.5.5 M/R-Method for Curved Box Girders**

A final note on the analysis of curved girders should include the historically cited computation method that is often used in curved steel bridges, which is the work of Tung and Fountain (1970) on the approximation of torsion by the M/R-Method. The idea is to approximate the torsional component of response in a curved bridge by dividing the bending moment that develops at a given cross-section by the radius of curvature. This method provides a good approximation for use during preliminary design of box girders, but the method does not work for I-girder bridges because two of the assumptions implicit in the method are that there is no cross sectional distortion and there is negligible warping torsion. While these assumptions are generally reasonable for box girders and for other closed or semi-closed sections with adequate bracing, I-girders have a significant amount of torsional distortion due to warping, rendering this method inappropriate for I-girder applications.

## **2.6 STATE OF PRACTICE (CODE REQUIREMENTS):**

There are several bridge design specifications that outline requirements for curved I-girders during construction. Some of these specifications provide detailed recommendations, while others only provide general guidance. The following paragraphs describe the requirements stated in several relevant specifications and include the preferred practices for the state of Texas. These paragraphs provide an understanding of the codified state of practice for bridges during construction.

### **2.6.1 AASHTO LRFD Bridge Design Specifications**

The AASHTO LRFD Bridge Design Specifications (2007) is published by the American Association of State Highway and Transportation Officials (AASHTO) and provides a Load and Resistance Factor Design (LRFD) guideline for bridge engineers to use in the design of all types of bridges. There is some coverage of construction issues in

the specifications, including Section 2.5.3 which discusses the design objectives during construction. This section states, “Constructibility issues should include, but not be limited to, consideration of deflection, strength of steel and concrete, and stability during critical stages of construction.” Chapter 4 is dedicated to the structural analysis of bridges; Section C4.6.1.2.1 includes the statement, “Since equilibrium of horizontally curved I-girders is developed by the transfer of load between the girders, the analysis must recognize the integrated behavior of all structural components. Bracing members are considered primary members in curved bridges since they transmit forces necessary to provide equilibrium.” This requirement suggests a certain level of analysis is required for curved bridges above that of a similarly complex straight bridge. The commentary continues by stating,

*Small-deflection theory is adequate for the analysis of most curved-girder bridges. However, curved I-girders are prone to deflect laterally when the girders are insufficiently braced during erection. This behavior may not be well recognized by small-deflection theory. Classical methods of analysis usually are based on strength of materials assumptions that do not recognize cross-section deformation. Finite element analyses that model the actual cross-section shape of the I-girders can recognize cross-section distortion and its effect on structural behavior.*

This commentary brings up two important ideas discussed in this dissertation: (1) the need for 3D finite element analysis and (2) the limitations of small-deflection theory. The recommendation of using finite element analyses to model a bridge’s cross-section and bracing members is accomplished by the UT Bridge program developed as part of this research and discussed later in Chapter 4 of this dissertation.

Chapter 6 of AASHTO LRFD Bridge Design Specification sets forth the specifications for the design of steel bridges. Section 6.5.1 specifies that the limit states should be investigated “for each stage that may be critical during construction, handling, transportation, and erection.” Section 6.7.4.2 establishes specific limitations on the unbraced length of curved I-girder bridges by mandating the spacing limit ( $L_b$ ) between all intermediate cross frames or diaphragms as follows:

$$L_b \leq L_r \leq \frac{R}{10} \leq 30' \quad \text{Equation 2.7}$$

where:

$L_r$  = Limiting unbraced length  
 $R$  = Radius of curvature of the bridge

$$L_r = \pi r_t \sqrt{\frac{E}{F_{yr}}} \quad \text{Equation 2.8}$$

In Equation 2.9, the following definitions are used:

$r_t$  = Effective cross sectional radius of gyration for lateral torsional buckling (given below)  
 $F_{yr}$  = Compression-flange stress at the onset of nominal yielding within the cross-section

$F_{yr}$ , including residual stress effects—but not including compression-flange lateral bending—is taken as the smaller of  $0.7F_{yc}$  and  $F_{yw}$ , but not less than  $0.5F_{yc}$ , where  $F_{yc}$  and  $F_{yw}$  are the yield stress of the compression flange and the web, respectively.

$$r_t = \frac{b_{fc}}{\sqrt{12 \left( 1 + \frac{1}{3} \frac{D_c t_w}{b_{fc} t_{fc}} \right)}} \quad \text{Equation 2.9}$$

where:

$b_{fc}$  = Width of the compression flange  
 $t_{fc}$  = Thickness of the compression flange  
 $t_w$  = Thickness of the web  
 $D_c$  = Depth of the web in compression in the elastic range.

Equation 2.7 gives very specific cross-frame spacing requirements depending on the cross-sectional properties used by the designer. Section 6.10.2.2 of the AASHTO specifications provides other provisions for cross-sectional proportioning, including an equation limiting the flange width to one-sixth of the depth of the web. This provision would allow a twelve-foot deep beam to have a two-foot wide flange. The limit of flange width to depth ratio of 1/6 can lead to relatively slender girders that may experience buckling or deformational problems during early stages of construction.

## **2.6.2 AASHTO LRFD Bridge Construction Specifications**

The AASHTO LRFD Bridge Construction Specifications (2004) provide required construction practices as stated by AASHTO. The provisions of Section 11.6 specify the erection of steel structures and states in Section 11.6.4.3 that “Cross frames and diagonal bracing shall be installed to provide stability and ensure correct geometry. Temporary bracing, if necessary at any stage of erection, shall be provided by the Contractor.” Section 11.6 provides suggestions, but it does not give guidance as to how to determine whether or not temporary bracing is in fact “necessary.” There is no standard on the level of analysis or the factor of safety that should be provided to determine the need for temporary supports.

## **2.6.3 AASHTO/NSBA Steel Bridge Erection Guide Specification**

The AASHTO/NSBA Steel Bridge Erection Guide Specification (2007) is published jointly by AASHTO and the National Steel Bridge Alliance (NSBA) with the intent to standardize and to facilitate construction of steel bridges in the United States. Chapter 2 of this document addresses the erection procedure and requires that a contractor provide a detailed erection plan to the owner prior to the start of construction. Section 2.3 b) states the submitted plan should contain, “calculations to substantiate structural adequacy and stability of girders for each step of bridge assembly.” There is no mention of the type of procedure or the level of analysis required. Instead, the specification only stipulates that these calculations be completed as part of the erection plan. Chapter 6 of this document specifies the lifting procedure and states that “. . . crane and materials must be located such that the lift is safe and within the crane manufacture’s capacity. . .” Section 6.3 states, “Girders shall be stabilized with falsework, temporary bracing, and/or holding cranes until a sufficient number of adjacent girders are erected with diaphragms and/or cross frames connected to provide the necessary lateral stability and to make the structure self-supporting.” Again, this requirement is given without guidance for accomplishing the task. The details for the level of analysis or factor of safety to employ are not discussed. The commentary

associated with Section 6.3 states that “Removal of falsework, temporary bracing, and holding cranes shall be in accordance with stability provided in the erection procedure.”

#### **2.6.4 TxDOT Preferred Practices for Steel Bridge Design, Fabrication, and Erection**

Engineers not satisfied with the previously mentioned guidelines and specifications can find other sources of information, including the TxDOT Preferred Practices for Steel Bridge Design, Fabrication, and Erection. This document is published by the Texas Department of Transportation (TxDOT) to provide optimal quality and value in steel bridge design within Texas. In Section 2.2.1 it states that “for curved girders, flange width should be approximately one-third the web depth and no less than 30 percent of the web depth. The extra width for curved girders enhances handling stability and helps keep lateral bending stresses within reason.” This limit of one-third the web depth is twice as wide as the one-sixth limit specified by the AASHTO LRFD Bridge Design Specification. Thus, one of the goals of the current project is to investigate the influence of the ratio of the flange width to the web depth on the behavior of curved girders so that the disparity between the AASHTO provisions and those by TxDOT can be clarified. The Preferred Practices also state, “... flange width affects girder stability during handling, erection, and deck placement. Keep the girder length (field section length) to flange width ratio below 85.” This last recommendation gives guidance on the length of field sections and provides for a conservative limit to ensure transportation and erection safety. Section 2.2.4 provides additional cross-sectional proportioning recommendations and states that the recommended depth given in AASHTO 2.5.2.6.3 should be increased by 10% to 20% for curved girders. The total superstructure depth to span length ratio should be 1: 0.033 – 1: 0.04 (or span to depth of 25 to 30) according to the TxDOT Preferred Practices. Section 2.6 states that for curved girders, TxDOT prefers that diaphragms or cross frames be placed at a spacing of 15 to 20 ft maximum to help limit flange bending stresses and cross frame/diaphragm member forces.



### 2.6.5 NCHRP Synthesis 345 Report

Another source of information about the current state of practice in construction and erection of curved I-girders is the recent NCHRP Synthesis 345 report (2005). This report, titled *Steel Bridge Erection Practices, a Synthesis of Highway Practices*, documents a survey sent to state departments of transportation, contractors, and fabricators. Chapter four summarizes the erection issues and solutions encountered by the survey participants. With respect to the lifting of curved girders, it was noted that picking up a girder at two points usually eliminates any lateral stability problems, as long as the line between the “pick” points runs through the center of gravity of the girder. The erectors also provided rules of thumb for cross-sectional proportioning, stating that an unbraced length to compression flange width ( $L/b_f$ ) of 60 or less provides stability during transportation and erection, but they also stated that it could increase to as much as 80 with further stress calculations to verify the safety. Any  $L/b_f$  value greater than 80 would require a temporary support (falsework or holding crane) to provide stability according to the erectors. These rules of thumb from the experience of the erectors provide valuable guidance to designers, but they do not provide the analysis process to accomplish “further stress calculations.” Chapter 5 reports the problems experienced by the survey participants, including five states reporting stability problems with girders at various stages of construction. Instabilities were reported for girders without adequate cross-frame bracing attached, cantilevered girders over the pier to a field splice, and also due to wind loadings during construction. Another problem reported by eight states was unanticipated lateral or rotational deformations of the girders during the deck placement. These concerns highlight the need for robust computational tools to assist engineers in predicting the behavior of these bridges during construction when a bridge is at its most vulnerable state.

## **2.7 RECENT WORK:**

### **2.7.1 Field Study in Austin, Texas – Bridge 88:**

Recently, as a component of the current research project, Schuh (2008) reported results from field monitoring of a direct connector near the Austin Bergstrom International Airport in Austin, Texas. The curved bridge selected for instrumentation was Unit 6 of Bridge 88, the direct connector for eastbound US 71 to northbound SH 130. Unit 6 is a three-span, continuous bridge comprised of a four-girder system. The three spans (Spans 14, 15, and 16) comprised a horizontally curved steel I-girder unit of the 23-span bridge. The exterior girder of the four-girder cross-section had span lengths of 185, 210, and 158 ft. respectively. The center-to-center spacing of the girders was 10 ft. – 4 in. The radius of curvature of the outside fascia girders was 1235.727 feet. Figure 2.7 shows the plan layout of the bridge, with Span 14 magnified to show the location of the instrumented girders and cross-frames. The outside fascia girder, Girder 4, and the adjacent inside girder, Girder 3, of Span 14 were selected for instrumentation. In addition, two cross-frames (X1 and X2) connecting these two girders were also instrumented. Figure 2.7 gives an elevation view of Girders 3 and 4 with the instrumented cross-sections detailed.

Figure 2.8 is a photo of part of the instrumented girder along with the data acquisition system used to record strains during the entire erection process. Campbell Scientific 5000 data loggers were used along with multiplexers to increase the number of channels that could be recorded for each data logger. A total of 64 strain gages were used to monitor the behavior of the girder. It should also be noted that significant time and consideration was spent in protecting the gages and the data acquisition system from both environment elements (sun, rain, wind, etc.) and human elements (construction workers, equipment, etc.). Additionally during the concrete placement, 16 rotation gages were used near midspan along with vertical deflection measurements at 1/8<sup>th</sup> points in span 14 using a laser distance meter. Figure 2.9 is a photo of Bridge 88 Span 14 with instrumentation locations identified.

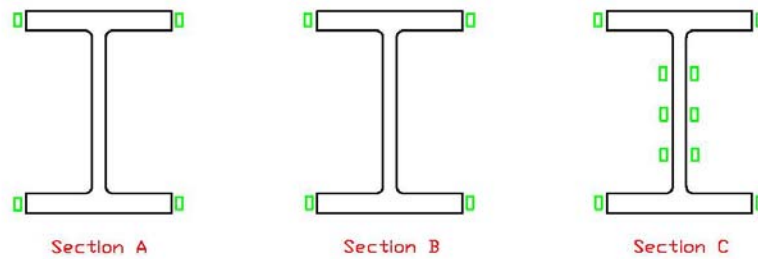
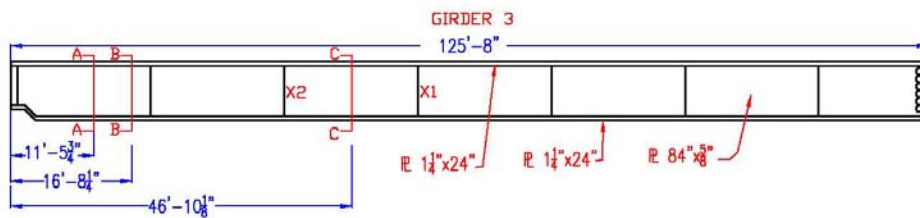
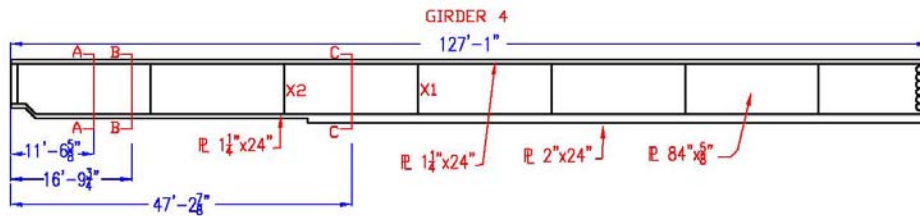
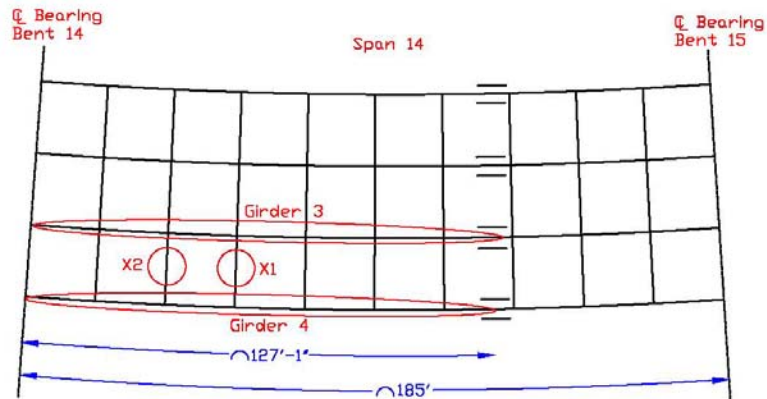
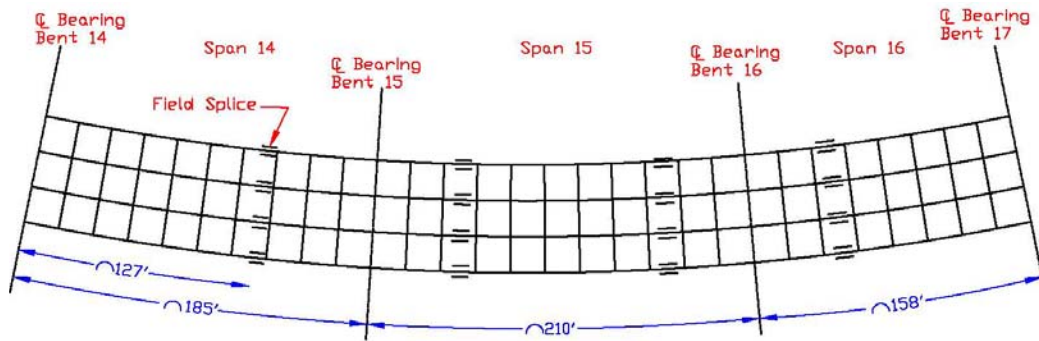


**Figure 2.7: Unit 6 Bridge Layout & Girder Elevations w/ Gage Locations (Schuh 2008)**

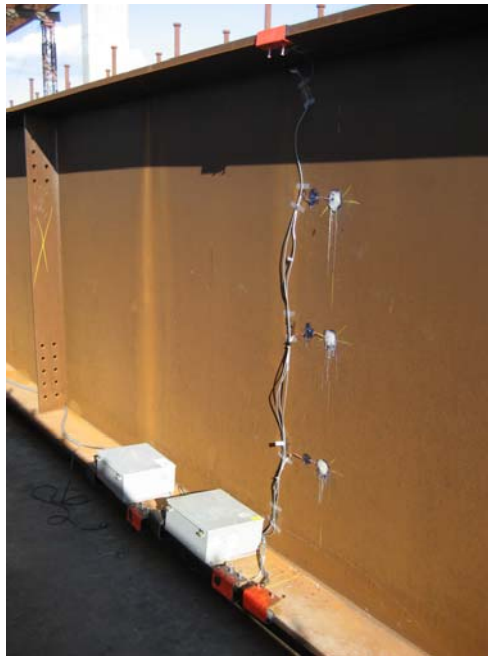


**Figure 2.8: Instrumented Girder Cross Section with Data Acquisition System**

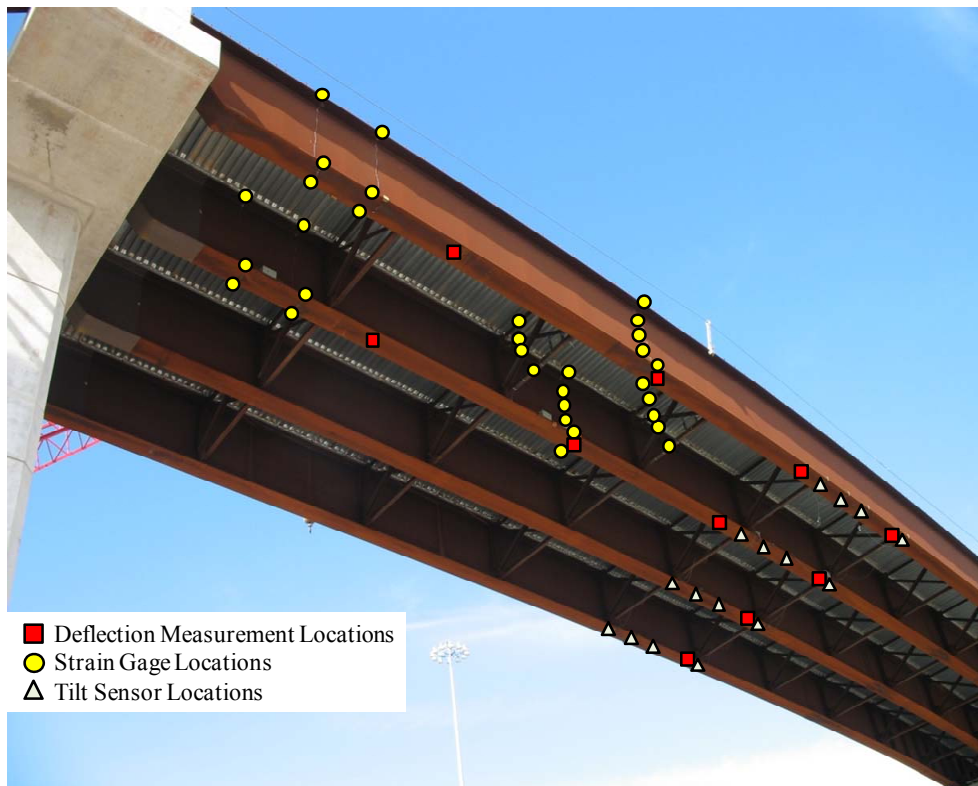


**Figure 2.9: Instrumentation Locations on Bridge 88 Span 14**

The instrumentation was installed after the girders had been delivered to the site and before they were lifted into place. Strain readings were recorded while the girders

were lifted, during erection, and as the concrete deck was cast. Strain gages were placed on the flange tips, and the measured strains were converted to stresses. These stresses can be decomposed into their bending and warping components as shown in Figure 2.10 and Figure 2.11. The equations describing this decomposition are given in Equation 2.10 and Equation 2.11.

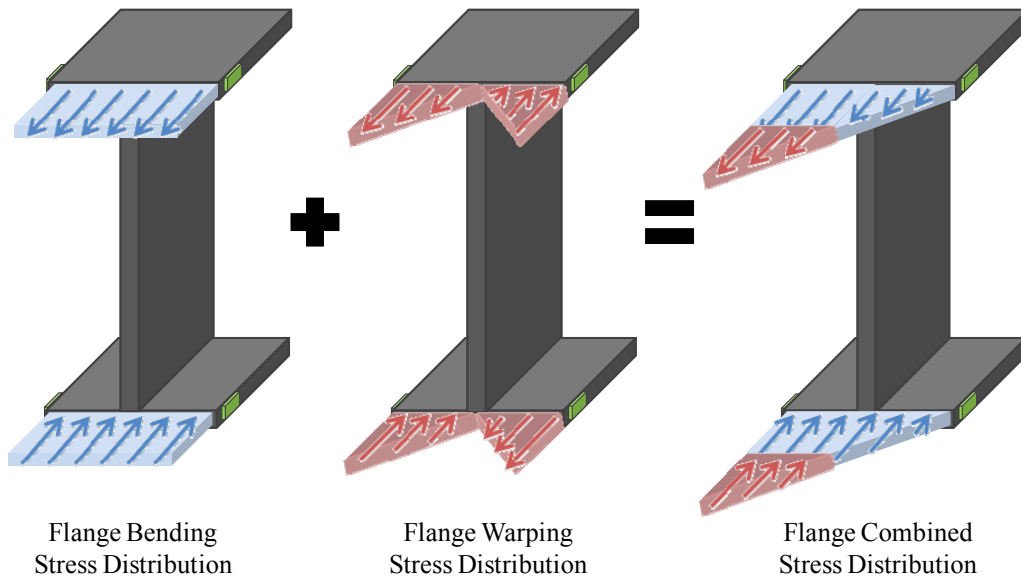


**Figure 2.10: Curved I-girder Flange Stress Distribution (Schuh 2008)**

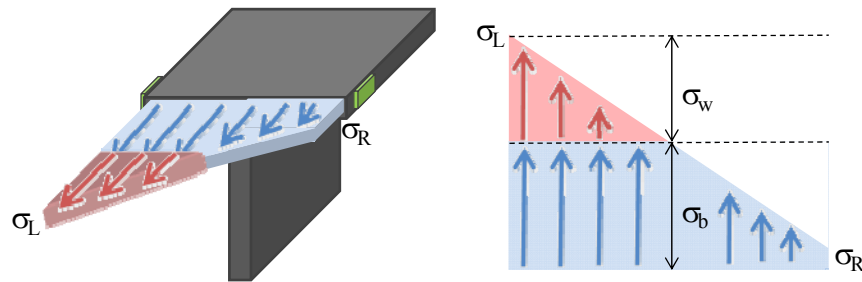


**Figure 2.11: Bending and Warping Stress Isolation (Schuh 2008)**

$$\sigma_{bending} = \frac{(\sigma_L + \sigma_R)}{2} \quad \text{Equation 2.10}$$

$$\sigma_{warping} = \frac{(\sigma_L - \sigma_R)}{2} \quad \text{Equation 2.11}$$

Several graphs documenting the stress verse time in the girders during erection were provided by Schuh (2008), and Figure 2.12 and Figure 2.13 are two representative plots. The data shown in these figures indicate that the stresses encountered during this

stage of construction were low and were dominated by the erection process, including attaching and detaching cranes and installing cross-frames.

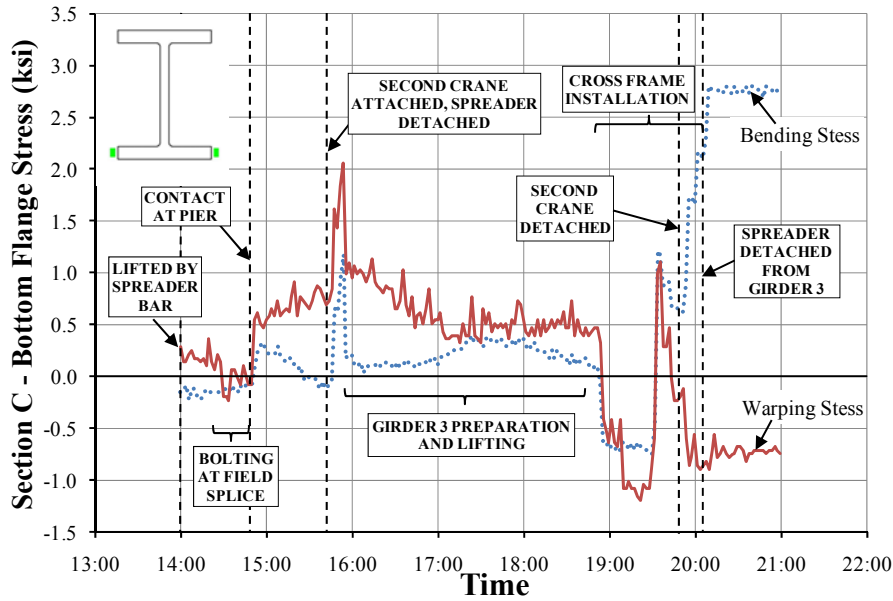


**Figure 2.12: Girder 4 at Section C Bottom Flange Stress Changes (Schuh 2008)**

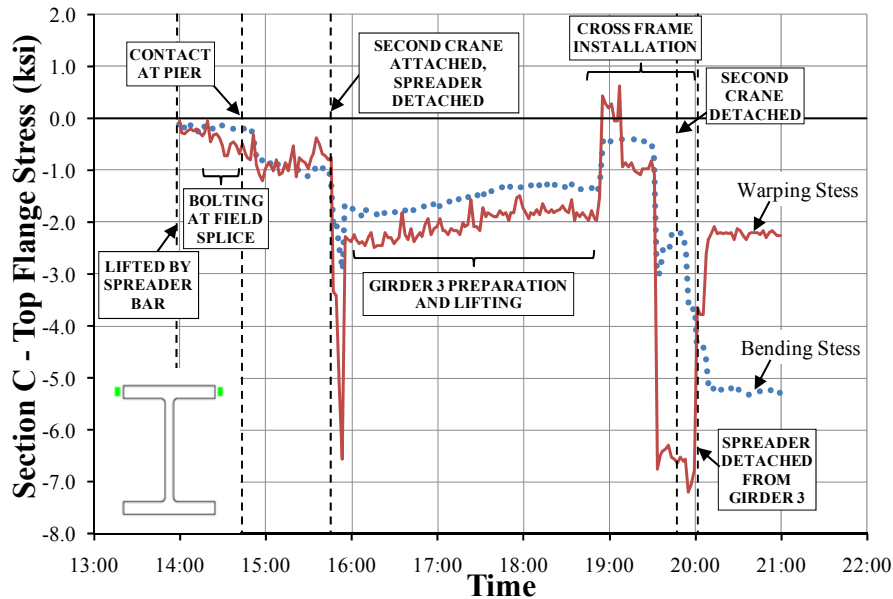


**Figure 2.13: Girder 4 at Section C Top Flange Stress Changes (Schuh 2008)**

While the data collected during erection provided only a general indication that all girders remained well below yielding during lifting, the specific state of stress was difficult to ascertain due to the lack of specific knowledge of the initial condition of the

girder. The girders were offloaded from the transporting trucks onto large wooden timbers, which made accurate computational modeling of the girder difficult. Figure 2.14 is a picture of a girder supported on the large wooden timbers prior to lifting. Due to the uncertain support conditions, identifying the stress change when the girders were lifted from the timbers was difficult to model.



**Figure 2.14: Large Wooden Support Timbers**

Later, during the concrete deck placement, larger stresses were observed relative to those recorded during erection, which allowed for improved confidence in the conclusions that could be drawn from the test. In addition to the strain gage readings, rotation and vertical displacement was measured during the deck placement. The rotation information is reported by Fasl (2008). The concrete placement process, along with forces in two cross-frames and vertical displacement data, are reported by Farris (2008). The vertical displacement measurements were taken in the same span as the strain gage readings, span 14. The readings were taken on all four girders at the midspan of span 14 and on Girders 3 and 4, proceeding back station toward pier 14 at  $3/8^{\text{th}}$ ,  $1/4^{\text{th}}$ , and  $1/8^{\text{th}}$  of span 14. Figure 2.15 includes a set of tables with the vertical deflection given in inches for the girders at different times during the concrete deck placement process. The deck was cast starting at pier 17 and placed continuously toward pier 14. For the data shown, positive deflection is defined as downward, and a negative deflection value is upward, indicating an uplift of the girders at times during the deck placement. Additional details of the measurement technique can be found in Farris (2008).

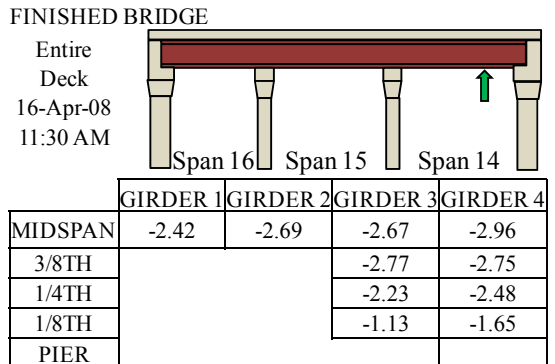
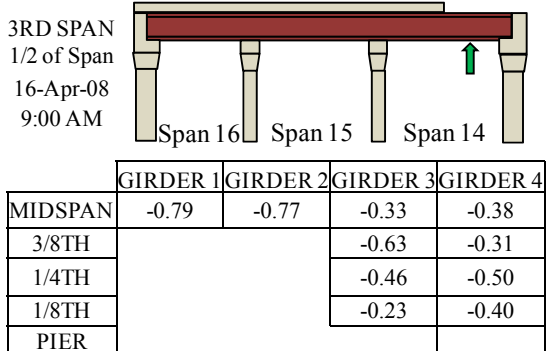
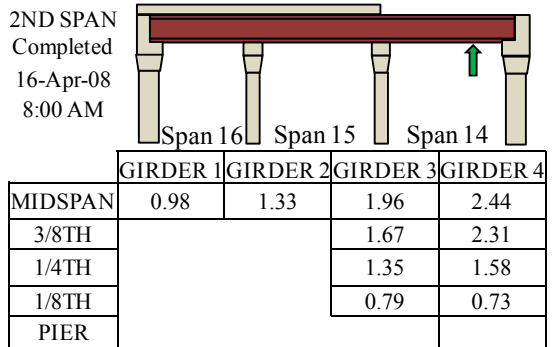
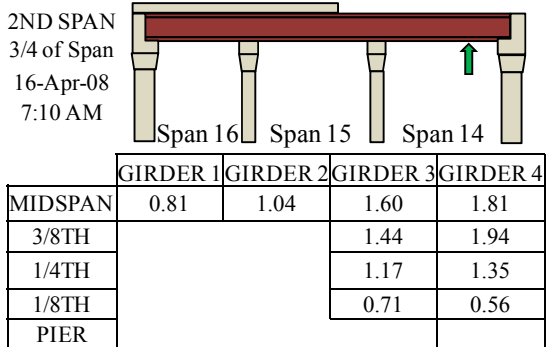
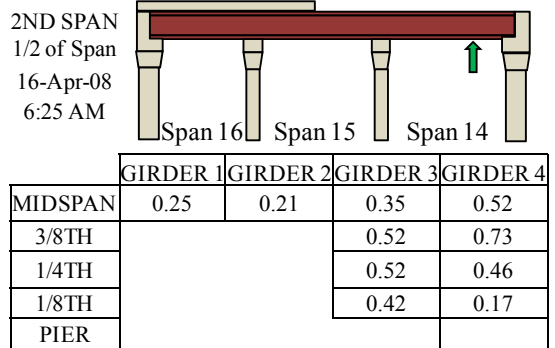
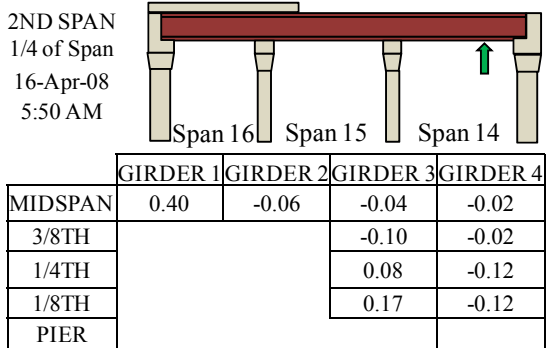
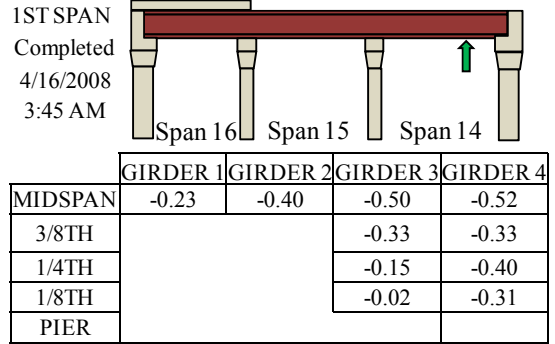
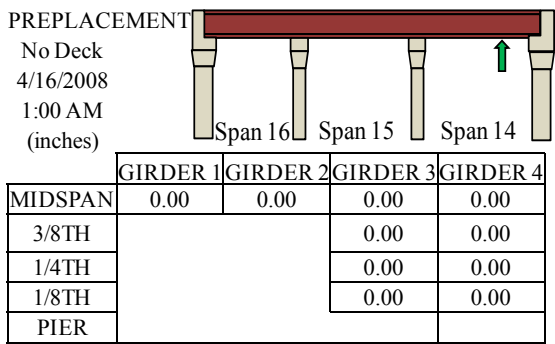


**Figure 2.15: Bridge 88 Concrete Placement Girder Deflection Readings (inches)**



### **2.7.2 Field Study San Angelo, Texas – Hirschfeld Lift Test:**

The data collected from Span 14 during lifting did not result in adequate stress change to verify the computational model. Additionally, the pre-lift stress state was not attainable due to the large uneven wood timbers used to support the girders prior to lifting as shown in Figure 2.14. The width of the series of timbers used for support ranged from 10 ft. to 15 ft. along the length of the bridge; due to the compressibility of the timber, as well as the uneven surface on the ground, determining the boundary conditions prior to lifting was challenging, making the computation of changes in stress difficult. Although an additional test was conducted on another girder at the job site, the most useful data were obtained from two girders that were instrumented and tested at the Hirschfeld Steel Company fabrication yard in San Angelo, Texas.

An important aspect of the second set of tests was to lift the girders from known support conditions so that reliable data could be obtained for validation of computational models. The support system shown in Figure 2.16 was fabricated for this purpose. The supports consisted of wooden 2" × 6" pieces bolted together for the base and two 4" × 4" struts that were hinged to the base. The struts were positioned on the outside of the curves and reacted at the intersection of the top flange and web to prevent twist of the girders. Because the supports were leveled prior to the tests, the support conditions were well known, and the resulting boundary conditions for the girder could be replicated computationally.



***Figure 2.16: Fabricated Wood Supports for Girder Lift***

The girders that were tested at the Hirschfeld storage yard were two curved girders that would eventually be part of the structural system of Bridge 88. The girders were moved into a staging area in the steel yard where they were instrumented with strain gages, tilt sensors, and the data acquisition system. The Hirschfeld tests were undertaken to capture the stress and rotational change associated with lifting a curved girder that was initially supported with well established boundary conditions. Multiple lifts were conducted to ensure reliability in the data. Two different girder support locations were tested. In addition, two identical supports were used, yielding a statically determinate structure with known support conditions. The girders were lifted using a MI-JACK lifting crane with a lift clamp spacing of approximately 40 ft. For both girders, the data loggers were programmed to scan every 12 seconds. For each location, the girder was placed on the supports for approximately 1-2 minutes, lifted up for approximately 1-2 minutes, replaced on the supports for 1-2 minutes, and lifted again while the supports were moved to a new location.

Two different girder segments were lifted in the Hirschfeld tests. The first segment was a prismatic girder that was 124 ft. – 1 in. long with an 84 in. deep web plate that was 5/8 in. thick. The top and bottom flange had a uniform thickness along the girder length of 1.25 in. and a uniform width of 24 in. The radius of curvature was 1215

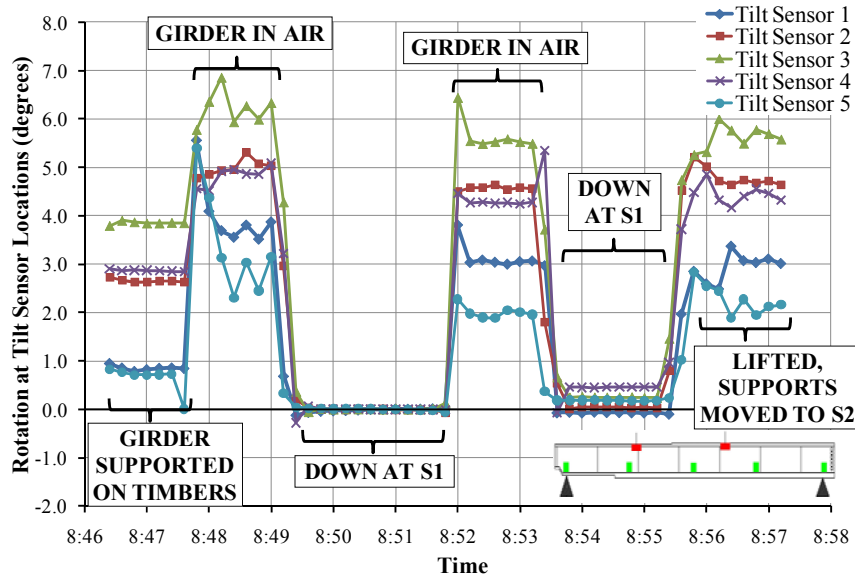
ft. The second girder segment was 127 ft. – 4 in. long and had a non-prismatic section with an 84 in. deep web plate that was 5/8 in. thick along the entire girder length. The top flange had a thickness transition 53 ft. – 4 in. from the dapped end from 1.25 in. to 1.75 in. The bottom flange had a thickness transition of 1.25 in. to 2.5 in. at 27 ft. – 3 in. from the dapped end. Both the top and bottom flanges had a uniform width of 24 in. The radius of curvature was 1236 ft. Although data from both tests were useful in validating computational models of girder response, only results for the prismatic girder are presented in this chapter. Additional details of the test program and data analyses can be found in Schuh (2008) and Farris (2008).

Strain gages were installed at the quarter points and midspan of the segment. Gages were installed at mid-thickness of the four flange tips. The flange gages were used to measure bending and warping stresses in the flanges. Five tilt sensor locations were selected at sections that were sequentially numbered 1-5. These locations were intended to capture rotational changes at the ends, quarter points, and midspan of the girder. The tilt sensors were located on the bottom flange on the interior side relative to the girder's horizontal curvature.

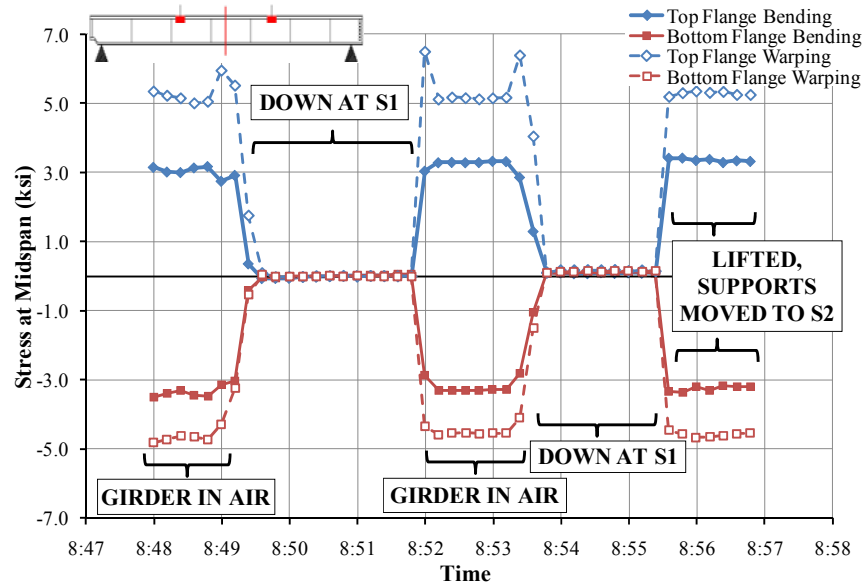
Figure 2.17 shows a graph generated using the data collected from the five tilt sensors attached to the prismatic girder. The tilt sensors record the rotational change of the girder at the sensor location. These data were zeroed based upon the twist of the girder on the fabricated support. The measured rotation change is the angular change of the lifted girder relative to the girder supported on the wooden supports located near the ends, which are referred to as the S1 support locations. Figure 2.18 is a graph of the stress change that was calculated from the strain gage data for the same test configuration. The change in bending and warping stresses are calculated for the top and bottom flanges at midspan. The stresses were zeroed for the girder on the fabricated supports, and the resulting change in stress for the girder lifted in the air is shown.

Figure 2.19 shows a graph that was developed using the data from the five tilt sensors attached to the prismatic girder under different boundary conditions than those shown in Figure 2.17. Similarly to the first test, the data were zeroed for the girder while

it was on the fabricated wooden supports located near the quarter points, which is referred to as the S2 support location, and the measured rotation change corresponds to the case when the girder was lifted in the air. A graph of the change in bending and warping stresses for the top and bottom flanges at midspan for the S2 support location is shown in Figure 2.20.



**Figure 2.17: Prismatic Girder Rotational Change for the S1 Support (Adapted from Schuh 2008)**



**Figure 2.18: Prismatic Girder Stress Change for the S1 Support (Adapted from Schuh 2008)**

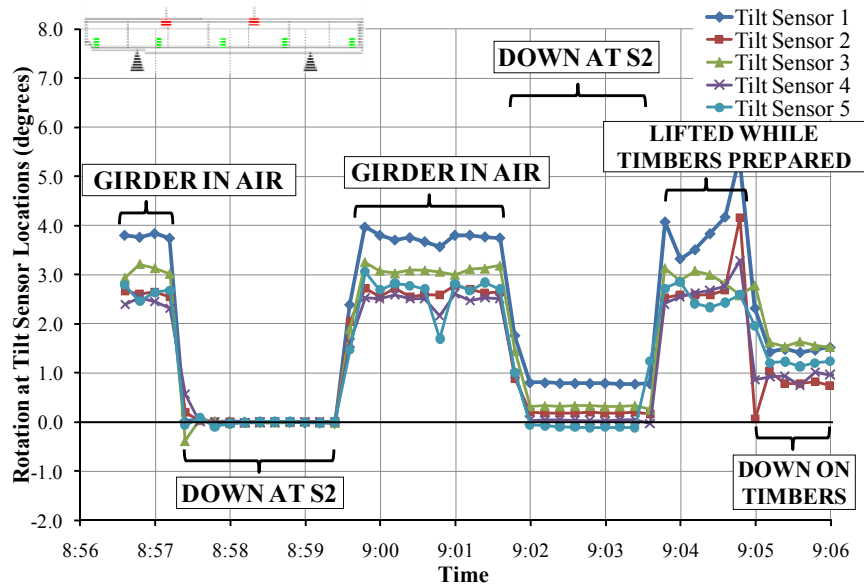


**Figure 2.19: Prismatic Girder Rotational Change for the S2 Support (Adapted from Schuh 2008)**

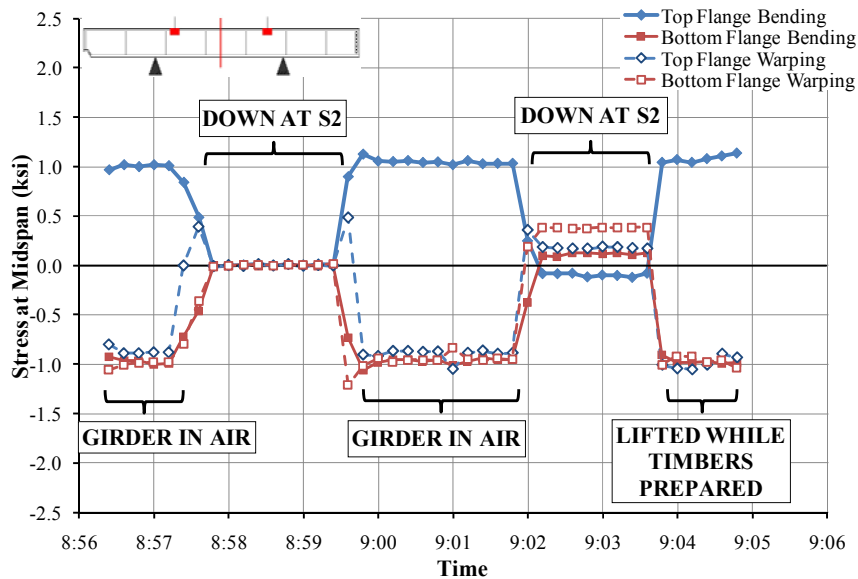


**Figure 2.20: Prismatic Girder Stress Change for the S2 Support (Adapted from Schuh 2008)**

There are several observations to note in these graphs. First, on the graph of S1 (Figure 2.17) the greatest rotation was at Tilt Sensor 3, the sensor located at midspan, while the minimum rotation was at Tilt Sensors 1 and 5 at the ends where the wooden supports prevent girder rotation. The Tilt Sensor 5 rotational change corresponds to the rigid body rotation of the girder while in the air, and the difference between Sensors 3

and 5 is the cross-sectional twist due to the induced torsion from the self weight of the curved girder. This observation is verified in the rotation graph for S2 in which much less relative cross-sectional twist occurs because the lifting points and support points are very close to each other. In this case, the tilt sensors record a similar rigid body rotation due to the lifting process. Second, the bending stresses are approximately equal for the top and bottom flange, which would be expected for a symmetric girder. Third, the warping stresses are equal to or greater than the bending stresses, which indicate the importance of their inclusion in design. Finally, the warping of the flange for the S2 case initially seemed incorrect because the two flanges are subjected to the same sign for the warping stress. However, this behavior was also predicted by subsequent computation models of the lifting test. This “warping” stress includes the effects of lateral flange bending. Because the girders experienced rigid body rotation in the lifting process, the weak axis bending stress due to self weight is significant and affects the apparent warping stress.

The data for the non-prismatic girder revealed many of the same trends as the prismatic girder with a few exceptions. Most notably, the bending stresses were not equal for the top and bottom flange, which is expected for an unsymmetric girder. The top flange at Cross Section B is 1.25 in., while the bottom flange is 2.5 in., and the data reflect this geometric difference. The recorded stress change for the bottom flange was approximately half the recorded stress change for the top flange.

### **2.7.3 Computational Parametric Studies**

#### **2.7.3.1 Introduction**

The buckling of I-girders is a concern, especially when the unbraced length is relatively large in conjunction with low lateral or torsional stiffness. These conditions may be present at various stages during the construction process. When an individual girder segment is lifted, there is generally no bracing provided, which makes the segment prone to excessive deformations and susceptible to buckling. The most critical scenario from the perspective of buckling is a girder segment lifted with two lift points (single

point lifts are impractical except for very short segments). This configuration is the minimum number of supports necessary to lift a girder, but it maximizes the unbraced length and provides no restraint against rigid body rotation about the axis defined by the lift points. Thus, the parametric finite element analysis that was conducted as part of this project focused on this critical lifting procedure, and conclusions concerning other, more stable, lifting methods are discussed in the conclusions.

The most straightforward analytical check of girder stability is a linear eigenvalue buckling analysis. An eigenvalue buckling analysis predicts the buckled shape (eigenvector) and the multiplier (eigenvalue) of the applied load that will cause the stiffness of the system under consideration to become zero (i.e., buckle). Utilizing this approach, some insight into the behavior of I-girders during lifting is obtained, but conclusive results for curved I-girders are limited by the assumptions inherent in the analysis technique. A linear eigenvalue buckling analysis assumes that the pre-buckling deformations of the system being analyzed are small. This assumption is reasonable for straight girders, but it does not accurately describe a curved girder system. Conceptually, the curvature can be thought of as an initial imperfection. Under such conditions, system displacements increase as load is applied, leading to second-order effects that decrease the buckling capacity of a curved girder system relative to that of a straight girder system. Thus, a geometric nonlinear analysis that takes the effects of deformations into account as load is applied was utilized in this research to predict the large deflection response associated with curved girder systems. Both eigenvalue and geometric nonlinear analyses were performed as part of a parametric study conducted to establish the design guidelines necessary for safe and economic lifting of curved I-girders and to evaluate how the eigenvalue analysis results compare with those of the nonlinear analyses. A description of the methods used and a summary of the results are provided in the following section.

### 2.7.4 Parametric Finite Element Model

To understand the behavior of curved girders during lifting, it was desirable to perform a series of analyses over a wide range of support and loading conditions. The parametric study was completed using the finite element analysis software, ANSYS (2007), which provides a user-defined parametric language. The parametric language allows a user to develop a manageable set of input files that cover a wide range of modeling scenarios and to quickly change specific user-defined variables. For the problems studied on this research project, the flexible parametric language allowed for variation in the radius of curvature, girder depth, girder length, plate thicknesses, and lift locations. The variables considered in the parametric study included radius of curvature ( $R$ ), flange width to depth ( $b_f/D$ ), length to depth ( $L/D$ ), and lift point location ( $a/L$ ), which are shown with their range in Table 2.4. Figure 2.21 shows a schematic of a girder with the parameters defined.

**Table 2.4: Eigenvalue Parametric Study Variables**

| Variable                          | Maximum  | Minimum |
|-----------------------------------|----------|---------|
| Radius of Curvature ( $R$ )       | Straight | 250'    |
| Flange Width to Depth ( $b_f/D$ ) | 1/3      | 1/6     |
| Length to Depth ( $L/D$ )         | 10       | 25      |
| Lift Point Location ( $a/L$ )     | 0.1      | 0.4     |



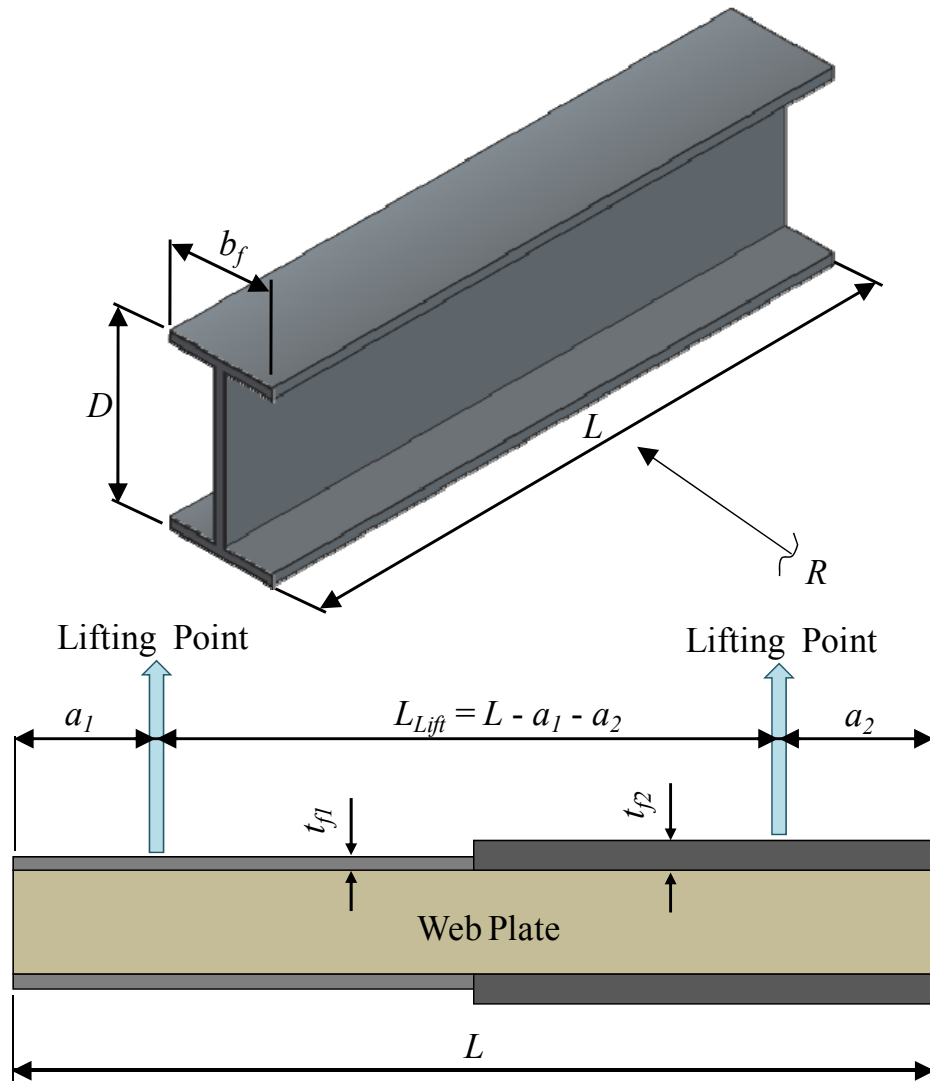


**Figure 2.21: Girder Parameter Definitions (Adapted from Farris 2008)**

The average lifting location was used for  $a$  when non-prismatic girders were lifted with  $a_1 \neq a_2$ . This situation is shown in Equation 2.12.

$$a = \frac{a_1 + a_2}{2} \quad \text{Equation 2.12}$$

The model consisted of 8-node shell elements (SHELL93) that have six degrees of freedom at each node. These shell elements were used to model the flanges, web, and stiffeners. The boundary conditions that constrain the girder during lifting were initially troublesome due to the mathematical singularity in the stiffness matrix. The singularity results from a lack of global degree of freedom constraints, namely the rotation about a

line defined by the lifting points. In actuality, the girder rotates such that the center of gravity is at its lowest point, rendering the minimum potential energy of the system. To find the solution with the computational model, a flexible spring was added to the bottom of the girder at the lifting locations in the direction perpendicular to the longitudinal axis of the girder to provide a small amount of restraint to rigid body rotation. Field results from the Hirschfeld lift tests were used to ensure that the stiffness of the lateral springs provided a system similar to that found in practice because the spring is used to account for friction in the lifting clamp. Figure 2.22 and Figure 2.23 are two screen shots of the ANSYS model used to calculate the buckling capacity of a curved I-girder during lifting. Figure 2.24 is a picture from one of the tests conducted at Hirschfeld Steel Plant.

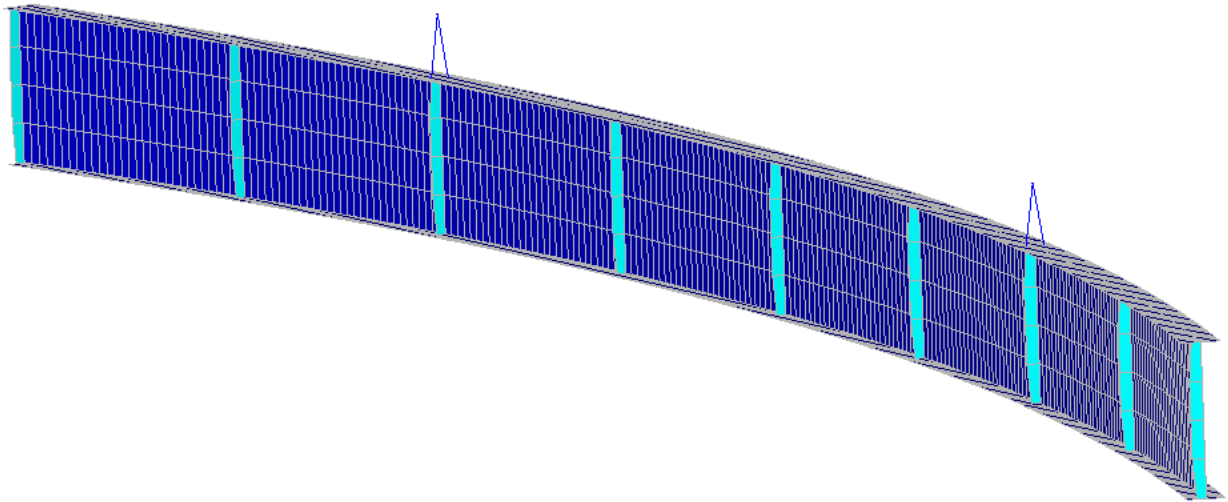


***Figure 2.22: ANSYS Model of a Curved I-girder during Lifting***

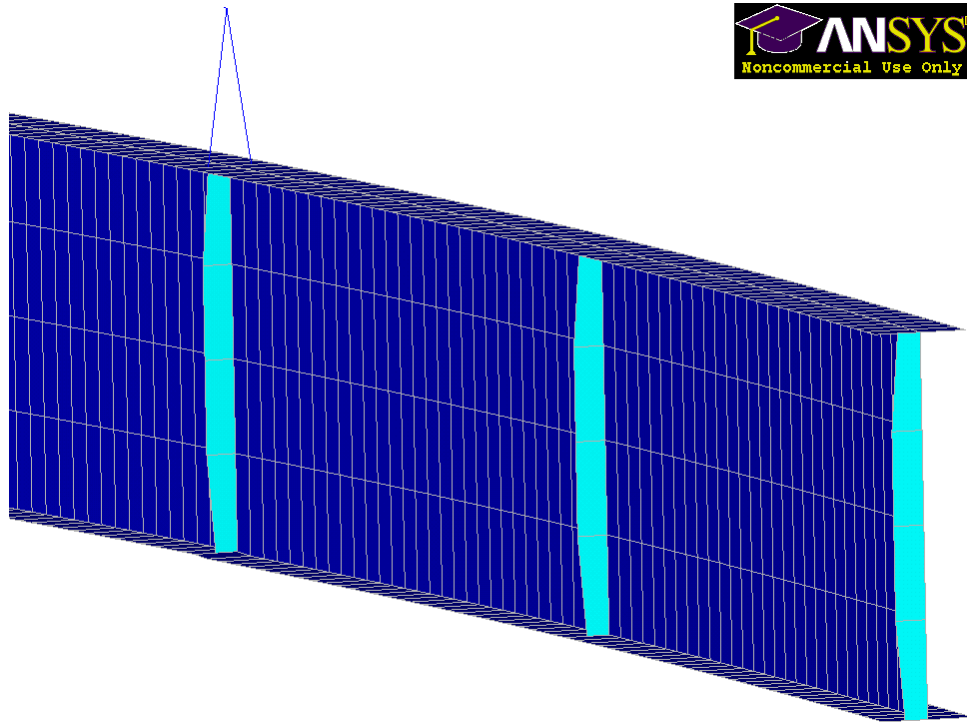


*Figure 2.23: Close-up of the ANSYS Model of a Curved I-girder during Lifting*



*Figure 2.24: Actual I-girder Lifted during Field Test*

### 2.7.5 Eigenvalue Buckling

As mentioned earlier, the eigenvalue is a multiplier of the applied loads that will cause buckling. For all the cases studied, the only load considered was the girder self weight; thus, an eigenvalue less than 1.0 indicates that the girder will buckle under its own weight, which is clearly undesirable. In practice, however, it is uncommon for engineers to perform a 3-D eigenvalue analysis of a girder, and simplified methods have been developed to provide essential design information without the need for carrying out a complicated analysis. In most situations the simplifying assumption that is commonly used is that lateral-torsional buckling will control the stability behavior of a girder during lifting. This assumption is reasonable and one that was evident in the buckled shapes produced by the analysis and shown in Figure 2.25 for several lifting locations.

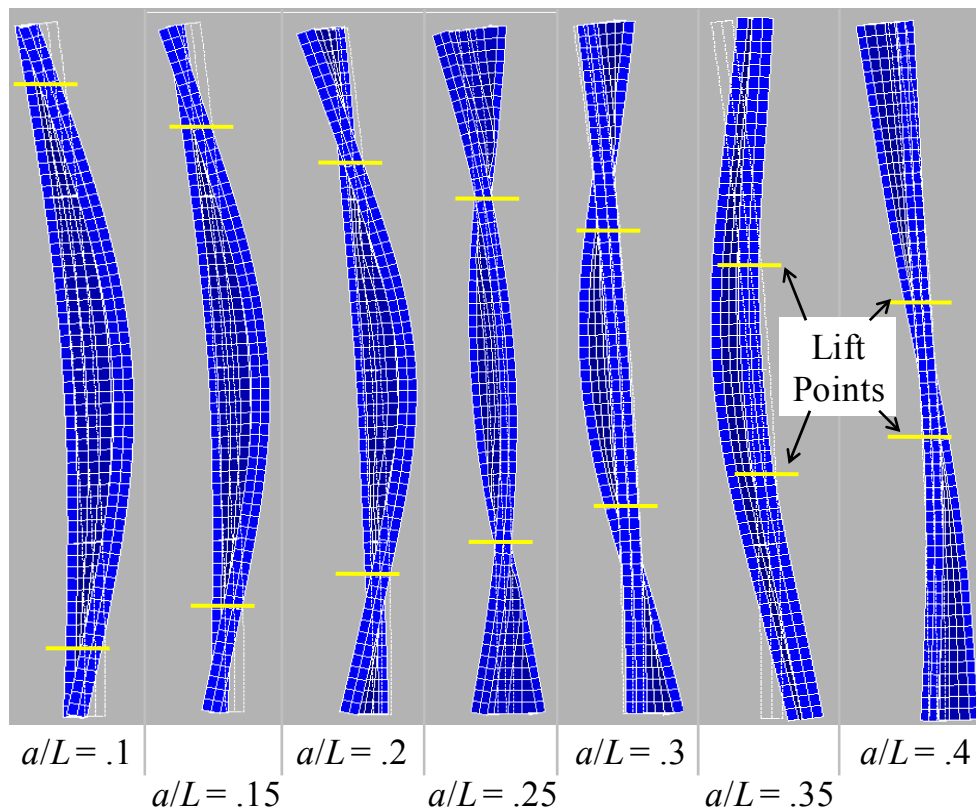


**Figure 2.25: Buckled Shape of I-girder during Lifting (Schuh 2008)**

The solution for lateral-torsional buckling of a beam under uniform moment can be found in Timoshenko and Gere (1961). This solution, however, can provide overly

conservative solutions if significant moment gradient exists along the length of the beam being analyzed. Accordingly, a moment gradient factor,  $C_b$ , is applied to the critical buckling moment to account for non-uniform bending moment. This approach has been applied to several structural systems when considering buckling (Helwig et al. 1997; SSRC 1998; Salmon et al. 2009). The  $C_b$  approach allows the engineer to utilize the solution derived for uniform moment loading and account for the wide range of longitudinal or transverse load distributions found in practice. The cases of girders during lifting pose a particularly difficult problem since there is neither a clearly defined unbraced length nor a general expression for the  $C_b$  that should be used. Engineers often are unsure whether they should assume the lifting point is a braced point or use the full length of the girder segment. Therefore, gaining an understanding of the behavior of prismatic and non-prismatic girders during lifting was a primary objective for the research study as outlined in the following two subsections. In evaluating the behavior of the girders during lifting, two different approaches were considered for defining the unbraced length for the uniform moment solution. Schuh (2008) approached the problem by using the spacing between the lift points ( $L_{LIFT}$ ) for the unbraced length. Farris (2008) found that using the full length of the girder segment ( $L$ ) as the unbraced length might be easier to apply in design. Therefore the material that is presented in the subsection on prismatic girders is based upon the original work by Schuh (2008), but the expressions were adjusted based upon defining the unbraced length as the full length of the girder segment for consistency and found in Stith et al. (2009). The radius of curvature was found to have little effect on the calculated eigenvalue, but a range of radii from 500 ft. to straight was investigated.

#### **2.7.5.1 Prismatic Girders**

The study of prismatic girders during lifting was completed by Schuh (2008), and a full description of the parametric study conducted for this research project can be found in his thesis. A representative graph presented by Schuh is provided in this section along with the resulting equation derived to account for the effect of moment gradient on buckling of I-girders during lifting.

The parameter with the greatest influence on the eigenvalue of the girder during lifting is the lifting location ( $a/L$ ). The following graphs present the effect of varying  $a/L$  on the eigenvalue for beams with various degrees of horizontal curvature, span-to-depth ratios, and also flange-width-to-depth ratio ( $b_f/D$ ).

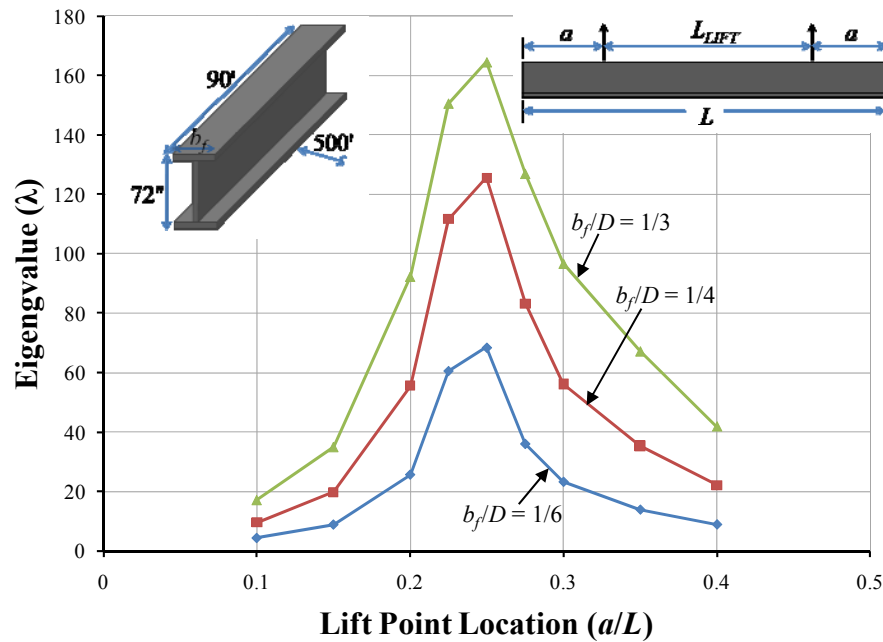


**Figure 2.26: Effect of Lift Location and  $b_f/D$  on the Eigenvalue (Adapted from Schuh 2008)**

As shown in Figure 2.26, the maximum eigenvalues are achieved at an  $a/L$  of approximately 0.25. The eigenvalue decreases quickly when the lift location deviates from this configuration. The smallest eigenvalues occur at the extremes of the lifting points that were considered—at values of  $a/L$  of 0.1 and 0.4. The effect of changing  $a/L$  is similar in all of the cases studied. Additionally, the radius of curvature had a negligible effect on the eigenvalue, while the  $b_f/D$  and  $L/D$  had some effect, but less than the lifting location ( $a/L$ ).

Once the eigenvalue is obtained from the results, the proposed adjustment factor to account for the effects of lifting on curved I-girders,  $C_b$ , can be observed from the trends. The  $C_b$  value from the FEA studies was found for a given lifting geometry by comparing the eigenvalue buckling capacity with the equation for uniform moment

loading given by Timoshenko and Gere (1961). The  $C_b$  factor is established as the ratio of the maximum moment along the girder length to the buckling capacity for uniform moment given by Timoshenko and Gere. The expressions used to evaluate  $C_b$  are given in the following equations and figure.

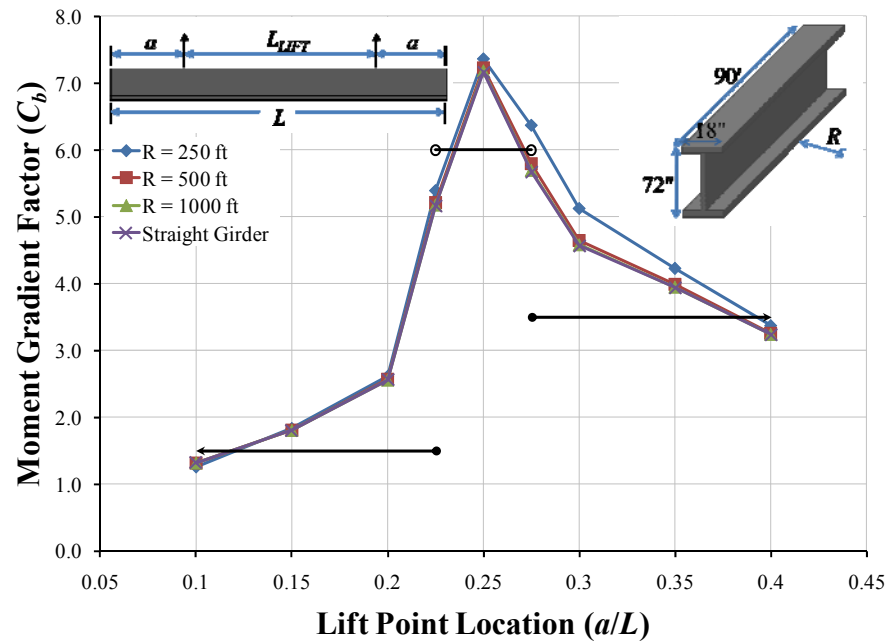


**Figure 2.27  $C_b$  vs.  $a/L$  for Given Radius of Curvatures (Adapted from Schuh 2008)**

From the trends presented in the figures, the expression for  $C_b$  was formulated and given in Equation 2.13 below. This expression is shown in Figure 2.27 as a black trend line.

$$\begin{aligned}
 C_b &= 1.5 \quad \text{for} \quad \frac{a}{L} \leq 0.225 \\
 C_b &= 6.0 \quad \text{for} \quad 0.225 < \frac{a}{L} < 0.275 \\
 C_b &= 3.5 \quad \text{for} \quad \frac{a}{L} \geq 0.275
 \end{aligned}
 \tag{Equation 2.13}$$

### 2.7.5.2 Non-prismatic Girders

The study of non-prismatic girders during lifting was completed by Farris (2008), and a full description of the parametric study she performed is given in her thesis. The following is a representative sample of the graphs presented by Farris along with the

resulting equation derived to account for moment gradient. The parametric study began with a non-prismatic girder with two flange plate transitions. The flange sizes were varied by changing the thickness of the flange. The first and third cross-sections of the girder had top and bottom flange thicknesses of 1.25 in. The second (middle) cross-section has a top and bottom flange thickness of 2.00 in. The comparison studies within this section were all analyzed with symmetric lifting points.

The graph in Figure 2.28 presents the effect of varying  $a/L$  on the eigenvalue ( $\lambda$ ), and it shows this effect for various flange-width-to-depth ratios ( $b_f/D$ ).

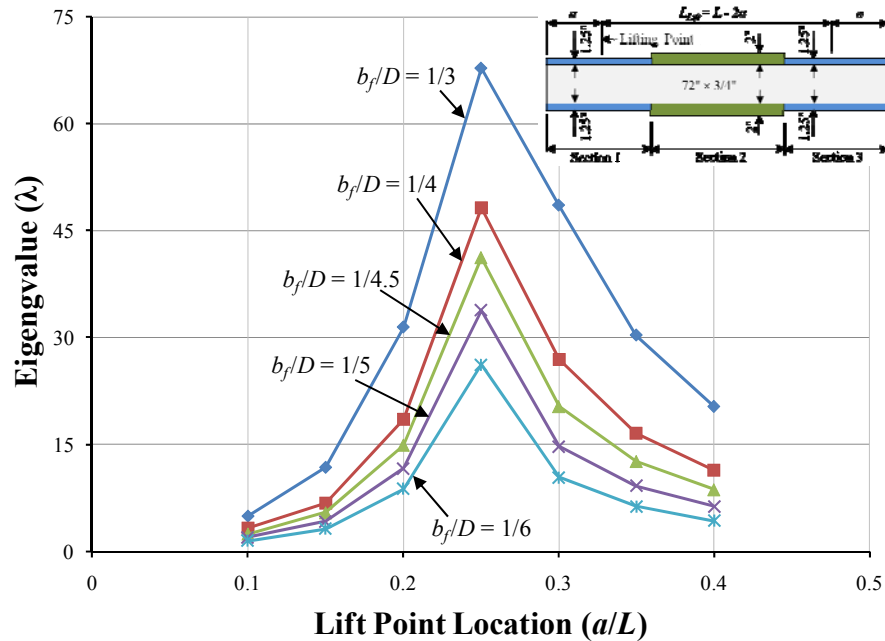


**Figure 2.28: Effect of Lift Location and  $b_f/D$  on the Eigenvalue (Adapted from Farris 2008)**

The purpose of presenting the  $b_f/D$  study is to illustrate the behavior of the eigenvalue as a function of girder lifting point. The flange width-to-depth ratio has some effect, but not as significant as the lift locations. The range of  $b_f/D$  spans the limits set by AASHTO Specifications ( $b_f/D \geq 1/6$ ) and the Texas Preferred Practices ( $b_f/D \geq 1/3$ ). In general, the girder is the least stable when the lifting points are very close to the ends of the girder ( $a/L = 0.10$ ) compared to lifting points that are moved closer towards the mid



section of the girder ( $a/L = 0.4$ ). The highest buckling capacity was observed at an  $a/L$  value of 0.25.

The length of a spreader beam ( $L_{Lift}$ ) was varied from 20 ft. to 85ft to determine the effect on the buckling capacity. As  $L_{Lift}$  decreases, the length of the overhang regions (lengths  $a_1$  and/or  $a_2$ ) increases. The length of the girder segment was fixed at 120 ft. The web plate was 72 in.  $\times$   $\frac{3}{4}$  in., which produces a girder with an  $L/d$  ratio of approximately 20. The location of the top and bottom flange plate transition was varied to investigate the behavior of the I-girder as the sections were modified. Depending on the lifting geometry, different regions of the girders controlled the buckling mode.

The optimal spreader beam length ( $L_{Lift}$ ) was calculated with the spreadsheet UT Lift, which is discussed in detail in Chapter 3. The optimal length is selected as the length of a spreader bar that, when used to lift a curved I-girder, produces zero rigid body rotation or tilt. The optimal lifting location did not generally result in the maximum eigenvalue.

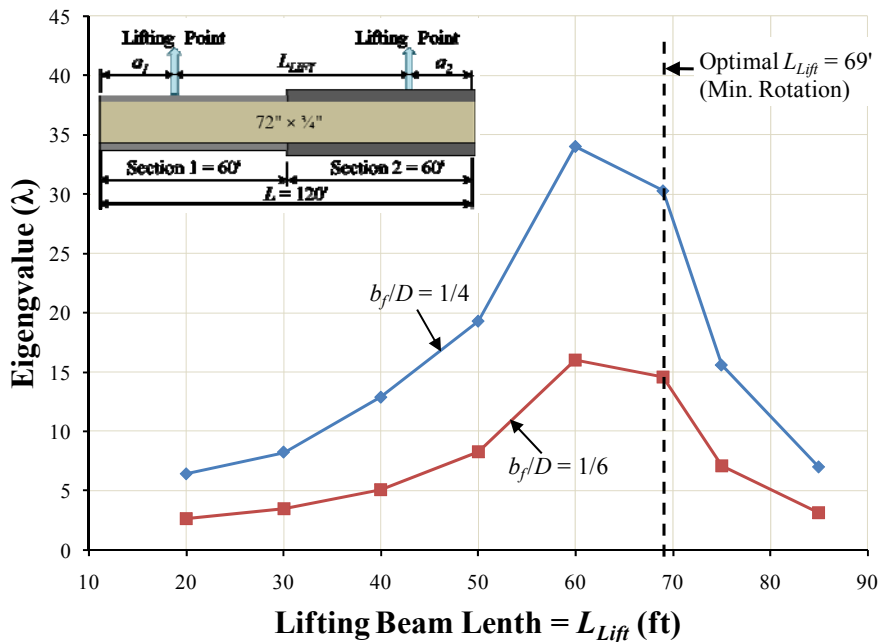
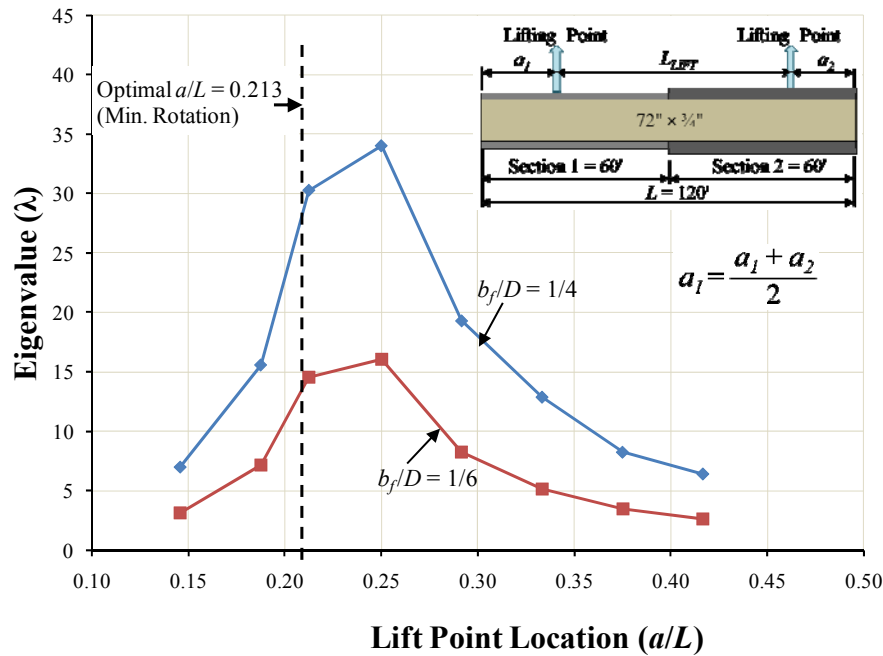


Figure 2.29:  $\lambda$  vs.  $L_{Lift}$  (Section 1=Section 2 = 60') (Adapted from Farris 2008)



**Figure 2.30:  $\lambda$  vs. Average  $a/L$  (Section 1=Section 2 = 60') (Adapted from Farris 2008)**

For the cases shown, the eigenvalue is greater for a  $b_f/D$  ratio of  $1/4$  compared to one of  $1/6$ , which can be expected because the longer flanges add stability during lifting. The optimal spreader beam length is approximately 70 ft. for zero rotation during lifting, but the length between lift points ( $L_{Lift}$ ) that produces zero rigid body motion is not the optimum location for maximum stability. Despite these differences, however, the location that produces zero rigid body rotation is near the maximum stability location; therefore, it is reasonable to select the lifting locations based on this location.

Finally, the simplification described previously for prismatic girders, namely that lateral-torsional buckling is the governing mode of response, was applied to non-prismatic girders, and a moment gradient factor,  $C_b$ , was derived. A complexity with non-prismatic girders that is not encountered with the study of prismatic girders is the question of what section properties ( $J$ ,  $I_y$ ,  $C_w$ ) to use in the lateral-torsional buckling equation. To develop an improved understanding of the response of non-prismatic girders, the unbraced length ( $L_b$ ) was varied to determine how changes in this parameter affect the moment gradient factor. Based on extensive parametric studies on the buckling capacity of non-prismatic girders, it was concluded that a conservative approach should

be taken. Thus, it was recommended that, in calculating the lateral-torsional buckling capacity ( $M_o$ ), the entire length of the lifted section should be used for the unbraced length and the cross-section with the smallest geometric properties should be used. The maximum moment occurs at either the lift locations or in the region between the lift locations. Depending on the location of the lift points, the girder will buckle in one of these two locations—the cantilever or the mid region. The controlling maximum moment should be taken as the absolute maximum moment, regardless of where it occurs.

It should be noted that the graphs and equations given for prismatic girders are different from those given in Schuh's thesis due to a change in the assumed unbraced length ( $L_b$ ). To ensure consistency, the unbraced length was altered to match the work of Farris, which assumes the entire girder length as the unbraced length rather than using the longer of the cantilever overhang or the distance between the lift points as defined by Schuh. When these modifications were made, it became clear that the recommended expressions given in Equation 2.13 and Equation 2.14 were inconsistent and that the equations used by Farris were slightly unconservative. The reason for this discrepancy is that Farris assumed the smallest cross-sectional properties for the entire length, while the eigenvalue buckling analysis accounted for the "stiffer" portion of the nonprismatic beam. The result was a higher moment gradient factor ( $C_b$ ). The expressions used to evaluate  $C_b$  are given in the following figures and equations.

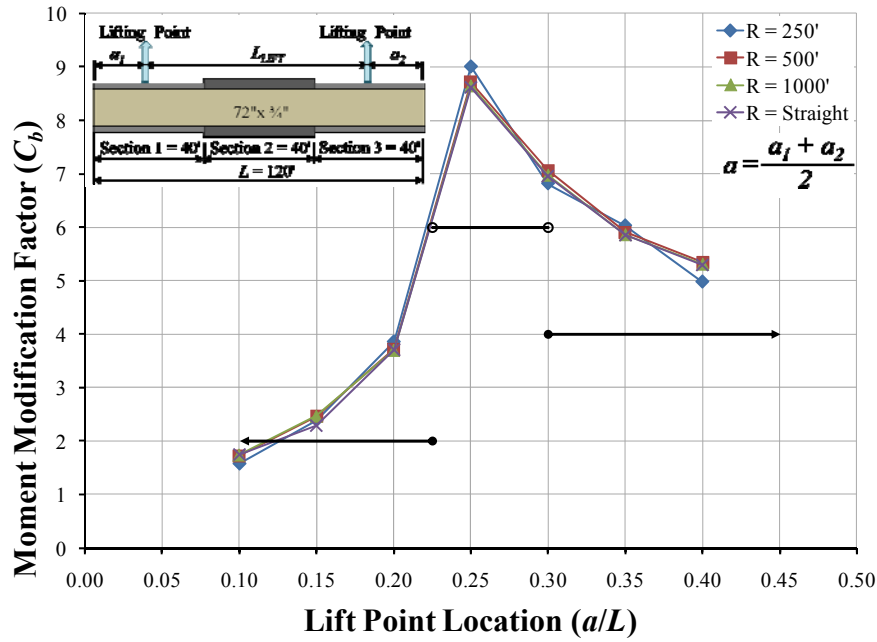


Figure 2.31:  $C_b$  vs.  $a/L$  for Given Radius of Curvatures (Symmetric Lift) (Farris 2008)

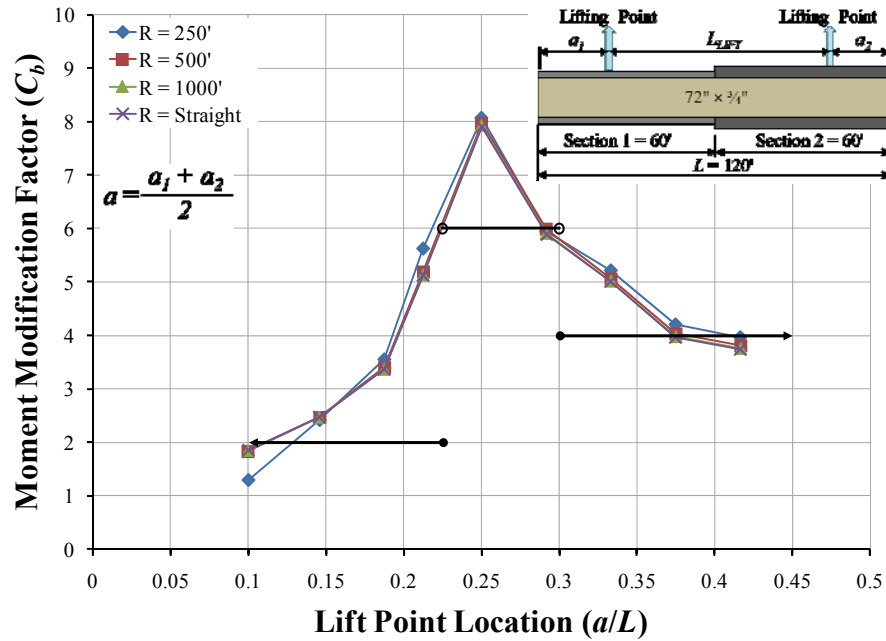


Figure 2.32:  $C_b$  vs.  $a/L$  for Given Radius of Curvatures (Unsymmetric Lift) (Farris 2008)

The expression in Equation 2.14 was formulated for the moment gradient factor,  $C_b$ , using the trends presented in the previous figures. This expression is represented as the black trend line in the previous figures.

$$C_b = 2.0 \quad \text{for} \quad \frac{a}{L} \leq 0.225$$

$$C_b = 6.0 \quad \text{for} \quad 0.225 < \frac{a}{L} < 0.3$$

$$C_b = 4.0 \quad \text{for} \quad \frac{a}{L} \geq 0.3$$

**Equation 2.14**

Results from the eigenvalue buckling analyses described in this section showed that the radius of curvature had very little effect on the critical buckling load. In addition, the magnitudes of the eigenvalues showed that the critical load was often significantly higher than the girder self weight. While the effect of girder curvature does not significantly impact the eigenvalue solution, girder curvature does have an impact on the actual girder displacements. The next section describes the nonlinear behavior of the girders as a function of girder curvature and lifting geometry. The eigenvalue solutions presented in this chapter serve as an important limit for evaluating girder behavior.

### **2.7.5.3 Eigenvalue Buckling Analysis Conclusions**

The basic assumptions that were made in performing the eigenvalue analyses presented above are that the girders experienced small displacements prior to buckling, had a linear stiffness, and failure was controlled by lateral-torsional buckling rather than a local instability. The eigenvalue buckling analysis provides a straightforward and accurate assessment of the response of straight I-girders, and it also provides an indication of stability for curved girders. Thus the following assumptions were included in the development of the moment gradient factor:

- 1) Lateral-torsional buckling is the dominant buckling mode.
- 2) Girders experience small displacements prior to buckling.
- 3) The unbraced length used to calculate the moment capacity is the entire length of the girder segment.
- 4) The smallest geometric properties are used to calculate the moment capacity for non-prismatic girders.

The following recommendations are given for the lifting of I-girders:

- 1) The  $C_b$  factors derived for prismatic girders should also be used for non-prismatic girders.
- 2) The predicted buckling capacity provides accurate solutions for straight girders.
- 3) The predicted buckling capacity provides an indication of the stability for curved girders.
- 4) The lifting location is the greatest factor in determining girder stability. Overall stability is maximized for an  $a/L$  approximately equal to 0.25; for prismatic girders, it is maximized for  $a/L = 0.238$ .

### 2.7.6 Geometric Nonlinear Buckling

The result of the eigenvalue parametric studies showed that girders lifted near their quarter points have the most stable response. As many of the previous figures showed, however, the radius of curvature did not significantly affect the eigenvalue buckling capacity. A set of eigenvalue analyses were performed to determine the affect of the radius of curvature on the eigenvalue at a relatively small interval, and the results are shown graphically in Figure 2.33.

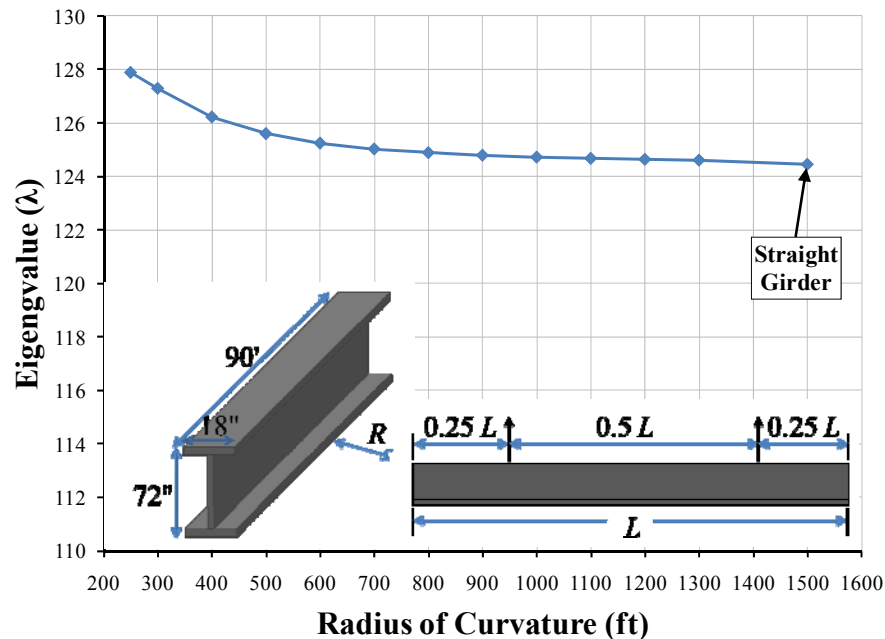
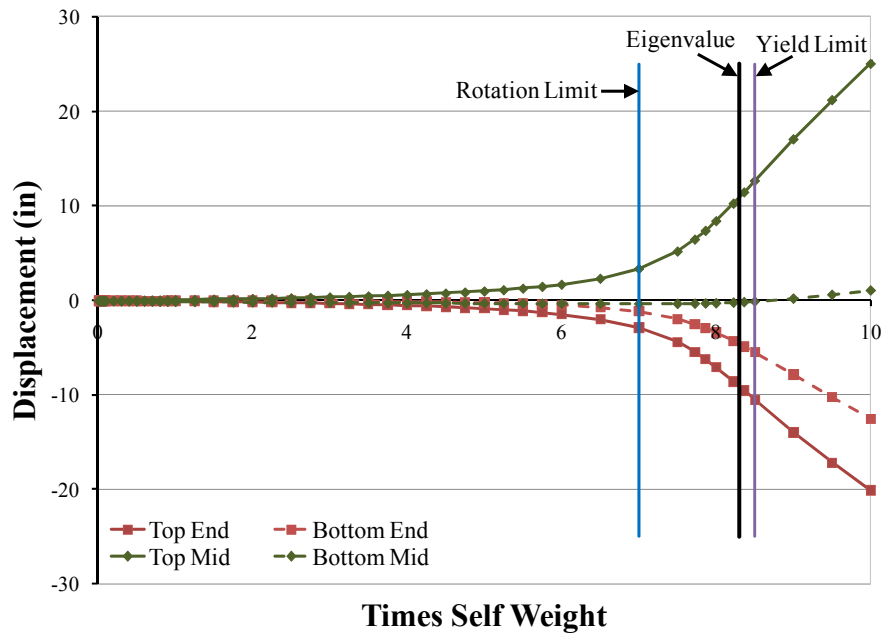


Figure 2.33: Effect of Radius of Curvature on the Eigenvalue (Schuh 2008)

These results indicate a slight increase in the eigenvalue with a decrease in the radius of curvature. This behavior has been attributed to two primary factors: 1) the small displacement assumption associated with an eigenvalue analysis and 2) the arching effect in resisting the buckling mode. The first factor is extremely important to the conclusions drawn from this research. The eigenvalue buckling analysis assumes small displacements of the system prior to buckling, which is generally true for straight girders as the load does not induce out-of-plane displacements before buckling occurs. However, such is not the case for curved girders, which can have both torsional and weak-axis bending stresses develop as a result of out-of-plane displacements. Under these conditions, the assumptions used for assessing stability using an eigenvalue solution are no longer valid. It may seem that these displacements would reduce the eigenvalue, but it is also notable that the buckled shape given by the eigenmode does not have a magnitude associated with it. Thus, for a given displaced shape, both positive and negative mode shapes are possible; for highly curved girders, the eigenmode must bend the girder against the curvature, thereby providing the system with a kind of arching restraint. These two features limit the applicability of eigenvalue buckling solutions for highly curved girders.

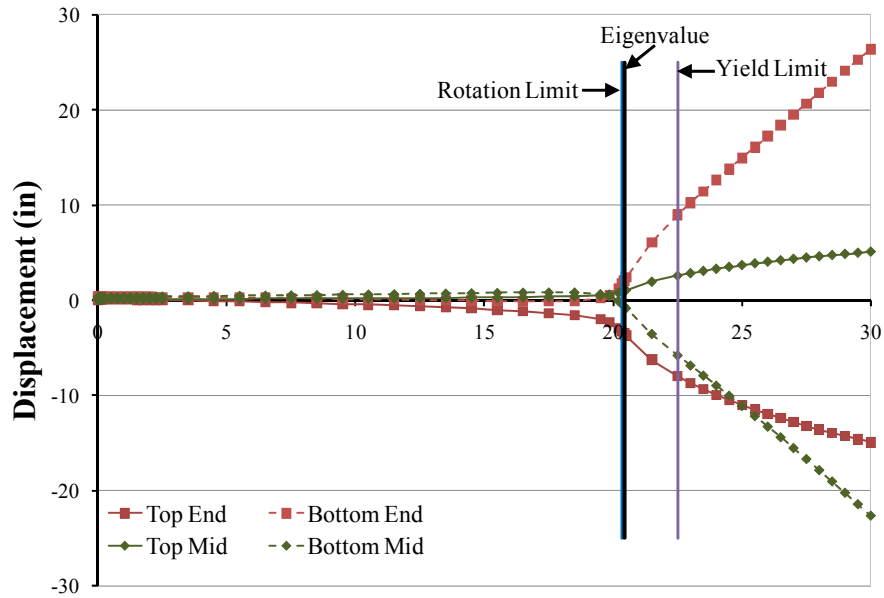
Accordingly, a 3-D geometric nonlinear analysis was performed to capture the behavior of curved I-girders during lifting. Due to the linear elastic material properties utilized in the models, two criteria were identified to limit the applicability of the solutions to fit practical conditions. Based upon the information gained from a survey of erectors, contractors, and engineers (Farris 2008), a serviceability limit state of 1.5 degrees of girder rotation was used to ensure proper girder fit-up for aerial splices. In addition, a strength limit state of one-half of the yield stress ( $F_y/2$ ) was established to prevent yielding from occurring as a result of the combination of residual stresses with lifting. For all nonlinear analyses conducted, only gravity load was acting on the girders. Although other loads such as wind are possible, erectors typically have stringent limits on wind speed that would preclude girder lifting in windy conditions. As discussed previously, the eigenvalue represents the multiple of the applied load that will cause

buckling. Because only gravity load acted on the girder, the abscissa in the following figures is a multiple of the self weight, with the ordinate representing the out-of-plane displacement of the top and bottom of the girders. Displacements are shown for both the end and the middle of the girder. All cases presented in this section have a flange-to-depth ratio of  $\frac{1}{4}$ . Figure 2.34 and Figure 2.35 represent “straight” girders with an L/500 imperfection, which is representative of manufacturing tolerances for I-girders. Figure 2.36 and Figure 2.37 are curved girders with a radius of curvature equal to 500 ft. Two lift locations are used in these examples:  $a/L = 0.2$  and  $a/L = 0.25$ . Three vertical lines showing the load limits corresponding to the rotation limit of 1.5 degrees, half the yield stress, and the eigenvalue are labeled on the graphs.

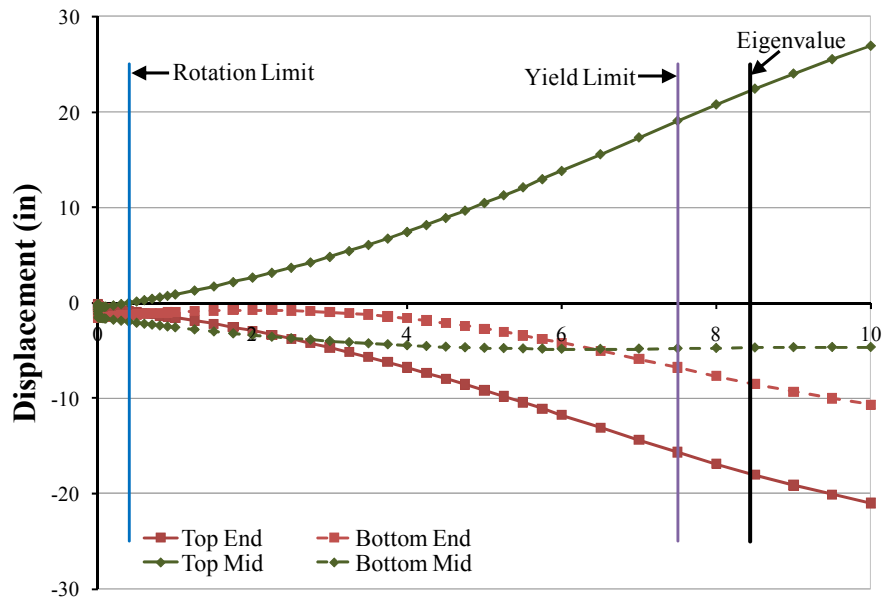


**Figure 2.34: Flange Lateral Displacement for Girder with  $a/L = 0.2$   $b_f/D = 0.25$   $R = Str$ .**





**Times Self Weight**  
**Figure 2.35: Flange Lateral Displacement for Girder**  
**with  $a/L = 0.25$   $b_f/D = 0.25$   $R = Str.$**



**Times Self Weight**  
**Figure 2.36: Flange Lateral Displacement for Girder**  
**with  $a/L = 0.2$   $b_f/D = 0.25$   $R = 500'$**

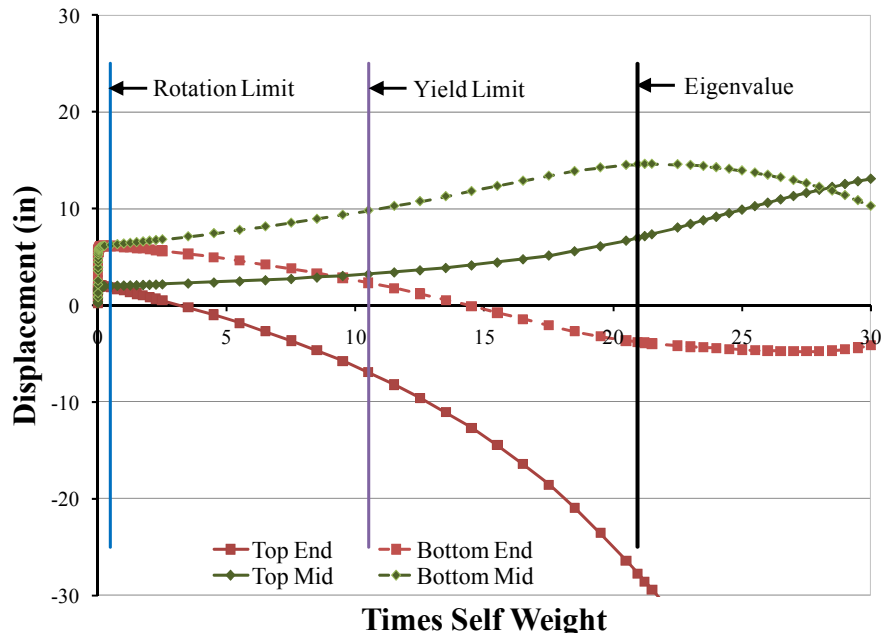


**Figure 2.37: Flange Lateral Displacement for Girder  
with  $a/L = 0.25$   $b_f/D = 0.25$   $R = 500'$**

The straight girder systems shown in Figure 2.34 and Figure 2.35 generally behave as expected and show good correlation with the eigenvalue analyses. The girders deflect very little until they approach the eigenvalue buckling load; they then diverge quickly afterwards. This response indicates that the eigenvalue provides a good estimate of the buckling capacity of straight girders. On the contrary, results for the girders with significant curvature shown in Figure 2.36 and Figure 2.37 experience substantial displacements early in their response, with the rotation limit quickly reached. In both of the cases corresponding to the response of curved girders, the rotation limit is reached first, then the yield limit is reached, and finally the eigenvalue limit is reached. These results suggest that the eigenvalue is an unconservative estimate for the limiting capacity of highly curved girders. It should be noted that for Figure 2.37, the girder is lifted such that an initial rigid body rotation occurs; thus, the additional rotation necessary to reach a limit is relatively small. For more detail on the nonlinear parametric study performed for this research, see Petruzzi (2010).

The most important finding from all of the analyses conducted is that the rotation limit controls the response for practically all curved I-girders. Accordingly, engineers

need efficient methods for accurately predicting girder rotation during lifting. Chapter 3 provides an overview of analytical expressions that were developed as part of this study for predicting the rigid body rotation for curved girders with various lifting locations.

## **2.8 CONCLUSIONS**

Research on curved steel I-girders has advanced considerably over the past 40 years due in large part to the CURT and CSBRP projects. Moreover, the accessibility of the microcomputer has allowed computational techniques to become increasingly sophisticated during this time period. Despite these advances, there still exists a significant lack of full-scale data for curved I-girders during lifting, erection, and concrete deck placement. Recent work at the University of Texas at Austin provides much of the information necessary to begin filling some of the existing knowledge gaps. The data collected allows for the validation of computational models that can be utilized to predict the behavior of these complex systems during the early stages of a bridge's life when it is most prone to failure. The following chapters of this dissertation provide both theoretical predictions of the behavior of these systems and analysis tools that allow engineers to ensure public safety and to optimize construction practices.

## CHAPTER 3:

# BEHAVIOR OF CURVED I-GIRDERS DURING LIFTING

---

### 3.1 INTRODUCTION

Data collected from field tests and results of computational simulations described in the previous chapter indicate that the rotational response often controls the overall behavior during lifting of curved girder segments. The rotational response can be decomposed into a rigid body rotation and a cross-sectional twist. For straight girders, this rotational behavior is not problematic, and the results of a linear eigenvalue buckling analysis will accurately predict the behavior of these girders while they are lifted. For curved girders, an eigenvalue buckling analysis does not accurately predict the response as displacements accrue as soon as the girder segment is lifted. Thus, based upon feedback from erectors, a serviceability limit state was introduced in the previous chapter to ensure that curved girders do not experience large displacements during construction. Accordingly, it was imperative to derive an analytical approach to predict the behavior of curved I-girders during lifting.

As indicated above, the rotational behavior of a curved girder during lifting has two components: a rigid body rotation ( $\theta_{\text{rigid}}$ ) and a cross-sectional twist ( $\theta_{\text{twist}}$ ). The rigid body rotation is a function of the girder geometry and the lifting locations and is independent of the girder stiffness. Calculation of the cross-sectional twist must consider both the St. Venant and the torsional warping stiffness. There are exact solutions for the torsional response of open sections for specific boundary conditions and loadings, but not for the general case (Seaburg and Carter 1997). It was therefore necessary to find an approximate solution to the twist of an open section subjected to non-uniform torque. After a search of the literature, a 1-D, two-node, 2 degree-of-freedom per node  $C^1$  continuous finite element formulation was found for open sections subjected to non-uniform torsion (Mohareb and Nowzartash 2003). A displacement-based  $C^1$  continuous finite element has the property that the primary variable (i.e., displacements) and the

derivative of the primary variable are continuous at the boundary between two elements. For this particular element, the cross-sectional angle of twist ( $\theta_{\text{twist}}$ ) and the change in the cross-sectional angle of twist ( $\theta_{\text{twist}}$ ) are continuous at the element boundaries. It is by combining the rigid body rotation and the cross-sectional twist that an accurate prediction of a curved girder's behavior can be determined; thus, if  $\theta_{\text{rigid}} + \theta_{\text{twist}} < 1.5^\circ$  at all critical points along a curved girder, the girder satisfies the serviceability limit state.

### 3.2 RIGID BODY ROTATION

For a straight girder, the center of gravity (C.G.) of the girder segment lies along the girder's centerline. For any lifting configuration of the girder, there is no eccentricity between the line of support created by the lift points and the center of gravity. Therefore, no rigid body rotation will occur about the longitudinal axis of the girder when it is being lifted in the air. Curved girders, conversely, have the property that the C.G. of the segment is shifted from the girder centerline. In roadway design, it is typical convention to use circular geometry for the horizontal alignment and parabolic geometry for the vertical alignment. Figure 3.1 is a plan view schematic drawing that shows how the C.G. of both a straight and curved girder.

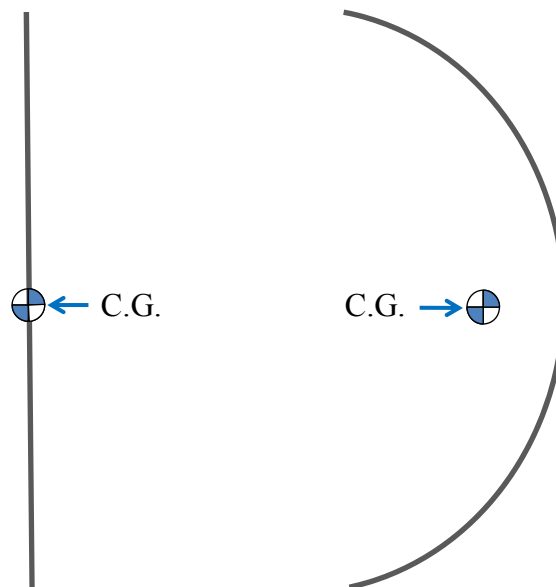


*Figure 3.1: Plan View Schematic of Curved and Straight Girder Center of Gravity (Schuh 2008)*

The line of support for lifting is defined by a line that passes through the lifting apparatus. Many girders are lifted with a single crane and spreader beam, resulting in two lift clamps defining the line of support. Figure 3.2 is a picture of a girder being lifted in this manner.



***Figure 3.2: Lifting of a Horizontally Curved Steel I-Girder with 1 Crane & 2 Lift Clamps***

For a system in which the center of gravity does not occur collinearly with the line of support, the girder will rotate about the line of support until the center of gravity is collinear with the lift clamps. The rotation stabilizes the system by minimizing the total potential energy. Two factors contribute to the rigid body rotation: the center of gravity location (a function of the girder geometry) and the lift locations. The rigid body rotation is not affected by the girder stiffness. In order to determine the center of gravity, a set of equations was derived for non-prismatic girders with any arrangement of cross frames attached to the girder. The process utilizes polar coordinates with the origin at the center of radius of the girder. Figure 3.3 is a schematic of an example curved girder that defines many of the variables needed for this development. The curved girder in the example has two different cross-sections with lengths  $L_1$  and  $L_2$ . Additionally, five cross frames are attached to the inside of the girder at locations  $L_{xi}$  from the beginning of the girder. The

following derivation uses the example bridge girder to demonstrate the variable definitions and to develop the equations for a simple case. Then, the final generalized equations that are useful for all girders are provided.

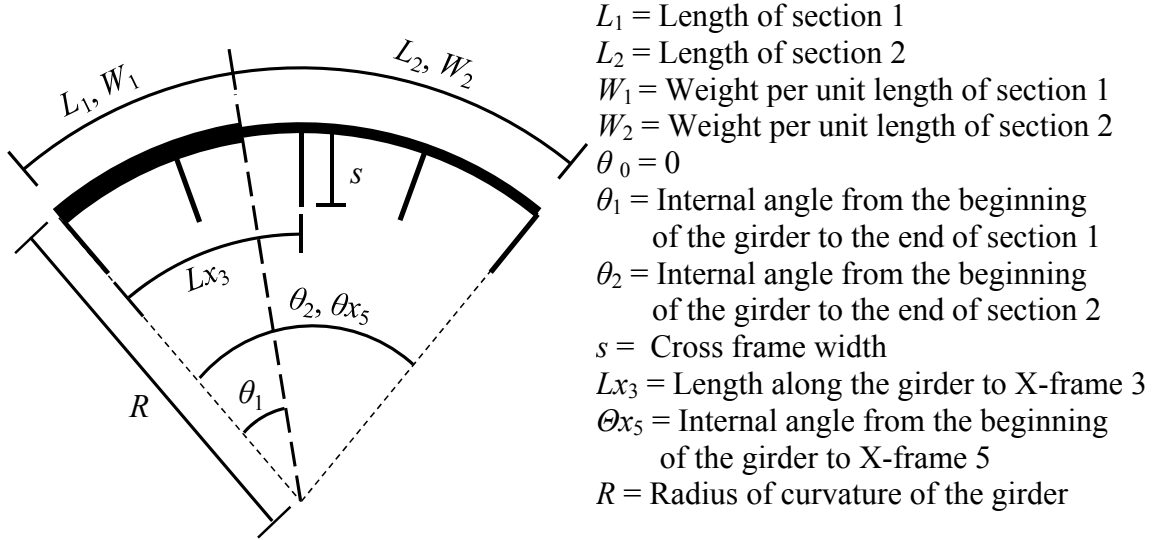


**Figure 3.3: Variable Definition for C.G.**

where  $\theta_1$  and  $\theta_2$  are given in Equation 3.1 and Equation 3.2:

$$\theta_1 = \frac{L_1}{R} \quad \text{Equation 3.1}$$

$$\theta_2 = \frac{L_2}{R} + \theta_1 \quad \text{Equation 3.2}$$

The internal angle from the beginning of the girder to a given cross-section or cross frame can be generalized and is given in Equation 3.3 and Equation 3.4, respectively:

$$\theta_i = \frac{L_i}{R} + \theta_{i-1} \quad \text{Equation 3.3}$$

$$\theta_{x_i} = \frac{Lx_i}{R} \quad \text{Equation 3.4}$$

The weight of the girder from Figure 3.3 can be defined below with Equation 3.6:

$$\text{Total Girder Weight} = \int_{\theta_0}^{\theta_1} W_1 R d\theta + \int_{\theta_1}^{\theta_2} W_2 R d\theta \quad \text{Equation 3.5}$$

$$= W_1 R (\theta_1 - \theta_0) + W_2 R (\theta_2 - \theta_1) \quad \text{Equation 3.6}$$

The generalized form of the total girder weight equation is shown in Equation 3.7 and Equation 3.8:

$$\text{Total Girder Weight} = \sum_i^n \int_{\theta_{i-1}}^{\theta_i} W_i R d\theta \quad \text{Equation 3.7}$$

$$= R \sum_i^n W_i (\theta_i - \theta_{i-1}) \quad \text{Equation 3.8}$$

The total weight of the cross frames can be defined as the sum of the weight of each cross frame as given in Equation 3.9:

$$\text{Total X - Frame Weight} = \sum_j^m Wx_j \quad \text{Equation 3.9}$$

The total weight can thus be defined by Equation 3.10:

$$\text{Total Weight} = R \sum_i^n W_i (\theta_i - \theta_{i-1}) + \sum_j^m Wx_j \quad \text{Equation 3.10}$$

where:

- $n$  = Number of different girder cross sections
- $m$  = Number of cross frames
- $Wx_j$  = Weight of cross frame  $j$

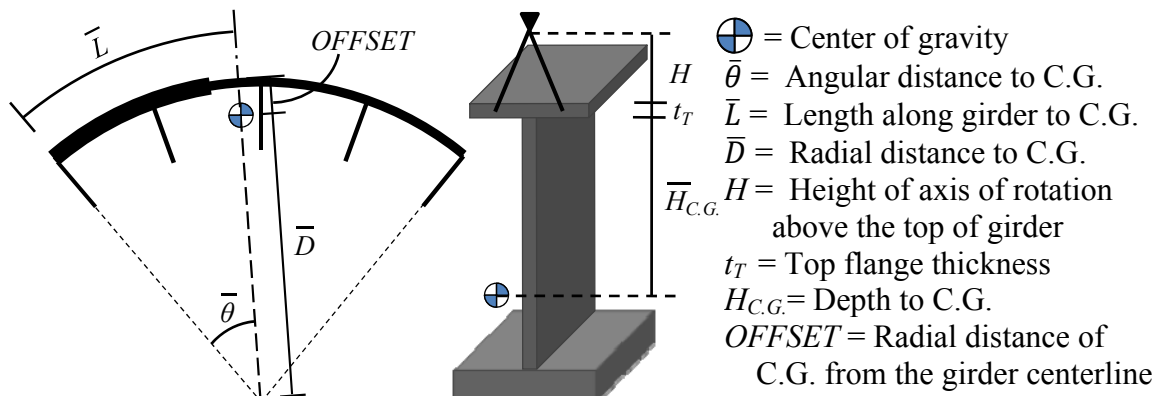


**Figure 3.4: C.G. Location**

The angular distance from the beginning of the girder to the center of gravity is determined from a weighted average of the segment's centroids located at the angular



center of each cross section. For the girder shown in Figure 3.4, the expression is developed using Equation 3.11a-Equation 3.11c:

$$\bar{\theta} = \frac{\frac{\theta_1 + \theta_0}{2} \int_{\theta_0}^{\theta_1} W_1 R d\theta + \frac{\theta_2 + \theta_1}{2} \int_{\theta_1}^{\theta_2} W_2 R d\theta + \sum_j^m W x_j \theta x_j}{\int_{\theta_0}^{\theta_1} W_1 R d\theta + \int_{\theta_1}^{\theta_2} W_2 R d\theta + \sum_j^m W x_j} \quad \text{Equation 3.11a}$$

$$\bar{\theta} = \frac{W_1 R \frac{(\theta_1 + \theta_0)(\theta_1 - \theta_0)}{2} + W_2 R \frac{(\theta_2 + \theta_1)(\theta_2 - \theta_1)}{2} + \sum_j^m W x_j \theta x_j}{W_1 R(\theta_1 - \theta_0) + W_2 R(\theta_2 - \theta_1) + \sum_j^m W x_j} \quad \text{Equation 3.11b}$$

$$\bar{\theta} = \frac{\frac{W_1 R(\theta_1^2 - \theta_0^2) + W_2 R(\theta_2^2 - \theta_1^2)}{2} + \sum_j^m W x_j \theta x_j}{W_1 R(\theta_1 - \theta_0) + W_2 R(\theta_2 - \theta_1) + \sum_j^m W x_j} \quad \text{Equation 3.11c}$$

The generalized expression for the angular distance to the center of gravity for a curved girder is determined by the following expression:

$$\bar{\theta} = \frac{\frac{R \sum_i^n W_i (\theta_i^2 - \theta_{i-1}^2)}{2} + \sum_j^m W x_j \theta x_j}{R \sum_i^n W_i (\theta_i - \theta_{i-1}) + \sum_j^m W x_j} \quad \text{Equation 3.11}$$

The distance along the length of a girder to the center of gravity can then be calculated as follows:

$$\bar{L} = \bar{\theta} R \quad \text{Equation 3.12}$$

The radial distance to the center of gravity is determined by taking the weighted average of the girder projected onto the  $\bar{\theta}$  radial line. This situation is shown schematically in Figure 3.5.

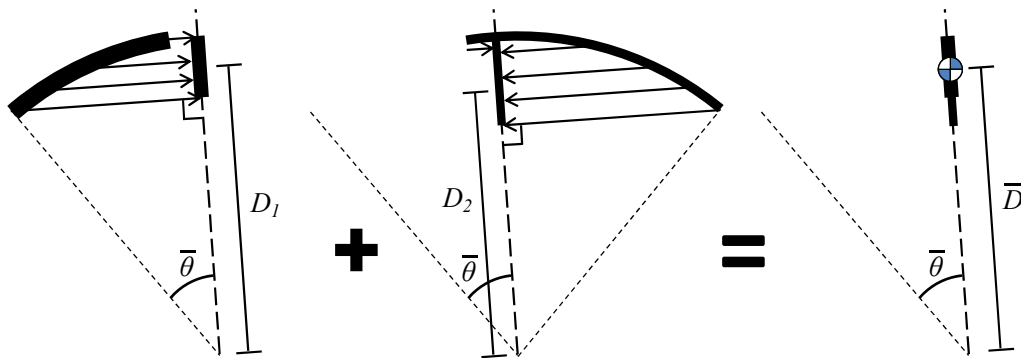


Figure 3.5: Schematic of Method used to Obtain Radial Distance to C.G.

The equation resulting from Figure 3.5 is given by Equation 3.13a and Equation 3.13b

$$\bar{D} = \frac{\int_{\theta_0}^{\theta_1} W_1 R \cos(\theta - \bar{\theta}) R d\theta + \int_{\theta_1}^{\theta_2} W_2 R \cos(\theta - \bar{\theta}) R d\theta + \sum_j^m W x_j (R + \alpha \frac{S}{2}) \cos(\theta x_j - \bar{\theta})}{\int_{\theta_0}^{\theta_1} W_1 R d\theta + \int_{\theta_1}^{\theta_2} W_2 R d\theta + \sum_j^m W x_j}$$

**Equation 3.13a**

$$\bar{D} = \frac{W_1 R^2 [\sin(\theta_1 - \bar{\theta}) - \sin(\theta_0 - \bar{\theta})] + W_2 R^2 [\sin(\theta_2 - \bar{\theta}) - \sin(\theta_1 - \bar{\theta})] + \sum_j^m W x_j (R + \alpha \frac{S}{2}) \cos(\theta x_j - \bar{\theta})}{W_1 R(\theta_1 - \theta_0) + W_2 R(\theta_2 - \theta_1) + \sum_j^m W x_j}$$

**Equation 3.13b**

The radial distance can be determined by the generalized form of Equation 3.13b and is given in Equation 3.13:

$$\bar{D} = \frac{R^2 \sum_i^n W_i [\sin(\theta_i - \bar{\theta}) - \sin(\theta_{i-1} - \bar{\theta})] + (R + \alpha \frac{S}{2}) \sum_j^m W x_j \cos(\theta x_j - \bar{\theta})}{R \sum_i^n W_i (\theta_i - \theta_{i-1}) + \sum_j^m W x_j}$$

**Equation 3.13**

where:

$$\alpha = \begin{cases} -1 & \text{if cross frames are only on the inside of the curve} \\ 0 & \text{if cross frames are only on both sides of the girder} \\ 1 & \text{if cross frames are only on the outside of the curve} \end{cases}$$

The offset of the center of gravity from centerline of the girder is given by Equation 3.14:

$$OFFSET = R - \bar{D}$$

**Equation 3.14**

The depth of the center of gravity is determined from a weighted average of each cross section's C.G. measured from the bottom of the top flange. For the girder shown in Figure 3.4, the expression is given by Equation 3.15a and Equation 3.15b:

$$\bar{H}_{C.G.} = \frac{H_{C.G.} \int_{\theta_0}^{\theta_1} W_1 R d\theta + H_{C.G.} \int_{\theta_1}^{\theta_2} W_2 R d\theta + \sum_j^m W x_j H_{C.G.j}}{\int_{\theta_0}^{\theta_1} W_1 R d\theta + \int_{\theta_1}^{\theta_2} W_2 R d\theta + \sum_j^m W x_j}$$

**Equation 3.15a**

$$\bar{H}_{C.G.} = \frac{W_1 H_{C.G.1} R(\theta_1 - \theta_0) + W_2 H_{C.G.2} R(\theta_2 - \theta_1) + \sum_j^m W x_j H_{C.G.j}}{W_1 R(\theta_1 - \theta_0) + W_2 R(\theta_2 - \theta_1) + \sum_j^m W x_j}$$

**Equation 3.15b**

The generalized form of this equation is given by Equation 3.15:

$$\bar{H}_{C.G.} = \frac{R \sum_i^n W_i H_{C.G.i} (\theta_i - \theta_{i-1}) + \sum_j^m W x_j \theta x_j}{R \sum_i^n W_i (\theta_i - \theta_{i-1}) + \sum_j^m W x_j}$$

Equation 3.15

To prevent rigid body rotation, the line of support must intersect the center of gravity defined by the previous equations. There are an infinite number of lines that intersect the C.G. as demonstrated by the two examples in Figure 3.6; however, the lift clamp capacity requirements are minimized by requiring equal lift forces, which allows for a unique solution to this problem. This positioning of the lifting clamps gives an optimum solution with respect to the rigid body rotation.

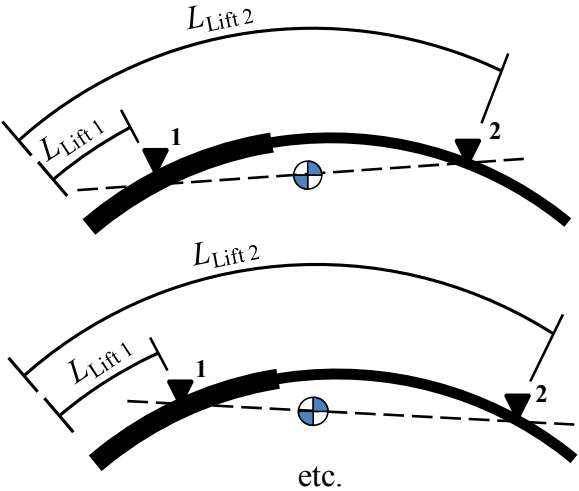
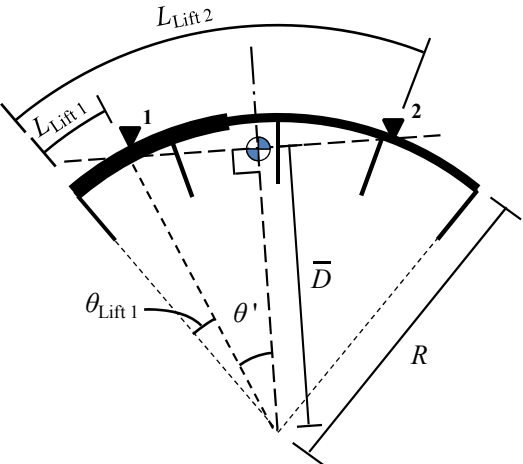


Figure 3.6: Possible Lines of Support that Intersect the C.G.



- $L_{Lift 1}$  = Length along girder to lift pt. 1
- $L_{Lift 2}$  = Length along girder to lift pt. 2
- $\theta_{Lift 1}$  = Angular distance to lift pt. 1
- $\theta_{Lift 2}$  = Angular distance to lift pt. 2
- $\oplus$  = Center of gravity
- $\theta'$  = Angular distance from lift pts. to Center of gravity
- $\bar{D}$  = Radial distance to C.G.
- $R$  = Radius of curvature of the girder

Figure 3.7: Zero Rotation/Equal Force Lift Location

The lift points will have equal forces if they are an equal distance from center of gravity. These lift point locations are determined by the following sequence of equations:

$$\cos(\theta') = \frac{\bar{D}}{R} \quad \text{Equation 3.16}$$

$$\theta' = \cos^{-1}\left(\frac{\bar{D}}{R}\right) \quad \text{Equation 3.17}$$

$$\theta_{Lift\ 1} = \bar{\theta} - \theta' \quad \text{Equation 3.18}$$

$$L_{Lift\ 1} = R\theta_{Lift\ 1} \quad \text{Equation 3.19}$$

$$L_{Lift\ 2} = R(\theta_{Lift\ 1} + 2 * \theta') \quad \text{Equation 3.20}$$

A spreader bar is commonly used by a single crane in lifting a girder and can be represented as a chord between the lift points. Figure 3.8 is a picture of a crane using a spreader bar to lift a girder. The practical application of the equations developed in this section allows for the design of the spreader bar length. Equation 3.21 gives the length of the spreader bar necessary to prevent rotation and minimize the lift clamp capacity requirements.



**Figure 3.8: Spreader Bar used by a Single Crane Lifting a Girder**

$$\Delta L = 2R \sin(\theta') \quad \text{Equation 3.21}$$

The lift clamp capacity requirements are defined by Equation 3.22:

$$\text{Lift Load} = \frac{\text{Total Girder Weight}}{2} \quad \text{Equation 3.22}$$

In general, the optimum spreader bar length is not available to the contractor for all girders. It is therefore important to calculate the rigid body rotation for a given girder and spreader bar length.

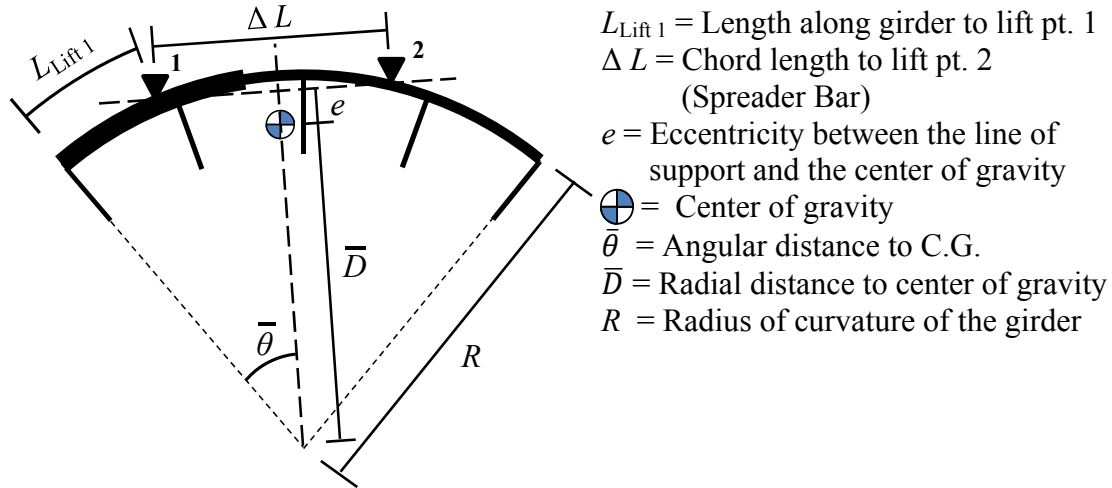


**Figure 3.9: Predicted Rotation and Lift Reactions**

The eccentricity between the line of support and the center of gravity must be determined. This determination is made by giving coordinate locations for three critical points: lift clamp 1, lift clamp 2, and the center of gravity. Then, the minimum distance to the center of gravity from the line of support is determined (mathworld.wolfram.com). Equation 3.23 through Equation 3.26 define the coordinates of the three critical points, and Equation 3.27 can be used to compute the eccentricity:

$$L_{\text{Lift } 1}: (x_1, y_1) = \left( R \sin\left(\frac{L_{\text{Lift } 1}}{R}\right), R \cos\left(\frac{L_{\text{Lift } 1}}{R}\right) \right) \quad \text{Equation 3.23}$$

$$\Delta L_{\text{Arc Length}} = 2R \sin^{-1}\left(\frac{\Delta L}{2R}\right) \quad \text{Equation 3.24}$$

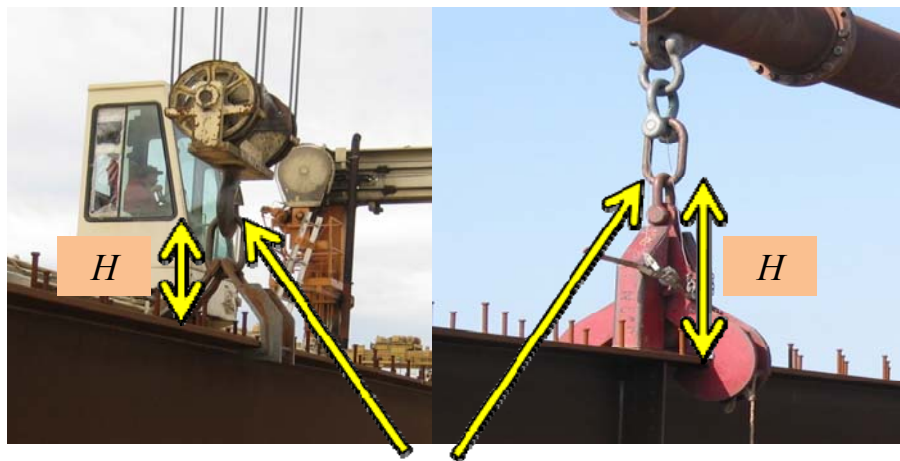
$$L_{\text{Lift } 2}: (x_2, y_2) = \left( R \sin\left(\frac{L_{\text{Lift } 1} + \Delta L_{\text{Arc Length}}}{R}\right), R \cos\left(\frac{L_{\text{Lift } 1} + \Delta L_{\text{Arc Length}}}{R}\right) \right) \quad \text{Equation 3.25}$$

$$\text{C. G.}: (x_0, y_0) = (R \sin(\bar{\theta}), R \cos(\bar{\theta})) \quad \text{Equation 3.26}$$

$$e = \frac{|(x_2 - x_1)(y_1 - y_0) - (x_1 - x_0)(y_2 - y_1)|}{\sqrt{(x_2 - x_1)^2 + (y_2 - y_1)^2}} \quad \text{Equation 3.27}$$

(mathworld.wolfram.com)

The distance above the top of the girder to the axis of rotation ( $H$ ) is the only remaining quantity needed to calculate the rigid body rotation of a curved girder lifted at two points using a spreader bar. A complete definition and a detailed parametric study of the effect of  $H$  on the rotation and stability of curved girders is given in Schuh (2008). This parameter can be defined by the lowest location of the lifting apparatus that is free to rotate as shown in Figure 3.10. The smaller the assumed value for  $H$ , the more conservative the computed results will be for calculation purposes. 24 in. is a practical yet conservative estimate for the height of the axis of rotation for situations where an engineer has no information regarding the lifting apparatus. Figure 3.11 provides a schematic of the rigid body rotation.



Assumed Axis of Rotation

**Figure 3.10: Approximating the Height of the Axis of Rotation (Schuh 2008)**

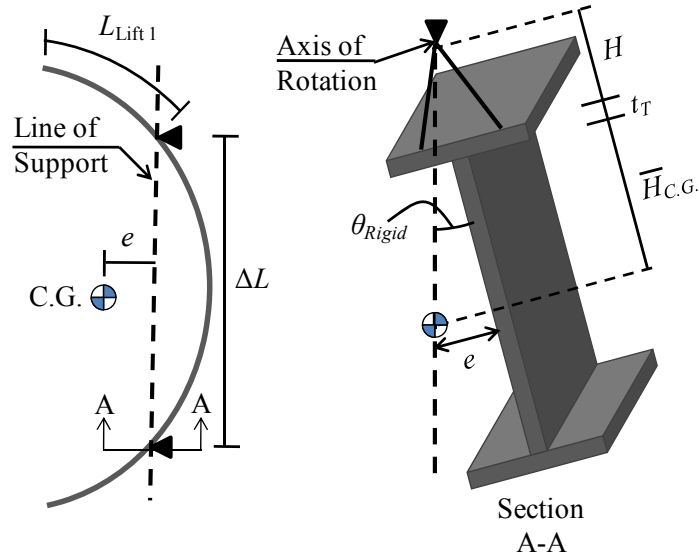


**Figure 3.11: Schematic of the Rigid Body Rotation**

The rigid body rotation of a girder, given the height of the axis of rotation above the top of the girder, can be found using the following expression:

$$\theta_{Rigid} = \tan^{-1} \left( \frac{e}{H + t_T + \bar{H}_{C.G.}} \right) \quad \text{Equation 3.28}$$

The lift clamp reactions are calculated by their relative distance from the girder's center of gravity. The equations used to calculate these reactions are given by Equation 3.29 through Equation 3.32. These equations assume that the lifting apparatus acts independently as would be the case for two cranes lifting a girder; for a single girder with a spreader bar, the lift clamp reactions must be equal or the girder will rotate along the length of the girder.

$$R_{Lift 1} = Total Weight * \frac{(L_{Lift 2} - \bar{L})}{(\Delta L_{Arc Length})} \quad \text{Equation 3.29}$$

$$R_{Lift 1} = \left[ R \sum_i^n W_i (\theta_i - \theta_{i-1}) + \sum_j^m W x_j \right] \frac{(L_{Lift 2} - \bar{L})}{(\Delta L_{Arc Length})} \quad \text{Equation 3.30}$$

$$R_{Lift 2} = Total Weight * \frac{(\bar{L} - L_{Lift 1})}{(\Delta L_{Arc Length})} \quad \text{Equation 3.31}$$

$$R_{Lift\ 2} = \left[ R \sum_i^n W_i (\theta_i - \theta_{i-1}) + \sum_j^m W x_j \right] \frac{(\bar{L} - L_{Lift\ 1})}{(\Delta L_{Arc\ Length})} \quad \text{Equation 3.32}$$

### 3.3 CROSS-SECTIONAL TWIST

#### 3.3.1 Torque on an Open Cross Section

The second part of the rotational behavior of curved girders is the cross-sectional twist that occurs due to the torque induced by a girder's self-weight. The torsional stiffness of a girder segment is often divided into the St. Venant and torsional warping components. The St. Venant stiffness is related to the uniform torsional stiffness while the warping stiffness is related to the non-uniform torsional stiffness. The warping stiffness is a function of the length of the segment. For box girder segments, the warping stiffness is often neglected since the St. Venant stiffness is very large for closed cross sections. For open cross sections, the importance of the contribution of the two stiffness components needs to be considered. Figure 3.12 is a schematic of the induced stresses resulting from a torsional load on an I-girder.

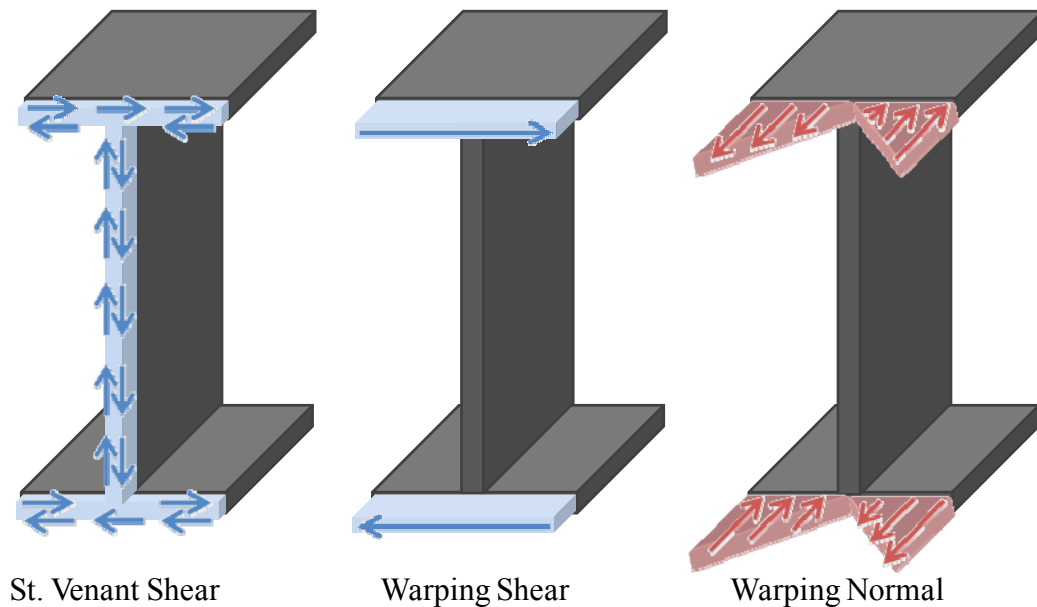


**Figure 3.12: Torsion Induced Stresses (Schuh 2008)**



For any section, torsion is resisted by St. Venant shear stresses ( $T_{SV}$ ) and warping restraint ( $T_W$ ); therefore, the sum of the two must be equal to the total torsion acting on the cross-section under consideration as indicated by Equation 3.33.

$$T(z) = T_{SV}(z) + T_W(z) \quad \text{Equation 3.33}$$

where:

$$T_{SV}(z) = GJ\varphi'(z) \quad \text{Equation 3.34}$$

$$T_W(z) = EC_W\varphi'''(z) \quad \text{Equation 3.35}$$

Thus, the differential equation for torsional equilibrium is given by Equation 3.36:

$$\frac{T(z)}{EC_W} = \frac{1}{k^2}\varphi' + \varphi''' \quad \text{Equation 3.36}$$

where:

$$k = \sqrt{\frac{EC_W}{GJ}} \quad \text{Equation 3.37}$$

The general solution to this differential equation is given by Equation 3.38:

$$\varphi(z) = A + B \cosh\left(\frac{z}{k}\right) + C \sinh\left(\frac{z}{k}\right) + \varphi_p(z) \quad \text{Equation 3.38}$$

$\varphi(z)$  is the general solution to the nonhomogenous differential equation for torsion. The constants  $A$ ,  $B$ , and  $C$  are determined by the boundary conditions of the problem under consideration (Engelhardt 2008). The particular solution of the differential equation,  $\varphi_p(z)$ , depends on the applied distributed twisting moments,  $t(z)$ , acting on the beam. These twisting moments are given by (Mohareb and Nowzartash 2003):

$$t(z) = EC_W\varphi_p^{IV} - GJ\varphi_p'' \quad \text{Equation 3.39}$$

For specific boundary conditions and loading cases, AISC has summarized the solution to the differential equation and has given guides for design (Seaburg and Carter 1997). However, for the general case, there is no exact solution; thus, an approximate solution can be developed. A search of the literature revealed a 1-D, two-node, 2 degree-of-freedom per node  $C^1$  continuous finite element formulation for open sections subjected

to non-uniform torsion (Mohareb and Nowzartash 2003). By utilizing this formulation, a reasonable approximation of the cross-sectional twist of a curved I-girder during lifting was achieved.

The formulation utilizes a displacement-based finite element procedure with the general equilibrium equations shown in Equation 3.40:

$$[K_e]\{\varphi\} = \{G_{eFE}\} + \{G\} \quad \text{Equation 3.40}$$

where:

- $[K_e]$  = Exact stiffness matrix
- $\{\varphi\}$  = Nodal displacements (i.e., nodal rotation and change of rotation)
- $\{G_{eFE}\}$  = Exact nodal fixed end forces
- $\{G\}$  = External nodal forces (i.e., applied torques)

$[K_e]$  is derived from the element stiffness matrix and has the form:

$$K_{mn} = \delta(GJ s_{mn} + EC_W w_{mn}) \quad \text{Equation 3.41}$$

where  $m$  and  $n$  range between 1 and 4, and  $\delta$  is defined as :

$$\delta = \frac{1}{(2 - 2 \cosh kl + kl \sinh kl)^2} \quad \text{Equation 3.42}$$

The terms  $s_{mn}$  and  $w_{mn}$  are defined as:

$$s_{11} = k(\cosh kl - 1)(kl \cosh kl - 3 \sinh kl + 2kl) \quad \text{Equation 3.43}$$

$$s_{12} = (\cosh kl - 1)[-2 \cosh kl + 0.5kl \sinh kl + 0.5(kl)^2 + 2] \quad \text{Equation 3.44}$$

$$s_{22} = \frac{1}{k} [kl - 0.5(kl)^3 + kl \cosh kl (1 - 2 \cosh kl) + \sinh kl (\cosh kl - 1) + 0.5(kl)^2 \sinh kl (2 + \cosh kl)] \quad \text{Equation 3.45}$$

$$s_{24} = \frac{1}{k} [0.5(kl)^2 (kl \cosh kl - 3 \sinh kl) + (\cosh kl - 1)(3kl - \sinh kl)] \quad \text{Equation 3.46}$$

$$w_{11} = k^3(\cosh kl - 1)(\sinh kl - kl) \quad \text{Equation 3.47}$$

$$w_{12} = k^2[0.5(kl)(\cosh kl - 1)(\sinh kl - kl)] \quad \text{Equation 3.48}$$

$$w_{22} = k[(\cosh kl - 1)(\sinh kl - kl \cosh kl) + \sinh kl (kl)^2 (0.5 \cosh kl - 1) + 0.5(kl)^3] \quad \text{Equation 3.49}$$

$$w_{24} = k(\cosh kl - 0.5(kl)^2 - 1)(kl \cosh kl - \sinh kl) \quad \text{Equation 3.50}$$

The remaining terms in the element stiffness matrix are calculated as:

$$[K] = \begin{bmatrix} K_{11} & K_{12} & -K_{11} & K_{12} \\ & K_{22} & -K_{12} & K_{24} \\ & & K_{11} & -K_{12} \\ sym & & & K_{22} \end{bmatrix} \quad \text{Equation 3.51}$$

$\{G_{eFE}\}$  is calculated by integrating the product of the shape functions  $\{N_i(z)\}$  and the applied distributed twisting moment  $t(z)$  as shown in Equation 3.52.

$$\{G_{eFE}\} = \int_{z=0}^{z=l} \{N_i(z)\}t(z)dz \quad \text{Equation 3.52}$$

where the element shape functions are:

$$\{N(z)\} = \frac{1}{2 - 2C + kls} \left\{ \begin{array}{l} (1 - C) \cosh kz + S \sinh kz - Skz + (1 - C + kls) \\ \frac{1}{k} [(S - klC) \cosh kz + (1 - C + kls) \sinh kz + (1 - C)kz - (S - klC)] \\ -(1 - C) \cosh kz - S \sinh kz + Skz + (1 - C) \\ \frac{1}{k} [(kl - S) \cosh kz - (1 - C) \sinh kz + (1 - C)kz + (S - kl)] \end{array} \right\}$$

$$\text{Equation 3.53}$$

with:

$$C = \cosh kl$$

$$S = \sinh kl$$

The distributed twisting moment acting on a curved girder is the distribution of forces that causes non-uniform torque. Physically, it is similar to a shear force that causes a change in the bending moment of a beam; thus, it can similarly be calculated by taking the derivative of the moment diagram. For this particular case, the distributed twisting moment is calculated by taking the derivative the torsional moment diagram.

### 3.3.2 Calculating the Torsional Moment Diagram

The torsional moment diagram is similar to a bending moment diagram; however, rather than depending upon applied transverse loads, it is a function of the torque applied to a cross-section, which varies with position along the length of a given beam. To obtain the diagram, the girder is cut at some location along its length  $x$ , and equilibrium is

established between the applied loads and the internal forces. The torsion acting on a cross-section is equal to the product of the applied loads and the eccentricity of the load with respect to the cross-sectional shear center. However, unlike straight girders, these girders are curved in the 2-D plan view space, which complicates the process. To calculate the eccentricity of the applied load with respect to the cross-sectional shear center at a cut located along the girder segment at  $x = "X"$ , a line tangent to the girder's curve at the cut is drawn. The eccentricity ( $e_{Tx}$ ) is the perpendicular distance of the applied load from the tangent line. Figure 3.13 shows a schematic of this concept, which utilizes similar triangles to calculate the eccentricity.

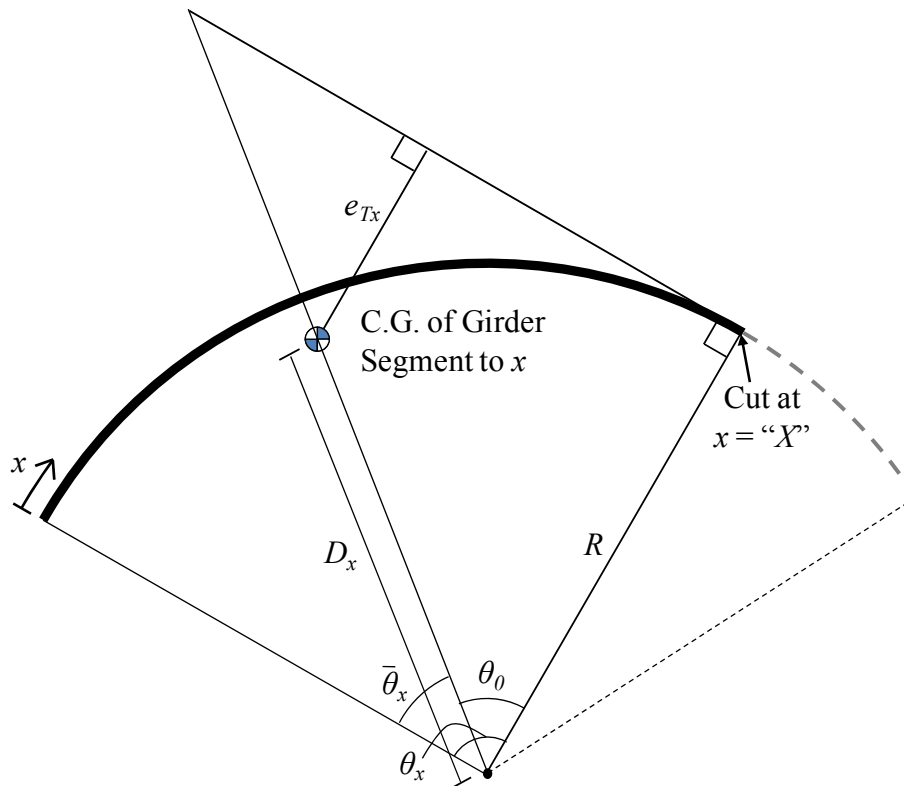


**Figure 3.13: Basic Idea for Calculating Torsion Diagram**

Where:

$x$  = Length along girder

$D_x$  = Radial distance to C.G. of the girder segment of length " $X$ "

$R$  = Radius of curvature

$\theta_x$  = Angular distance from the beginning of the girder to the cut at " $X$ "

$\bar{\theta}_x$  = Angular distance from the beginning of the girder to the C.G. of the girder segment of length " $X$ "

$e_{Tx}$  = Eccentricity between C.G. and a tangent line at the cut

The eccentricity is calculated by Equation 3.54 - Equation 3.56.

$$\theta_x = \frac{x}{R} \quad \text{Equation 3.54}$$

$$\theta_o = \theta_x - \bar{\theta}_x \quad \text{Equation 3.55}$$

$$e_{Tx} = \left( \frac{R}{\cos \theta_o} - D_x \right) \cos \theta_o \quad \text{Equation 3.56}$$

This basic idea can be expanded to consider the general case. In general, a girder will experience a rigid body rotation, which can be calculated using Equation 3.28. In a plan view, as a girder rotates, the reactions at the lift points will not be on the same plan view arc of the girder as the shear center. The shear center is a geometric property of a cross-section and is shown schematically in Figure 3.14.

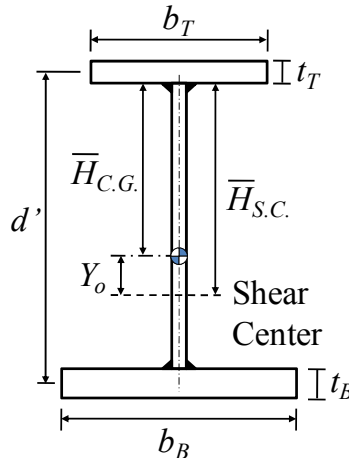


**Figure 3.14: Shear Center of a Plate Girder**

The equations needed to calculate the shear center can be found in a variety of sources (e.g., CISC 2002) and are provided in Equation 3.57 - Equation 3.59.

$$\alpha = \frac{1}{\left( 1 + \left( \frac{b_T}{b_B} \right)^3 \left( \frac{t_T}{t_B} \right) \right)} \quad \text{Equation 3.57}$$

$$\bar{H}_{S.C.} = \alpha d' - \frac{t_T}{2} \quad \text{Equation 3.58}$$

$$Y_o = \bar{H}_{C.G.} - \bar{H}_{S.C.} \quad \text{Equation 3.59}$$

The eccentricity of a girder's center of gravity from the line of support is also necessary to calculate the rigid body rotation. This rigid body rotation results in an eccentricity of the cross-sectional center of gravity and cross-sectional shear center from the line of support. The center of gravity eccentricity and shear center eccentricity are not constant for an unsymmetrical girder. Figure 3.15 shows a schematic of this concept.

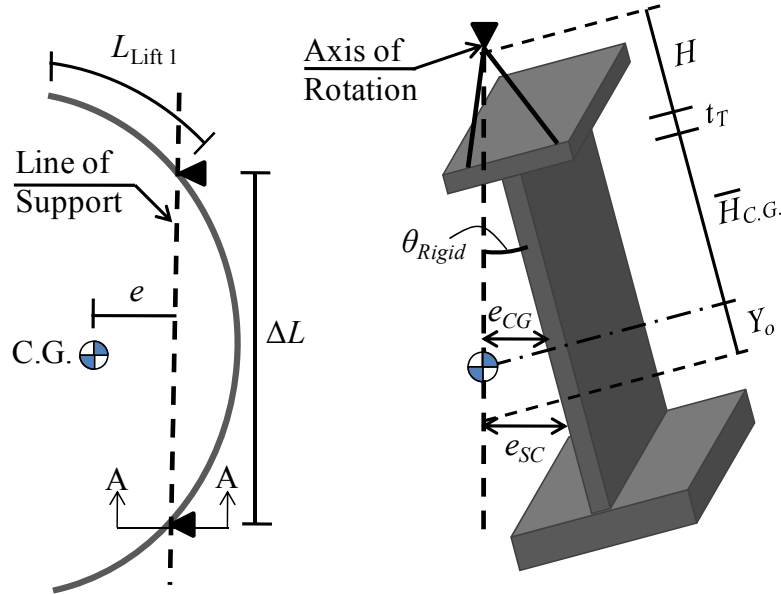


**Figure 3.15: Center of Gravity Eccentricity and Shear Center Eccentricity**

$$e_{CGi} = e \frac{(H + t_T + H_{CGi})}{(H + t_T + \bar{H}_{CG})} \quad \text{Equation 3.60}$$

$$e_{SCj} = e \frac{(H + t_T + H_{SCj})}{(H + t_T + \bar{H}_{CG})} \quad \text{Equation 3.61}$$

$$e_{Yoj-i} = e_{SCj} - e_{CGi} \quad \text{Equation 3.62}$$

To demonstrate the method used to calculate the torque applied by the lift clamp at a given location for a prismatic girder, the following figures and equations represent a step-by-step process for lift clamp 1. It can be shown that a similar formulation could be used for lift clamp 2. Figure 3.16 gives the angular distance to the lift clamps (Equation 3.63 and Equation 3.64) and calculates the line perpendicular to the line of support (Equation 3.65 and Equation 3.66). This perpendicular line represents the direction of girder movement in the plan view.

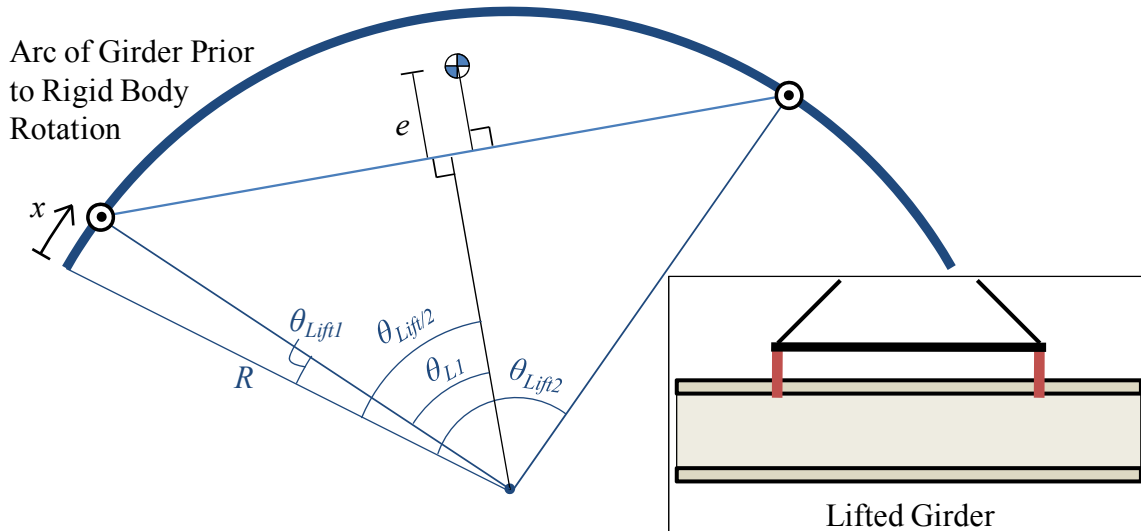


**Figure 3.16: Schematic 1<sup>st</sup> Step in Calculating Torque Applied by Lift Clamps**

where:

$e$  = Eccentricity of the girder's center of gravity from the line of support

$$\theta_{Lift1} = \frac{L_{Lift1}}{R} \quad \text{Equation 3.63}$$

$$\theta_{Lift2} = \frac{L_{Lift2}}{R} \quad \text{Equation 3.64}$$

$$\theta_{Lift/2} = \frac{\theta_{Lift1} + \theta_{Lift2}}{2} \quad \text{Equation 3.65}$$

$$\theta_{L1} = \theta_{Lift/2} - \theta_{Lift1} \quad \text{Equation 3.66}$$

Once the rigid body rotation occurs, the arc representing the shear center moves in the plan view by an amount  $e_{SC1}$  in the direction calculated in step 1. Figure 3.17 shows schematically the distance from the center of the shear center arc to the lift clamp ( $c$ ) and the angular location ( $\theta'_{L1}$ ), with the process given by Equation 3.67 - Equation 3.69.

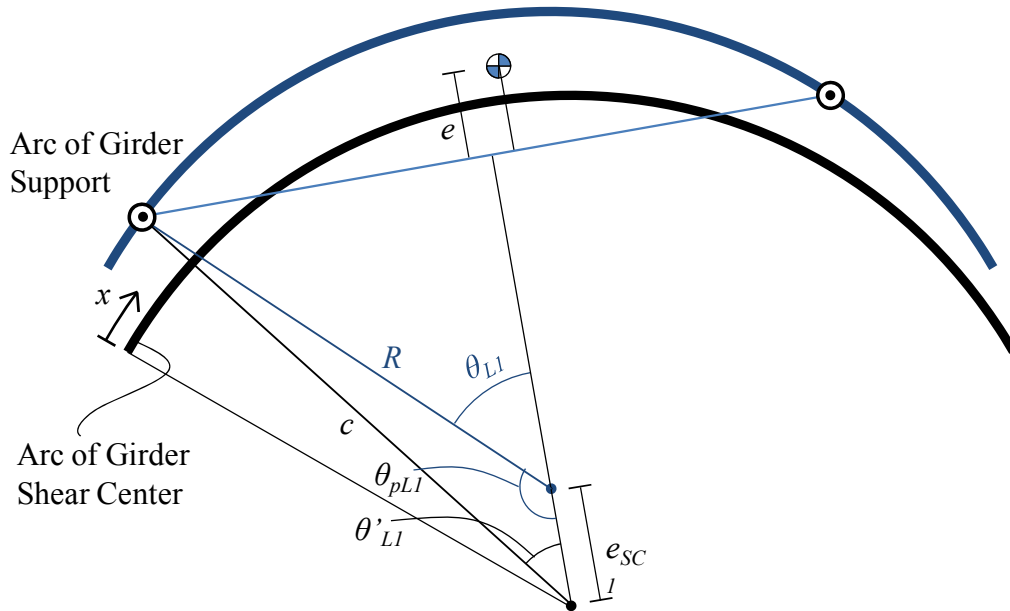


**Figure 3.17: Schematic 2<sup>nd</sup> Step in Calculating Torque Applied by Lift Clamps**

where:

$e_{SC1}$  = Shear center eccentricity for the girder's 1<sup>st</sup> cross section

$$\theta_{\pi L1} = \pi - \theta_{L1} \quad \text{Equation 3.67}$$

By the Law of Cosines:

$$c = (R^2 + e_{SC1}^2 - 2 \cdot R \cdot e_{SC1} \cdot \cos(\theta_{\pi L1}))^{1/2} \quad \text{Equation 3.68}$$

By the Law of Sines:

$$\theta'_{L1} = \sin^{-1} \left( \frac{R \cdot \sin(\theta_{\pi L1})}{c} \right) \quad \text{Equation 3.69}$$

With the necessary geometry calculated, similar triangles can be drawn, and the eccentricity can be calculated. The lift clamp reactions are determined from a static analysis and are given by Equation 3.30 for lift clamp 1 and Equation 3.32 for lift clamp 2. Figure 3.18 shows the final step in calculating the torque applied by lift clamp 1 on a cross-section of the girder located at  $x = "X"$  and is calculated using Equation 3.70 - Equation 3.72.



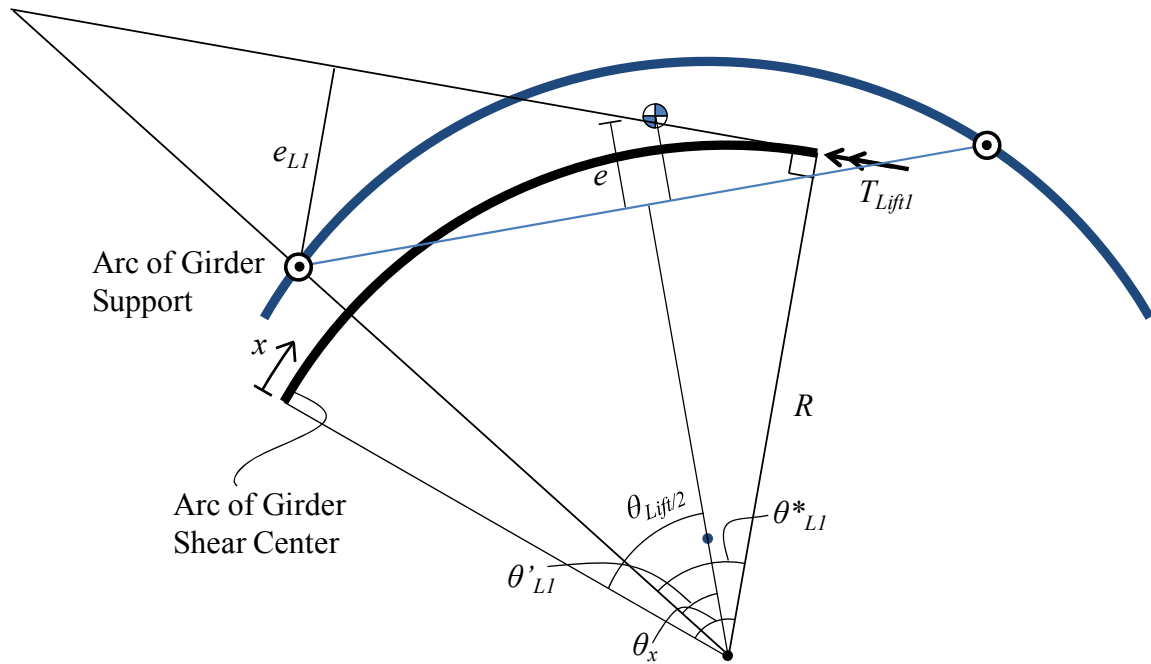


**Figure 3.18: Schematic 3<sup>rd</sup> Step in Calculating Torque Applied by Lift Clamps**

where:

$e_{L1}$  = Eccentricity of lift clamp 1 from the tangent line of the shear center

$R_{Lift1}$  = Vertical lift clamp 1 reaction

$T_{Lift1}$  = Torque applied to the cross-section by lift clamp 1

$$\theta^*_{L1} = \theta_x + (\theta'_{L1} - \theta_{Lift/2}) \quad \text{Equation 3.70}$$

$$e_{L1} = \left( \frac{R}{\cos(\theta^*_{L1})} - c \right) \cos(\theta^*_{L1}) \quad \text{Equation 3.71}$$

$$T_{Lift1} = R_{Lift1} \cdot e_{L1} \quad \text{Equation 3.72}$$

This procedure can be also be utilized for the other lift clamp. The only complication for determining the torque applied by the lift clamp for a non-prismatic girder occurs with the use of Equation 3.68. The eccentricity of the shear center should be taken as  $e_{SCi}$  for a cut on cross-section  $i$ .

The other contributor to the torsion diagram is the girder's self weight. To highlight the complications of an unsymmetrical, non-prismatic girder, the following figures demonstrate the procedure for calculating the torque acting on a cross section located at  $x = "X"$  due to the girder self weight. Figure 3.19 shows schematic diagram of



$$c = (D_{x1}^2 + e_{Yo2-1}^2 - 2 \cdot D_{x1} \cdot e_{Yo2-1} \cdot \cos(\theta_{\pi Lx1}))^{1/2} \quad \text{Equation 3.78}$$

$$\theta'_{Lx1} = \sin^{-1} \left( \frac{D_{x1} \cdot \sin(\theta_{\pi Lx1})}{c} \right) \quad \text{Equation 3.79}$$

$$\theta^*_{Lx1} = \theta_{x1} + (\theta'_{Lx1} - \theta_{Lift/2}) \quad \text{Equation 3.80}$$

$$e_{Tx1} = \left( \frac{R}{\cos(\theta^*_{Lx1})} - c \right) \cos(\theta^*_{Lx1}) \quad \text{Equation 3.81}$$

$$T_{x1} = W_{x1} \cdot e_{Tx1} \quad \text{Equation 3.82}$$

Figure 3.20 is a schematic diagram of the method to calculate the eccentricity between the girder's 2<sup>nd</sup> cross-section and the tangent line to the girder at the cut located at  $x = "X"$ , with the necessary equations to derive the applied torque given by Equation 3.83 - Equation 3.92.

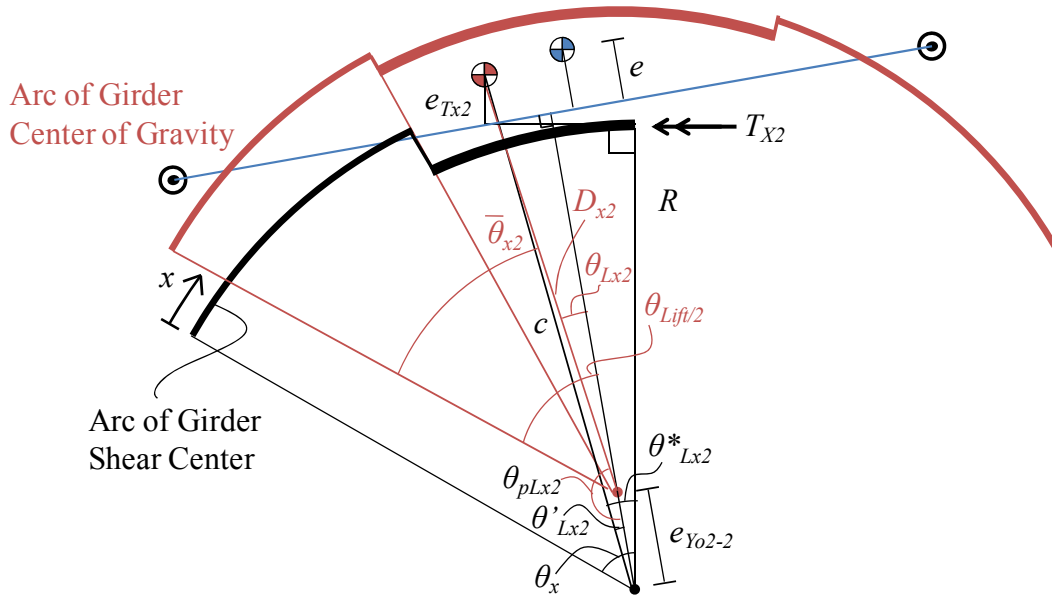


**Figure 3.20: Schematic of Unsymmetrical Non-prismatic Girder Self Weight Torque** where:

$\bar{\theta}_{x2}$  = Angular distance from the beginning of the girder to the C.G. of the portion of the girder from the beginning of 2<sup>nd</sup> cross-section to the cut at  $x = "X"$ :

$$\bar{\theta}_{x2} = \frac{\theta_2 + \theta_1}{2} \quad \text{Equation 3.83}$$

$D_{x2}$  = Radial distance to the C.G. of the portion of the girder from the beginning of 2<sup>nd</sup> cross-section to the cut at  $x = "X"$ :

$$D_{x2} = \left( \frac{2R^2}{L_2 - x} \right) \sin \left( \frac{L_2 - x}{2R} \right) \quad \text{Equation 3.84}$$

$W_{x2}$  = Weight of the portion of the girder from the beginning of 2<sup>nd</sup> cross-section to the cut at  $x = "X"$ :

$$W_{x2} = W_2 R (\theta_x - \theta_1) \quad \text{Equation 3.85}$$

$$\theta_{Lx2} = \theta_{Lift/2} - \bar{\theta}_{x2} \quad \text{Equation 3.86}$$

$$\theta_{\pi Lx2} = \pi - \theta_{Lx2} \quad \text{Equation 3.87}$$

$$c = (D_{x2}^2 + e_{Y_{O2-2}}^2 - 2 \cdot D_{x2} \cdot e_{Y_{O2-2}} \cdot \cos(\theta_{\pi Lx2}))^{1/2} \quad \text{Equation 3.88}$$

$$\theta'_{Lx2} = \sin^{-1} \left( \frac{D_{x2} \cdot \sin(\theta_{\pi Lx2})}{c} \right) \quad \text{Equation 3.89}$$

$$\theta^*_{Lx2} = \theta_{x2} + (\theta'_{Lx2} - \theta_{Lift/2}) \quad \text{Equation 3.90}$$

$$e_{Tx2} = \left( \frac{R}{\cos(\theta^*_{Lx2})} - c \right) \cos(\theta^*_{Lx2}) \quad \text{Equation 3.91}$$

$$T_{x2} = W_{x2} \cdot e_{Tx2} \quad \text{Equation 3.92}$$

The generalized forms of the above expressions are presented below in Equation 3.93 - Equation 3.99.

$$\theta_{Lxi} = \theta_{Lift/2} - \bar{\theta}_{xi} \quad \text{Equation 3.93}$$

$$\theta_{\pi Lxi} = \pi - \theta_{Lxi} \quad \text{Equation 3.94}$$

$$c = (D_{xi}^2 + e_{Y_{Oj-i}}^2 - 2 \cdot D_{xi} \cdot e_{Y_{Oj-i}} \cdot \cos(\theta_{\pi Lxi}))^{1/2} \quad \text{Equation 3.95}$$

$$\theta'_{Lxi} = \sin^{-1} \left( \frac{D_{xi} \cdot \sin(\theta_{\pi Lxi})}{c} \right) \quad \text{Equation 3.96}$$

$$\theta^*_{Lxi} = \theta_{xi} + (\theta'_{Lxi} - \theta_{Lift/2}) \quad \text{Equation 3.97}$$

$$e_{Txi} = \left( \frac{R}{\cos(\theta^*_{Lxi})} - c \right) \cos(\theta^*_{Lxi}) \quad \text{Equation 3.98}$$

$$T_{xi} = W_{xi} \cdot e_{Txi} \quad \text{Equation 3.99}$$

where:

$i$  = Cross-sectional number of the girder segment under consideration

$j$  = Cross-sectional number at the location of the cut

The torque acting on a girder along its length is the sum of the torque applied by the lift clamps and that attributed to the self-weight and is given by the following expression:

$$T(x) = \sum_{i=1}^n (W_{xi} \cdot e_{Txi}) - T_{Lift1} - T_{Lift2} \quad \text{Equation 3.100}$$

where:

$n$  = Number of different cross sections to the location of the cut at  $x = "X"$

To demonstrate the expected results from a 125-foot prismatic girder lifted at two points, the following graphs show the typical torsion diagram. The graphs show how the response changes as a function of the location along the span where the girder is lifted symmetrically and the first lifting location is positioned 25 ft., 26.375 ft., 29.75 ft., and 31.25 ft. from the beginning of the girder, respectively.

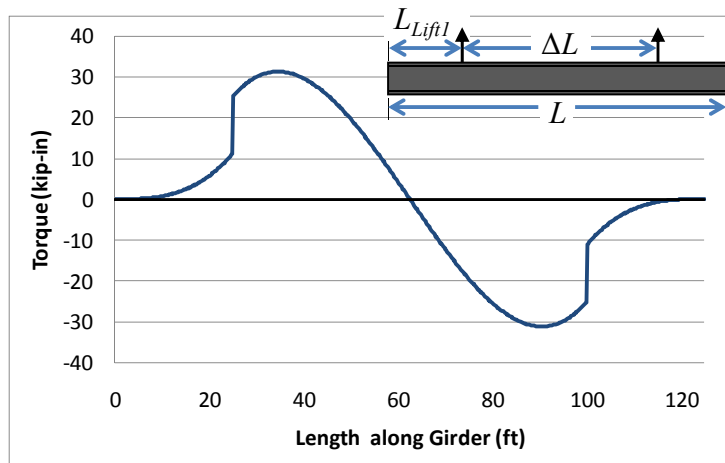


**Figure 3.21: Torsion Diagram for  $L_{Lift1}/L = 0.2$**

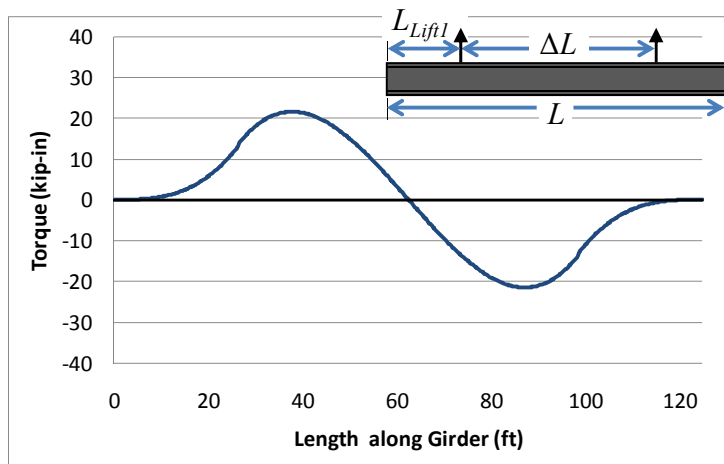


**Figure 3.22: Torsion Diagram for  $L_{Lift}/L = 0.211$**

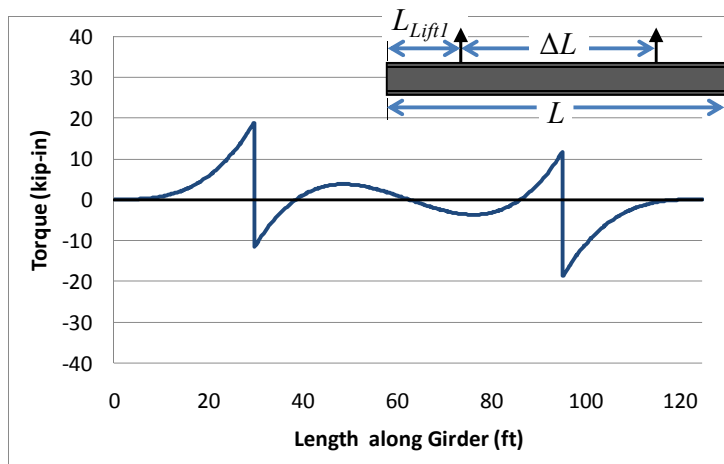


**Figure 3.23: Torsion Diagram for  $L_{Lift}/L = 0.238$**

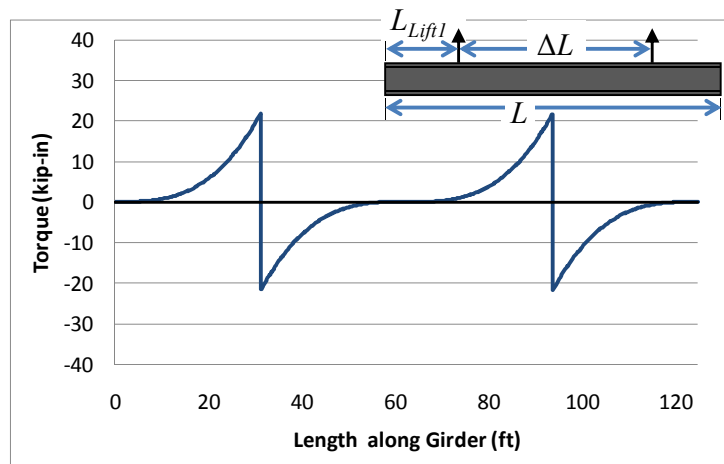


**Figure 3.24: Torsion Diagram for  $L_{Lift}/L = 0.25$**

With the torsion diagram determined, the derivative of the function can be calculated to obtain the distributed torsional moment. The derivative can be computed numerically with many schemes such as central difference, forward difference, or backwards difference. Equation 3.101 – Equation 3.103 give these linear approximations. Rather than using any of these schemes, however, a higher-order approximation of the derivative was chosen—called a five-point one dimensional stencil (Numerical Differentiation [www.Wikipedia.org](http://www.Wikipedia.org))—to provide results that were deemed suitably accurate by the researchers and using a minimum number of elements. This numeric differentiation scheme utilizes a quadratic approximation of the derivative. An arbitrarily small  $h$  is chosen, and the function is given by Equation 3.104.

Central Difference: 
$$t(x) = \frac{dT}{dx} = \frac{T(x - h) + T(x + h)}{2h} \quad \text{Equation 3.101}$$

Backward Difference: 
$$t(x) = \frac{dT}{dx} = \frac{T(x - h) + T(x)}{h} \quad \text{Equation 3.102}$$

Forward Difference: 
$$t(x) = \frac{dT}{dx} = \frac{T(x) + T(x + h)}{h} \quad \text{Equation 3.103}$$

Five-Point 1-D stencil:

|  |                       |
|--|-----------------------|
| $t(x) = \frac{dT}{dx} = \frac{T(x - 2h) - 8 * T(x - h) + 8 * T(x + h) - T(x + 2h)}{12h}$ | <b>Equation 3.104</b> |
|--|-----------------------|

With the distributed torsional moment computed, Equation 3.52 can be calculated by means of numerical integration. A frequently used numerical integration technique utilizes Gaussian Quadrature to approximate the integral of a function. The interval of integration must be transformed from the arbitrary points  $[a,b]$  to  $[-1,1]$ , which is accomplished using Equation 3.105. By evaluating  $f(x)$  at the Gauss points and multiplying by the appropriate weighting function, Equation 3.106 is obtained.

$$\int_a^b f(x)dx = \frac{(b - a)}{2} \int_{-1}^1 f\left(\frac{b - a}{2}x + \frac{a + b}{2}\right) dx \quad \text{Equation 3.105}$$

$$\frac{b-a}{2} \sum_{i=1}^n w_i f\left(\frac{b-a}{2}x_i + \frac{a+b}{2}\right) \quad \text{Equation 3.106}$$

To increase the accuracy of the integration with a minimum of elements, a 5-point integration was performed with the following integration points and weighting functions:

| Integration Points                           | Weighting Function                         |
|--|--|
| $x_1 = -\frac{\sqrt{245 + 14\sqrt{70}}}{21}$ | $\omega_1 = \frac{322 - 13\sqrt{70}}{900}$ |
| $x_2 = -\frac{\sqrt{245 - 14\sqrt{70}}}{21}$ | $\omega_2 = \frac{322 + 13\sqrt{70}}{900}$ |
| $x_3 = 0$                                    | $\omega_3 = \frac{128}{225}$               |
| $x_4 = \frac{\sqrt{245 - 14\sqrt{70}}}{21}$  | $\omega_4 = \frac{18 + 13\sqrt{30}}{36}$   |
| $x_5 = \frac{\sqrt{245 + 14\sqrt{70}}}{21}$  | $\omega_5 = \frac{322 - 13\sqrt{70}}{900}$ |

### 3.4 CALCULATION OF DISPLACEMENTS AND LONGITUDINAL STRESSES

The previous sections described the method used to calculate the cross-sectional twist along the length of the girder by discretizing the girder into 1-D finite elements for comparison to a serviceability limit. In addition, it is important that stresses do not exceed a strength limit state. The longitudinal stress was calculated by combining the strong-axis bending stress, weak-axis bending stress, and the warping normal stress. The strong and weak axis bending stresses were calculated by combining the Euler beam bending stiffness terms to the element stiffness matrix for the discretized girder.

Figure 3.25 is a schematic diagram of an I-girder with the two nodes of the represented 1-D beam element and the element degrees of freedom. Previously, the stiffness terms associated with the  $\theta_{x1}$ ,  $\theta'_{x1}$ ,  $\theta_{x2}$ , and  $\theta'_{x2}$  degrees of freedom were described. The necessary beam stiffness terms can be found in McGuire et al. (2000). The appropriate stiffness terms, associated displacement degrees of freedom, and fixed-end force vector are given by Equation 3.107. In computing the response of a curved



girder while being lifted, the self-weight of the girder is decomposed into components as a result of the rigid body rotation ( $\theta_{Rigid}$ ), which results in the fix-end force vector.

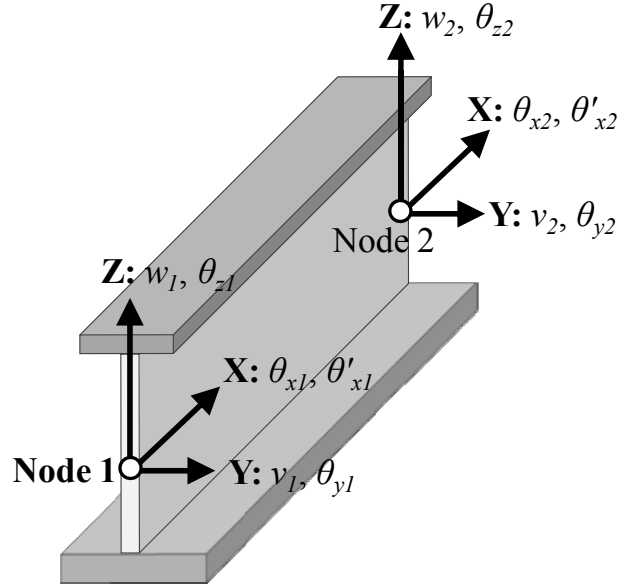


**Figure 3.25: Discretized Girder 1-D Beam Element Degrees of Freedom**

$$\begin{bmatrix} \frac{12EI_z}{L^3} & \frac{6EI_z}{L^2} & 0 & 0 & -\frac{12EI_z}{L^3} & \frac{6EI_z}{L^2} & 0 & 0 \\ & \frac{4EI_z}{L} & 0 & 0 & -\frac{6EI_z}{L^2} & \frac{2EI_z}{L} & 0 & 0 \\ & & \frac{12EI_y}{L^3} & -\frac{6EI_y}{L^2} & 0 & 0 & -\frac{12EI_y}{L^3} & -\frac{6EI_y}{L^2} \\ & & & \frac{4EI_y}{L} & 0 & 0 & \frac{6EI_y}{L^2} & \frac{2EI_y}{L} \\ & & & & \frac{12EI_z}{L^3} & -\frac{6EI_z}{L^2} & 0 & 0 \\ & & & & & \frac{4EI_z}{L} & 0 & 0 \\ & & & & & & \frac{12EI_y}{L^3} & \frac{6EI_y}{L^2} \\ & & & & & & & \frac{4EI_y}{L} \\ & & & & & & & & \text{sym.} \end{bmatrix} \begin{Bmatrix} v_1 \\ \theta_{y1} \\ w_1 \\ \theta_{z1} \\ v_2 \\ \theta_2 \\ w_2 \\ \theta_2 \end{Bmatrix} = \begin{Bmatrix} -\frac{wL}{2} \sin(\theta_{Rigid}) \\ -\frac{wL^2}{12} \sin(\theta_{Rigid}) \\ -\frac{wL}{2} \cos(\theta_{Rigid}) \\ \frac{wL^2}{12} \cos(\theta_{Rigid}) \\ -\frac{wL}{2} \sin(\theta_{Rigid}) \\ \frac{wL^2}{12} \sin(\theta_{Rigid}) \\ -\frac{wL}{2} \cos(\theta_{Rigid}) \\ -\frac{wL^2}{12} \cos(\theta_{Rigid}) \end{Bmatrix}$$

**Equation 3.107**

where:

$w$  = Self weight of the girder per unit length

The element forces at any node point were calculated from the product of the element stiffness matrix and nodal displacements with the addition of the element fixed-

end forces. The element forces were calculated so that both the strong and weak axis bending moments could be utilized to calculate the longitudinal stresses. Additionally, the bending moments were compared to the critical buckling moment used in the stability check. The stress was calculated separately for each flange tip, because the combination of the longitudinal stresses result in a nonuniform stress distribution. The absolute maximum stress was required for the strength limit check. Figure 3.26 is a schematic of the individual components that make up the longitudinal flange stress. The strong-axis bending stress was calculated using Equation 3.108. The weak-axis bending stress was calculated using Equation 3.109. The warping normal stress was calculated using Equation 3.110. The combination of these three equations results in the longitudinal stress as shown in Equation 3.111.

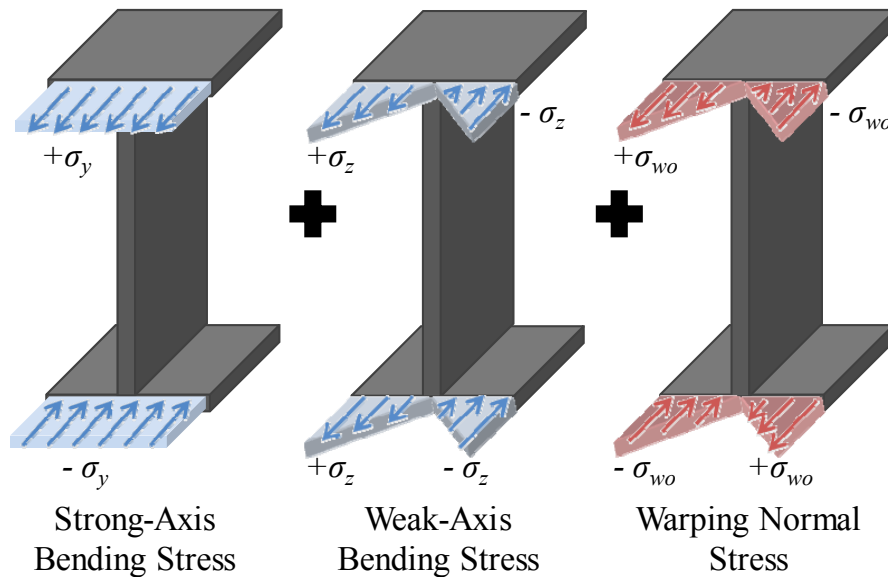


**Figure 3.26: Longitudinal Stress Components**

$$\sigma_y = \frac{M_y z}{I_y} \quad \text{Equation 3.108}$$

$$\sigma_z = \frac{M_z y}{I_z} \quad \text{Equation 3.109}$$

$$\sigma_{wo} = EW_{no} \theta''_x \quad \text{Equation 3.110}$$

$$\sigma_L = \sigma_y + \sigma_z + \sigma_{wo} \quad \text{Equation 3.111}$$

where:

$M_y$  = Moment in the y-axis

$z$  = Z-distance from the flange tip to the centroid

$I_y$  = Moment of inertia of the girder about the y-axis

$M_z$  = Moment in the z-axis

$y$  = Y-distance from the flange tip to the centroid

$I_z$  = Moment of inertia of the girder about the z-axis

$E$  = Young's modulus of girder

$W_{no}$  = Normalized warping constant, and

$$W_{no} = \frac{b_f D}{4}$$

$b_f$  = Flange width

$D$  = Girder depth

$\theta''_x$  = Second derivative of the cross-sectional twist

The second derivative of the cross-sectional twist was obtained using a central difference scheme as shown in Equation 3.101 and the change in twist ( $\theta'_x$ ) obtained from the analysis of the girder. The maximum moment was compared to the critical buckling moment obtain from the modification to Timoshenko's lateral-torsional buckling equation with a  $C_b$  factor as described in Chapter 2.

Utilizing the calculated out-of-plane displacement, the slight change in the location of the center of gravity was determined. A revised eccentricity of the line of support and center of gravity and then used to recalculate the rigid body rotation to provide additional accuracy.

## 3.5 UT LIFT SPREADSHEET

### 3.5.1 Introduction and Purpose

To facilitate the use of the expressions that were developed in the last sections, a macro-enabled Excel spreadsheet program was developed and named "UT Lift." This computational tool is capable of predicting the behavior of curved I-girders during lifting. The program allows a user to input information about the girder being analyzed, and then the spreadsheet utilizes the previously developed equations and procedures to provide a linear approximation of a girder's deformational behavior during lifting.

The spreadsheet provides a tool that will primarily be used by erectors or erection engineers. The program can be used to determine the ideal location for girder lifting as well as the girder deformations for locations different than the ideal location. The program also provides an indication of the safety of a girder during lifting. The program was developed assuming the girder segment is lifted with one crane and two lift clamps. This lifting technique one of the most economical due to the use of a single crane and is commonly used in the construction of curved I-girder bridges as shown in Figure 3.27. The program is conservative if a lifting scenario with more than 2 lifting points is used.



***Figure 3.27: Lifting of a Horizontally Curved Steel I-Girder  
with 1 Crane & 2 Lift Clamps***

The spreadsheet was developed with clearly indicated input cells for information on the lifting geometry and cell highlighting to call attention to the calculated results. Green-colored cells are designated for input to be given, and blue-colored cells highlight the notable calculated results. The current spreadsheet allows for the analysis of a girder segment with up to eight different cross-sections and 18 cross-frame locations along the length of the girder segment.

### 3.5.2 Girder Input Sheet

The spreadsheet is divided into four separate tabs. The first tab (**Girder Input**) contains two pages that are dedicated to the required geometric properties of the girder and the cross-frame information including:

- 1) the number of different cross-sections along the girder,
- 2) the radius of curvature of the girder segment,
- 3) the plate dimensions for each cross-section,
- 4) the arc length measured along the girder's centerline of each cross-section,
- 5) the number of cross-frames attached to the girder segment during lifting,
- 6) the cross-frame width,
- 7) the weight of each cross-frame,
- 8) the location of the cross-frames, and
- 9) the positioning of the cross-frames, including cross-frames only on the inside of the curve, only on the outside of the curve, or on both sides of the girder.

Screen shots of these pages are shown in Figure 3.28 and Figure 3.29.

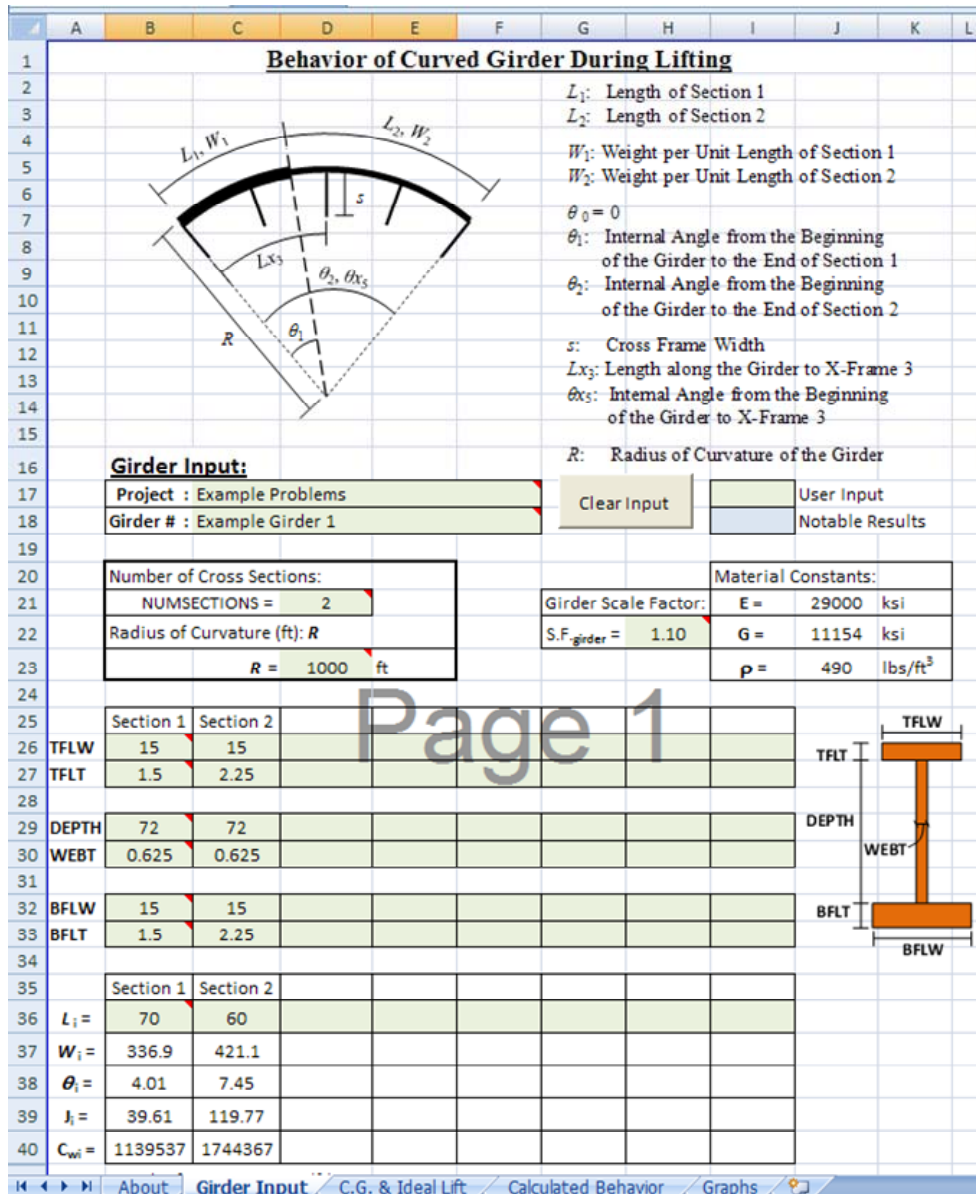


**Figure 3.28: Screen Shot of UT Lift Girder Geometric Input**

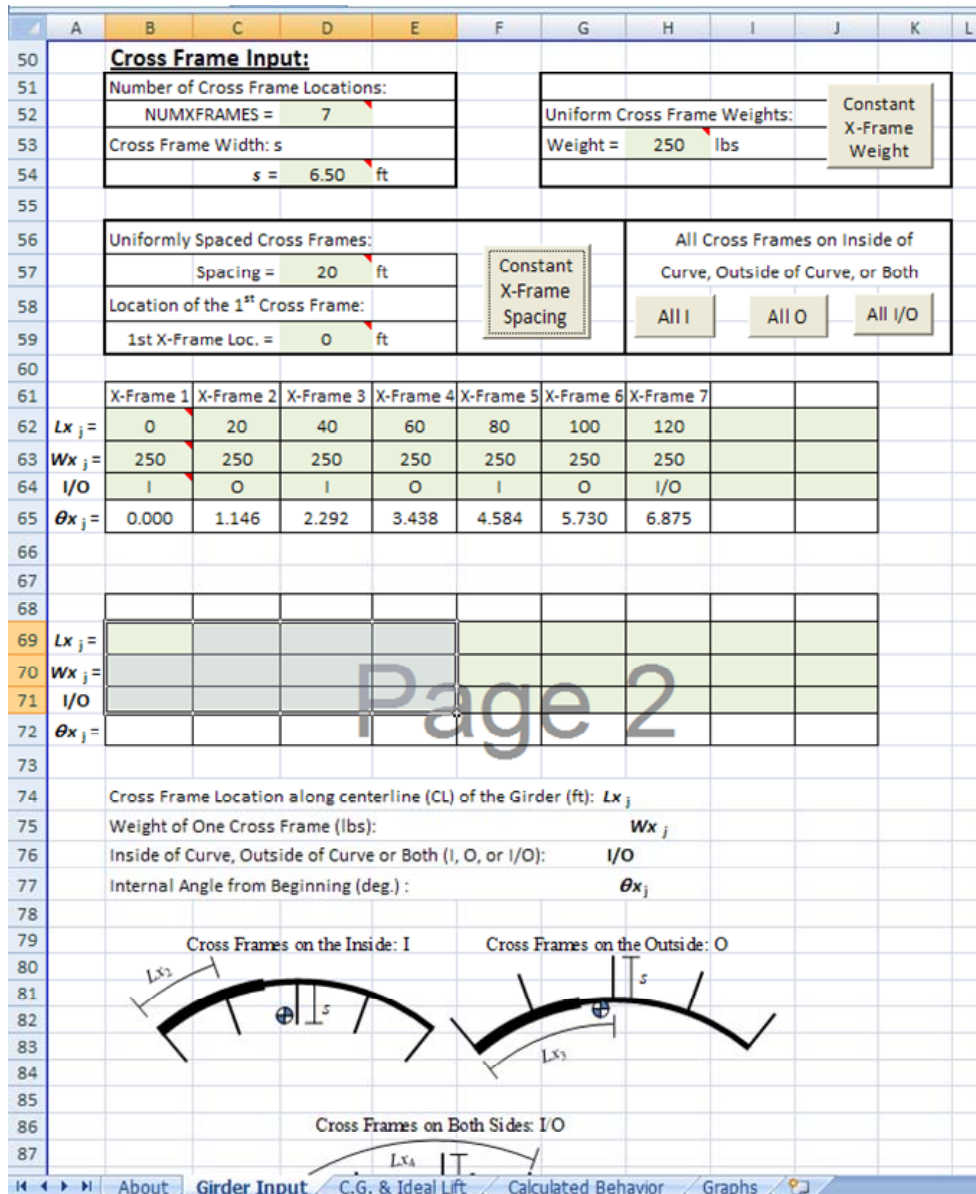


**Figure 3.29: Screen Shot of UT Lift Girder Cross Frame Input**

The project name and the name of the specific girder analyzed can be specified for record-keeping purposes. The girder scale factor is multiplied by the girder self-weight and allows an engineer to match shipping weight if available or it accounts for other auxiliary elements (shear studs, stiffeners etc.). The sign convention for the radius of curvature is positive for a right curve looking ahead station from the girder's beginning. A "Clear Input" button is available to allow a user to quickly erase all input values that are entered. Once pressed, it will prompt a user to confirm that they want all

the input cells to be deleted before proceeding with the operation. Figure 3.30 provides a schematic of a girder cross-section with the necessary plate dimensions, including:

- 1) top flange width (TFLW),
- 2) top flange thickness (TFLT),
- 3) web depth (DEPTH),
- 4) web thickness (WEBT),
- 5) bottom flange thickness (BFLT), and
- 6) bottom flange width (BFLW).

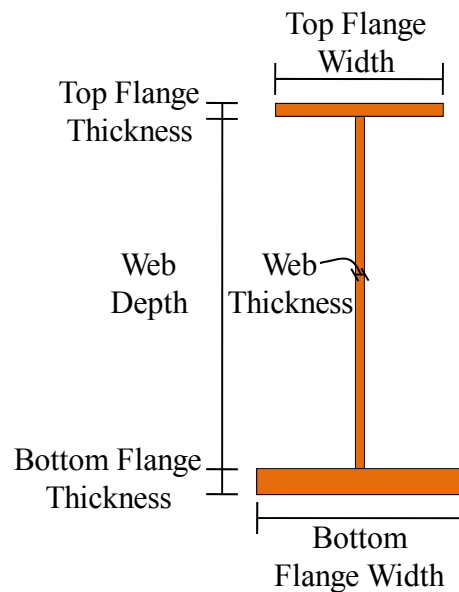


**Figure 3.30: Plate Dimensions**

The cross-frame width is needed to determine the center of gravity of an individual cross-frame. The cross-frame center of gravity is assumed to be located midway between adjacent girders (girder spacing divided by two). Therefore, the girder spacing should be specified as the cross-frame width. The weight of a cross-frame should only include the weight of a single cross-frame even if they are located on both sides of the girder for a given location. The cross-frames need to be specified as either located on the inside of the curve, on the outside of the curve, or on both sides of the curve for a given cross-frame location as shown in Figure 3.31. By selecting “I/O”, the weight will be multiplied by two for locations where cross-frames are present on both



sides of the girder. The positioning of each cross-frame—on the inside, outside, or both sides of the girder—is specified for each cross-frame location and does not necessarily have to be consistent down the length of the girder. The cross-frame locations must be specified in ascending order down the length of the girder. The flexibility of specifying cross frame locations as inside the curve, outside the curve, or both sides for each individual cross-frame allow an erector to adjust the cross-frames included in the lift in case they need to adjust the rigid body rotation of a given segment.

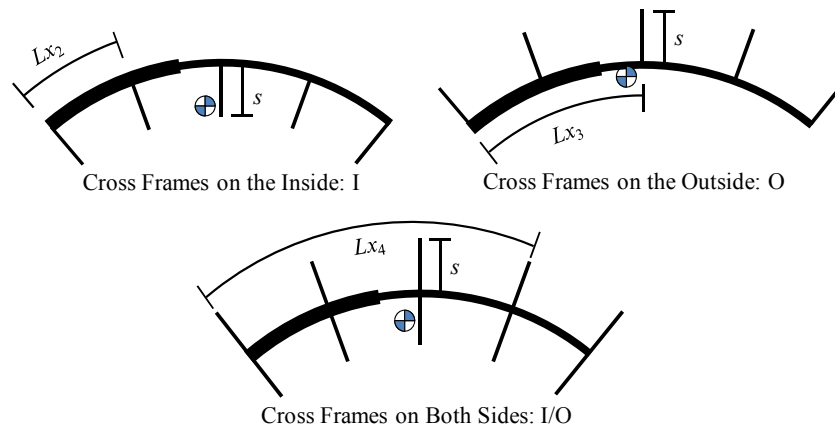


**Figure 3.31: Options of Cross Frame Location**

For girders with constant cross-frame spacing, the “Uniformly Spaced Cross Frame:” section allows a user to specify the cross-frame spacing and the first cross-frame location. Then, the correct input will appear in the cells once the “Constant X-Frame Spacing” button is pressed. There are three buttons for quickly specifying the positioning of the cross-frames: “All I”, “All O”, and “All I/O”. By pressing one of these buttons, all of the cross-frame location cells will be propagated with the appropriate value. The program does not require uniform cross-frame locations, but these buttons assist users with girders that have constant spacing. Once the number of cross-sections and the number of cross-frames are specified, any input located in columns associated with cross-sections or cross-frames beyond the specified values will be ignored and can be deleted without affecting the analysis.

### 3.5.3 C.G. & Ideal Lift Sheet

The spreadsheet calculates several useful pieces of information for future calculations as well as comparisons to known information for checking the computed results including:

- 1) the total girder length,
- 2) the total girder weight,
- 3) the longitudinal and radial location of the girder segment's center of gravity,
- 4) the lift clamp locations that result in zero rigid body rotation and equal lift clamp forces, and
- 5) the reactions at the lift clamps for the zero rigid body rotation location.

The location of the girder segment's center of gravity is given as the length along the girder and an offset from the girder centerline. The center of gravity offset is assumed to be on the inside of the curve; thus, this direction is considered a positive offset. There are an infinite number of lines that intersect the curve at two points and pass through the center of gravity. However, there exists a unique line that passes through the center of gravity and gives a lift clamp location that results in equal minimized forces. This positioning of the lift clamps is optimal with regard to the girder's rigid body rotation. The reaction for these lift clamps is equal to the total girder weight divided by two. A screen shot of the page in UT Lift that performs these calculations is shown in Figure 3.32.

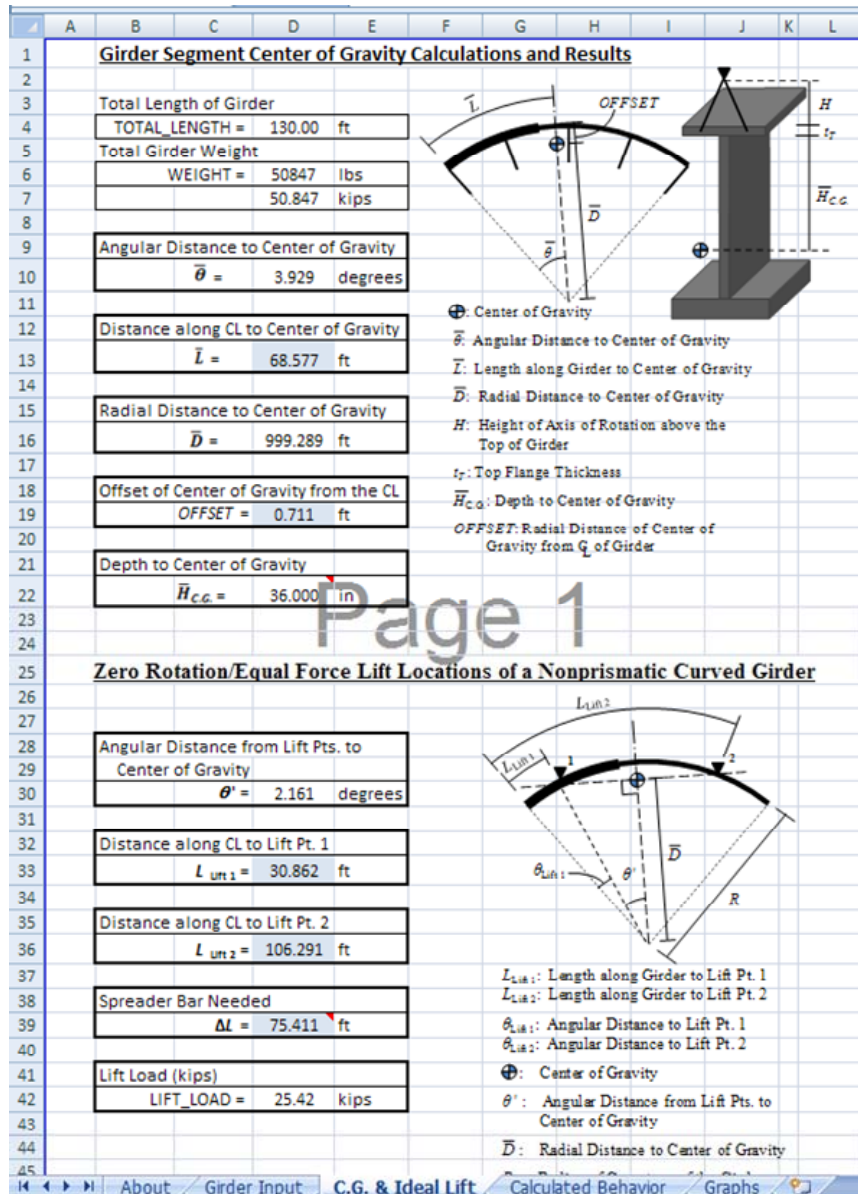
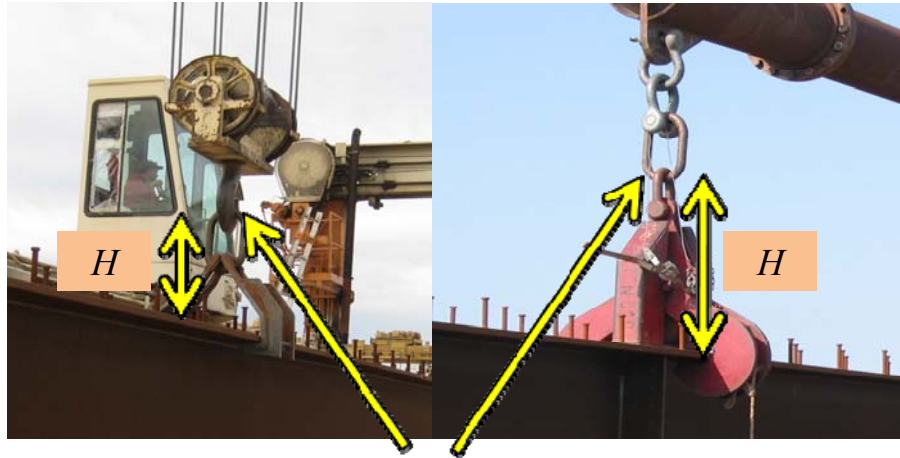


Figure 3.32: Screen Shot of UT Lift C.G. & Ideal Lift Output

### 3.5.4 Calculated Behavior Sheet

This sheet allows for the behavior of a girder segment lifted at specified locations to be analyzed. This analysis requires both the location of the lift clamps and the location of the axis of rotation above the top of the girder to be specified by the user. The axis of rotation is the location within the lifting apparatus where rotation is free to occur. For the case of a single crane with two lift clamps separated by a spreader bar, this location is the

point on the lift clamp that allows for rotation. Figure 3.33 demonstrates the assumed axis of rotation for two different lift clamps. In the figure, this height is approximately 30 in., and based on parametric studies, this value has been determined to provide reasonable predictions of response. It should be noted, however, that a smaller value will result in larger calculated rigid body rotations (i.e., a more conservative estimate of response).



Assumed Axis of Rotation

**Figure 3.33: Definition of the Height to Axis of Rotation (Schuh 2008)**

Based on the user specified lift locations, the eccentricity of the center of gravity from the line of support is calculated, and the subsequent rigid body rotation is computed. The reactions at the lift clamps are also provided; it is important to note that they may not be equal as the analysis treats them as independent lift points. For girders lifted with a single crane and a spreader bar, the lift clamp forces must be equal for static equilibrium. A warning is issued for unequal lift forces, but the program will compute an answer even if the forces are not the same. Such a situation may arise in the case where a girder is lifted with two cranes. When the “**Calculate Rotation & Stress**” button is pressed, a macro within the spreadsheet will carry out the linear finite element analysis described previously to approximate the girder’s cross-sectional twist.

The results of the analysis are provided on this sheet and include the predicted total rotations and stresses for the lifted girder. The rotations include both the rigid body rotation and an approximation of the cross-sectional twist. The reported stresses include the strong axis bending stresses, the weak axis bending stresses, and the warping normal

stresses. The maximum stresses are reported at both lift locations and at the midpoint between the lift clamps. The maximum rotations are reported at both ends of the girder as well as the midpoint between the lift clamps. The spreadsheet also provides an estimate of the critical buckling load as determined from a modified form of Timoshenko's lateral torsional buckling equation. The modified equation and detailed description of its development are provided in Schuh (2008) and Farris (2008), a summary of which is provided in Chapter 2. The critical buckling load rarely controls the design for lifting of curved girders, but it is a reasonable estimate for the lifting of straight girders and mildly curved girders.

Screen shots of the pages described in this section are shown in Figure 3.34 and Figure 3.35.

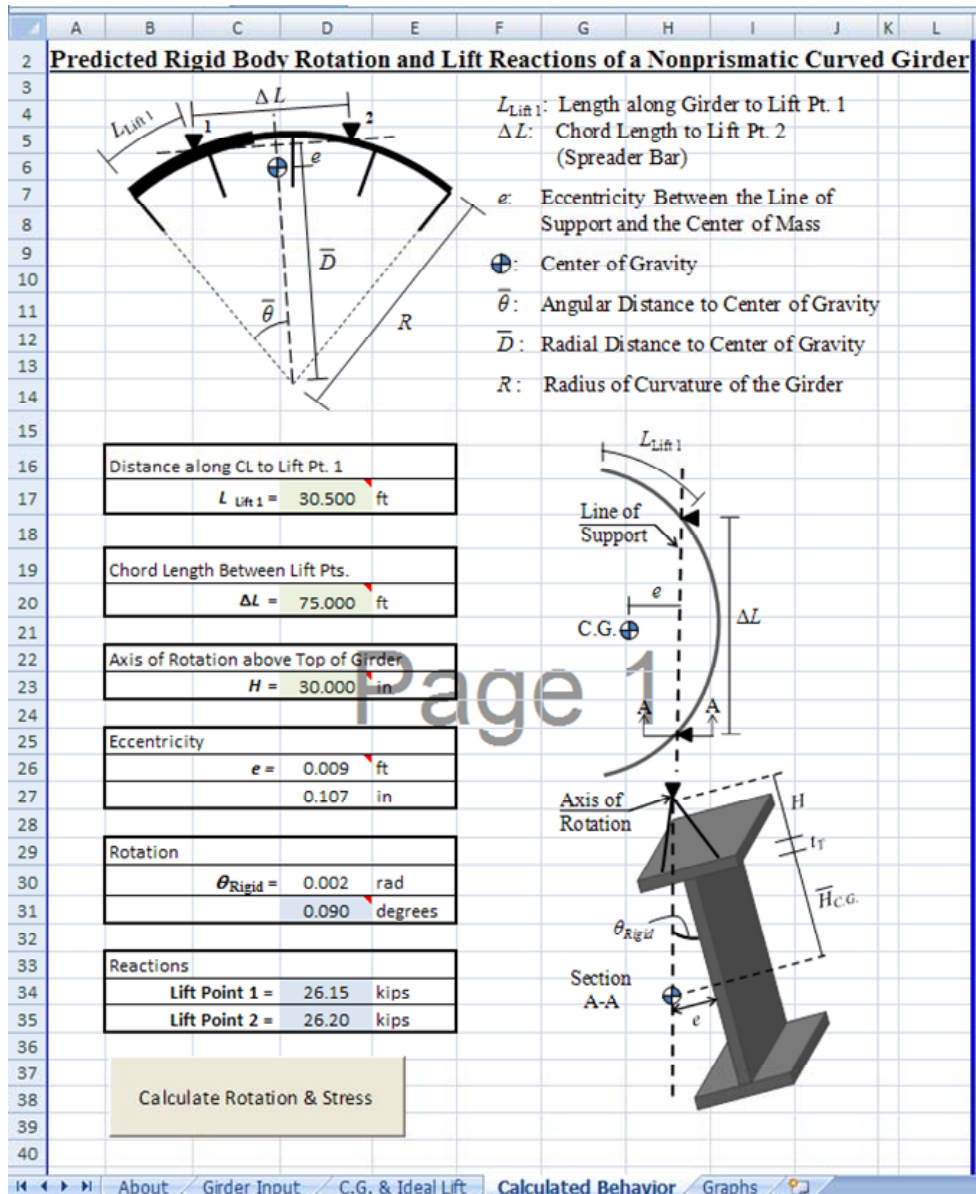
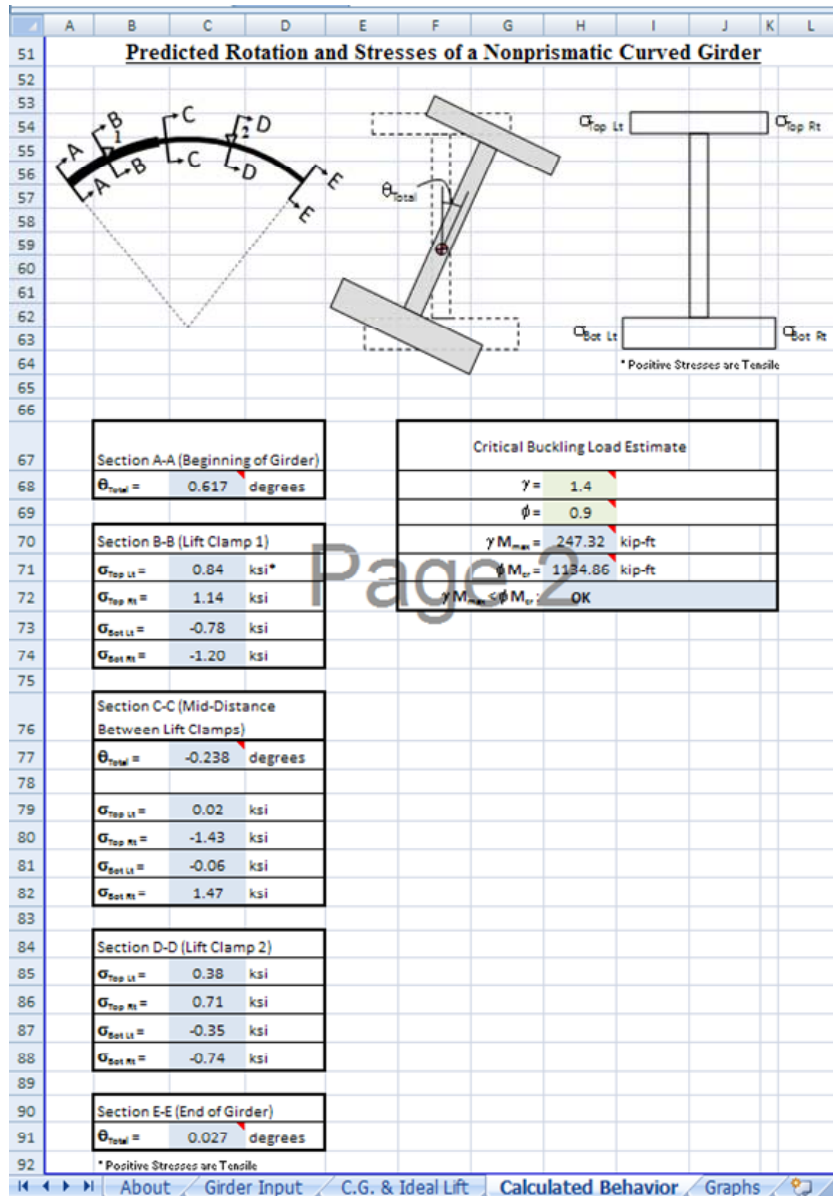


Figure 3.34: Screen Shot of UT Lift Calculated Behavior Input



**Figure 3.35: Screen Shot of UT Lift Calculated Behavior Output**

### 3.5.5 Girder Deformations and Torsional Diagrams

The analysis tool also provides three useful graphs to assist an engineer in evaluating the behavior of a girder during lifting. The first graph is an out-of-plane displacement diagram that gives the displacement of the top and bottom of the girder along its length. The second graph, and possibly the most important one, provides the total rotation of the girder along the length. For an infinitely stiff girder this graph would

be a horizontal line with a value equal to the rigid body rotation. As the girder becomes more torsionally flexible, the graph will have greater variation in the rotation along the length, an indication of potential stability issues during lifting. Finally, the third graph provided is the torsion diagram, which gives an indication of the torsional forces acting on the girder during lifting. A screen shot of this page with all three graphs is shown in Figure 3.36.

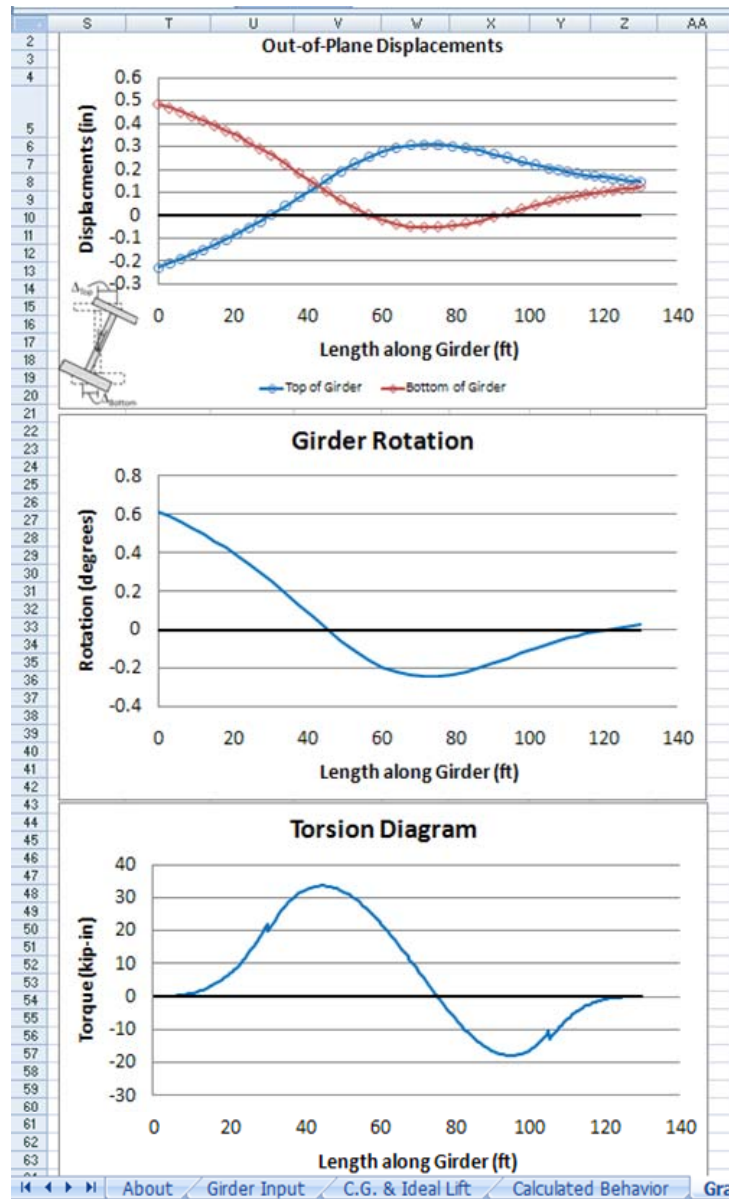


**Figure 3.36: Screen Shot of UT Lift Graphical Output**



Users of the program should be aware of its limitations so that they can understand the applicability of the results to the problem being solved. The limits on geometric input was outlined early in this chapter. The cross-sectional twist is calculated using a linear finite element analysis and does not iterate to account for nonlinear effects. Research carried out during this project has found that second-order effects are generally minimal if the analysis is limited to small total rotations ( $< \sim 1.5$  degrees). The specific allowable rotation limit should be controlled by the erector's preference.

### 3.5.6 Verification of UT Lift

Verification of the UT Lift analysis tool was carried out by comparing analysis results obtained from the spreadsheet program with those from the 3-D nonlinear finite element model developed in ANSYS and utilized in the parametric study described previously. In particular, the cross-sectional twist and the rigid body rotation were calculated within UT Lift, and the total rotation was compared to a geometric nonlinear analysis in ANSYS. Figure 3.37 – Figure 3.40 show a set of comparisons between the rotational behavior predicted by UT Lift and the calculated rotation of the mid-height of the girder from the 3-D analysis in ANSYS.

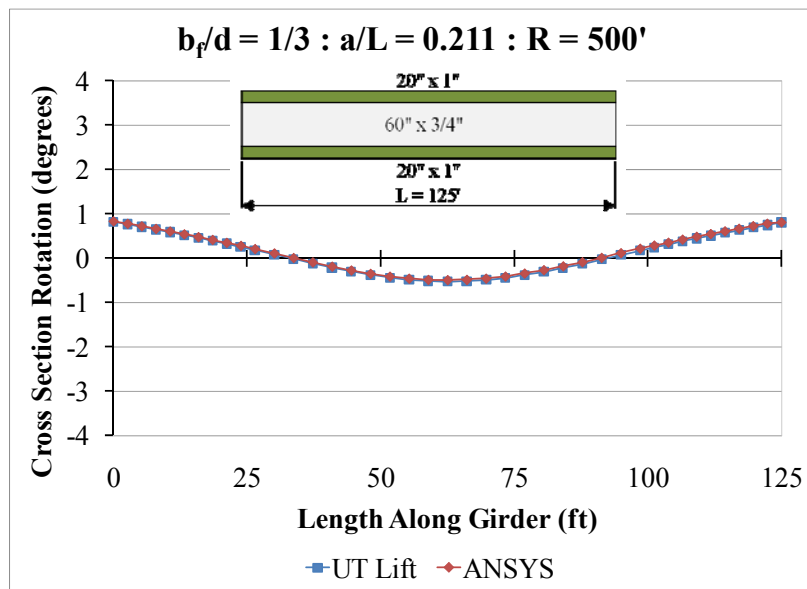


**Figure 3.37: UT Lift Validation Graph 1**

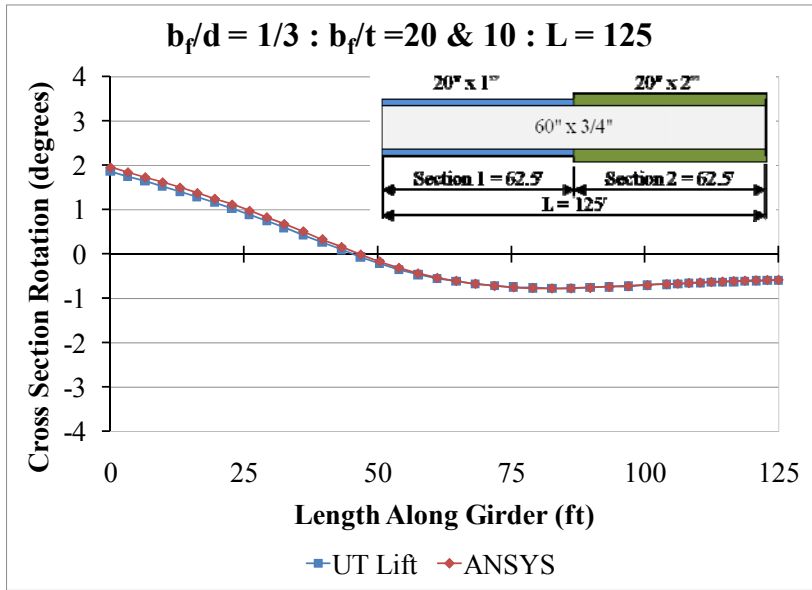


**Figure 3.38: UT Lift Validation Graph 2**

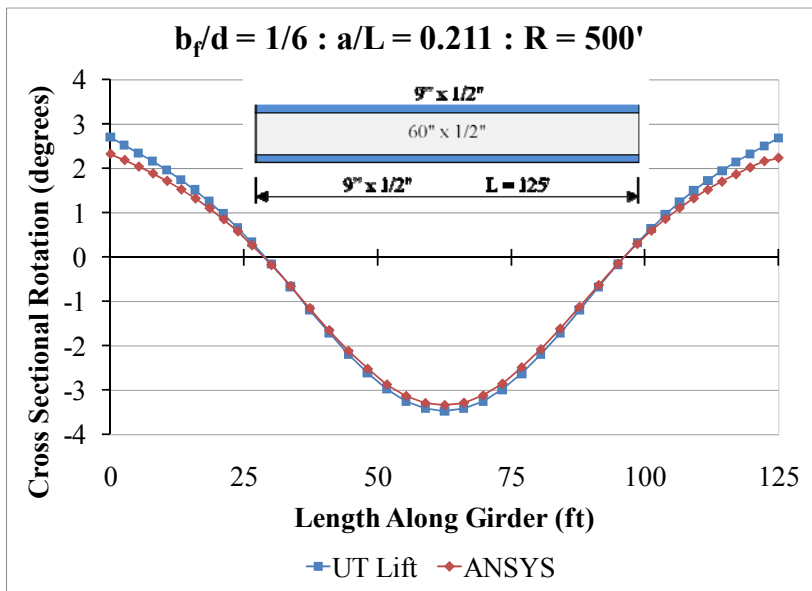


**Figure 3.39: UT Lift Validation Graph 3**

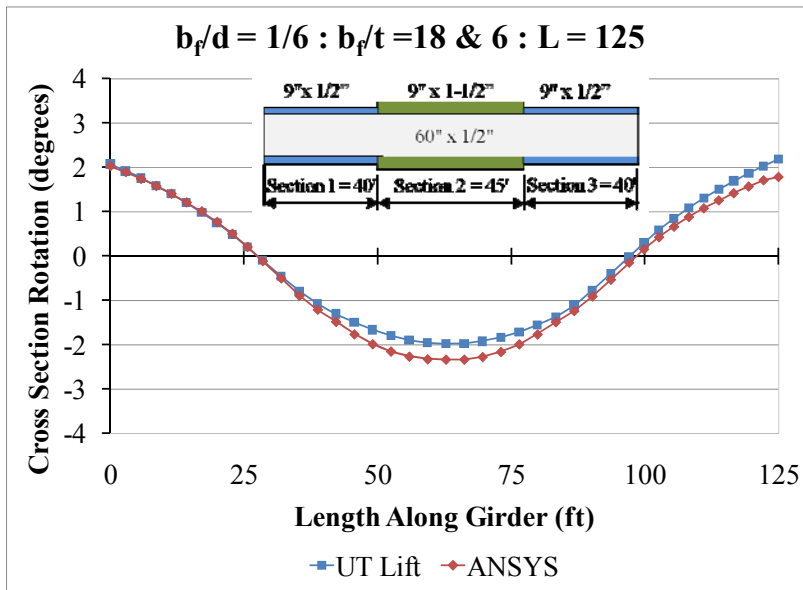


**Figure 3.40: UT Lift Validation Graph 4**

It should be noted that, for the comparisons shown above, the rigid body rotations were relatively small, which led to good agreement of the total rotation between UT Lift and the ANSYS model. For cases with larger rigid body rotations than those indicated in the above examples, the linear approximation obtained from UT Lift deviates from the nonlinear analysis results, especially for the case of slender girders ( $b_f/D \leq 1/6$ ). Nevertheless, UT Lift provides a quick, accurate, user-friendly analysis tool for engineers and erectors.

This section has provided detailed information and analytical solutions for a girder lifted at two points. Another common method for lifting curved girders utilizes two or more cranes for the lifting of long, heavy segments, often with four or more lift points. Several parametric analyses were completed to study this behavior, and it was found that the use of more than two lift points greatly increases the moment gradient of the girder along its length. This increase in moment gradient has a significant stabilizing effect on the girder, but it does not entirely prevent the possibility of buckling. It is advantageous for an erector to space the lifting points along the length to maximize the moment gradient. Additionally, the height of the axis of rotation from the center of gravity is generally increased for two cranes with separate spreader bars; the axis of rotation is the top of the lifting harness close to the top of the cranes. This increase in the

height of the axis of rotation reduces the rigid body rotation experienced by the girder, thus reducing weak axis bending effects. In general, the addition of lifting points is beneficial, but for a simplified analysis procedure such as the one implemented in UT Lift, a conservative approach is recommended. Accordingly, in the case where a girder is lifted with two cranes, an engineer can utilize the previous equations and assume the girder is lifted at the center of the two spreader bars.

### 3.5.7 UT Lift Example

The capabilities of UT Lift are outlined with the following example from a 2-span bridge with skewed supports and varying cross-frame locations. The girder under consideration is over the middle pier and has three cross-sections and 13 cross-frame locations. Figure 3.41 provides a plan view of the bridge, and Figure 3.42 is an elevation view of the girder. The bridge has a girder spacing of 8 ft. and the radius of curvature of the girder is 1200 ft.

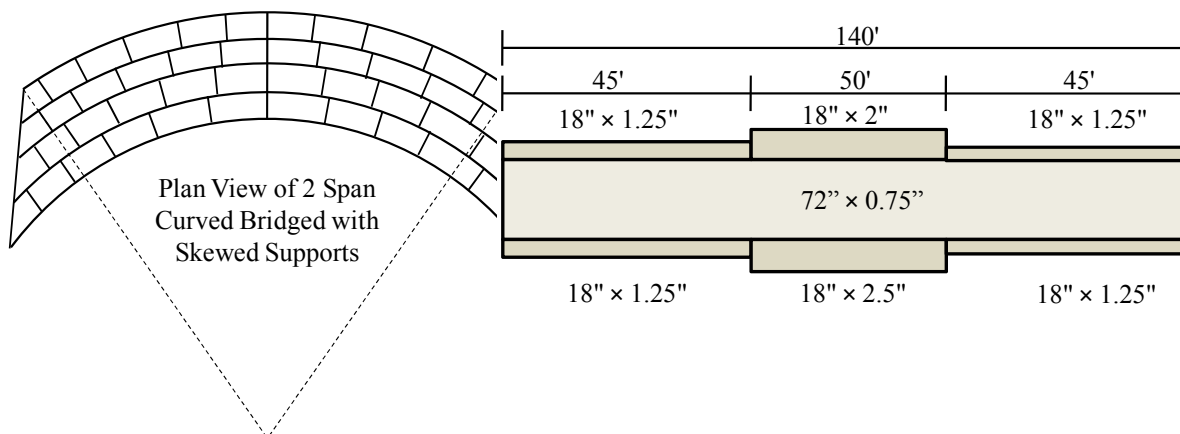


**Figure 3.41: Plan View of a 2 Span Bridge with Skewed Supports**

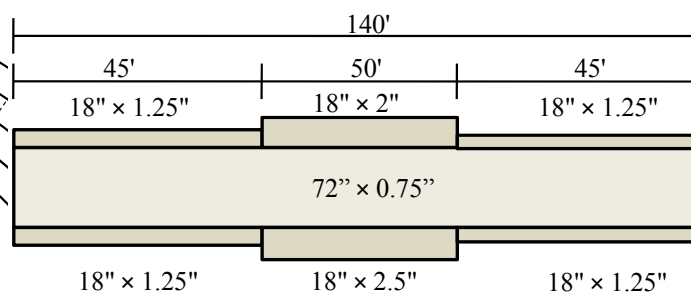


**Figure 3.42: Elevation View of a Girders**

UT Lift calculates that if the first lift point location is 31.45 ft. from the beginning of the girder and a 77.09 ft. spreader bar is used, the girder will not have any rigid body rotation. However, due to practical constraints, it would be reasonable to assume a spreader bar length of 75 ft. is used for the lifting. The program then calculates an initial rigid body rotation for such a spreader bar to be 0.33°. The Excel macro can then be run and the total rotation calculated. The maximum predicted rotation of 0.77° is given at the

beginning of the girder, and a maximum stress of 1.43 ksi is given at the 1<sup>st</sup> lift point. While the predicted buckling capacity is over-predicted for curved girders using an eigenvalue analysis, it is instructive to note that the predicted reduced buckling capacity,  $\phi M_{cr}$ , is 3673 k-ft and the maximum factored moment,  $\gamma M_{max}$ , is 315 k-ft, which is only one-tenth of the predicted capacity, thereby indicating a relatively stable girder. UT Lift provides three graphic outputs: 1) the out-of-plane displacements of the top and bottom flanges relative to the girder's original vertical position as a function of position along the length of the girder, 2) the total rotational deformations of the girder along its length, and 3) the torsion diagram of the girder in the lifted state. Figure 3.43, Figure 3.44, and Figure 3.45 are the three graphical outputs for this girder, respectively.

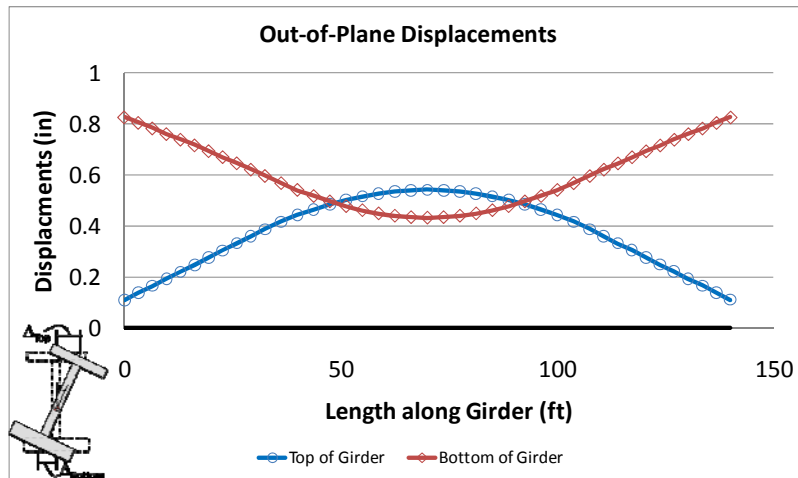


**Figure 3.43: Out-of-Plane Displacements of the Girder**

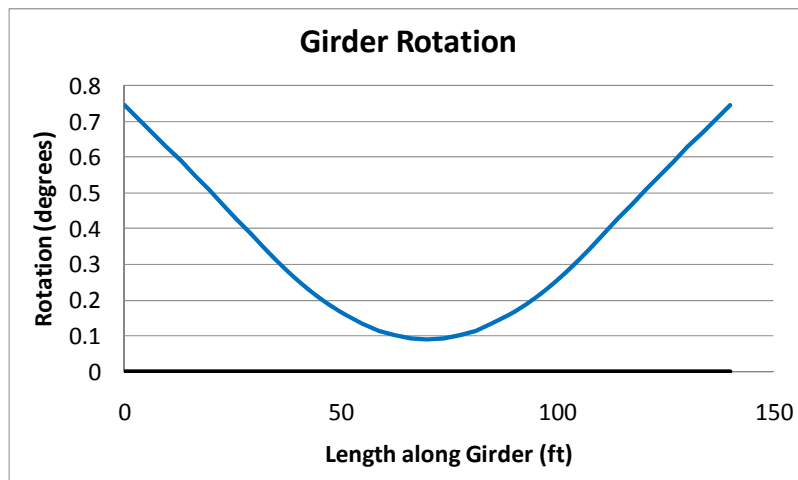


**Figure 3.44: Total Rotations of the Girders**

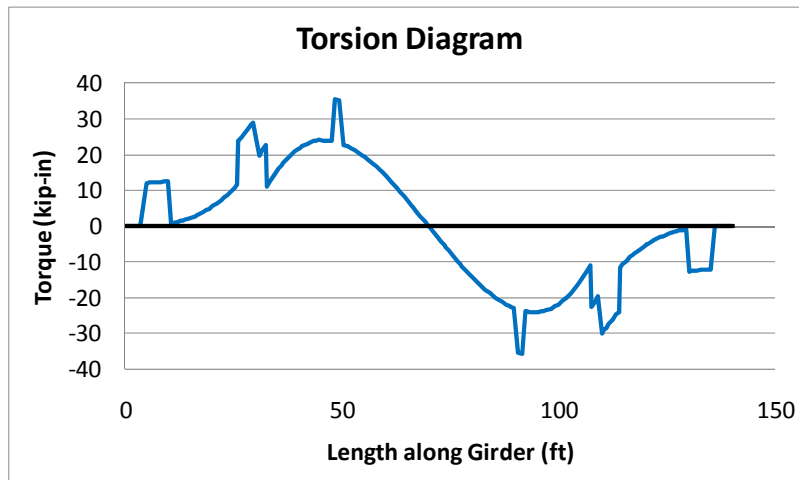


*Figure 3.45: Torsion Diagram of the Girder*

### 3.6 CONCLUSION

Extensive research was carried out to develop an improved understanding of the response of curved I-girders during lifting. A nationwide survey of the state-of-practice was conducted to determine the most common methods used to lift curved girders and to establish the greatest challenges facing engineers. Parametric studies utilizing eigenvalue buckling analyses and geometric nonlinear finite element analyses were conducted to develop a detailed understanding of curved girder behavior. Following these initial tasks, equations were derived to calculate the center of gravity of non-prismatic girders with cross-frames attached. These equations can be used to predict the rigid body rotation that will occur during the lifting of curved I-girders. A linear finite element for approximating the rotation of open sections was found in the literature that was dependent on the torsion diagram for the girder. A procedure for developing this diagram was established, and the entire process was implemented into an Excel-based spreadsheet called UT Lift. UT Lift requires input readily available to an engineer and provides a prediction of the behavior of curved I-girders during lifting. Based on the results of detailed parametric studies, the following recommendations are given for the safe lifting of curved I-girders:

- 1) Maximize the moment gradient by lifting a girder near the quarter points of the girder segment.

- 2) Minimize the rigid body rotation by lifting a girder such that the line of support passes through the center of gravity.
- 3) Minimize weak axis bending by reducing the rigid body rotation.
- 4) Widening the top flange to increase the warping stiffness is the most economical way to increase the torsional stiffness of the open section I-girder and reduce the cross-sectional twist.
- 5) The girders should remain elastic during lifting. Limiting service load stresses to a value of  $F_y/2$  should result in adequate performance. The stress check should include strong axis bending stresses, weak axis bending stresses, and warping normal stresses.
- 6) Girder segments should be checked for the serviceability limit state so as not to result in excessive rotation of the girders that can complicate air splicing. A value of 1.5 degrees was used by the researchers based upon feedback from erectors. The rotational check should include both the rigid body rotation and the cross-sectional twist.

Once a girder is lifted into place the partially constructed bridge must be maintained as a stable system. Each step in the erection process should be checked for excess deflections or stresses. Prior to the concrete deck hardening, the noncomposite bridge must safely support the deck load and all other construction live loads. Chapter 4 describes the development of UT Bridge, which is a computational tool capable of analyzing an I-girder bridge for each of these construction steps.

# **CHAPTER 4:**

## **UT BRIDGE: A 3-D FINITE ELEMENT ANALYSIS PROGRAM FOR I-GIRDERS DURING CONSTRUCTION**

---

### **4.1 INTRODUCTION**

There are several critical stages in the life of a bridge. The construction stage often represents the most complicated phase for analysis due to the wide variation in the support conditions that bridge components may experience. The construction stage can be divided into three phases that the need to be considered to ensure an efficient bridge can be safely constructed: 1) girder lifting, 2) girder erection, and 3) casting of the concrete bridge deck. The spreadsheet program UT Lift that was described in Chapter 3 provides an analytical tool for predicting the behavior of girder segments during lifting. This chapter focuses on the development of a computer program, UT Bridge, which provides a tool for modeling the other two critical phases. The chapter includes an overview of the development of the computer program as well as verification of the software with both field data and commercially available software.

### **4.2 GENERAL INFORMATION:**

UT Bridge is a three-dimensional finite element program capable of modeling the steel girder system of a bridge at various stages in the erection process as well as modeling the girder system during the concrete deck placement. The program is capable of modeling curved or straight girders with a variety of support conditions. UT Bridge can perform a linear elastic analysis and an eigenvalue buckling analysis during girder erection and also placement of the concrete bridge deck. The program allows for material self-weight, wind loading, point loading, and temporary supports. The program is comprised of three parts: a pre-processor, processor, and post-processor. A comprehensive online help menu is included with the program, providing guidance to the user and explaining important features.



### 4.2.1 Finite Element Analysis

The UT Bridge program utilizes a three-dimensional finite element analysis. The finite element method is one of the most widely-used analysis methods available to engineers and scientist today. The flexibility and accuracy of the method has resulted in its favorable use for a wide range of problems in a variety of disciplines. In the field of structural engineering, the method has been used to model a variety of complex structural systems. The origins of the finite element method reside in mathematics by Courant (1943), but were first implemented by engineers in the aerospace industry during the 1950s. In the early 1950s, Jon Turner of Boeing Airplane Company extended a one-dimensional structural analysis to two dimensions by discretizing a portion of an airplane wing into constant strain triangles (Turner, et al. 1956). The term “finite element method” was utilized by Clough a few years later to describe the use of two-dimensional discretization of continuous structural surfaces to approximate the displacements, stresses, and strains over the surface (Clough 1960). The finite element method was an extension of the direct stiffness method that was commonly utilized by structural engineers for structural analysis. To demonstrate the discretization process, Figure 4.1 below shows a frame discretized with beam elements as is customary with the direct stiffness method. The bridge deck in Figure 4.1 shows the discretization of the area with quadrilateral elements. The boundaries and connection points of adjacent elements are defined by nodes with coordinates that represent the position of the elements in space.

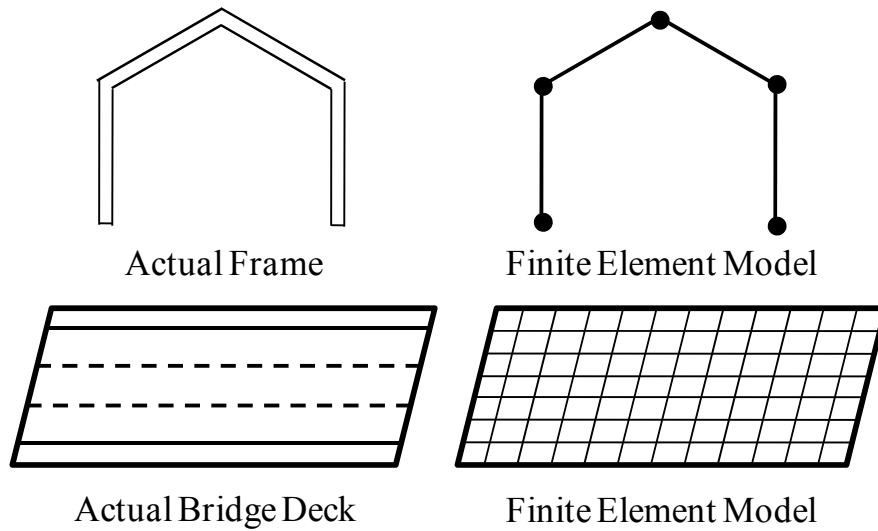


**Figure 4.1: Finite Element Idealization**

The displacements are obtained at the node locations and at all other locations the displacements are approximated. The stiffness of the structure at the node locations is obtained by summing the stiffness of all the elements attached to a node. The general procedure of the finite element method includes discretization, generating local element stiffness matrices, combining element stiffness matrices into a global system of equations, applying loads and boundary conditions, solving the mathematical model, and processing the results.

The simplest form of the set of equations to be solved in the finite element process is:

$$[K]\{\Delta\} = \{P\} \quad \text{Equation 4.1}$$

where:

$[K]$  = Structural stiffness matrix,  
 $\{\Delta\}$  = Nodal displacements, and  
 $\{P\}$  = Loads on the structure.

Thus, the displacements can be obtained by inverting the stiffness matrix and multiplying by the loads as shown in Equation 4.2.

$$\{\Delta\} = [K]^{-1}\{P\} \quad \text{Equation 4.2}$$

The basic framework for the UT bridge finite element program can be divided into three basic steps as depicted in Figure 4.2: pre-processor, processor, and post-

processor. A brief overview of the individual parts of UT Bridge is provided in the remainder of this section. A more in-depth discussion of all three parts of UT Bridge are provided later in the chapter with particular emphasis placed on the framework of the processor step.

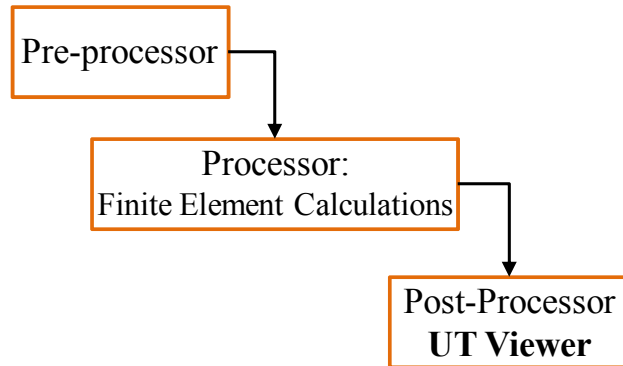


*Figure 4.2: UT Bridge Basic Program Architecture*

#### **4.2.2 Pre-processor:**

Starting the UT Bridge software initiates the pre-processor for the program. The pre-processor was developed in Visual Basic and prompts the user to enter the information readily available from bridge plans so that the model geometry can be developed. The program systematically prompts the user for information on a series of fourteen input forms. A flowchart showing the structure of the UT Bridge pre-processor is shown in Figure 4.3. The first nine forms define the bridge properties, the next three forms define the construction analysis cases, and the last two forms allow the user to define the kinds of analyses to perform.

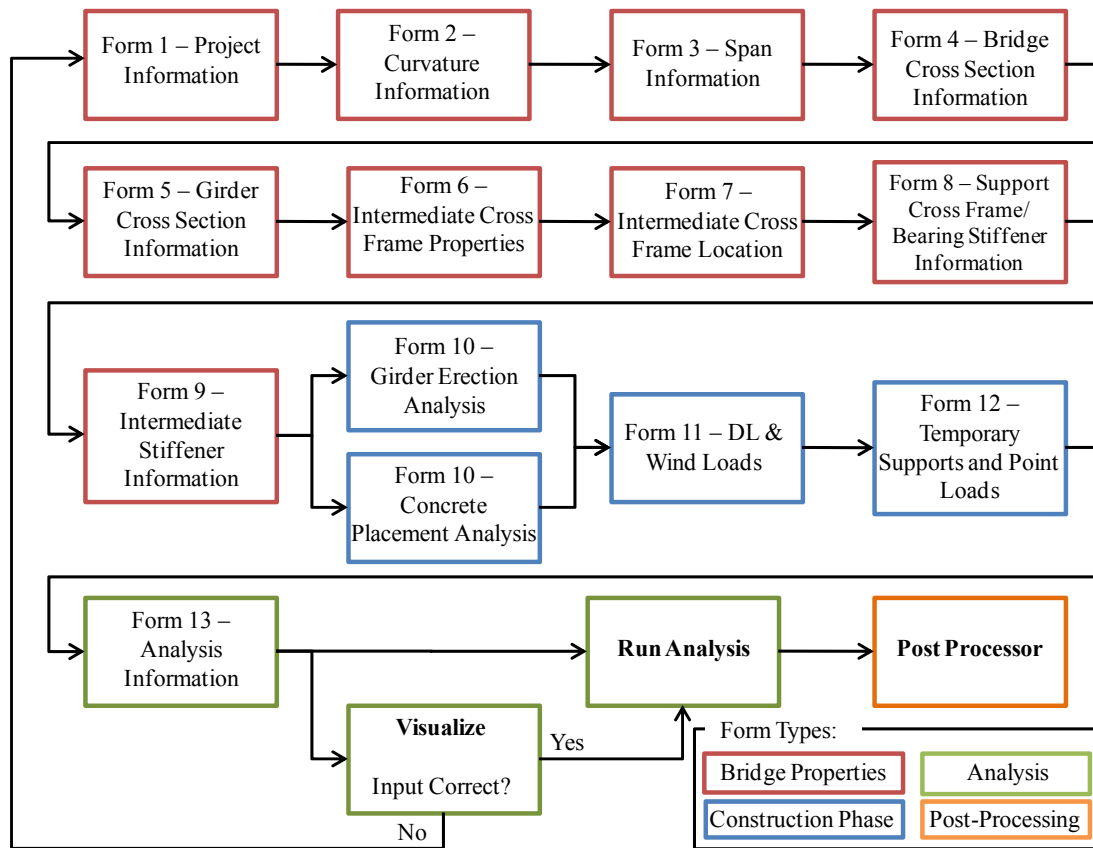


**Figure 4.3: Flow Chart of UT Bridge**

### 4.2.3 Processor:

The processor within UT Bridge is a FORTRAN program that assembles the user-defined input from the pre-processor and develops the analytical model of the bridge. The model is defined by the nodes and elements necessary for the three-dimensional finite element analysis. The global stiffness matrix is formed by combining the individual stiffness matrices for the shell elements, beam elements, truss elements, and spring elements that make up the full model. Once the global stiffness matrix and load vector are assembled, the structural analysis is conducted for the various load stages and the output is provided so that the post-processor (UT Viewer) can display the information.

The processor performs a linear elastic analysis for each analysis case specified by the user. The eigenvalue buckling analysis is only performed if it is specified by the

user. The linear elastic analysis assumes small displacement theory; thus, for each erection sequence stage, the global stiffness matrix is formed and the resulting equilibrium equations are solved assuming that elastic redistribution of deflections and stresses will occur from the previous analysis case. The concrete placement analysis has a time-dependent component in which the concrete material properties vary from analysis case to analysis case. Therefore, the concrete placement analysis is a linear incremental analysis that calculates the deflections and stresses of each analysis based upon newly applied loads in the corresponding construction stage and utilizing the current system global stiffness. The total deflections and stresses are calculated by summing the cumulative effects of all the previous analyses. Accordingly, adding an intermediate shore tower during a concrete placement analysis will not result in zero displacement at the shore tower location, but rather only zero incremental displacement for the analysis case during which the shower tower exists. A flow chart showing the structure of the UT Bridge processor is provided in Appendix A.

#### **4.2.4 Post-Processor:**

The post-processor for UT Bridge is called UT Viewer and was developed using C++. UT Viewer has the capabilities to show the user a full three-dimensional view of the user-defined bridge as well as display the results from the specified analysis. After UT Bridge has completed a full analysis, the user can display graphs of the stresses, displacements, and rotations of the bridge at tenth points along each span. UT Viewer also provides the cross-frame forces and support reactions for each analysis case. Additionally, the numerical data is available in tabular form in case the user wishes to further manipulate the data in a program of their choice, such as Microsoft Excel.

### **4.3 UT BRIDGE PRE-PROCESSOR**

The UT Bridge pre-processor is a series of fourteen forms that allow the engineer to take information readily available from typical engineering plans and enter the necessary input in order to perform a robust three-dimensional finite element analysis. This philosophy was central to the development of UT Bridge with the ultimate goal of

providing a tool that an engineer can use to efficiently and accurately analyze complex systems. Prior to the development of UT Bridge, these types of analyses were only completed for specialized cases due to the complexity of curved I-girder bridges, which requires significant modeling effort and computational resources. To fully utilize the capabilities of the program, the assumptions implicit in the development need to be understood. Figure 4.4 is a screen shot from a sample form in the UT Bridge pre-processor. This particular form prompts the user to input the number of spans, the length of the spans, and the substructure information.

Span Information - [3/14]

Number of Spans:  
3

Span Information

| Span Number | Span Length (ft) |
|-------------|------------------|
| 1           | 236.46           |
| 2           | 254.28           |
| 3           | 238.08           |

Note: The span length is specified assuming the horizontal alignment line is the center line of girder 1 and is measured from center line to center line.

Substructure Information

| Substructure Unit | Skew Angle (deg.) | Support Condition |
|-------------------|-------------------|-------------------|
| 1                 | 0                 | Expansion Bearing |
| 2                 | 0                 | Fixed Bearing     |
| 3                 | 0                 | Fixed Bearing     |
| 4                 | 0                 | Expansion Bearing |

Note: Skew angle sign convention assumes a right forward skew is positive and a left forward skew is negative. (See schematic for clarity)

Back Next Save & Close

**Figure 4.4: Screen Shot of a UT Bridge Form**

The program has some basic limitations and is based upon some predefined assumptions that bound the problem and provide simplifications to the input process. It is critical for the user to understand these assumptions to ensure the bridge is modeled with sufficient accuracy. Bridge engineers define the bridge geometry based on a predefined profile grade line (PGL) provided by the transportation engineer. This location varies from roadway project to roadway project. The PGL can be the center of the roadway, the edge of a lane, or the center of a divided highway, which for a bridge

may not lie on the bridge. Thus, a standard PGL was established for all bridges in the UT Bridge program, and it is set at the centerline of girder 1, which is defined as the left-most girder on a cross-sectional view looking ahead station. All bridge geometry is specified relative to this line including span length, skew angle, etc. Figure 4.5 is a schematic of a typical bridge cross-section with the girders numbered and the coordinate axis shown at the profile grade line. UT Bridge will analyze both straight and curved girder bridges. For a bridge curving to the left looking ahead station, a positive radius of curvature is specified, while a negative radius of curvature is specified for a bridge curving to the right. A schematic of a pair of bridges with different signs for the radius of curvature is provided in Figure 4.6 indicating the direction of curvature consistent with the program.

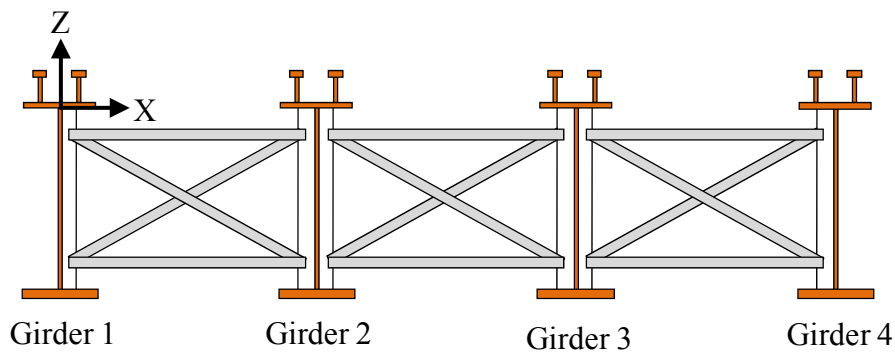


**Figure 4.5: Typical Bridge Cross-Section Looking Ahead Station**

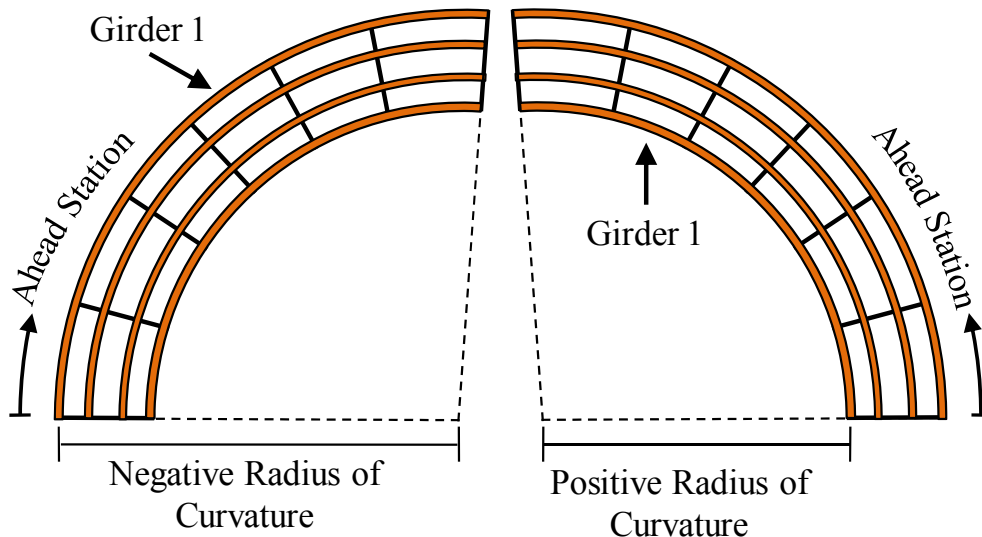


**Figure 4.6: Sign Convention for Curved Bridges**

UT Bridge allows for any number of girders and any number of spans; however very large systems may have issues with the problem size (this will be described in more detail later in the chapter). Additionally, the program allows for substructure skew. The sign convention within UT Bridge is arbitrarily chosen such that a right forward skew or a counterclockwise substructure rotation in the plan view is a positive skew angle, while a left forward skew or a clockwise substructure rotation in the plan view is a negative skew angle. Figure 4.7 is a schematic of a bridge where the first abutment's skew angle ( $\theta_1$ ) is negative, because it is a left forward skew. The bridge's middle pier is at no skew ( $\theta_2 = 0$ ) or perpendicular to Girder 1, and the end abutment's skew angle ( $\theta_3$ ) is positive or a right forward skew.

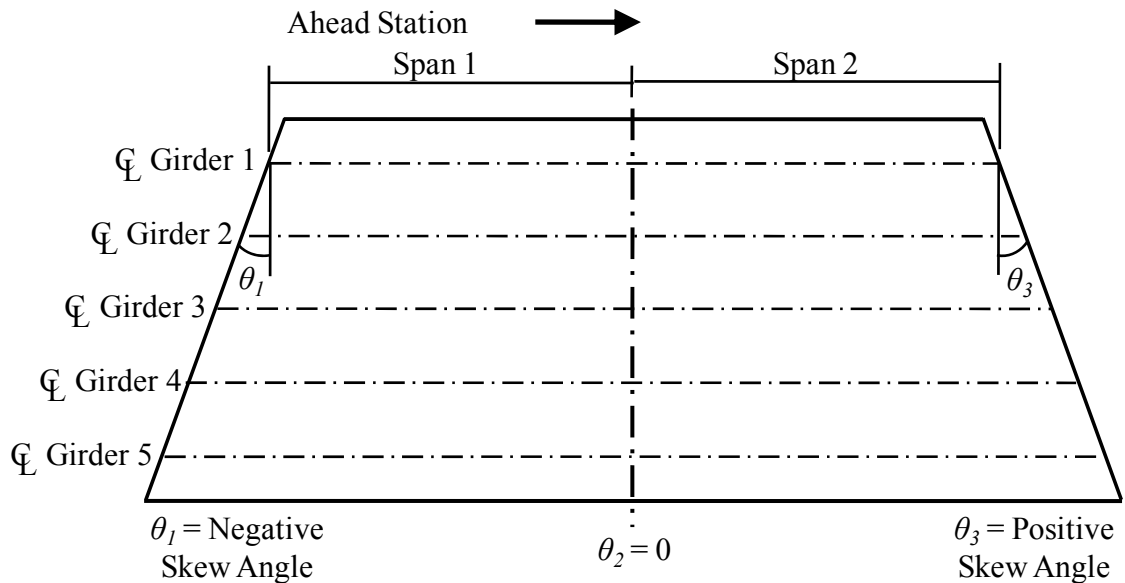


**Figure 4.7: Skew Angle Sign Convention**

The program assumes that all cross-frames are an X-type cross-frame, which is the specified standard for curved I-girder bridges in the state of Texas. For the purposes of cross-frame stiffness, the diagonal chords are assumed to be comprised of tension-only members, which is a conservative assumption with regard to the X-type cross-frames. Assuming a tension only cross-frame system results in the cross-frames behaving as if there is a single tension diagonal, and the reported output is given as such with one diagonal having zero force and the other diagonal having a tensile force. Cross-frames



are assumed to be attached to girders by stiffener plates and thus all girders have stiffeners located at the cross-frame location. Additional intermediate stiffeners can be specified in the pre-processor to stiffen the web and prevent web buckling in regions of high shear. Support cross-frame and bearing stiffeners are assumed to exist at each substructure unit. For some curved bridges with highly skewed supports, cross-frames are placed radially and do not exist along interior supports. To account for this in UT Bridge, the user can simply specify a small cross-sectional area for these members, and their contribution can be negated. Another important assumption regarding bearing stiffeners is that the program assumes they will exist on both sides of the girder. Therefore, when specified by the user, they only need to input one bearing stiffener and the program will automatically place one on the other side. Figure 4.8 is a typical X-type cross-frame with the individual chords labeled. The necessary input for each chord is the cross-sectional area of the chord.

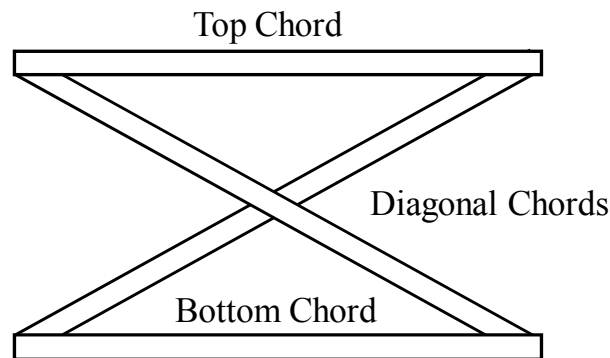


**Figure 4.8: Typical X-Type Cross-Frame**

A powerful feature of the UT Bridge program is the ability to fully analyze the bridge erection sequence. The program allows for each step in the erection process to be analyzed individually to determine deflections, stresses, and rotations throughout the bridge. The bridge model is assumed to be erected from one end of the bridge toward the other. The erection sequence of the bridge can be completed ahead station or back station. Accordingly, a bridge built from each end and completed with a central drop-in section cannot be modeled explicitly. The program treats each set of lifted girders as an analysis case. The lifting sequence to be analyzed can be a single girder or multiple girders depending on the erection plans. The critical stage for stability will often be the

case when a single girder segment is erected or cantilevers over a support since minimal bracing is present. Subsequent intermediate construction phases may be less critical because cross-frames will often be installed prior to releasing the lifting crane. To avoid analyzing construction stages that are not critical, the engineer can specify only critical stages during the bridge erection procedure to accelerate the analysis time. This flexibility provides the erection engineer with options previously unavailable by current bridge analysis software. Figure 4.9 – Figure 4.11 are a set of screen shots from the UT Bridge post-processor, UT Viewer, showing a model of a bridge with associated pictures of the erection process being modeled. With one input file, all these analysis cases can be completed at once.



**Figure 4.9: Bridge Erection Sequence with Associated UT Bridge Model**

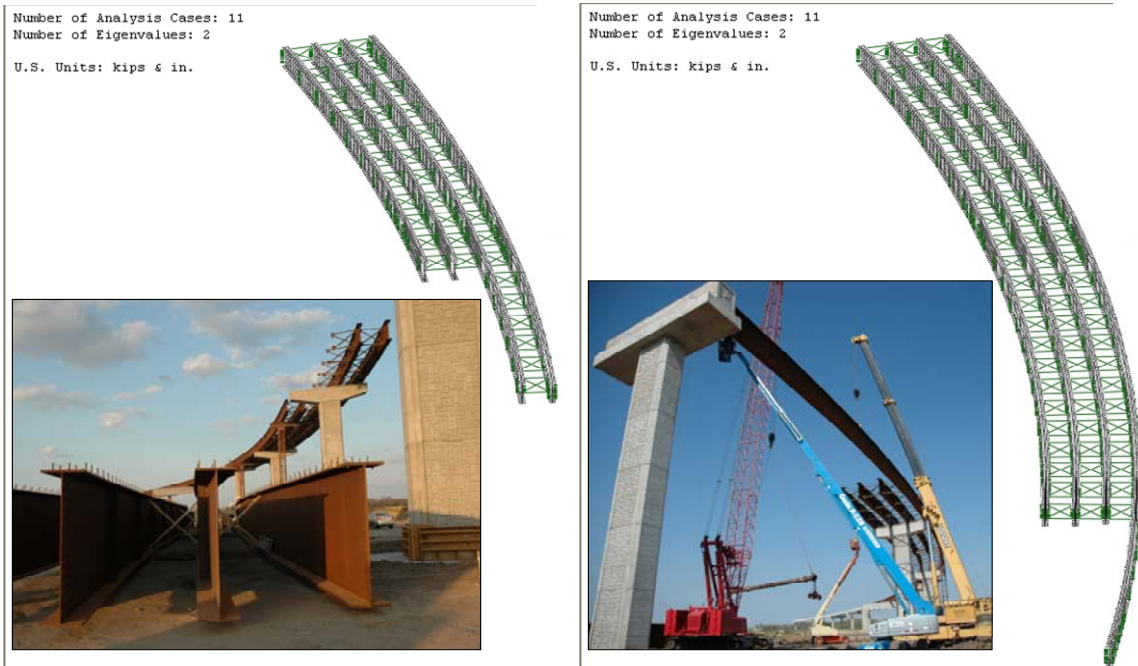


**Figure 4.10: Bridge Erection Sequence with Associated UT Bridge Model**



**Figure 4.11: Bridge Erection Sequence with Associated UT Bridge Model**

The other option for analysis is the ability to model the concrete bridge deck placement. The user can specify the sequence of the deck placement and analyze the state of stress for each stage of the concrete placement. Modeling the concrete deck

placement requires the early age concrete to be modeled in a time-dependent nature. As such, a linear incremental analysis technique was developed in which the loads in a given analysis case are applied to the corresponding system stiffness. The increment of displacement and stresses is then summed with all previous analyses to obtain the current state of stress. The method for modeling the interaction of the shear studs and the early age concrete was based upon recommendations from Topkaya (2002). Depending upon the concrete strength and age, an interpolation is conducted in UT Bridge for the modulus of elasticity of the concrete and the shear stud spring stiffness using Topkaya's results. The research study by Topkaya (2002) is based upon a series of push-out tests with shear studs in early-age concrete. The concrete used was a Class-S type concrete commonly used in bridge decks in the state of Texas. The requirements for Class-S concrete include:

- Minimum 28 day Compressive Strength: 4000 psi
- Minimum 7 day Flexural Strength: 570 psi
- Maximum Water/Cement Ratio: 0.47
- Desired Slump: 3 inches (4 inches maximum)

The shear studs used in the laboratory test were 3/4-in. diameter and with a 5-in. height, a conservative (small) size for typical bridges. Figure 4.12 is a schematic of the deformation pattern commonly encountered during the push-out tests. Figure 4.13 is a schematic of the push-out test setup, and Figure 4.14 is an actual picture of the test setup.

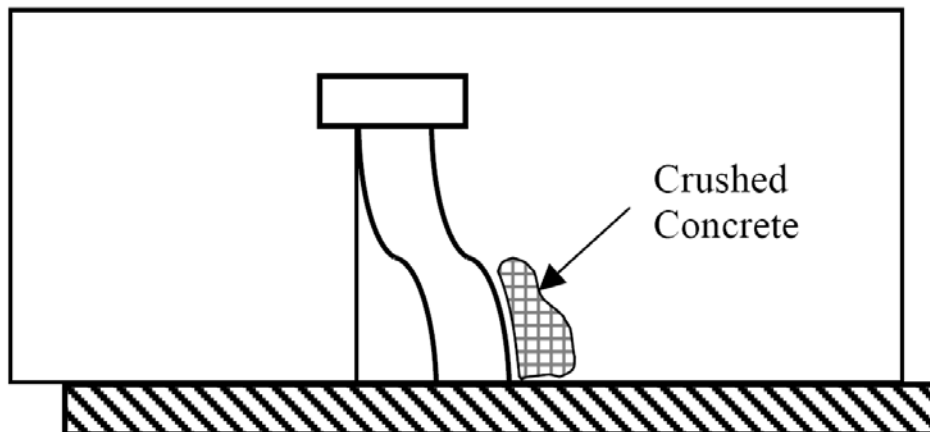


*Figure 4.12: Deformation Pattern for Shear Studs in Concrete Deck (Topkaya 2002)*

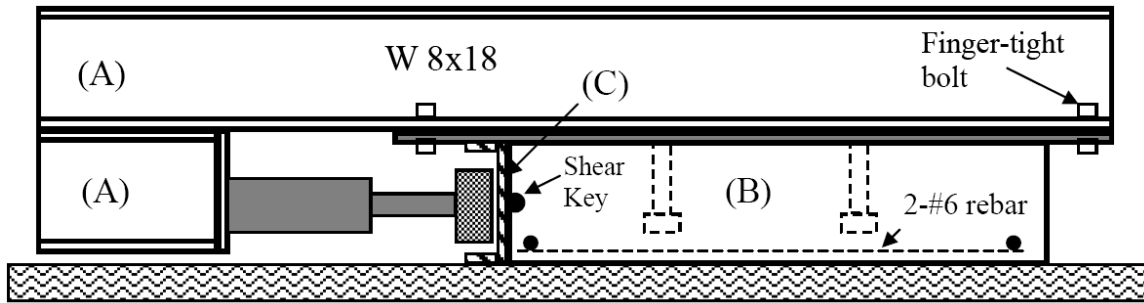


**Figure 4.13: Schematic View of Push-out Test (Topkaya 2002)**



**Figure 4.14: Picture of Push-out Test Setup (Topkaya 2002)**

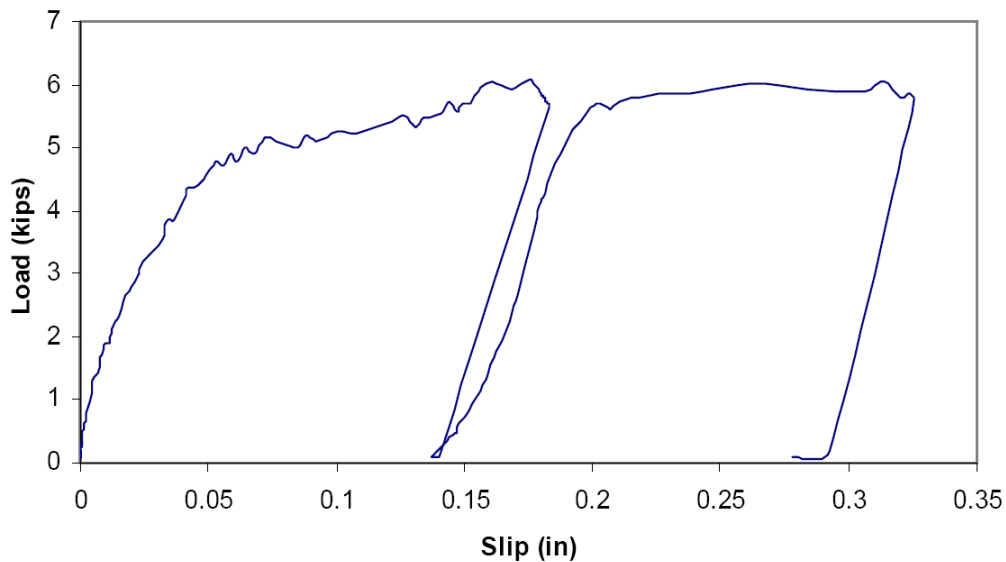


**Figure 4.15: Typical Load Displacement Graph (4 hr Concrete) (Topkaya 2002)**

A typical load-displacement curve for the push-out test is shown in Figure 4.15. The design strength of the shear stud was determined at a slip of 0.03 inches. In addition to the push-out test, Topkaya (2002) conducted simultaneous compressive strength and

modulus tests so that interpolation for the early age concrete modulus could be conducted. The displacement values along with the design loads given in Table 4.1 provide the shear stud spring stiffness interpolation for UT Bridge.

**Table 4.1: Push-out Test Results (Topkaya 2002)**

| Time   | Stud Design Strength, $Q_d$ (kips) |      |      |             | Stud Maximum Strength, $Q_{max}$ (kips) |      |      |             |
|--------|------------------------------------|------|------|-------------|---|------|------|-------------|
|        | Specimen Number                    |      |      | Average     | Specimen Number                         |      |      | Average     |
|        | 1                                  | 2    | 3    |             | 1                                       | 2    | 3    |             |
| 4 hr   | 3.6                                | 4.4  | 3.7  | <b>3.9</b>  | 6.0                                     | 6.2  | 6.1  | <b>6.1</b>  |
| 8 hr   | 8.1                                | 6.3  | 6.9  | <b>7.1</b>  | 10.2                                    | 8.85 | 10.0 | <b>9.6</b>  |
| 13 hr  | 10.1                               | 7.7  | 9.00 | <b>8.9</b>  | 13.5                                    | 10.1 | 14.7 | <b>12.7</b> |
| 22 hr  | 11.9                               | 13.0 | 11.5 | <b>12.1</b> | 17.5                                    | 17.6 | 17.5 | <b>17.5</b> |
| 3 day  | 13.8                               | 14.5 | 13.0 | <b>13.7</b> | 17.5                                    | 19.4 | 19.1 | <b>18.7</b> |
| 7 day  | 14.9                               | 15.0 | 14.9 | <b>14.9</b> | 18.4                                    | 20.2 | 19.8 | <b>19.4</b> |
| 14 day | 15.3                               | 16.0 | xxx  | <b>15.6</b> | 19.2                                    | 20.1 | 21.2 | <b>20.2</b> |
| 28 day | 18.3                               | 16.4 | 17.0 | <b>17.2</b> | 21.0                                    | 21.0 | 21.0 | <b>21.0</b> |

Instead of using the results from Topkaya (2002), the program also permits the user to independently input the modulus of elasticity of the concrete and the shear stud spring stiffness. However, the user is cautioned that such input should be based upon a clear understanding of the actual properties as determined from independent tests.

A final important option allowed by the pre-processor is the ability to vary the discretization of the bridge along the length. UT Bridge discretizes the bridge into nodes and elements required for a three-dimensional finite element analysis. The most accurate element is a square element with a ratio of the width to length (aspect ratio) of 1.0. However, because the geometry of bridge girders vary widely, the cross-section was set such that two elements represent the flanges and four elements represent the web of each girder. The deck has two elements representing each overhang, two elements over each flange, and three elements representing the deck between the girders. The element length was set by attempting to minimize the aspect ratio for a range of typical girders.

It should be noted that within finite element theory, mesh refinement generally improves the solution accuracy. However, for computational efficiency and for solutions

that are acceptably accurate, extremely fine meshes are not often necessary. UT Bridge offers three meshing options: Course, Normal, and Fine. The *Normal Mesh* has been assessed to be reasonable for a typical bridge. However, it has been noted that for very large problems (several girders and long bridge lengths) the number of nodes—and thus the number of degrees of freedom—requires more memory to solve than that available on a typical workstation. Therefore, the *Course Mesh* option is available to reduce the problem size and to provide the capacity to model large bridge systems. The *Fine Mesh* option is also available if the user desires to increase the number of elements used to model the girder system.

The default mesh density is *Normal Mesh*. A *Normal Mesh* density places an element at approximately every two feet for U.S. Units and approximately every 700 mm for SI Units. Changing the mesh density only changes the number of element divisions along the length of the girders. There is still the same number of elements across the flange widths or through the depth of the girders. For a *Coarse Mesh*, the element lengths are multiplied by a factor of two and for a *Fine Mesh*, the element mesh is divided by a factor of two. Examples of Coarse, Normal, and Fine meshes are shown for a given girder system in Figure 4.16 – Figure 4.18, respectively.

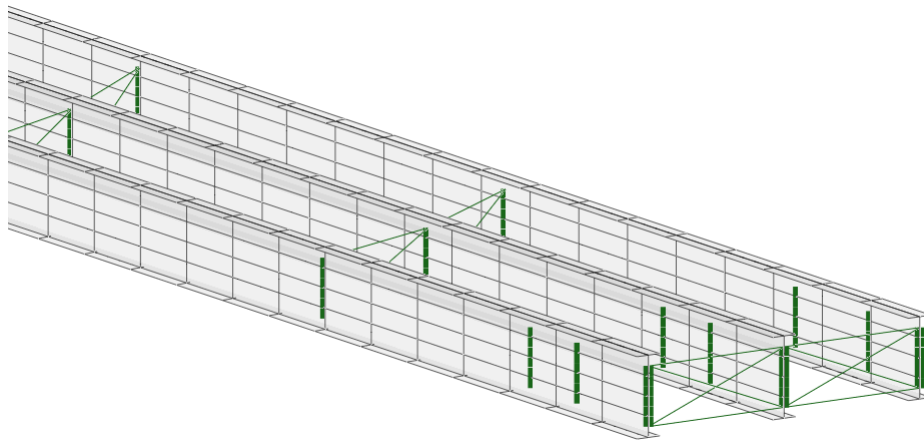


**Figure 4.16: Coarse Mesh Density**



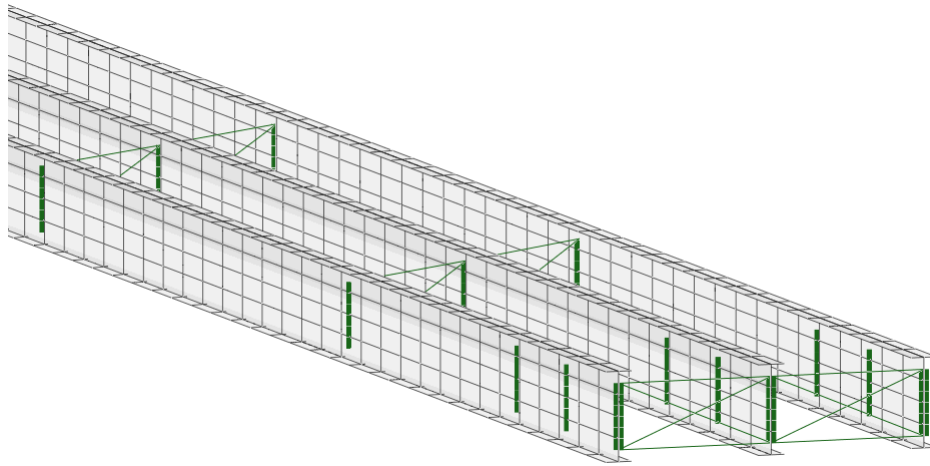


**Figure 4.17: Normal Mesh Density**

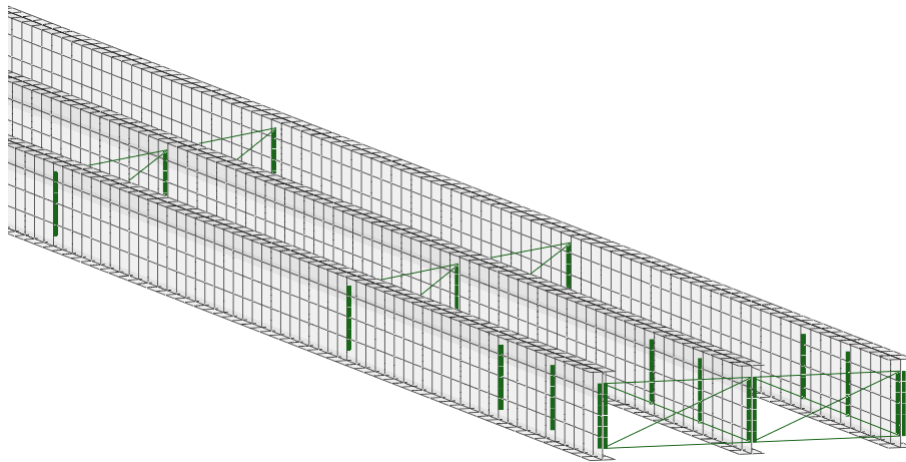


**Figure 4.18: Fine Mesh Density**

For a workstation with 3.50 GB of RAM, the approximate capacity is 100,000 nodes for an eigenvalue buckling problem and approximately 150,000 nodes for a linear elastic analysis. The approximate number of nodes can be calculated by using Equation 4.3 and Equation 4.4. The expression in Equation 4.3 is used for erection analysis, and Equation 4.4 is used for the deck placement analysis.

$$\# \text{ Nodes} = (17 * \text{Number of Girders}) * \frac{\text{Length}}{\text{Unit Factor}} * \text{Mesh Density} \quad \text{Equation 4.3}$$

$$\# \text{ Nodes} = (27 * \text{Number of Girders} + 3) * \frac{\text{Length}}{\text{Unit Factor}} * \text{Mesh Density} \quad \text{Equation 4.4}$$

where:



|                     |   |                                     |                        |
|---------------------|---|-------------------------------------|------------------------|
| <i>Length</i>       | = | Total Length of bridge in <i>ft</i> | (U.S. Customary Units) |
|                     | = | Total Length of bridge in <i>mm</i> | (SI Units)             |
| <i>Unit Factor</i>  | = | 1                                   | (U.S. Customary Units) |
|                     | = | 350                                 | (SI Units)             |
| <i>Mesh Density</i> | = | 1                                   | if Normal Mesh         |
|                     | = | 2                                   | if Fine Mesh           |
|                     | = | 0.5                                 | if Coarse Mesh         |

## 4.4 UT BRIDGE PROCESSOR

### 4.4.1 Node Numbering

The first step in the finite element process is to discretize the structure of interest. The following section explains the node numbering approach implemented in the UT Bridge program. The program generates node locations by an algorithm developed to allow for curved or straight I-girder bridges. Although for large problems difficulties may be encountered with computer memory or disk space, there is not a limit on the number of girders or the number of spans. The algorithm allows for skewed substructures to be included with positive skew being defined as a right forward skew and negative skew being defined as a left forward skew. A help screen with a picture is available in the pre-processor to ensure the user is aware of the sign convention. Figure 4.19 shows the cross-sectional node numbering scheme. There are two shell elements per flange, which corresponds to five flange nodes. In addition, there are four shell elements per web, which corresponds to nine web nodes. In practice, the profile grade line varies depending on the bridge; however a standard must be made for the purposes of this program. The profile grade line was chosen to be the center line of the left most girder, which is defined as Girder 1. Therefore, the span lengths and substructure skews are designated along the center line of Girder 1.

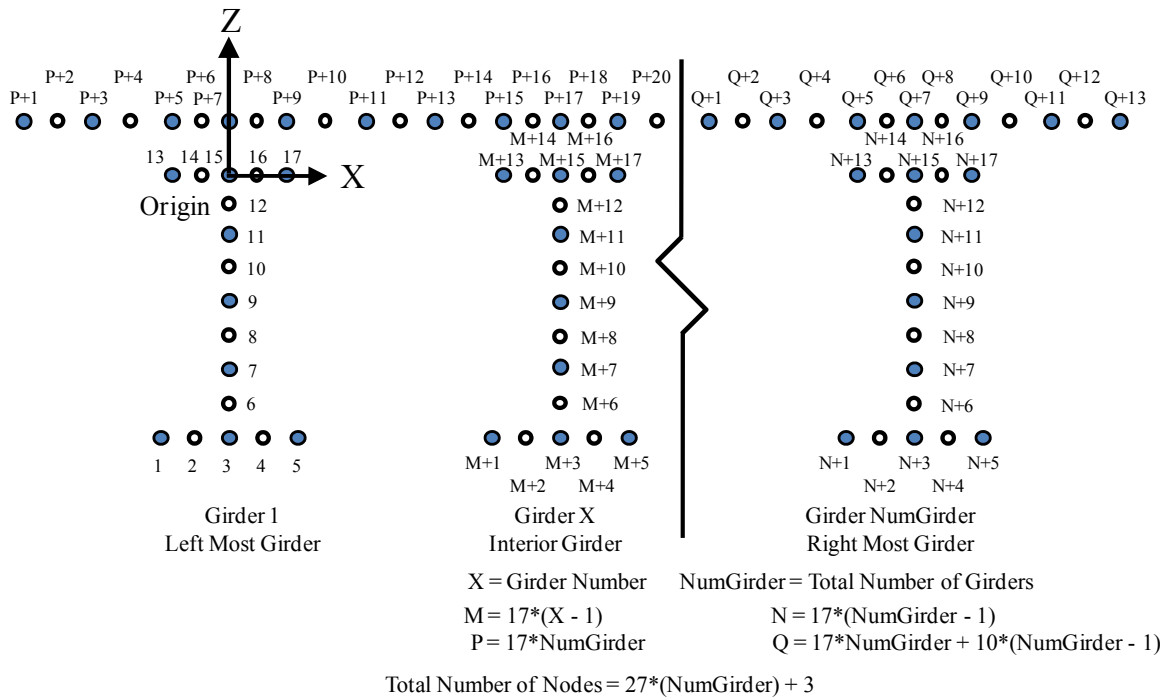


**Figure 4.19: Schematic of the Node Numbering Used in UT Bridge**

Element connectivity defines the relationship between the elements and the nodes associated with each element. Nine-node shell elements are used to model the steel plates of the girder and the concrete deck. The cross-frames are comprised of truss elements, beam elements are used for the stiffeners, and springs elements are used to simulate the shear stud interaction between the concrete deck and the girders. All girders consist of an equal number of elements along their length to ensure a regular element layout for the deck. To ensure an equal number of elements, the centerline length of each span is calculated from the skew, girder spacing, and Girder 1 information. The length is then divided into the number of segments that result in approximately two-foot elements. By utilizing the nine-node shell elements, the resulting nodal cross-sections are at approximately one foot intervals along the length of the bridge for the normal mesh density option. For spans with varying skewed substructures, the element length will be larger on one side of the bridge centerline and smaller on the other side. This discretization scheme works well for most typical bridges, but may have trouble for short span bridges with a large skew differential from one support unit to the next as this situation may result in very small element lengths on one side of the bridge and long

element lengths on the other. Figure 4.20 is a schematic of the nodal cross-section layout of a bridge with skewed supports.

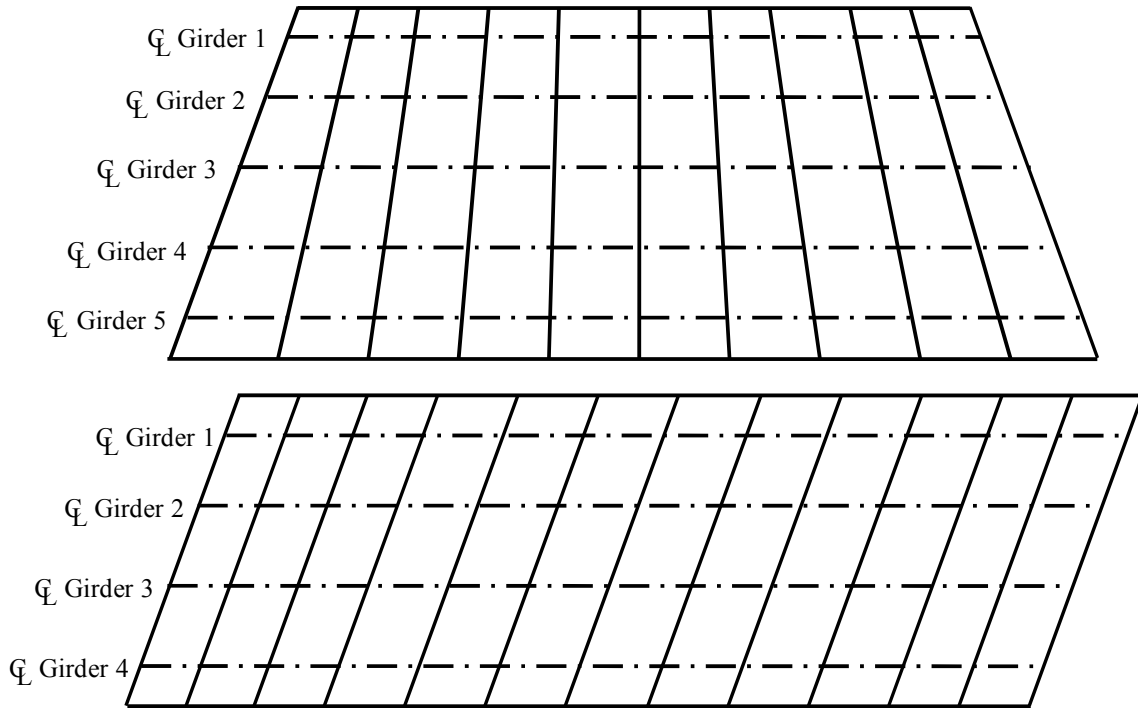


**Figure 4.20: Skewed Bridge Nodal Cross-Section Schematic**

The element length (approximately 2 feet) was chosen to give acceptable element aspect ratios for typical steel plate girder bridges. The aspect ratio for a shell element is the ratio of the element's length to width. For a square, the aspect ratio is one and it varies for all other quadrilaterals. During the assembly of the global stiffness matrix for the finite element analysis, each individual shell element is transformed to a square master element, and the stiffness is calculated following the algorithm discussed later in this chapter. The transformation to the master element introduces computational error inherent in finite element analysis, but this error can be minimized by maintaining an aspect ratio as close to one as possible. Considering the typical depth of the plate girder and flange widths, it was deemed appropriate to use elements with an approximate length of 2 feet without a significant error. A similar aspect ratio was used in the development of U-TrAp (Toykaya 2002), which is software for analyzing trapezoidal box girders. The capitalization in the program name serves the dual reference that it is applicable to trapezoidal shaped girders and was also developed at the University of Texas at Austin.

Another issue related to the aspect ratio is the skew of the individual elements. The element skew will also introduce a certain amount of numerical error as it is transformed to the master element. U-TrAp 2.0 does not have the capability to allow for skewed substructure supports, and thus this issue was not addressed previously. During this research investigation, the numerical error from the effects of the element skew angle for typical bridges was found to be negligible.

#### **4.4.2 Aspect Ratio Parametric Study:**

To quantify the error associated with various aspect ratios, a parametric study was conducted to ensure adequate accuracy of the model. The numerical error is associated with calculating the element's Jacobian matrix, which translates the master element's natural coordinates to the element's actual global coordinates. An attempt was made to quantify the error of the shell element by utilizing a general purpose finite element program, ANSYS. ANSYS does not have the exact nine-node shell element utilized in UT Bridge, but it does have an equivalent eight-node shell element (SHELL93) that has similar shape functions and was used for the error estimation analysis. The analytical study was multifaceted with initial studies utilizing a two-dimensional plate discretized into rectangular elements with various aspect ratios and then divided into parallelogram elements with various skew angles. Finally, a three-dimensional beam element was developed with the top and bottom flange elements consisting of parallelograms with various skews to simulate the actual discretization scheme proposed for UT Bridge.

##### **4.4.2.1 Rectangular Element Parametric Study:**

Many two-dimensional plate bending problems have been solved exactly for specific boundary conditions (Timoshenko and Woinowsky-Krieger 1959). For a rectangular plate simply supported along the edge with a point load at the center, the maximum deflection of the plate is give by Equation 4.5.

$$\Delta_{max} = \frac{\alpha P a^2}{D} \qquad \text{Equation 4.5}$$

where:

$$D = \frac{Eh^3}{12(1 - \nu^2)}$$

**Table 4.2: Constant ( $\alpha$ ) Depending on Ratio of the Rectangle's Side Lengths (Timoshenko and Woinowsky-Krieger 1959)**

|            |        |         |         |         |        |
|------------|--------|---------|---------|---------|--------|
| $b/a$      | 1      | 1.1     | 1.2     | 1.4     | 1.6    |
| $\alpha =$ | 0.0116 | 0.01265 | 0.01353 | 0.01484 | 0.0157 |

**Table 4.3: Constant ( $\alpha$ ) Depending on Ratio of the Rectangle's Side Lengths (Timoshenko and Woinowsky-Krieger 1959)**

|            |        |         |        |          |
|------------|--------|---------|--------|----------|
| $b/a$      | 1.8    | 2       | 3      | $\infty$ |
| $\alpha =$ | 0.0162 | 0.01654 | 0.0169 | 0.01695  |

where:

- $P$  = Point load (kips)
- $a$  = Length of the small side of the rectangle
- $b$  = Length of the long side of the rectangle
- $E$  = Young's Modulus (29,000 ksi for steel)
- $\nu$  = Poisson's Ratio (0.3 for steel)
- $h$  = Shell thickness (in)
- $\alpha$  = Constant used in Equation 4.5

This solution assumes small deflections of a laterally loaded plate. It does not include membrane action or shear deformation. Nevertheless, the solution provides a powerful basis to verify the legitimacy of the analysis approach taken in UT Bridge. Figure 4.21 is a screen shot from an ANSYS analysis modeling a 10"  $\times$  10" shell that is 1" thick and has a 1 kip point load at the center. The theoretical maximum plate deflection given by Equation 4.5 is 0.4368". The results of the parametric study are summarized in Table 4.4.

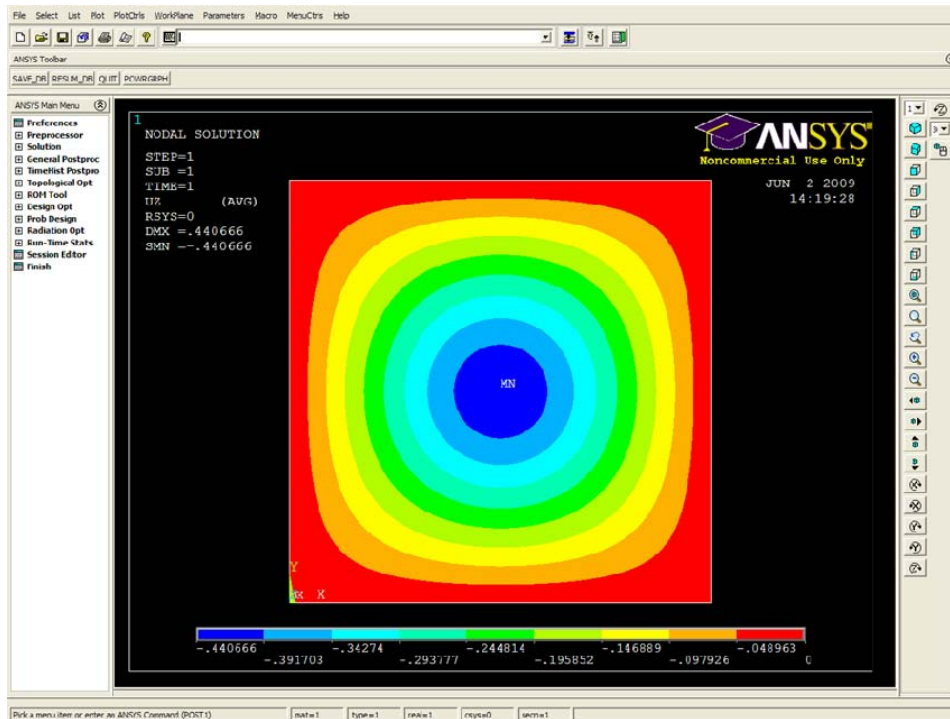


**Figure 4.21: ANSYS Screen Shot of Plate Bending Problem**

**Table 4.4: Plate Bending Aspect Ratio Parametric Summary**

| Aspect Ratio | Element Size (in)     | $\Delta_{\max}$ (in) | % Difference |
|--------------|-----------------------|----------------------|--------------|
| 1            | $0.2 \times 0.2$      | 0.44067              | 0.8860       |
| 2            | $0.25 \times 0.125$   | 0.44071              | 0.8951       |
| 3            | $0.333 \times 0.111$  | 0.44072              | 0.8974       |
| 4            | $0.333 \times 0.083$  | 0.44078              | 0.9112       |
| 5            | $0.417 \times 0.083$  | 0.44077              | 0.9089       |
| 10           | $0.5 \times 0.05$     | 0.44086              | 0.9295       |
| 60           | $0.417 \times 0.0069$ | 0.44113              | 0.9913       |

It should be noted that the theoretical deflection for an ideal aspect ratio of 1 is slightly larger (0.89%) than the ANSYS predicted deflections. This overestimation of the deflections is counterintuitive because the process of discretizing a region and numerically approximating the deflections (a finite element analysis) results in a stiffer system and thus smaller deflections than what is expected of an actual continuum. However, in this particular situation, the predicted deflection given by Timoshenko is for plate bending only and does not include the shear deformations that are included in the

ANSYS formulation. The difference in the modeling assumptions can account for the error, but it is also notable that for aspect ratios of up to 60, the change in predicted deflection is  $\sim 0.1\%$ . The relatively small variation in the predicted deflections suggest that if UT Bridge is targeted to maintain an aspect ratio less than approximately 10, the discretization of the model does not generally introduce significant error.

The previous approach was taken for rectangular plates with various slide lengths. Additionally, the boundary conditions of the plate were changed from simply supported to fixed, and the theoretical plate bending solution given by Timoshenko was compared to the ANSYS shell. The results of all of these analyses confirmed the previous assumption that aspect ratios will not dramatically affect the analysis unless they are extreme, significantly greater than 10.

#### **4.4.2.2 Parallelogram Element Parametric Study:**

After studying the aspect ratio of rectangles the effects of using parallelogram elements was studied. The elements were compared using their acute (smallest) angle to define the parallelogram used. It was necessary in developing the various skewed angles to vary the element's aspect ratio, but the same square plate was used initially to compare to the data given for the aspect ratio study. Table 4.5 shows the acute angle and the maximum deflection (deflection under the point load) for a variety of cases with various parallelograms. It also reports the percent difference between the ANSYS results and Timoshenko's prediction. It is notable that as the acute angle decreases, the predicted deflection also decreases. This trend indicates a stiffening effect resulting from the use of highly skewed parallelograms.

***Table 4.5: Plate Bending Parallelogram Parametric Summary***

| Acute Angle<br>(deg.) | $\Delta_{\max}$<br>(in) | %<br>Difference |
|-----------------------|-------------------------|-----------------|
| 84.29                 | 0.44084                 | 0.9249          |
| 78.69                 | 0.44075                 | 0.9043          |
| 75.96                 | 0.44076                 | 0.9066          |
| 71.57                 | 0.4407                  | 0.8929          |
| 63.43                 | 0.44067                 | 0.8860          |
| 45.00                 | 0.44044                 | 0.8333          |

|       |         |        |
|-------|---------|--------|
| 26.57 | 0.44016 | 0.7692 |
| 18.26 | 0.43969 | 0.6616 |
| 14.04 | 0.43963 | 0.6479 |
| 11.31 | 0.43904 | 0.5128 |
| 5.71  | 0.43818 | 0.3159 |

While the deflections are greater than those predicted by Timoshenko, a similar argument was made for the increase as stated previously when discussing the aspect ratio results. The stiffening that occurs with the change in skew angle is larger than for the aspect ratios study, but for almost all cases the difference is less than 1%. Historically the issue of aspect ratio and skew angle affected the overall results more due to the lack of accuracy in storing the numeric data. Existing programs such as ANSYS utilize double precision accuracy in the storage of numbers, which means that more digits past the decimal place are stored and thus round-off error is reduced in converting the element global coordinates to the master element coordinates.

#### **4.4.2.3 Girder Flange Parallelogram Parametric Study:**

The final part of the parametric study was focused on the proposed element layout to be used in the UT Bridge program, which consisted of two shell elements across the flanges and four elements through the web depth. For this analysis, the flange shell elements were skewed into parallelograms, and variations in the degree of the flange skew were studied. Individual simply supported beams were modeled with a point load at the middle of the span and with a uniformly distributed load. The results were compared to predictions of the deflections and stress using standard Bernoulli-Euler beam theory. Additionally, the torsional effect was calculated by applying a point torque to the end of a cantilever beam with skewed flange elements. The torsion study was conducted because the torsional behavior will significantly affect the lateral-torsional buckling capacity predicted by UT Bridge. Screen shots are shown in Figure 4.22 from the ANSYS analysis with a distributed load applied to a simply supported girder and a torque applied to a cantilever with skew flange shell elements. Table 4.6 is a summary of the results from the simply supported girder with the percent difference from the ANSYS analysis and beam theory for the deflection and the stresses at midspan. Table 4.7 is a



summary of the results from the cantilever with an applied torque comparing the end rotations and the fixed-end stress at a length of one girder depth from the fixed end. Stress comparisons were made a girder depth from the fixed end to minimize the effects from stress concentrations from the boundary conditions that would be included in the ANSYS results but not in the theoretical solutions.

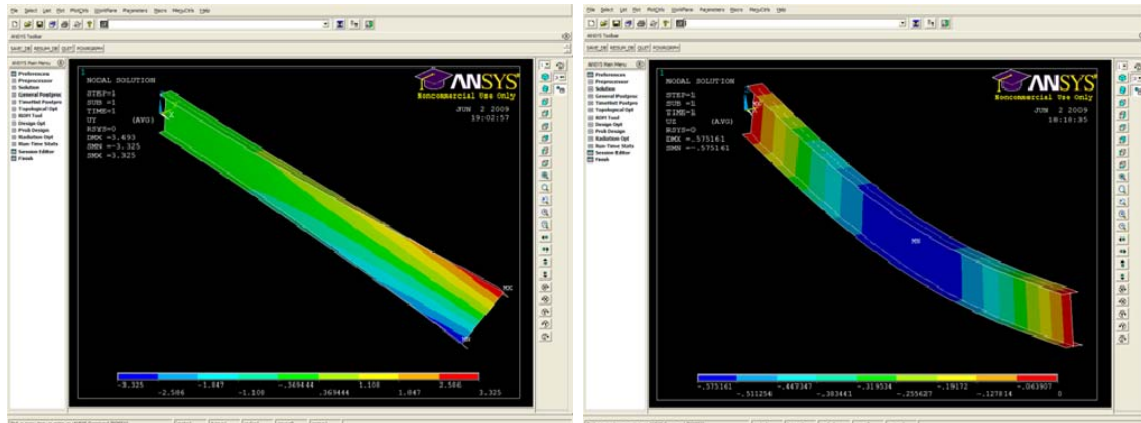


**Figure 4.22: ANSYS Screen Shots of Girder Flange Parallelogram Parametric Study**

**Table 4.6: Girder Flange Parallelogram Parametric Summary**

| Distributed Load on Simple Span |                                 |                             |
|---------------------------------|---------------------------------|-----------------------------|
| Acute Angle (deg.)              | MidSpan Deflection % Difference | MidSpan Stress % Difference |
| 84.29                           | 0.9102                          | 0.0315                      |
| 60.02                           | 0.8049                          | -0.0485                     |
| 45                              | 0.4099                          | -0.0773                     |
| 29.94                           | 0.7499                          | -0.0792                     |
| 5.71                            | -0.4711                         | -0.6089                     |

**Table 4.7: Girder Flange Parallelogram Parametric Summary**

| Torque on Cantilever |                                |  |
|----------------------|--------------------------------|--|
| Acute Angle (deg.)   | Free End Rotation % Difference | Depth from Fixed End Stress % Difference |
| 84.29                | 1.2167                         | 0.4072                                   |
| 60.02                | 1.2231                         | 0.4219                                   |
| 45                   | 1.1931                         | 0.4953                                   |
| 29.94                | 1.2136                         | 0.5980                                   |
| 5.71                 | -0.5327                        | 3.3263                                   |

It can be seen from Table 4.6 and Table 4.7 that while the variation of aspect ratio has some effect on the reported results, the skew angle does not significantly reduce the accuracy of the shell elements with double precision accuracy. The magnitudes of the error for skew angles greater than  $60^\circ$  (thus an acute angle of  $30^\circ$ ) may become more significant and additional verifications may be necessary for these extreme cases.

#### **4.4.3 Activation of Nodes**

The final step before calculating the individual element stiffness matrices is to define which elements to include in a given analysis case. To accomplish this task, an algorithm was developed to activate and deactivate the appropriate nodes. One of the primary features of the program is the ability to input one file and analyze several erection steps or concrete deck placement stages. To produce a single input file and accomplish several analysis steps, UT Bridge has two routines depending on whether the analysis is simulating erection or the concrete deck placement. The entire bridge model geometry is developed and the nodes are activated depending on the analysis run. For the erection analysis, all the nodes are initially deactivated. For each analysis step, the nodes associated with the lifted portion are activated for the next analysis step and remain activated for the remainder of the analysis steps. For the concrete placement analysis, all the girder nodes are activated and then deck nodes are deactivated. For each analysis, the portion of the deck placed is activated and added to the model. When developing the global stiffness matrix for the each load step, the activated elements are determined by making sure all nodes associated with the elements are active; otherwise, the element is deactivated and not included in the stiffness matrix.

#### **4.4.4 Element Elastic Stiffness Formulations:**

A critical step in any finite element program is the accurate formation of the global stiffness matrix. The global stiffness matrix is a combination of all the active element stiffness matrices in a given analysis case. UT Bridge utilizes four types of elements to model a bridge: shell elements, truss elements, beam elements, and spring elements. The shell elements model the steel girder flanges, web, and concrete deck.

The truss elements model the cross-frames. The beam elements model the stiffeners. The spring elements model the shear studs. Each element type has different properties and thus a different element stiffness formulation. The following sections describe both the elastic stiffness formulations for the element types used in UT Bridge and the geometric stiffness formulations for the element types subject to buckling.

#### **4.4.4.1 Shell Element Elastic Stiffness Formulations:**

The first finite elements developed to model thin plates in bending were shells based on Kirchhoff plate theory, which neglects shear deformations. These relatively simple shell element formulations superimposed a plate bending stiffness formulation and a plane stress membrane stiffness formulation. The result is a flat shell element that can be used to model flat components or used to model general curved shells as an assemblage of flat elements. The use of flat elements to represent a curved structure requires a relatively large number of elements to accurately represent the geometry. Additionally, the use of this theory presented difficulties in satisfying inter-element continuity on the displacements and edge rotations because the rotations are calculated from the transverse displacements (Bathe 1996). The Kirchhoff plate theory is analogous to Bernoulli-Euler Beam theory for beam elements. The more general shell element formulation used in UT Bridge separates the displacements and rotations of the surface normal vector into independent variables and allows interelement continuity to be satisfied directly. The separation of the displacements and rotations accounts for shear deformations in the shell element similar to a Timoshenko Beam theory.

UT Bridge utilizes a nine-node isoparametric displacement-based shell element (Figure 4.23) originally developed by Ahmad, Irons, and Zienkiewicz (1970) and modified to prevent shear and membrane locking (Bathe 1996) to model the steel plates of the girders and the concrete deck as shown in Figure 4.24. Some details of the formulation are given in varying degrees in Bathe (1996), Topkaya (2002), and Popp (2004). An isoparametric element uses the same shape functions to define the geometry and the displacements. The shape functions, also called interpolation functions, are a set of equations that approximate the solution (displacement, etc.) at all points within an

element given the solution of the finite element analysis at each node. Displacement-based finite element procedures obtain the solution by directly applying the variational principle in the finite element space, which discretizes the space of admissible displacements for the structure (Chapelle & Bathe 2003). A functional is constructed which includes all the intrinsic features of the problem, such as the governing equations, boundary conditions, and constraints. For a structural or solids problem the functional also represents the total energy of the system. Direct variational principles make use of methods such as the principle of virtual work and the principle of minimum total potential energy to determine approximate solutions to various problems (Reddy 2006). The space of admissible displacements corresponds to the smooth space of the functional without discontinuities that violate the physics of the problem.

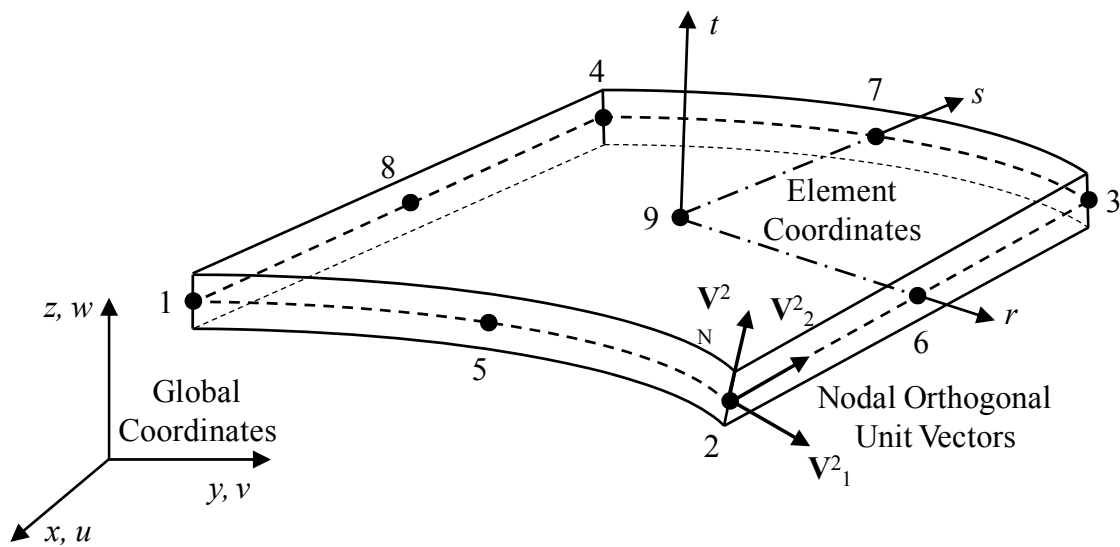


**Figure 4.23: Nine-Node Shell Element Schematic**

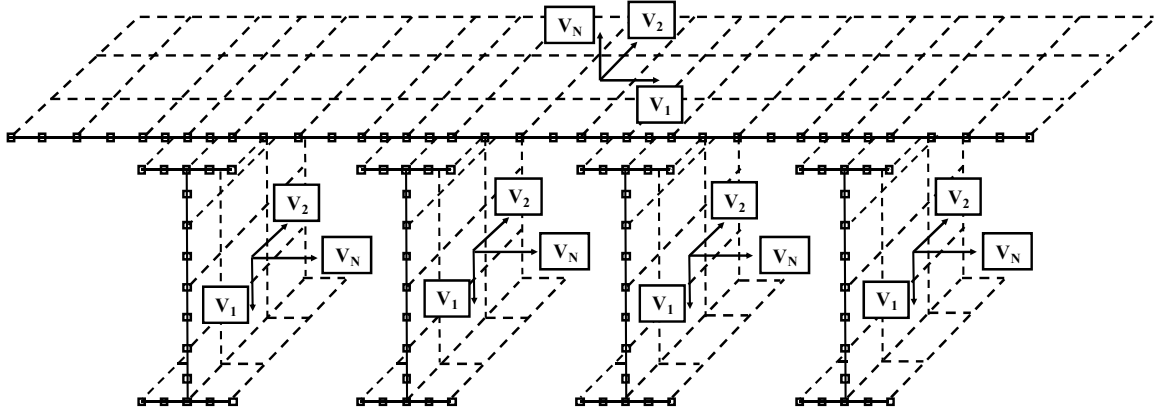


**Figure 4.24: Schematic of Bridge Shell Elements**

The first step in developing the shell formulation is to define a set of mutually orthogonal unit vectors at each node. The unit vectors are defined with  $V_N^i$  specifying the direction normal to the shell surface at each node location. In general,  $V_2^i$  is defined along the length of the bridge,  $V_N^i$  is always defined through the thickness, and  $V_1^i$  is orthogonal to  $V_2^i$  and  $V_N^i$ . The element is mapped from global  $(x, y, z)$  coordinates to natural element coordinates  $(r, s, t)$  utilizing the following equation:

$$\mathbf{x}(r, s, t) = \sum_{i=1}^9 \left[ \left( \mathbf{x}_i + t \frac{h}{2} \mathbf{V}_N^i \right) N_i(r, s) \right] \quad \text{Equation 4.6}$$

where:

- $\mathbf{x}$  = Cartesian coordinates of any point in the element,
- $\mathbf{x}_i$  = Cartesian coordinates of node point  $i$ ,
- $h$  = Thickness of the shell in the  $t$  direction at node point  $i$ ,
- $\mathbf{V}_N^i$  = Components of the unit normal vector at node point  $i$ ,
- $N_i$  = Lagrangian interpolation function (See Figure 4.25).

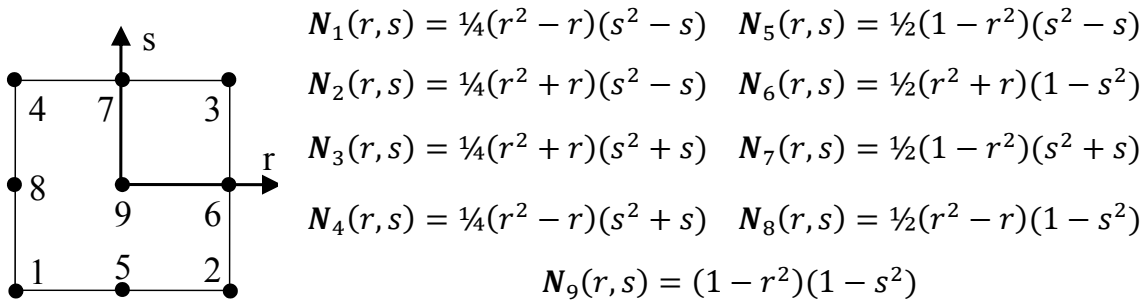


**Figure 4.25: Natural Coordinate System and Lagrangian Shape Functions**

As noted previously, the shell element used in UT Bridge is an isoparametric shell element formulation that uses the same shape functions to define the geometry and displacements. Therefore, the form of Equation 4.6 is used when the displacements of the element  $u$ ,  $v$ , and  $w$  are mapped from global  $(x, y, z)$  coordinates to natural element coordinates  $(r, s, t)$  utilizing the following equation:

$$\mathbf{u}(r, s, t) = \sum_{i=1}^9 \left[ \left( \mathbf{u}_i + t \frac{h}{2} \mathbf{V}_N^i \right) N_i(r, s) \right] \quad \text{Equation 4.7}$$

where:

$\mathbf{u}$  = Displacements of any point in the element,

$\mathbf{u}_i$  = Displacements of node point  $i$ ,

The remaining variables are similarly defined in Equation 4.6.

In addition to the displacements, two rotations are defined for each node ( $\alpha$  and  $\beta$ ) corresponding to the rotation of  $\mathbf{V}_N^i$  about the previously mentioned nodal orthogonal unit vectors  $\mathbf{V}_1^i$  and  $\mathbf{V}_2^i$ , respectively. Because  $\alpha$  and  $\beta$  are assumed to be small angles and the rotation of an infinitely-thin straight material line can be defined by the rotation of the vectors normal to that line, it can be shown that:

$$\mathbf{V}_N^i = -\mathbf{V}_2^i \alpha + \mathbf{V}_1^i \beta \quad \text{Equation 4.8}$$

Combining Equation 4.7 and Equation 4.8 results in the following expression for the element displacements  $\mathbf{u}$ :

$$\mathbf{u}(r, s, t) = \sum_{i=1}^9 \left[ \left( \mathbf{u}_i + t \frac{h}{2} (-\mathbf{V}_2^i \alpha_i + \mathbf{V}_1^i \beta_i) \right) N_i(r, s) \right] \quad \text{Equation 4.9}$$

This shell formulation has five degrees of freedom at each node corresponding to the displacement degrees of freedom  $u$ ,  $v$ , and  $w$  and the rotational degrees of freedom  $\alpha$  and  $\beta$ . The shell element does not have the sixth, “drilling”, degree of freedom corresponding to a rotation about the  $\mathbf{V}_N^i$  vector. The absence of a “drilling” degree of freedom is in keeping with the Reissner-Mindlin kinematical assumptions, which pertain to the admissible displacement profile through the shell thickness (Chapelle & Bathe 2003). The Reissner-Mindlin shell theory assumes that a straight line normal to the

undeformed mid-surface of the shell remains straight during deformation, not necessarily normal to the deformed mid-surface (Bathe 1996). This shell theory is analogous to the Timoshenko beam used in 1-D problems. Additionally, this “drilling” rotation in the plane of the element is small and stores relatively little strain energy. Accordingly, the drilling rotation can be disregarded without sacrificing accuracy in the solution (Popp 2004). Another result of using a shell element without a “drilling” degree of freedom is that the model is defined to have five degrees of freedom per node except at the web flange intersection nodes. These nodes have six degrees of freedom as the drilling degree of freedom of one shell corresponds to a rotation degree of freedom of the other and vice versa.

To evaluate the element stiffness matrix of the shell, the strain-displacement matrix ( $\mathbf{B}$ ) is needed. This matrix relates the element strains in terms of the derivatives of the element displacements with respect to the global coordinates to the element displacements.

$$\boldsymbol{\varepsilon}_0 = \mathbf{B}\hat{\mathbf{u}} \quad \text{Equation 4.10}$$

where:

$$\boldsymbol{\varepsilon}_0 = \left\{ \frac{\partial u}{\partial x} \quad \frac{\partial v}{\partial y} \quad \frac{\partial w}{\partial z} \quad \frac{\partial v}{\partial x} + \frac{\partial u}{\partial y} \quad \frac{\partial w}{\partial x} + \frac{\partial u}{\partial z} \quad \frac{\partial w}{\partial y} + \frac{\partial v}{\partial z} \right\}^T \quad \text{Equation 4.11}$$

$$\hat{\mathbf{u}} = \{u_1 \quad v_1 \quad w_1 \quad \alpha_1 \quad \beta_1 \quad u_2 \quad \dots\}^T \quad \text{Equation 4.12}$$

where:

$\hat{\mathbf{u}}$  = Vector of element displacements at each node of the element.

The shear strain terms of the strain matrix ( $\boldsymbol{\varepsilon}_0$ ) are ordered such that they are consistent with the original formulation used in U-TrAp (Topkaya 2002) and are consistent in this formulation and the implementation of the program. However, the element displacements are defined in terms of the natural coordinate system as defined by taking the derivatives with respect to the natural coordinate of Equation 4.9 as follows:

$$\left\{ \begin{array}{l} \frac{\partial u}{\partial r} \\ \frac{\partial u}{\partial s} \\ \frac{\partial u}{\partial t} \\ \frac{\partial v}{\partial r} \\ \frac{\partial v}{\partial s} \\ \frac{\partial v}{\partial t} \\ \frac{\partial w}{\partial r} \\ \frac{\partial w}{\partial s} \\ \frac{\partial w}{\partial t} \end{array} \right\} = \left[ \begin{array}{cccccc} \frac{\partial N_1}{\partial r} & 0 & 0 & -t \frac{h}{2} \frac{\partial N_1}{\partial r} V_{2x}^1 & t \frac{h}{2} \frac{\partial N_1}{\partial r} V_{1x}^1 & \frac{\partial N_2}{\partial r} & \dots \\ \frac{\partial N_1}{\partial s} & 0 & 0 & -t \frac{h}{2} \frac{\partial N_1}{\partial s} V_{2x}^1 & t \frac{h}{2} \frac{\partial N_1}{\partial s} V_{1x}^1 & \frac{\partial N_2}{\partial s} & \dots \\ 0 & 0 & 0 & -\frac{h}{2} N_1 V_{2x}^1 & \frac{h}{2} N_1 V_{1x}^1 & 0 & \dots \\ 0 & \frac{\partial N_1}{\partial r} & 0 & -t \frac{h}{2} \frac{\partial N_1}{\partial r} V_{2y}^1 & t \frac{h}{2} \frac{\partial N_1}{\partial r} V_{1y}^1 & 0 & \dots \\ 0 & \frac{\partial N_1}{\partial s} & 0 & -t \frac{h}{2} \frac{\partial N_1}{\partial s} V_{2y}^1 & t \frac{h}{2} \frac{\partial N_1}{\partial s} V_{1y}^1 & 0 & \dots \\ 0 & 0 & 0 & -\frac{h}{2} N_1 V_{2y}^1 & \frac{h}{2} N_1 V_{1y}^1 & 0 & \dots \\ 0 & 0 & \frac{\partial N_1}{\partial r} & -t \frac{h}{2} \frac{\partial N_1}{\partial r} V_{2z}^1 & t \frac{h}{2} \frac{\partial N_1}{\partial r} V_{1z}^1 & 0 & \dots \\ 0 & 0 & \frac{\partial N_1}{\partial s} & -t \frac{h}{2} \frac{\partial N_1}{\partial s} V_{2z}^1 & t \frac{h}{2} \frac{\partial N_1}{\partial s} V_{1z}^1 & 0 & \dots \\ 0 & 0 & 0 & -\frac{h}{2} N_1 V_{2z}^1 & \frac{h}{2} N_1 V_{1z}^1 & 0 & \dots \end{array} \right] \left\{ \begin{array}{l} u_1 \\ v_1 \\ w_1 \\ \alpha_1 \\ \beta_1 \\ u_2 \\ \vdots \end{array} \right\} \quad \text{Equation 4.13}$$

To relate the derivatives of the global coordinates and the derivatives of the natural coordinates, the chain rule of partial differentiation is necessary and results in a matrix transformation defined as follows:

$$\left\{ \begin{array}{l} \frac{\partial}{\partial r} \\ \frac{\partial}{\partial s} \\ \frac{\partial}{\partial t} \end{array} \right\} = \left[ \begin{array}{ccc} \frac{\partial x}{\partial r} & \frac{\partial y}{\partial r} & \frac{\partial z}{\partial r} \\ \frac{\partial x}{\partial s} & \frac{\partial y}{\partial s} & \frac{\partial z}{\partial s} \\ \frac{\partial x}{\partial t} & \frac{\partial y}{\partial t} & \frac{\partial z}{\partial t} \end{array} \right] \left\{ \begin{array}{l} \frac{\partial}{\partial x} \\ \frac{\partial}{\partial y} \\ \frac{\partial}{\partial z} \end{array} \right\} \quad \text{Equation 4.14}$$

$$\frac{\partial}{\partial \mathbf{r}} = \mathbf{J} \frac{\partial}{\partial \mathbf{x}} \quad \text{Equation 4.15}$$

where:

$\mathbf{J}$  = Jacobian operator

The Jacobian operator relates the natural coordinate derivatives to the global coordinate derivatives and is obtained from the derivatives of Equation 4.6. However  $\partial/\partial \mathbf{x}$  is required and therefore the inverse of the Jacobian is necessary ( $\mathbf{J}^{-1}$ ) (Bathe



1996). By combining Equation 4.13 and Equation 4.14, the strain-displacement matrix ( $\mathbf{B}$ ) can be formulated as follows:

$$\begin{Bmatrix} \varepsilon_x \\ \varepsilon_y \\ \varepsilon_z \\ \varepsilon_{xy} \\ \varepsilon_{zx} \\ \varepsilon_{yz} \end{Bmatrix} = \begin{bmatrix} \frac{\partial H_1}{\partial x} & 0 & 0 & -\frac{h}{2}V_{2x}^1G_x^1 & \frac{h}{2}V_{1x}^1G_x^1 & \frac{\partial H_2}{\partial x} & \dots \\ 0 & \frac{\partial H_1}{\partial y} & 0 & -\frac{h}{2}V_{2y}^1G_y^1 & \frac{h}{2}V_{1y}^1G_y^1 & 0 & \dots \\ 0 & 0 & \frac{\partial H_1}{\partial z} & -\frac{h}{2}V_{2z}^1G_z^1 & \frac{h}{2}V_{1z}^1G_z^1 & 0 & \dots \\ \frac{\partial H_1}{\partial y} & \frac{\partial H_1}{\partial x} & 0 & -\frac{h}{2}(V_{2x}^1G_y^1 + V_{2y}^1G_x^1) & \frac{h}{2}(V_{1x}^1G_y^1 + V_{1y}^1G_x^1) & \frac{\partial H_2}{\partial y} & \dots \\ \frac{\partial H_1}{\partial z} & 0 & \frac{\partial H_1}{\partial x} & -\frac{h}{2}(V_{2z}^1G_x^1 + V_{2x}^1G_z^1) & \frac{h}{2}(V_{1z}^1G_x^1 + V_{1x}^1G_z^1) & \frac{\partial H_2}{\partial z} & \dots \\ 0 & \frac{\partial H_1}{\partial z} & \frac{\partial H_1}{\partial y} & -\frac{h}{2}(V_{2y}^1G_z^1 + V_{2z}^1G_y^1) & \frac{h}{2}(V_{1y}^1G_z^1 + V_{1z}^1G_y^1) & 0 & \dots \end{bmatrix} \begin{Bmatrix} u_1 \\ v_1 \\ w_1 \\ \alpha_1 \\ \beta_1 \\ u_2 \\ \vdots \end{Bmatrix}$$

**Equation 4.16**

where:

$$\begin{aligned} \frac{\partial H_i}{\partial x} &= J_{11}^{-1} \frac{\partial N_i}{\partial r} + J_{12}^{-1} \frac{\partial N_i}{\partial s} & G_x^i &= t \left( \frac{\partial H_i}{\partial x} \right) + J_{13}^{-1} N_i \\ \frac{\partial H_i}{\partial y} &= J_{21}^{-1} \frac{\partial N_i}{\partial r} + J_{22}^{-1} \frac{\partial N_i}{\partial s} & G_y^i &= t \left( \frac{\partial H_i}{\partial y} \right) + J_{23}^{-1} N_i \\ \frac{\partial H_i}{\partial z} &= J_{31}^{-1} \frac{\partial N_i}{\partial r} + J_{32}^{-1} \frac{\partial N_i}{\partial s} & G_z^i &= t \left( \frac{\partial H_i}{\partial z} \right) + J_{33}^{-1} N_i \end{aligned}$$

$$J_{ij}^{-1} = \text{Element } (i, j) \text{ of } \mathbf{J}^1$$

$$V_{1x}^i = \text{X-component of the } \mathbf{V}_1^i \text{ matrix at the } i \text{ nodal location}$$

$$V_{2x}^i = \text{X-component of the } \mathbf{V}_2^i \text{ matrix at the } i \text{ nodal location.}$$

The other piece of information needed to form the element stiffness matrix is the constitutive relationships. This shell formulation is a degenerated brick element that utilizes the three-dimensional generalized stress-strain matrix for an isotropic material. In keeping with the normal shell assumptions, the stress normal to the surface of the shell ( $\sigma_z$ ) is assumed to be zero. The constitutive relationship ( $\mathbf{C}^{local}$ ), which is the

mathematical representation of the behavior of a material that relates stresses to strains, in natural coordinates, is defined as follows:

$$\begin{Bmatrix} \sigma_x \\ \sigma_y \\ \sigma_z \\ \sigma_{xy} \\ \sigma_{zx} \\ \sigma_{yz} \end{Bmatrix} = \frac{E}{1-\nu^2} \begin{bmatrix} 1 & \nu & 0 & 0 & 0 & 0 \\ & 1 & 0 & 0 & 0 & 0 \\ & & 0 & 0 & 0 & 0 \\ & & & \frac{1-\nu}{2} & 0 & 0 \\ \text{Sym.} & & & & k \frac{1-\nu}{2} & 0 \\ & & & & & k \frac{1-\nu}{2} \end{bmatrix} \begin{Bmatrix} \varepsilon_x \\ \varepsilon_y \\ \varepsilon_z \\ \varepsilon_{xy} \\ \varepsilon_{zx} \\ \varepsilon_{yz} \end{Bmatrix} \quad \text{Equation 4.17}$$

where:

$E$  = Young's modulus of the material

$\nu$  = Poisson's ratio of the material

$k$  = Shear correction factor.

It should be noted that the shear stress and shear strain terms ( $\sigma_{zx}$  and  $\sigma_{yz}$ ,  $\varepsilon_{zx}$  and  $\varepsilon_{yz}$ ) have been defined and ordered to correspond to the formulation used in U-TrAp 2.0. To transform the constitutive matrix from natural coordinates to global coordinates, a rotation matrix  $\mathbf{R}$  is formed from the direction cosines of local orthogonal coordinate axes consisting of unit vectors  $\mathbf{t}_1$ ,  $\mathbf{t}_2$ , and  $\mathbf{t}_3$  at the Gauss integration points. Vectors  $\mathbf{t}_1$ ,  $\mathbf{t}_2$ , and  $\mathbf{t}_3$  are formed by using the Jacobian matrix ( $\mathbf{J}$ ) and the following algorithm:

$$\mathbf{t}_1 = \frac{\partial \mathbf{x}}{\partial r} = \mathbf{J}_{1,n} \quad \mathbf{t}_2 = \frac{\partial \mathbf{x}}{\partial s} = \mathbf{J}_{2,n} \quad : \quad n = 1, 2, 3 \quad \text{Equation 4.18}$$

Form unit vectors:

$$\mathbf{t}_1 = \frac{\mathbf{t}_1}{|\mathbf{t}_1|} \quad \mathbf{t}_2 = \frac{\mathbf{t}_2}{|\mathbf{t}_2|} \quad \text{Equation 4.19}$$

Calculate the normal vector:

$$\mathbf{t}_3 = \mathbf{t}_1 \times \mathbf{t}_2 \quad \text{Equation 4.20}$$

While  $\mathbf{t}_1$  and  $\mathbf{t}_2$  are not chosen arbitrarily they are not necessarily orthogonal and thus to  $\mathbf{t}_2$  vector is re-oriented:

$$\mathbf{t}_2 = \mathbf{t}_3 \times \mathbf{t}_1 \quad \text{Equation 4.21}$$

Then the  $\mathbf{R}$  matrix can be defined as follows and has been modified from that shown in Bathe (1996) to correlate with the ordering of the stress and strain terms used in the program:

$$\mathbf{R} = \begin{bmatrix} l_1^2 & m_1^2 & n_1^2 & l_1 m_1 & n_1 l_1 & m_1 n_1 \\ l_2^2 & m_2^2 & n_2^2 & l_2 m_2 & n_2 l_2 & m_2 n_2 \\ l_3^2 & m_3^2 & n_3^2 & l_3 m_3 & n_3 l_3 & m_3 n_3 \\ 2l_1 l_2 & 2m_1 m_2 & 2n_1 n_2 & l_1 m_2 + l_2 m_1 & n_1 l_2 + n_2 l_1 & m_1 n_2 + m_2 n_1 \\ 2l_3 l_1 & 2m_3 m_1 & 2n_3 n_1 & l_3 m_1 + l_1 m_3 & n_3 l_1 + n_1 l_3 & m_3 n_1 + m_1 n_3 \\ 2l_2 l_3 & 2m_2 m_3 & 2n_2 n_3 & l_2 m_3 + l_3 m_2 & n_2 l_3 + n_3 l_2 & m_2 n_3 + m_3 n_2 \end{bmatrix} \quad \text{Equation 4.22}$$

Because the vectors are unit vectors, the direction cosines are specified as follows:

$$\begin{aligned} l_1 &= \mathbf{e}_x \cdot \mathbf{t}_1 & m_1 &= \mathbf{e}_y \cdot \mathbf{t}_1 & n_1 &= \mathbf{e}_z \cdot \mathbf{t}_1 \\ l_2 &= \mathbf{e}_x \cdot \mathbf{t}_2 & m_2 &= \mathbf{e}_y \cdot \mathbf{t}_2 & n_2 &= \mathbf{e}_z \cdot \mathbf{t}_2 \\ l_3 &= \mathbf{e}_x \cdot \mathbf{t}_3 & m_3 &= \mathbf{e}_y \cdot \mathbf{t}_3 & n_3 &= \mathbf{e}_z \cdot \mathbf{t}_3 \end{aligned}$$

The global rigidity matrix, the constitutive model rotated to global coordinates, is calculated as follows:

$$\mathbf{D} = \mathbf{R}^T \mathbf{C}^{local} \mathbf{R} \quad \text{Equation 4.23}$$

With all the necessary components, the elastic stiffness matrix is defined as:

$$\mathbf{K}_{Shell} = \int_V \mathbf{B}^T \mathbf{D} \mathbf{B} dV = \iiint_V \mathbf{B}^T \mathbf{D} \mathbf{B} \det \mathbf{J} dr ds dt \quad \text{Equation 4.24}$$

This integration is performed numerically using Gaussian quadrature with three integration points in the  $r$ - and  $s$ -directions and with two integration points through the thickness of the  $t$ -direction. The result is Equation 4.25:

$$\mathbf{K}_{Shell} = \sum_i^{18} \mathbf{B}^T \mathbf{D} \mathbf{B} \det(\mathbf{J}) w(i) \quad \text{Equation 4.25}$$

where:

$\det(\mathbf{J})$  = Determinant of the Jacobian matrix  
 $w(i)$  = Weighting factors at the integration point

To verify the accuracy of the shell, a preliminary patch test was performed to ensure the shell exhibited basic behavior necessary for accurate modeling of the bridge. Strong-axis bending typically dominates the behavior of a bridge, resulting in longitudinal stresses and strains in the shell elements. The patch test was performed to ensure the shell exhibits a constant strain behavior under uniform loading. The patch test was successfully verified for a single shell and for multiple shells connected in an orientation similar to that of a girder flange.

#### 4.4.4.2 Truss Element Elastic Stiffness Formulations:

As noted earlier, truss elements were used to model the cross-frames. Modeling cross-frames as trusses is legitimized by Alfred G. Bishara and Wassef E. Elmir (1990) when they assigned beam elements to the cross-frame members of a three-dimensional finite element analysis of a multi-beam composite steel bridge, and the analysis accounted for all six internal forces. According to Bishara and Elmir, the analysis results clearly showed that the axial force was the most significant internal stress resultant and the other internal forces were of no real significance for design purposes.

In UT Bridge, the cross-frame elements are assembled into a “superelement” from four three-dimensional 2-node truss elements. The cross-frame element has four nodes and twelve degrees of freedom with local element number defined by Figure 4.26 looking ahead station.

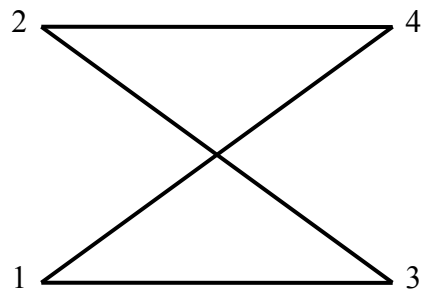


**Figure 4.26: Cross-Frame Schematic**

The truss elements that are used to form the cross-frame superelement are based off a standard 2-node truss element formulation found in many texts including Kassimali (1999) among others. The local element stiffness matrix is given by:

$$\mathbf{k} = \frac{EA}{L} \begin{bmatrix} 1 & -1 \\ -1 & 1 \end{bmatrix} \quad \text{Equation 4.26}$$

where:

$E$  = Young's Modulus of a particular cross-frame element  
 $A$  = Cross-sectional area of a particular cross-frame element  
 $L$  = Length of a particular cross-frame chords.

The matrix is converted to global coordinates by:

$$\mathbf{K} = \mathbf{T}^T \mathbf{k} \mathbf{T} \quad \text{Equation 4.27}$$

where:

$$\mathbf{T} = \begin{bmatrix} \cos \theta_x & \cos \theta_y & \cos \theta_z & 0 & 0 & 0 \\ 0 & 0 & 0 & \cos \theta_x & \cos \theta_y & \cos \theta_z \end{bmatrix} \quad \text{Equation 4.28}$$

where:

$$\cos \theta_x = \frac{(X_e - X_b)}{L} \quad \cos \theta_y = \frac{(Y_e - Y_b)}{L} \quad \cos \theta_z = \frac{(Z_e - Z_b)}{L}$$

$X_b$  = Global  $x$ -coordinate of the beginning node of the truss  
 $X_e$  = Global  $x$ -coordinate of the ending node of the truss  
 $Y_b$  = Global  $y$ -coordinate of the beginning node of the truss  
 $Y_e$  = Global  $y$ -coordinate of the ending node of the truss  
 $Z_b$  = Global  $z$ -coordinate of the beginning node of the truss  
 $Z_e$  = Global  $z$ -coordinate of the ending node of the truss

Then the truss element is combined into a cross-frame element as follows:

$$\mathbf{K}_{X-Frame} = \begin{bmatrix} \mathbf{K}_{13} & \mathbf{K}_{14} \\ \mathbf{K}_{23} & \mathbf{K}_{24} \end{bmatrix} \quad \text{Equation 4.29}$$

where:

$\mathbf{K}_{13}$  = Truss element stiffness matrix for the bottom chord of the cross-frame, the truss element from node 1 to node 3 (Figure 4.26).

$\mathbf{K}_{ij}$  = Similarly for the other submatrices, the truss element from node  $i$  to node  $j$ .

#### 4.4.4.3 Beam Element Elastic Stiffness Formulations:

Stiffeners in the UT Bridge program are modeled using beam elements. The stiffener elements are assembled into a “superelement” from eight three-dimensional two-node beam elements. The beam element used is a standard two-node beam element that

has been formulated in many texts including Kassimali (1999). The local stiffness matrix is given by:

$$\mathbf{k} = \begin{bmatrix}
 \frac{EA}{L} & 0 & 0 & 0 & 0 & 0 & -\frac{EA}{L} & 0 & 0 & 0 & 0 & 0 \\
 0 & \frac{12EI_y}{L^3} & 0 & 0 & \frac{6EI_y}{L^2} & 0 & 0 & -\frac{12EI_y}{L^3} & 0 & 0 & \frac{6EI_y}{L^2} & 0 \\
 0 & 0 & \frac{12EI_z}{L^3} & 0 & 0 & -\frac{6EI_z}{L^2} & 0 & 0 & -\frac{12EI_z}{L^3} & 0 & 0 & -\frac{6EI_z}{L^2} \\
 0 & 0 & 0 & \frac{GJ}{L} & 0 & 0 & 0 & 0 & 0 & -\frac{GJ}{L} & 0 & 0 \\
 0 & \frac{6EI_y}{L^2} & 0 & 0 & \frac{4EI_y}{L} & 0 & 0 & -\frac{6EI_y}{L^2} & 0 & 0 & \frac{2EI_y}{L} & 0 \\
 0 & 0 & -\frac{6EI_z}{L^2} & 0 & 0 & \frac{4EI_z}{L} & 0 & 0 & \frac{6EI_z}{L^2} & 0 & 0 & \frac{2EI_z}{L} \\
 -\frac{EA}{L} & 0 & 0 & 0 & 0 & 0 & \frac{EA}{L} & 0 & 0 & 0 & 0 & 0 \\
 0 & -\frac{12EI_y}{L^3} & 0 & 0 & -\frac{6EI_y}{L^2} & 0 & 0 & \frac{12EI_y}{L^3} & 0 & 0 & -\frac{6EI_y}{L^2} & 0 \\
 0 & 0 & -\frac{12EI_z}{L^3} & 0 & 0 & \frac{6EI_z}{L^2} & 0 & 0 & \frac{12EI_z}{L^3} & 0 & 0 & \frac{6EI_z}{L^2} \\
 0 & 0 & 0 & -\frac{GJ}{L} & 0 & 0 & 0 & 0 & 0 & \frac{GJ}{L} & 0 & 0 \\
 0 & \frac{6EI_y}{L^2} & 0 & 0 & \frac{2EI_y}{L} & 0 & 0 & -\frac{6EI_y}{L^2} & 0 & 0 & \frac{4EI_y}{L} & 0 \\
 0 & 0 & -\frac{6EI_z}{L^2} & 0 & 0 & \frac{2EI_z}{L} & 0 & 0 & \frac{6EI_z}{L^2} & 0 & 0 & \frac{4EI_z}{L}
 \end{bmatrix}$$

**Equation 4.30**

where:

- $E$  = Young's modulus of the material
- $G$  = Shear modulus of the material
- $A$  = Cross-sectional area of the stiffener
- $L$  = Length of the stiffener element
- $I_y$  = Moment of inertia about the local  $y$ -axis of the stiffener
- $I_z$  = Moment of inertia about the local  $z$ -axis of the stiffener
- $J$  = Torsion constant of the stiffener.

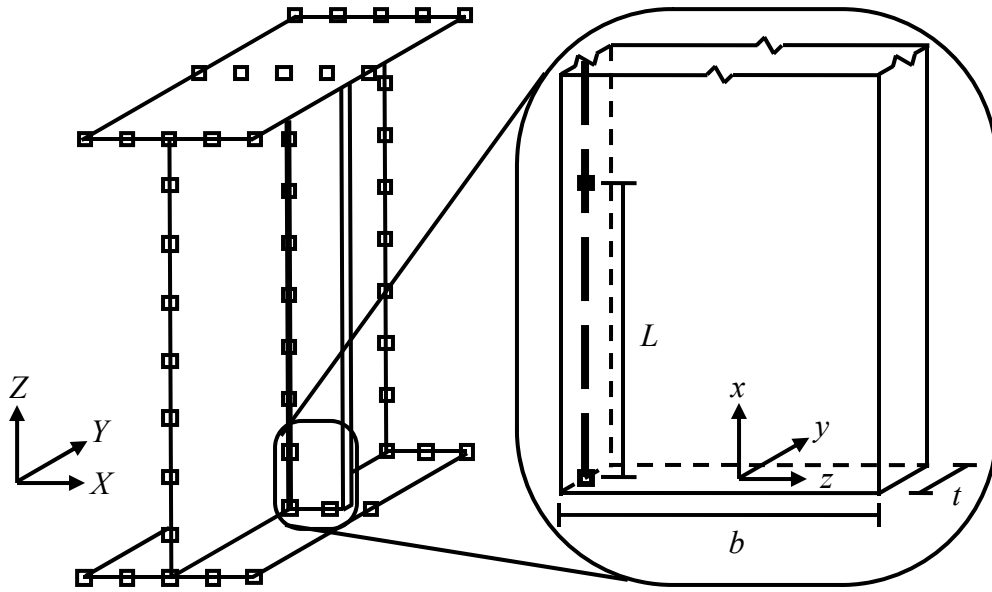


**Figure 4.27: Web Stiffener Schematic**

Figure 4.27 is a schematic of the web stiffener. The dimensions  $b$ ,  $t$ , and  $L$  are the width, thickness, and the distance between web nodes, respectively. The beam elements have six degrees of freedom (dof) per node which when combined results in 54 dof for the 9-node stiffener superelement. However, the web nodes only have five dof per node. Thus, the stiffener element could not be assembled directly from the two-node stiffness matrices, but require a matrix condensation that results in 9 nodes and 45 dof. To accurately account for the beam stiffness, the full 12 dof stiffness matrix ( $\mathbf{k}_{12}$ ) is formed, followed by a matrix condensation process performed as follows:

$$\mathbf{k}_{12} = \begin{bmatrix} \mathbf{k}_{10} & \mathbf{k}_{10x2} \\ \mathbf{k}_{10x2}^T & \mathbf{k}_2 \end{bmatrix} \quad \text{Equation 4.31}$$

$$\mathbf{k}_{10} = \mathbf{k}_{10} - \mathbf{k}_{10x2} * \mathbf{k}_2^{-1} * \mathbf{k}_{10x2}^T \quad \text{Equation 4.32}$$

where:

$\mathbf{k}_{10}$  = Submatrix related to the 10 dof remaining

$\mathbf{k}_2$  = Submatrix related to the seven dof that are being condensed out.

The element stiffness matrices are combined and the resulting 45 dof matrix is converted to global coordinates by:

$$\mathbf{K}_{stiffener} = \mathbf{T}^T \mathbf{k}_{45} \mathbf{T} \quad \text{Equation 4.33}$$

where:

$$T = \begin{bmatrix} R_5 & 0 & 0 & 0 & 0 & 0 & 0 & 0 & 0 \\ & R_5 & 0 & 0 & 0 & 0 & 0 & 0 & 0 \\ & & R_5 & 0 & 0 & 0 & 0 & 0 & 0 \\ & & & R_5 & 0 & 0 & 0 & 0 & 0 \\ & & & & R_5 & 0 & 0 & 0 & 0 \\ & & & & & R_5 & 0 & 0 & 0 \\ & & & & & & R_5 & 0 & 0 \\ & & & & & & & R_5 & 0 \\ & & & & & & & & R_5 \\ & & & & & & & & & \text{sym} \end{bmatrix} \quad \text{Equation 4.34}$$

$$R_5 = \begin{bmatrix} 0 & 0 & 1 & 0 & 0 \\ -V_{Nx} & V_{Ny} & 0 & 0 & 0 \\ -V_{Ny} & -V_{Nx} & 0 & 0 & 0 \\ 0 & 0 & 0 & 0 & 1 \\ 0 & 0 & 0 & 1 & 0 \end{bmatrix}$$

$V_{Nx}$  = X-component of the vector normal to the web shell element at the stiffener location

$V_{Ny}$  = Y-component of the vector normal to the web shell element at the stiffener location.

#### 4.4.4.4 Shear Stud Beam Element Elastic Stiffness Formulation:

Composite action between the steel girder and the concrete bridge deck is achieved by welding shear studs to the top flange of the bridge girders. Figure 4.28 is a schematic drawing depicting the difference in behavior for a beam with and without composite action. The result of composite action is an increase in the bridge stiffness and strength.



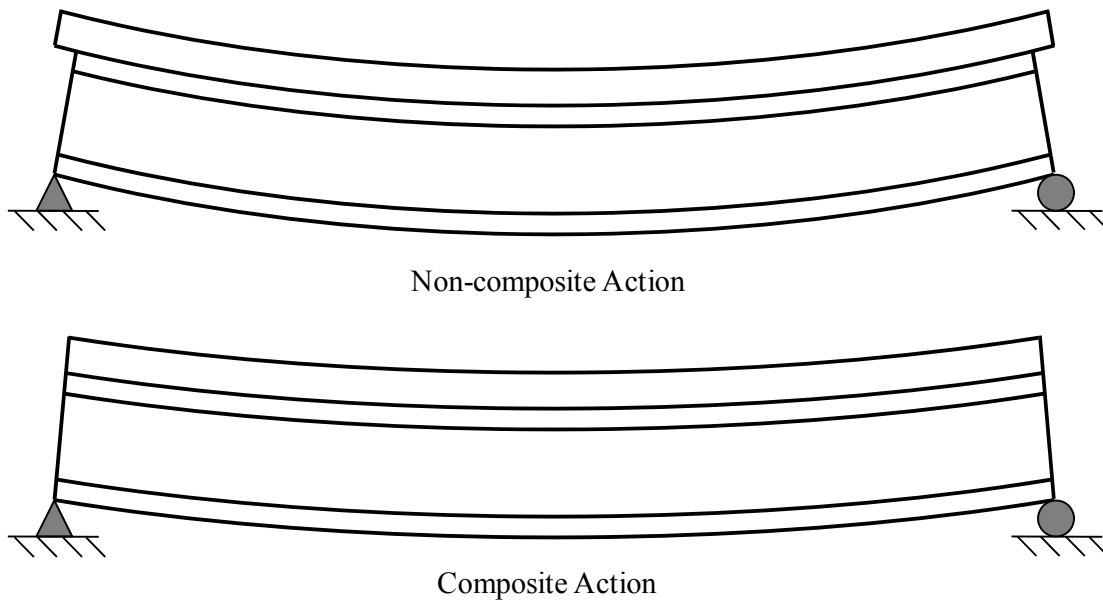


**Figure 4.28: Schematic Effect of Composite Action**

Spring elements were used in UT Bridge to model the shear stud connection between the steel girders and the concrete deck. Significant work was completed by Topkaya at the University of Texas at Austin on the shear stud strength in early aged concrete (Topkaya 2002; Topkaya et al. 2004). A major contribution of Topkaya's work is the ability to model the stiffening effects of early age concrete on the stiffness and stability of girder systems. A summary of this work was presented previously in this chapter. UT Bridge utilizes the experimental data reported by Topkaya by allowing the user to specify the age of the concrete for consideration in the analysis. An assumption in the program is that the bridge utilizes a similar concrete and shear stud type as Topkaya. The program applies a linear interpolation for a specific age concrete; alternatively, the user can provide the concrete modulus and shear stud stiffness.

The companion program U-TrAp 2.0 utilizes a standard three-dimensional two node spring to represent the shear studs. However, this approach requires the top flange and deck nodes to be coincident. To improve modeling capabilities, UT Bridge allows the height of the haunch to be included with a variation on the beam element similar to Equation 4.30 to represent the shear studs. The equation that accounts for the variation in the deck height as a function of the deck thickness and the haunch is shown in Equation 4.35. The haunch is the concrete placed above the top flange of a girder and below the

deck (~1 in. to 2 in.) that both assists in maintaining the deck geometry for variations in the girder haunch and provides a constant deck thickness for girders with variable top flange thickness.

$$\mathbf{k} = \begin{bmatrix}
 K_1 & 0 & 0 & 0 & \frac{K_1 L}{2} & -K_1 & 0 & 0 & 0 & \frac{K_1 L}{2} \\
 & K_2 & 0 & -\frac{K_2 L}{2} & 0 & 0 & -K_2 & 0 & -\frac{K_2 L}{2} & 0 \\
 & & K_3 & 0 & 0 & 0 & 0 & -K_3 & 0 & 0 \\
 & & & \frac{K_2 L^2}{3} & 0 & 0 & \frac{K_2 L}{2} & 0 & \frac{K_2 L^2}{6} & 0 \\
 & & & & \frac{K_1 L^2}{3} & -\frac{K_1 L}{2} & 0 & 0 & 0 & \frac{K_1 L^2}{6} \\
 & & & & & K_1 & 0 & 0 & 0 & -\frac{K_1 L}{2} \\
 & & & & & & K_2 & 0 & \frac{K_2 L}{2} & 0 \\
 & & & & & & & K_3 & 0 & 0 \\
 & & & & & & & & \frac{K_2 L^2}{3} & 0 \\
 & & & & & & & & & \frac{K_1 L^2}{3}
 \end{bmatrix}$$

*Sym*

**Equation 4.35**

where:

$K_1$  = In-plane shear stud stiffness

$K_2 = K_1$

$K_3$  = Vertical spring stiffness

$L$  = Spring length or the haunch thickness plus half the deck thickness

The vertical stiffness is calculated internally as an axial stiffness ( $EA/L$ ). Where the behavior is dominated by the concrete and thus  $E$  is equal to the Young's modulus of concrete,  $A$  is the tributary area of the shear stud in the model and  $L$  is defined above. To ensure convergence and prevent unrealistic movement, two checks are performed with regard to the spring stiffness. If the concrete is specified as newly placed, then the  $E \approx 0$  and  $K_1 \approx 0$ ; thus, the in-plane spring stiffness ( $K_1$ ) is set equal to the friction of the concrete against steel and  $E$  is set to an arbitrary small, but nonzero number to ensure

some material stiffness. The tributary area associated with a shear stud is the area of the top flange closest to the shear stud. Figure 4.29 is a schematic drawing of a top flange with three shear studs across the top of the girder and a crosshatched area showing the area contribution for the vertical stiffness of the shear stud.

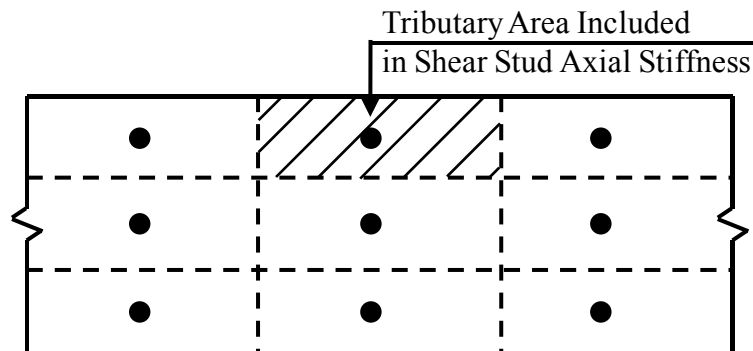


*Figure 4.29: Tributary Area of Shear Stud Stiffness*

#### 4.4.5 Eigenvalue Buckling Analysis:

In many structural applications, the determination of critical loads that might cause instabilities provide valuable information to understanding the strength and behavior of the structure. The critical loads are often determined by conducting an eigenvalue buckling analysis to determine the buckling load and the corresponding mode shape (eigenvector). The user can use UT Bridge to find the eigenvalue for each load case. Although the first mode is typically the mode shape of interest because it corresponds to the lowest buckling mode, the user can also request higher modes. This section provides an overview of the implementation of the eigenvalue analysis in UT Bridge.

##### 4.4.5.1 Mathematical Introduction

The standard eigenproblem in linear algebra takes the form given in Equation 4.36 and is commonly rearranged for solution purposes as shown in Equation 4.37.

$$Ax = \lambda x \quad \text{Equation 4.36}$$

$$(A - \lambda I)x = 0 \quad \text{Equation 4.37}$$

where:

$A$  = Matrix of interest,  
 $x$  = Eigenvector,  
 $\lambda$  = Eigenvalue,  
 $I$  = Identity matrix.

In order for Equation 4.37 to be true, either the vector  $x$  is zero, which is the trivial case, or the determinate of  $(A - \lambda I)$  must be zero as stated mathematically in Equation 4.38.

$$|A - \lambda I|x = 0 \quad \text{Equation 4.38}$$

The solution of this set of equations can be completed in a quick and computationally efficient manner.

The eigenproblem can also take a more broad form known as the generalized eigenproblem given in Equation 4.39 and Equation 4.40.

$$Ax = \lambda Bx \quad \text{Equation 4.39}$$

$$(A - \lambda B)x = 0 \quad \text{Equation 4.40}$$

where:

$A$  = Matrix of order  $m$ ,  
 $B$  = Matrix of order  $m$ .

There are a variety of techniques used to transform the generalized eigenproblem into the standard eigenproblem for the sake of computational ease.

#### 4.4.5.2 Eigenproblem in UT Bridge

The application of typical linear elastic structural analysis techniques includes the assumption that the stiffness of the structure is independent of the forces in the members. As the force approaches the buckling load however, the member will “soften” and the stiffness will decrease. The simplest method of identifying the critical load is an eigenvalue buckling analysis which has been implemented in UT Bridge. The generalized form of an eigenvalue analysis is given in Equation 4.41.

$$[K + \lambda K_g]\Delta = \lambda P \quad \text{Equation 4.41}$$

where:

$K$  = Elastic stiffness matrix

$\mathbf{K}_g$  = Geometric stiffness matrix  
 $\Delta$  = Displacement matrix  
 $\mathbf{P}$  = Load matrix

The geometric stiffness matrix is a function of the member forces. Buckling will occur when an incremental load  $d\mathbf{P}$  results in an infinitely large displacement; mathematically this occurs when the matrix  $[\mathbf{K} + \lambda\mathbf{K}_g]$  is singular. This mathematical fact leads to the generalized eigenproblem given in Equation 4.42.

$$\mathbf{K}\mathbf{x} = -\lambda\mathbf{K}_g\mathbf{x} \qquad \text{Equation 4.42}$$

where:

$\lambda$  = Amplifier for the applied loads that will cause buckling  
 $\mathbf{x}$  = Buckled shape.

The eigenvalue analysis assumes that the displacements prior to buckling are infinitesimal, which is consistent with the small displacement theory of linear elastic analyses. For some structural systems, this assumption may not apply since pre-buckling deformations may lead to second order effects ( $P$ - $\delta$  and  $P$ - $\Delta$ ) that change the response. To model such systems accurately, a large displacement nonlinear analysis must be performed. This type of analysis can be computationally intensive and for many problems, the eigenvalue buckling analysis can give an acceptable indication of the stability of the bridge system.

#### **4.4.6 Element Geometric Stiffness Formulations:**

As stated previously, the geometric stiffness matrix is necessary for an eigenvalue buckling analysis. Details for formulating the geometric stiffness matrix for the element types used in the buckling analysis are provided in the following sections.

##### **4.4.6.1 Shell Element Geometric Stiffness Formulations:**

To perform a stability analysis, the geometric stiffness matrix must be formulated for the shell element utilized in UT Bridge. Additional details of the formulation are given in Popp (2004). The general three-dimensional strain vector can be divided into infinitesimal and large displacement components:

$$\boldsymbol{\varepsilon} = \boldsymbol{\varepsilon}_0 + \boldsymbol{\varepsilon}_L \quad \text{Equation 4.43}$$

where:

$\boldsymbol{\varepsilon}_0$  = Infinitesimal strain or linear strain

$\boldsymbol{\varepsilon}_L$  = Large displacement strain

The infinitesimal strain is defined in Equation 4.11. The large displacement component is the higher order terms of the strain equation; taking the first higher order terms it can be shown that  $\boldsymbol{\varepsilon}_L$  is (McGuire et al. 2000):

$$\boldsymbol{\varepsilon}_L = \frac{1}{2} \begin{pmatrix} \left(\frac{du}{dx}\right)^2 + \left(\frac{dv}{dx}\right)^2 + \left(\frac{dw}{dx}\right)^2 \\ \left(\frac{du}{dy}\right)^2 + \left(\frac{dv}{dy}\right)^2 + \left(\frac{dw}{dy}\right)^2 \\ \left(\frac{du}{dz}\right)^2 + \left(\frac{dv}{dz}\right)^2 + \left(\frac{dw}{dz}\right)^2 \\ \frac{du}{dx} \frac{du}{dy} + \frac{dv}{dx} \frac{dv}{dy} + \frac{dw}{dx} \frac{dw}{dy} \\ \frac{du}{dx} \frac{du}{dz} + \frac{dv}{dx} \frac{dv}{dz} + \frac{dw}{dx} \frac{dw}{dz} \\ \frac{du}{dy} \frac{du}{dz} + \frac{dv}{dy} \frac{dv}{dz} + \frac{dw}{dy} \frac{dw}{dz} \end{pmatrix} \quad \text{Equation 4.44}$$

The strain defined by Equation 4.43 and given by the combination of Equation 4.11 and Equation 4.44 is known as the Green-Lagrange strain. The nonlinear strain terms can be written as follows with a new matrix  $\mathbf{A}$ :

$$\boldsymbol{\varepsilon}_L = \frac{1}{2} \begin{bmatrix} \boldsymbol{\theta}_x^T & 0 & 0 \\ 0 & \boldsymbol{\theta}_y^T & 0 \\ 0 & 0 & \boldsymbol{\theta}_z^T \\ \boldsymbol{\theta}_y^T & \boldsymbol{\theta}_x^T & 0 \\ \boldsymbol{\theta}_z^T & 0 & \boldsymbol{\theta}_x^T \\ 0 & \boldsymbol{\theta}_z^T & \boldsymbol{\theta}_y^T \end{bmatrix} \begin{Bmatrix} \boldsymbol{\theta}_x \\ \boldsymbol{\theta}_y \\ \boldsymbol{\theta}_z \end{Bmatrix} = \frac{1}{2} \mathbf{A} \boldsymbol{\theta} \quad \text{Equation 4.45}$$

where:

$$\boldsymbol{\theta}_x^T = \left\langle \frac{\partial u}{\partial x} \quad \frac{\partial v}{\partial x} \quad \frac{\partial w}{\partial x} \right\rangle$$

$$\boldsymbol{\theta}_y^T = \left\langle \frac{\partial u}{\partial y} \quad \frac{\partial v}{\partial y} \quad \frac{\partial w}{\partial y} \right\rangle$$

$$\boldsymbol{\theta}_z^T = \left\langle \frac{\partial u}{\partial z} \quad \frac{\partial v}{\partial z} \quad \frac{\partial w}{\partial z} \right\rangle$$

Taking the variation of Equation 4.45 to determine the minimum total potential energy and using the fact that  $\delta \mathbf{A}\boldsymbol{\theta} = \mathbf{A}\delta\boldsymbol{\theta}$  (Zienkiewicz 1977),

$$\boldsymbol{\varepsilon}_L = \frac{1}{2}\delta\mathbf{A}\boldsymbol{\theta} + \frac{1}{2}\mathbf{A}\delta\boldsymbol{\theta} = \mathbf{A}\delta\boldsymbol{\theta} \quad \text{Equation 4.46}$$

Then, relating these nonlinear strain terms to the displacements utilizing the same procedure as outlined in the elastic stiffness matrix formulation produces a nonlinear strain-displacement matrix ( $\mathbf{B}_{NL}$ ) as follows:

$$\boldsymbol{\theta} = \mathbf{B}_{NL}\mathbf{a} \quad \text{Equation 4.47}$$

Expanding this equation gives:

$$\begin{pmatrix} \frac{\partial u}{\partial x} \\ \frac{\partial v}{\partial x} \\ \frac{\partial w}{\partial x} \\ \frac{\partial u}{\partial y} \\ \frac{\partial v}{\partial y} \\ \frac{\partial w}{\partial y} \\ \frac{\partial u}{\partial z} \\ \frac{\partial v}{\partial z} \\ \frac{\partial w}{\partial z} \end{pmatrix} = \begin{bmatrix} \frac{\partial H_1}{\partial x} & 0 & 0 & -\frac{h}{2}V_{2x}^1G_x^1 & \frac{h}{2}V_{1x}^1G_x^1 & \frac{\partial H_2}{\partial x} & \dots \\ 0 & \frac{\partial H_1}{\partial x} & 0 & -\frac{h}{2}V_{2y}^1G_x^1 & \frac{h}{2}V_{1y}^1G_x^1 & 0 & \dots \\ 0 & 0 & \frac{\partial H_1}{\partial x} & -\frac{h}{2}V_{2z}^1G_x^1 & \frac{h}{2}V_{1z}^1G_x^1 & 0 & \dots \\ \frac{\partial H_1}{\partial y} & 0 & 0 & -\frac{h}{2}V_{2x}^1G_y^1 & \frac{h}{2}V_{1x}^1G_y^1 & \frac{\partial H_2}{\partial x} & \dots \\ 0 & \frac{\partial H_1}{\partial y} & 0 & -\frac{h}{2}V_{2y}^1G_y^1 & \frac{h}{2}V_{1y}^1G_y^1 & 0 & \dots \\ 0 & 0 & \frac{\partial H_1}{\partial y} & -\frac{h}{2}V_{2z}^1G_y^1 & \frac{h}{2}V_{1z}^1G_y^1 & 0 & \dots \\ \frac{\partial H_1}{\partial z} & 0 & 0 & -\frac{h}{2}V_{2x}^1G_z^1 & \frac{h}{2}V_{1x}^1G_z^1 & \frac{\partial H_2}{\partial x} & \dots \\ 0 & \frac{\partial H_1}{\partial z} & 0 & -\frac{h}{2}V_{2y}^1G_z^1 & \frac{h}{2}V_{1y}^1G_z^1 & 0 & \dots \\ 0 & 0 & \frac{\partial H_1}{\partial z} & -\frac{h}{2}V_{2z}^1G_z^1 & \frac{h}{2}V_{1z}^1G_z^1 & 0 & \dots \end{bmatrix} \begin{pmatrix} u_1 \\ v_1 \\ w_1 \\ \alpha_1 \\ \beta_1 \\ u_1 \\ \vdots \end{pmatrix} \quad \text{Equation 4.48}$$

where:

$$\frac{\partial H_1}{\partial x} = J_{11}^{-1} \frac{\partial N_i}{\partial r} + J_{12}^{-1} \frac{\partial N_i}{\partial s} \quad G_x^i = t \left( \frac{\partial H_i}{\partial x} \right) + J_{13}^{-1} N_i$$

$$\frac{\partial H_1}{\partial y} = J_{21}^{-1} \frac{\partial N_i}{\partial r} + J_{22}^{-1} \frac{\partial N_i}{\partial s} \quad G_y^i = t \left( \frac{\partial H_i}{\partial y} \right) + J_{23}^{-1} N_i$$

$$\frac{\partial H_1}{\partial z} = J_{31}^{-1} \frac{\partial N_i}{\partial r} + J_{32}^{-1} \frac{\partial N_i}{\partial s} \quad G_z^i = t \left( \frac{\partial H_i}{\partial z} \right) + J_{33}^{-1} N_i$$

$J_{ij}^{-1}$  = Element  $(i, j)$  of  $\mathbf{J}^{-1}$

$V_{1x}^i$  = X-component of the  $\mathbf{V}_1^i$  matrix at the  $i$  nodal location,

$V_{2x}^i$  = X-component of the  $\mathbf{V}_2^i$  matrix at the  $i$  nodal location.

Combining Equation 4.46 and Equation 4.47 gives:

$$\boldsymbol{\varepsilon}_L = \mathbf{A}\boldsymbol{\delta\theta} = \mathbf{A}\mathbf{B}_{NL}\boldsymbol{\delta a} = \mathbf{G}\boldsymbol{\delta a} \quad \text{Equation 4.49}$$

And thus the following mathematical operation provides:

$$\mathbf{G} = \mathbf{A}\mathbf{B}_{NL} \quad \text{Equation 4.50}$$

$$\mathbf{G}^T = \mathbf{B}_{NL}^T \mathbf{A}^T \quad \text{Equation 4.51}$$

$$\boldsymbol{\delta G}^T = \mathbf{B}_{NL}^T \boldsymbol{\delta A}^T \quad \text{Equation 4.52}$$

The geometric stiffness matrix can be defined as follows:

$$\mathbf{K}_G \boldsymbol{\delta a} = \int_V \boldsymbol{\delta G}^T \boldsymbol{\sigma} dV = \int_V \mathbf{B}_{NL}^T \boldsymbol{\delta A}^T \boldsymbol{\sigma} dV \quad \text{Equation 4.53}$$

where the initial stress vector ( $\boldsymbol{\sigma}$ ) is:

$$\boldsymbol{\sigma} = \langle \sigma_x \quad \sigma_y \quad \sigma_z \quad \tau_{xy} \quad \tau_{zx} \quad \tau_{yz} \rangle^T \quad \text{Equation 4.54}$$

These initial stresses are determined from a linear elastic analysis by the following algorithm:

$$\boldsymbol{\varepsilon} = \mathbf{B}\mathbf{u} \quad \text{Equation 4.55}$$

$$\boldsymbol{\sigma} = \mathbf{R}^T (\mathbf{C}^{local}) \mathbf{R} \boldsymbol{\varepsilon} = \mathbf{D} \boldsymbol{\varepsilon} \quad \text{Equation 4.56}$$

$$\boldsymbol{\sigma} = \mathbf{D}\mathbf{B}\mathbf{u} \quad \text{Equation 4.57}$$

where:

$\mathbf{B}$  = Elastic strain-displacement matrix,

$\mathbf{C}^{local}$  = Shell element constitutive relationship in natural coordinates,

$\mathbf{R}$  = Rotation matrix,



$\mathbf{D}$  = Rigidity matrix in global coordinates.

The rigidity matrix relates the displacements ( $\mathbf{u}$ ) to the stresses ( $\boldsymbol{\sigma}$ ) used for the geometric stiffness matrix and it can be shown that (Popp 2004):

$$\delta \mathbf{A}^T \boldsymbol{\sigma} = \begin{bmatrix} \sigma_x \mathbf{I}_3 & \tau_{xy} \mathbf{I}_3 & \tau_{zx} \mathbf{I}_3 \\ & \sigma_y \mathbf{I}_3 & \tau_{yz} \mathbf{I}_3 \\ \text{Sym.} & & \sigma_z \mathbf{I}_3 \end{bmatrix} \delta \boldsymbol{\theta} = \mathbf{M} \delta \boldsymbol{\theta} \quad \text{Equation 4.58}$$

where:

$\mathbf{I}_3 = 3 \times 3$  identity matrix.

By combining Equation 4.47, Equation 4.53, and Equation 4.58, the geometric stiffness matrix is defined as:

$$\mathbf{K}_G = \int_V \mathbf{B}_{NL}^T \mathbf{M} \mathbf{B}_{NL} dV = \iiint_V \mathbf{B}_{NL}^T \mathbf{M} \mathbf{B}_{NL} \det \mathbf{J} dr ds dt \quad \text{Equation 4.59}$$

This integration is performed numerically using Gaussian quadrature with three integration points in the  $r$ - and  $s$ -directions and with two integration points in the  $t$ -direction resulting in Equation 4.60:

$$\mathbf{K}_G = \sum_i^{18} \mathbf{B}_{NL}^T \mathbf{M} \mathbf{B}_{NL} \det(\mathbf{J}) w(i) \quad \text{Equation 4.60}$$

where:

$\det(\mathbf{J})$  = Determinant of the Jacobian matrix  
 $w(i)$  = Weighting factors at the integration point.

#### 4.4.6.2 Truss Element Geometric Stiffness Formulations:

The geometric stiffness matrix is formulated similarly to the elastic stiffness matrix with four truss elements assembled into a “superelement.” The formulation of the three-dimensional two-node geometric stiffness matrix is explained in great detail in Popp (2004) and given as:

$$\mathbf{k}_G = \frac{F_x}{L} \begin{bmatrix} 1 & 0 & 0 & -1 & 0 & 0 \\ 0 & 1 & 0 & 0 & -1 & 0 \\ 0 & 0 & 1 & 0 & 0 & 0 \\ -1 & 0 & 0 & 1 & 0 & -1 \\ 0 & -1 & 0 & 0 & 1 & 0 \\ 0 & 0 & -1 & 0 & 0 & 1 \end{bmatrix} \quad \text{Equation 4.61}$$

where:

$F_x$  = Member axial force in the truss element from the linear elastic analysis.

The member axial force is calculated as follows:

$$F_x = \frac{EA}{L} * (\mathbf{T}_x^T \Delta) \quad \text{Equation 4.62}$$

where:

$$\begin{aligned} \mathbf{T}_x &= \langle \cos \theta_x \quad \cos \theta_y \quad \cos \theta_z \rangle^T \\ \Delta &= \langle \delta_x \quad \delta_y \quad \delta_z \rangle^T \\ \delta_x &= \delta_{xe} - \delta_{xb} \quad \delta_y = \delta_{ye} - \delta_{yb} \quad \delta_z = \delta_{ze} - \delta_{zb} \end{aligned}$$

$\mathbf{T}_x$  = Direction cosines of the local  $x$ -axis about the global axis,  
 $\Delta$  = Relative nodal displacements in the three global directions,  
 $\delta_{xb}$  = Global  $x$ -axis nodal displacement of the beginning node of the truss,  
 $\delta_{xe}$  = Global  $x$ -axis nodal displacement of the ending node of the truss.

The direction cosines are defined in Equation 4.28.

The local geometric stiffness matrix is converted to global coordinates by:

$$\mathbf{K}_G = \mathbf{T}^T \mathbf{k}_G \mathbf{T} \quad \text{Equation 4.63}$$

where:

$$\mathbf{T} = \begin{bmatrix} \mathbf{T}_x & \mathbf{T}_y & \mathbf{T}_z & 0 & 0 & 0 \\ 0 & 0 & 0 & \mathbf{T}_x & \mathbf{T}_y & \mathbf{T}_z \end{bmatrix} \quad \text{Equation 4.64}$$

Truss elements do not have an explicit  $y$ - or  $z$ -axis and are chosen arbitrarily as follows:

$$\mathbf{T}_y = \mathbf{e}_z \times \mathbf{T}_x = \langle -\cos \theta_y \quad \cos \theta_x \quad 0 \rangle^T \quad \text{Equation 4.65}$$

$$\mathbf{T}_z = \mathbf{T}_x \times \mathbf{T}_y \quad \text{Equation 4.66}$$

$$\mathbf{T}_z = \begin{pmatrix} -\cos \theta_x \cos \theta_z \\ -\cos \theta_y \cos \theta_z \\ \cos^2 \theta_x + \cos^2 \theta_y \end{pmatrix}$$

The four truss elements are combined similarly to Equation 4.29.

#### 4.4.6.3 Beam Element Geometric Stiffness Formulations:

The geometric stiffness matrix is formulated in a similar fashion to the elastic stiffness matrix with eight beam elements assembled into a “superelement.” The full geometric stiffness matrix of the three-dimensional beam element is formulated by combining bending-axial force interaction, torsion-axial force interaction, and torsion-bending interaction into Equation 4.61. This formulation is explained in detail in McGuire, Gallagher, and Ziemian (2000) and given as follows:

$$\mathbf{k}_G = \begin{bmatrix} \frac{F_{x2}}{L} & 0 & 0 & 0 & 0 & 0 & -\frac{F_{x2}}{L} & 0 & 0 & 0 & 0 & 0 \\ & \frac{6F_{x2}}{5L} & 0 & \frac{M_{y1}}{L} & \frac{M_{x2}}{L} & \frac{F_{x2}}{10} & 0 & -\frac{6F_{x2}}{5L} & 0 & \frac{M_{y2}}{L} & -\frac{M_{x2}}{L} & \frac{F_{x2}}{10} \\ & & \frac{6F_{x2}}{5L} & \frac{M_{z1}}{L} & -\frac{F_{x2}}{10} & \frac{M_{x2}}{L} & 0 & 0 & -\frac{6F_{x2}}{5L} & \frac{M_{zy2}}{L} & -\frac{F_{x2}}{10} & -\frac{M_{x2}}{L} \\ & & & \frac{F_{x2}I_p}{AL} & -\frac{2M_{z1} - M_{z2}}{6} & \frac{2M_{y1} - M_{y2}}{6} & 0 & -\frac{M_{y1}}{L} & -\frac{M_{z1}}{L} & -\frac{F_{x2}I_p}{AL} & -\frac{M_{z1} + M_{z2}}{6} & \frac{M_{y1} + M_{y2}}{6} \\ & & & & \frac{2F_{x2}L}{15} & 0 & 0 & -\frac{M_{x2}}{L} & \frac{F_{x2}}{10} & -\frac{M_{z1} + M_{z2}}{6} & -\frac{F_{x2}}{30} & -\frac{M_{x2}}{2} \\ & & & & & \frac{2F_{x2}L}{15} & 0 & -\frac{F_{x2}}{10} & -\frac{M_{x2}}{L} & \frac{M_{y1} + M_{y2}}{6} & -\frac{M_{x2}}{2} & -\frac{F_{x2}}{30} \\ & & & & & & \frac{F_{x2}}{L} & 0 & 0 & 0 & 0 & 0 \\ & & & & & & & \frac{6F_{x2}}{5L} & 0 & -\frac{M_{y2}}{L} & \frac{M_{x2}}{L} & -\frac{F_{x2}}{10} \\ & & & & & & & & \frac{6F_{x2}}{5L} & -\frac{M_{z2}}{L} & \frac{F_{x2}}{10} & \frac{M_{x2}}{L} \\ & & & & & & & & & \frac{F_{x2}I_p}{AL} & \frac{M_{z1} - 2M_{z2}}{6} & -\frac{M_{y1} - 2M_{y2}}{6} \\ & & & & & & & & & & \frac{2F_{x2}L}{15} & 0 \\ & & & & & & & & & & & \frac{2F_{x2}L}{15} \end{bmatrix}$$

*Sym.*

Equation 4.67

where:

- $A$  and  $L$  = Defined as in Equation 4.30,
- $I_p$  = Polar moment of inertia ( $I_y + I_z$ ).
- $F_{x2}$  = Axial force at the end node
- $M_{x2}$  = Torsional moment at the end node,
- $M_{y1}$  = Moment about the y-axis at the beginning node,

$M_{y2}$  = Moment about the  $y$ -axis at the end node,  
 $M_{z1}$  = Moment about the  $z$ -axis at the beginning node  
 $M_{z2}$  = Moment about the  $z$ -axis at the end node.

These member end forces are not readily determined due to the fact that the rotation about the  $z$ -axis is not a free degree of freedom (dof) for the web nodes and thus  $M_z$  is not straightforward to determine. To determine all 54 member end forces for the nine nodes of the eight element stiffener, the condensed elastic stiffness matrix of the middle six elements with 35 dof is multiplied by the free nodal displacement ( $\Delta 35$ ), and the other 7 nodal displacements are determined as follows:

$$\Delta 7 = k7^{-1}(\mathbf{0} - k35x7^T * \Delta 35) \quad \text{Equation 4.68}$$

where:

$k7^{-1}$  and  $k35x7^T$  = Defined similar to Equation 4.31.

The zero indicates that there are no externally applied loads to the condensed degrees of freedom. Then the nodal displacements are combined and the 54 displacements are multiplied by the full 54-dof elastic stiffness matrix to compute the member end forces. The full geometric stiffness matrix is then condensed similarly to the elastic stiffness matrix and the transformation to global coordinates using equations similar to Equation 4.33 and Equation 4.34.

#### 4.4.7 Boundary Conditions and Loading Options

UT Bridge assumes that the bridge girders are supported at the beginning and end of each span on permanent supports. The program accounts for this by removing the vertical degree of freedom from the node at the bottom flange/web interface at each permanent support. The in-plane behavior is controlled by the specified support type given by the user, either expansion bearing or fixed bearing. At an expansion bearing substructure unit, the girder is assumed to have a slotted sole plate on an elastomeric pad. Accordingly, a stiff spring is applied out-of-plane or radially to the bottom flange/web interface node, and a flexible spring is added longitudinally or tangentially that the same node. The flexible spring prevents a rigid body mode that would result in a singular

global stiffness matrix and therefore make the matrix impossible to invert. For fixed bearings, the program removes the in-plane degrees of freedom preventing any in-plane translations. During the bridge erection analysis, a common first analysis is the placement of a single girder on the bridge. Because there is no support cross-frame to brace the girder, a temporary stiff spring is added out-of-plane to the top flange/web interface node as a stabilizing boundary condition. This spring is removed in subsequent analyses when a second girder is added and the support cross-frame exists.

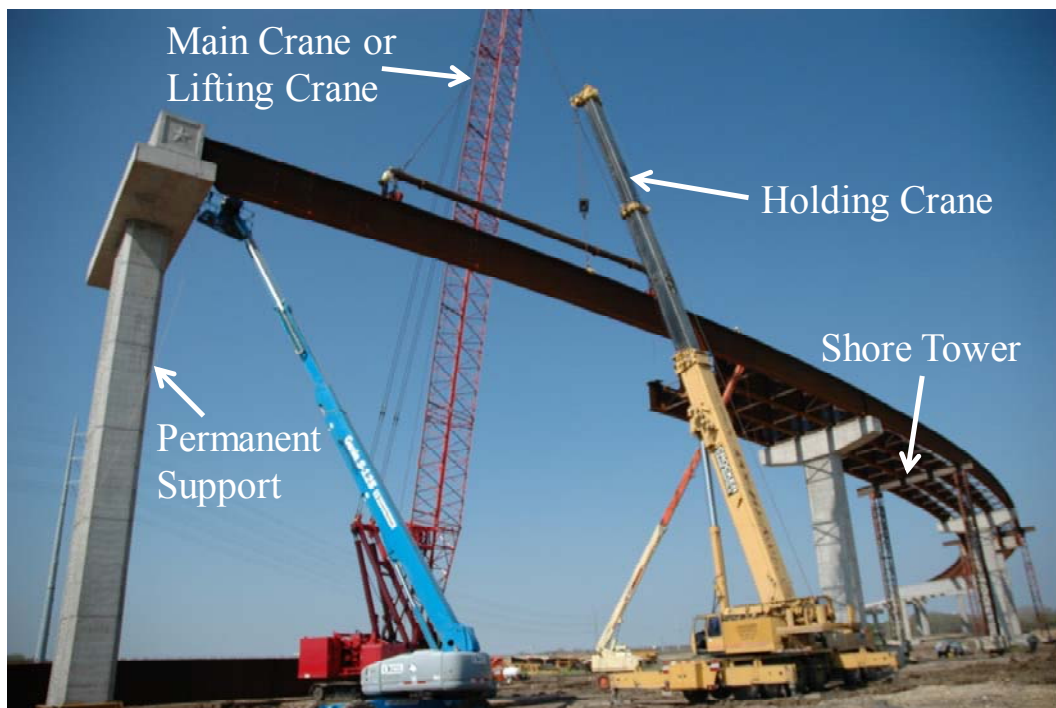


***Figure 4.30: Picture of Holding Crane and Shore Tower***

Figure 4.30 shows a curved I-girder bridge utilizing two effective methods of controlling excessive deformations and stresses during the construction process—shore towers and holding cranes. A shore tower is a temporary support placed under the bridge to control deformations and stresses during the construction process. To model this in UT Bridge, the program places a very stiff vertical spring at the bottom flange/web interface node at the location specified by the user. The shore tower is assumed to behave in-plane similarly to an expansion pier. Additionally, the program assumes that a brace is extended from the shore tower to the top flange of the girder since a cross-frame

is not necessarily located at the support. Thus, a stiff out-of-plane spring is added to the top flange/web interface node directly above the temporary support to provide stability. The temporary support is specified for each analysis case and can be removed prior to the end of construction. This modeling approach works well for the erection sequence analysis, but is problematic for the deck placement analysis as the analysis is linear incremental and the removal of a shore tower will not be accurately represented for such an analysis. A solution to this issue is to perform an analysis and determine the reaction forces from the temporary support. Then on a subsequent analysis apply the reactions after the support is removed to accurately calculate the total deflections and the current state of stress.

The holding crane is used commonly as a temporary vertical load to stabilize the bridge system during specific construction stages. To simulate this setup, UT Bridge allows a point load to be applied to any location on the bridge. The point load application was made general by allowing the user to not only apply a vertical load, but a horizontal point load as well. The load can be applied to the bottom flange/web interface node, the mid-height web node, or the top flange/web interface node. This flexibility allows for numerous load cases to be simulated with UT Bridge. The appropriate holding crane load may not be known prior an initial analysis. It is recommended that an initial analysis with a temporary support located at the holding crane location be performed to determine the reaction force. This reaction applied as a vertical load will prevent vertical deflection and provide an initial holding crane load that may require additional iterations as needed.

In addition to the point load, the self-weight of the bridge is computed by the processor. The weight of the girders, stiffeners, cross-frames, haunch, and deck are all included in the calculation with an optional load factor specified by the user. The area of the shell elements is calculated using the Bretschneider's formula for the area of a quadrilateral ([mathworld.wolfram.com](http://mathworld.wolfram.com)). A final loading option available in UT Bridge is a wind load. The wind load is specified as a pressure along a specific girder. Most

likely, the specified girder would be the exterior girder that is erected first. The specified girder has the pressure applied to the web along the erected portion for each analysis.

#### **4.4.8 Solvers:**

##### **4.4.8.1 Linear Elastic Solver:**

UT Bridge utilizes a highly optimized linear sparse solver developed at Compaq and included in Compaq's extended math library (CXML 2001). A "sparse" matrix is defined as one that has a large percentage of terms equal to zero. The direct sparse solver requires that the global stiffness matrix be given in a specifically formatted set of vectors. The vectors contain only the nonzero elements of the stiffness matrix, which leads to significant computational savings since the vast majority of the elements of the global stiffness matrix are zero and unnecessary to store. The locations of the nonzero elements are provided by the set of vectors, and the large set of linear equations is efficiently solved using a LU decomposition. The solver is further optimized because the stiffness matrix is always positive definite symmetric matrix allowing for the more efficient Cholesky factorization which requires only the upper triangular matrix to be solved (CXML 2001).

##### **4.4.8.2 Eigenvalue Solution Method:**

Popp (2004) provided a brief history of the solution to eigenproblems in his thesis going back to the work of Carl Gustav Jacob Jacobi in 1846. Popp also describes a few modern methods used to solve large eigenproblems in detail, including the inverse reciprocal approach and two variations of the spectral transformation approach. In his work, Popp compares the computational efficiencies of these approaches by implementing ARPACK into UTrAp. ARPACK (ARnoldi PACKage) is a collection of Fortran77 subroutines for solving large-scale eigenvalue problems developed at Rice University (Lehoucq et al. 1998). The following table is taken from Popp's work in which he considered the buckling of a single-girder bridge and varied the solver tolerance from  $10^{-8}$  to  $10^{-2}$ . He then compared the resulting eigenvalue to a known solution. The

Regular Inverse Mode corresponds to the inverse reciprocal approach and the Buckling Mode utilizes the spectral transformation approach.

**Table 4.8: Eigensolver Mode Comparison (Popp 2004)**

| Tolerance | Regular Inverse Mode |            | Buckling Mode |            |
|-----------|----------------------|------------|---------------|------------|
|           | Time (s)             | Error      | Time (s)      | Error      |
| $10^{-8}$ | 2.17                 | 0.0000000% | 2.00          | 0.0000001% |
| $10^{-7}$ | 2.11                 | 0.0000000% | 1.84          | 0.0000147% |
| $10^{-6}$ | 2.08                 | 0.0000000% | 1.42          | 0.5241094% |
| $10^{-5}$ | 1.92                 | 0.0000000% | 1.27          | 2.6114868% |
| $10^{-4}$ | 1.89                 | 0.0000000% | 1.25          | 2.6114868% |
| $10^{-3}$ | 1.75                 | 0.0000006% | 1.25          | 2.6114868% |
| $10^{-2}$ | 1.41                 | 0.5142611% | 1.25          | 2.6114868% |

From this study, although the inverse reciprocal approach is slower for some tolerance settings, the increased accuracy made it the logical choice for implementation in UT Bridge.

#### 4.4.8.3 Inverse Reciprocal Approach:

The inverse reciprocal approach is a technique to transform the generalized eigenproblem into a standard eigenproblem. Taking the generalized eigenproblem given in Equation 4.42, the matrices  $\mathbf{K}$  and  $\mathbf{K}_g$  can be interchanged by forming the following equation:

$$\mathbf{K}_g \mathbf{x} = \mu \mathbf{K} \mathbf{x} \quad \text{Equation 4.69}$$

where:

$$\mu = -\frac{1}{\lambda} \quad \text{Equation 4.70}$$

The problem can then be modified to fit the standard eigenproblem as shown in Equation 4.71:

$$\mathbf{K}^{-1} \mathbf{K}_g \mathbf{x} = \mu \mathbf{x} \quad \text{Equation 4.71}$$

where:

$$\mathbf{K}^{-1} \mathbf{K}_g = \mathbf{A} \text{ in the standard eigenproblem given in Equation 4.36.}$$



The largest negative eigenvalue can then be substituted into Equation 4.70, rendering the critical eigenvalue for the buckling problem. This solution is particularly well suited for structural analysis problems because the elastic stiffness matrix is symmetric, positive definite, and invertible; the geometric stiffness matrix, however, may not be positive definite and invertible.

For the eigenproblem to be defined, the geometric stiffness matrices for the various elements within the problem need to be computed. The previous section provides the geometric stiffness formulation for the shell, truss, and beam elements used in UT Bridge.

#### **4.4.8.4 Eigenvalue Solver:**

The eigenvalue solver used in UT Bridge was developed at Rice University and utilizes parts of the direct sparse solver used in the linear elastic analysis with additional subroutines to solve the eigenproblem using a direct inverse approach. This approach is utilized because it requires the inversion of the global elastic stiffness matrix. The global stiffness matrix can always be inverted for properly constrained systems and only requires the multiplication of the geometric stiffness matrix which may or may not be invertible. General information about the eigensolver method is provided in the previous section with additional details provided by Lehoucq (1998).

### **4.5 POST-PROCESSING WITHIN UT BRIDGE**

#### **4.5.1 Nodal Stress Recovery:**

The displacement-based finite element analysis used in UT Bridge leads to a solution in terms of the nodal displacements, which are the primary variables. The calculation of the nodal stresses is a derived or secondary variable that must be solved for after the program calculates the nodal displacements. This final step in the finite element analysis is referred to as post-processing. It should be noted that the numeric approximation of these secondary variables results in a lower accuracy level than that associated with the primary variable (i.e., displacements). For example, if the accuracy

level of the primary variable is 1%, the level of accuracy for a secondary variable may be in the range of 10% - 15% (Felippa 2004).

The calculation of element stresses has been previously discussed in the formulation of the shell element geometric stiffness matrix given in Equation 4.54 - Equation 4.57. However, the solution of the strain displacement matrix  $\mathbf{B}$  is calculated at the  $3 \times 3$  Gauss integration points, which results in the stress calculations at these locations. It is generally useful to report the stresses at the same locations as the displacements; these values, however, have been computed at the nodal positions. To allow the stresses and displacements to be reported at consistent locations, two approaches are possible:

- 1) Directly apply the nodal natural coordinates ( $r, s$ ) into the shape functions in the formulation of  $\mathbf{B}$  and obtain the nodal stresses using the approach in Equation 4.54 - Equation 4.57.
- 2) Evaluate the stresses at the Gauss points as has been discussed previously using the element stiffness integration rules and then extrapolate the element stress to the node points.

According to Felippa (2004), the second approach generally gives better stress values for quadrilateral elements whose geometry departs substantially from the rectangular shape. This conclusion is validated by “superconvergence” results in finite element approximation theory. For rectangular elements there is no difference between the previously mentioned approaches, but within UT Bridge parallelogram-shaped elements exist at highly skewed supports at the deck and flange elements. Therefore, the second approach was implemented in UT Bridge.

The extrapolation from the Gauss points to the node points is completed using a bi-quadratic extrapolation. The bi-quadratic extrapolation is an extension of a quadratic interpolation used in 1-dimensional analysis (Lagrange interpolation of displacements in a 3-noded finite element truss) to a two-dimensional surface. The extrapolation process is best understood by considering the region bounded by the Gauss points as a “Gauss element” ( $e'$ ) shown in Figure 4.31 and shaded blue.

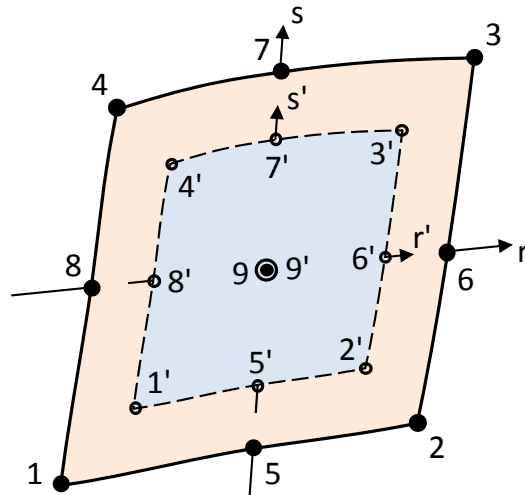


**Figure 4.31: Extrapolation from 3 × 3 "Gauss Element" (e') to 9-Noded Shell Element**

The stresses are calculated at the Gauss points designated as 1', 2', 3', 4', 5', 6', 7', 8', and 9' on the element specified by nodes numbered 1-9. The nodes and Gauss points are located at their natural coordinates ( $r, s$ ) given by the master element and shown in Table 4.9. The "Gauss element" has a similar scaled coordinate system ( $r', s'$ ) with the Gauss points located as shown in Table 4.10 and the node locations calculated for the Gauss element coordinate system by the simple relationship given in Equation 4.72.

$$r = \sqrt{5/3} r', \quad s = \sqrt{5/3} s', \quad r' = \sqrt{3/5} r, \quad s' = \sqrt{3/5} s \quad \text{Equation 4.72}$$

**Table 4.9: Natural Coordinates of 9-Node Shell Element**

| Nodes Number | Natural Coordinates |     | Gauss Element Coordinates |               |
|--------------|---------------------|-----|---------------------------|---------------|
|              | $r$                 | $s$ | $r'$                      | $s'$          |
| 1            | -1                  | -1  | $-\sqrt{5/3}$             | $-\sqrt{5/3}$ |
| 2            | 1                   | -1  | $\sqrt{5/3}$              | $-\sqrt{5/3}$ |
| 3            | 1                   | 1   | $\sqrt{5/3}$              | $\sqrt{5/3}$  |
| 4            | -1                  | 1   | $-\sqrt{5/3}$             | $\sqrt{5/3}$  |
| 5            | 0                   | -1  | 0                         | $-\sqrt{5/3}$ |
| 6            | 1                   | 0   | $\sqrt{5/3}$              | 0             |
| 7            | 0                   | 1   | 0                         | $\sqrt{5/3}$  |
| 8            | -1                  | 0   | $-\sqrt{5/3}$             | 0             |
| 9            | 0                   | 0   | 0                         | 0             |

**Table 4.10: Gauss Element Coordinates of 9-Node Shell Element**

| Gauss Number | Natural Coordinates |               | Gauss Element Coordinates |      |
|--------------|---------------------|---------------|---------------------------|------|
|              | $r$                 | $s$           | $r'$                      | $s'$ |
| 1'           | $-\sqrt{3/5}$       | $-\sqrt{3/5}$ | -1                        | -1   |
| 2'           | $\sqrt{3/5}$        | $-\sqrt{3/5}$ | 1                         | -1   |
| 3'           | $\sqrt{3/5}$        | $\sqrt{3/5}$  | 1                         | 1    |
| 4'           | $-\sqrt{3/5}$       | $\sqrt{3/5}$  | -1                        | 1    |
| 5'           | 0                   | $-\sqrt{3/5}$ | 0                         | -1   |
| 6'           | $\sqrt{3/5}$        | 0             | 1                         | 0    |
| 7'           | 0                   | $\sqrt{3/5}$  | 0                         | 1    |
| 8'           | $-\sqrt{3/5}$       | 0             | -1                        | 0    |
| 9'           | 0                   | 0             | 0                         | 0    |

The stresses  $\sigma$  whose values  $\sigma'_i$  at the Gauss points are known can be extrapolated through the bi-quadratic shape functions given in Figure 4.25 and expressed in terms of  $r'$  and  $s'$ :

$$\sigma(r', s') = [\sigma'_1 \quad \sigma'_2 \quad \cdots \quad \sigma'_9] \begin{bmatrix} N_1^{(e')} \\ N_2^{(e')} \\ \vdots \\ N_9^{(e')} \end{bmatrix} \quad \text{Equation 4.73}$$

where:

$$\begin{aligned} N_1^{(e')}(r', s') &= \frac{1}{4}(r'^2 - r')(s'^2 - s') & N_5^{(e')}(r', s') &= \frac{1}{2}(1 - r'^2)(s'^2 - s') \\ N_2^{(e')}(r', s') &= \frac{1}{4}(r'^2 + r')(s'^2 - s') & N_6^{(e')}(r', s') &= \frac{1}{2}(r'^2 + r')(1 - s'^2) \\ N_3^{(e')}(r', s') &= \frac{1}{4}(r'^2 + r')(s'^2 + s') & N_7^{(e')}(r', s') &= \frac{1}{2}(1 - r'^2)(s'^2 + s') \\ N_4^{(e')}(r', s') &= \frac{1}{4}(r'^2 - r')(s'^2 + s') & N_8^{(e')}(r', s') &= \frac{1}{2}(r'^2 - r')(1 - s'^2) \\ N_9^{(e')}(r', s') &= (1 - r'^2)(1 - s'^2) \end{aligned}$$

Expanding these equations for stresses at each node point  $i$  results in Equation 4.74.

$$\begin{bmatrix} \sigma_1(r', s') \\ \sigma_2(r', s') \\ \vdots \\ \sigma_9(r', s') \end{bmatrix} = \begin{bmatrix} N_1^{(e')}(r'_1, s'_1) & N_2^{(e')}(r'_1, s'_1) & \dots & N_9^{(e')}(r'_1, s'_1) \\ N_1^{(e')}(r'_2, s'_2) & N_2^{(e')}(r'_2, s'_2) & \dots & N_9^{(e')}(r'_2, s'_2) \\ \vdots & \vdots & \ddots & \vdots \\ N_1^{(e')}(r'_9, s'_9) & N_2^{(e')}(r'_9, s'_9) & \dots & N_9^{(e')}(r'_9, s'_9) \end{bmatrix} \begin{bmatrix} \sigma'_1 \\ \sigma'_2 \\ \vdots \\ \sigma'_9 \end{bmatrix} \quad \text{Equation 4.74}$$

#### 4.5.2 Inter-element Averaging:

The stress calculated by the previously discussed method is on an element-by-element basis. The result of using a 9-node shell element and quadratic displacement shape functions results in a linear approximation of the stress. However, unlike the displacements that have continuity enforced at the inter-element boundaries, the stresses have no such requirement and in general are not continuous. Thus, for convenience of the end user, a single stress value is computed for cases in which multiple elements are connected to a single node. The most common approach is an unweighted average of all elements connected to the node. The other option is to perform a weighted average where a weighting is assigned to the elements connected to a node.

For the shell elements used in UT Bridge, the stresses were calculated at the  $3 \times 3$  integration points in the plane of the shell, and also 2 layers through the thickness of the shell. The Gauss integration points are shown schematically in Figure 4.32.

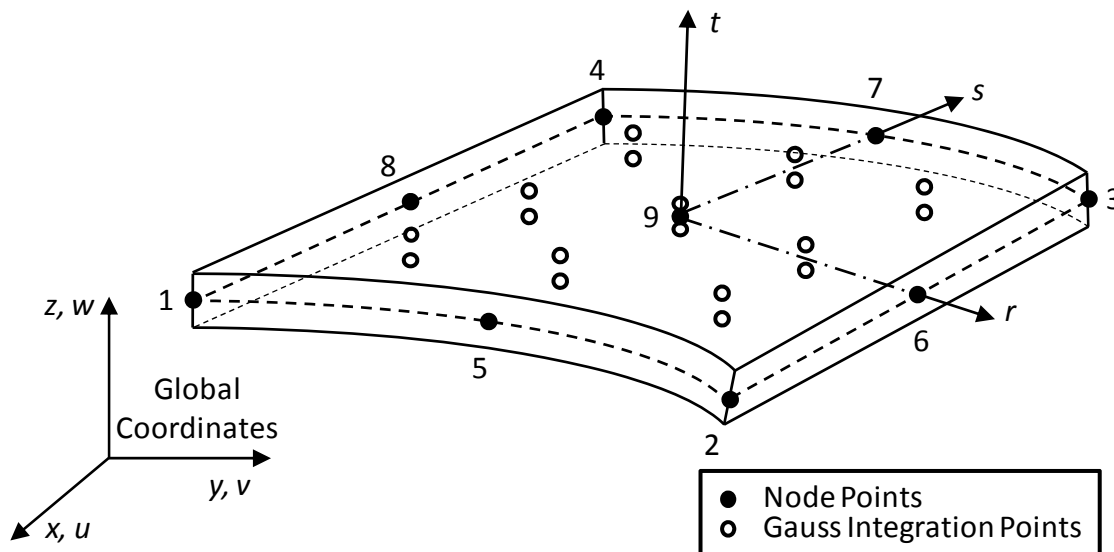
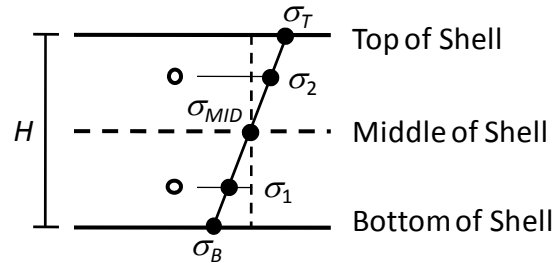


Figure 4.32: 18 Gauss Points of the  $3 \times 3 \times 2$  Integration

Assuming a linear variation through the thickness (no shear deformations) of the element allows for the stress at the top, middle, and bottom of the shell element to be calculated by Equation 4.75 - Equation 4.77.



**Figure 4.33: Through Thickness Stress Variation**

where:

$H$  = Shell thickness

$\sigma_1$  = Stress at the Gauss integration point layer located  $-H/2\sqrt{3}$  from the middle of the shell

$\sigma_2$  = Stress at the Gauss integration point layer located  $H/2\sqrt{3}$  from the middle of the shell

$$\sigma_B = 1/2 (\sigma_1 + \sigma_2) - \sqrt{3}/2 (\sigma_1 - \sigma_2) \quad \text{Equation 4.75}$$

$$\sigma_{MID} = 1/2 (\sigma_1 + \sigma_2) \quad \text{Equation 4.76}$$

$$\sigma_T = 1/2 (\sigma_1 + \sigma_2) + \sqrt{3}/2 (\sigma_1 - \sigma_2) \quad \text{Equation 4.77}$$

When performing stress checks in an analysis, the extreme fibers of the cross-section yield the maximum and minimum stress. Therefore it was desirable in UT Bridge to report the stresses at the bottom of the bottom flange, the midsurface of the web, and the top of the top flange and deck. When averaging the nodal stresses for nodes at certain locations, such as the web-flange interface, a simple unweighted average did not accurately give the extreme fiber stress in strong-axis bending. Therefore, the stresses were weighted such that the web elements were arbitrarily set to 1% of the weighting of a flange element. With this approach the web flange interfaces gave a stress for the extreme fibers in strong-axis bending.

### 4.5.3 Calculating Reactions:

The reactions are locations at the permanent supports where the displacements have been constrained to be zero. To recover the reactions at these supports, the full global stiffness matrix is partitioned to separate the free degrees of freedom and the restrained degrees of freedom as shown in Equation 4.78.

$$\begin{bmatrix} \mathbf{K}_{FF} & | & \mathbf{K}_{FR} \\ \hline - & + & - \\ \mathbf{K}_{RF} & | & \mathbf{K}_{RR} \end{bmatrix} \begin{Bmatrix} \Delta_F \\ \Delta_R = 0 \end{Bmatrix} = \begin{Bmatrix} \mathbf{F}_F \\ \mathbf{R} \end{Bmatrix} \quad \text{Equation 4.78}$$

where:

$$\begin{bmatrix} \mathbf{K}_{FF} & | & \mathbf{K}_{FR} \\ \hline - & + & - \\ \mathbf{K}_{RF} & | & \mathbf{K}_{RR} \end{bmatrix} = \text{Partitioned global stiffness matrix}$$

$\Delta_F$  = Free degrees of freedom.  
 $\mathbf{F}_F$  = Nodal forces.  
 $\mathbf{R}$  = Reactions at the restrained degrees of freedom.

$$\mathbf{R} = \mathbf{K}_{RF} * \Delta_F \quad \text{Equation 4.79}$$

Due to the efficient storage technique of the global stiffness matrix in UT Bridge, the terms associated with the restrained degrees of freedom are not stored prior to calculating the reactions. To recover the  $\mathbf{K}_{RF}$  matrix, the element stiffness matrix of all elements connected to the reaction node are calculated and multiplied by the corresponding displacements resulting in the calculation of  $\mathbf{R}$ .

### 4.6 POST-PROCESSOR, UT VIEWER

UT Viewer is the post-processor for the UT Bridge program and was created to help the user easily view and analyze the results from a set of bridge analyses. After the user loads the results file, they are then able to view a three-dimensional rendering of the bridge geometry, bridge displacements, and bridge stresses. Additionally, UT Viewer can also display numerous XY plots showing the displacements, rotations, and stresses at tenth points along the length of the bridge. The information used to generate the XY plots is also available in a tabular form, which allows the user to copy the information to

another program such as a spreadsheet for further analysis. Additionally, cross-frame forces and reactions are given graphically or in tabular form.

The three-dimensional graphics available in UT Viewer provide the engineer an invaluable tool to ensure the bridge intended to be modeled was properly input and key structural elements are located as indicated on the bridge plans. A *Visualization* option is provided in the pre-processor that quickly develops the bridge geometry, but does not actually perform an analysis. This option allows for a check of the input prior to the analysis. Figure 4.34 is screen shot of a bridge rendered in UT Viewer.

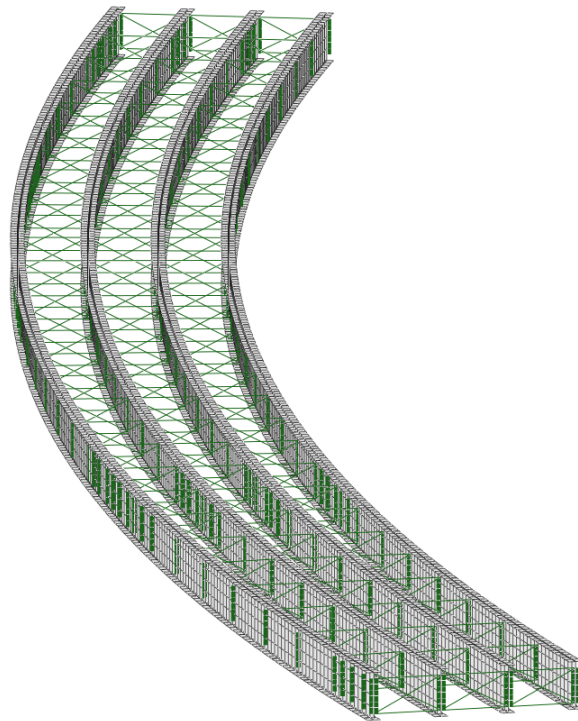


**Figure 4.34: UT Viewer Screen Shot of a Bridge**

In addition to geometric accuracy, UT Viewer can display the deformed shape of the bridge being analyzed for each analysis case. The deformed shape can also be viewed for the eigenvalue buckling analysis, providing the corresponding buckled shape (eigenvector) of the bridge system for each eigenvalue. An example of a bridge's buckled shape is shown in Figure 4.35. A three-dimensional contour plot of the stresses is also available to determine the maximum and minimum stress and the locations of high stress regions. Figure 4.36 is a screen shot of the UT Viewer stress contour for a concrete



deck placement analysis. The cross-frame forces are given for each of the members, but it is assumed that the diagonal member is a tension only member; therefore, one diagonal will report zero force. The reactions for both permanent and temporary supports are also given.

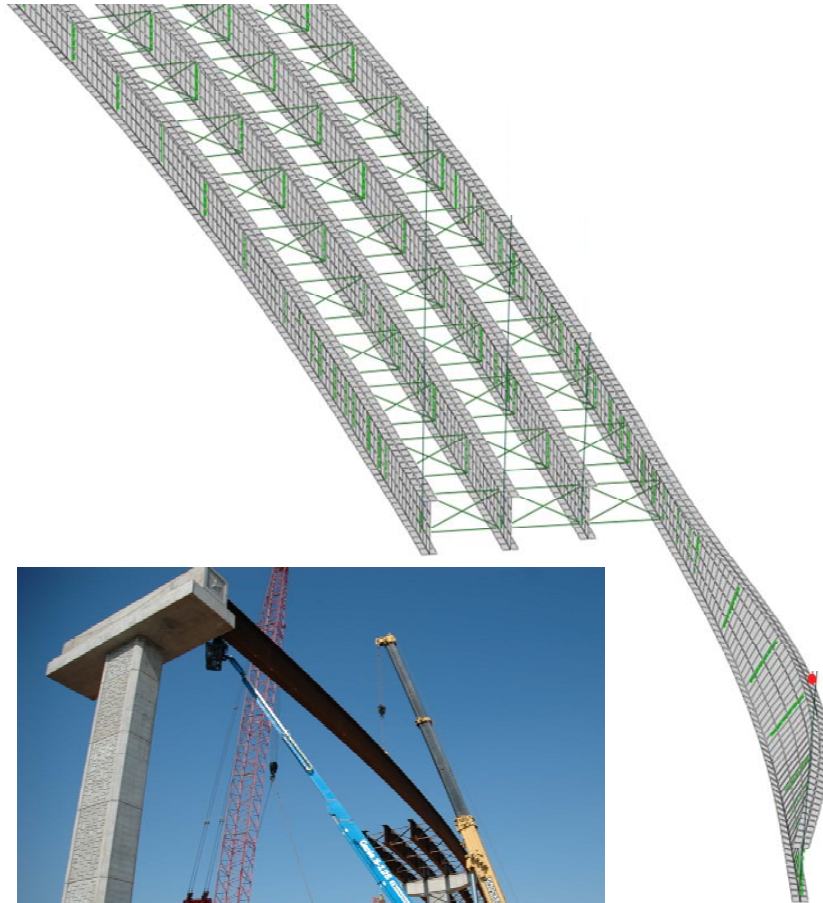


*Figure 4.35: UT Viewer Screen Shot of a Buckled Shape*

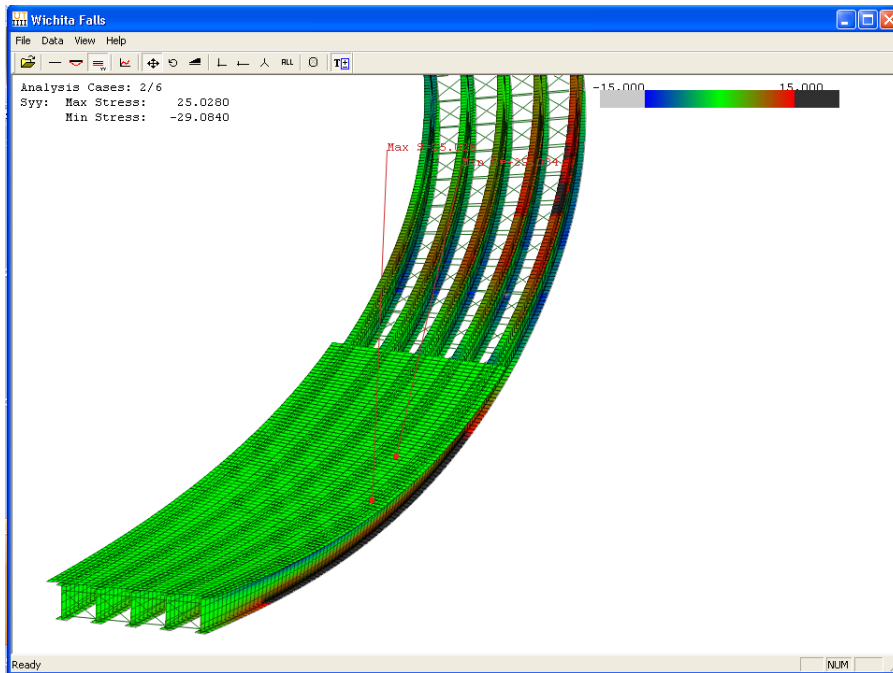


**Figure 4.36: UT Viewer Screen Shot of Stress Plot**

UT Viewer provides a range of two-dimensional graphs. The user can generate graphs of displacements, stresses, and rotations at tenth points along each span for each girder. These graphs provide a graphical indication of the relative displacement of the girders, the location of maximum rotation, or other pertinent information on the deformations or stresses. The data from the graphs are also given in a tabular form that can be copied and pasted into another program for additional data analysis. The tabular form of the data can provide designers with valuable information such as the necessary camber in highly curved or skewed bridge systems. Figure 4.37 is a screen shot of the graph of the vertical displacement of a three-span bridge with four girders.

**Displacement: Translation in Vertical Direction**  
Girder1      Girder2      Girder3      Girder4

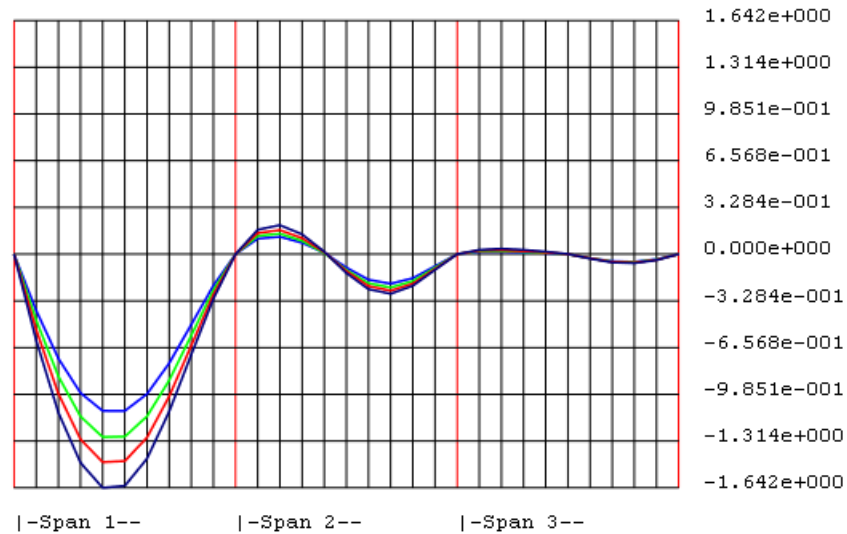


**Figure 4.37: Screen Shot of UT Bridge XY Plot for Concrete Placed in Span 1**

#### 4.7 VERIFICATION

Throughout the development of UT Bridge, verification studies were conducted on a continuous basis. Verification studies were conducted on individual elements, multiple-element systems, and entire bridge models. Although several different systems were considered, it is not possible to consider every possible scenario and thus it is recommended that the design engineer perform independent checks to ensure the accuracy of the program for the range of systems for which they might use the software. Two examples of actual bridges are provided with independent verification from field data, commercially available two-dimensional grillage models, and three-dimensional finite element analyses.

Bridge 88 was discussed previously in Chapter 3. The details of the collected field data were presented by Farris (2008). The displacement data were collected during the concrete deck placement. The deck was placed continuously starting from span 16 and progressing back station toward span 15 and finally over span 14. Displacement measurements were taken in the field in span 14 at  $1/8^{\text{th}}$  points from the beginning of the span to midspan on girders 3 and 4. The displacements were measured with a laser

distance meter that had an accuracy of 1/16<sup>th</sup> of an inch. Graphs comparing the field data with the predicted deflection values for Bridge 88 are presented in Figure 4.38 for the case when the deck was completely placed on span 16. The two graphs in Figure 4.38 represent the field data and results computed using UT Bridge for Girder 3 (a) and for Girder 4 (b). Figure 4.39 provides another pair of graphs with similar data, but they represent the time at which the first two spans (spans 15 and 16) were placed. Figure 4.40 and Figure 4.41 compare UT Bridge to the results of two separate commercially available grillage software programs, MDX (2009) and DESCUS (2008), as well as a three-dimensional finite element model developed in ANSYS (2007). The commercially available grillage software (MDX and DESCUS) were unable to perform the intermediate analysis; thus, they were only compared to the final bridge configuration with a fully installed deck. Some variations are observed between the measured data and the calculations from UT Bridge. Reasons for this discrepancy include the resolution of the laser, variations in the actual concrete placed as provided by the construction inspector (deck thickness varied from 8.5 in. to 10.25 in. and averaged 9.6 in.), and approximations in the amount of concrete deck placed at the time of the measurements.

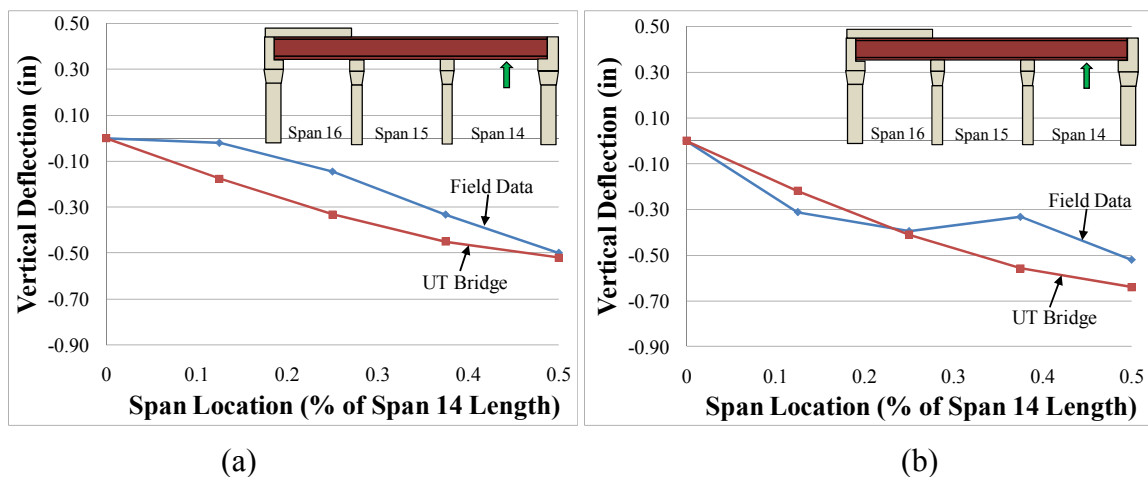


**Figure 4.38: UT Bridge Field Data Comparison for Girder 3 (a) and Girder 4 (b)**

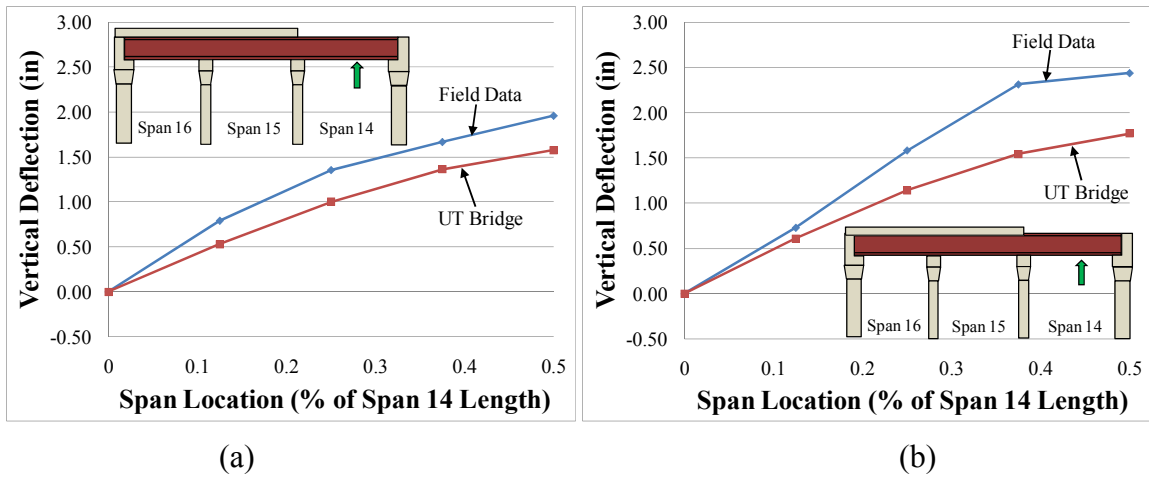


Figure 4.39: UT Bridge Field Data Comparison for Girder 3 (a) and Girder 4 (b)

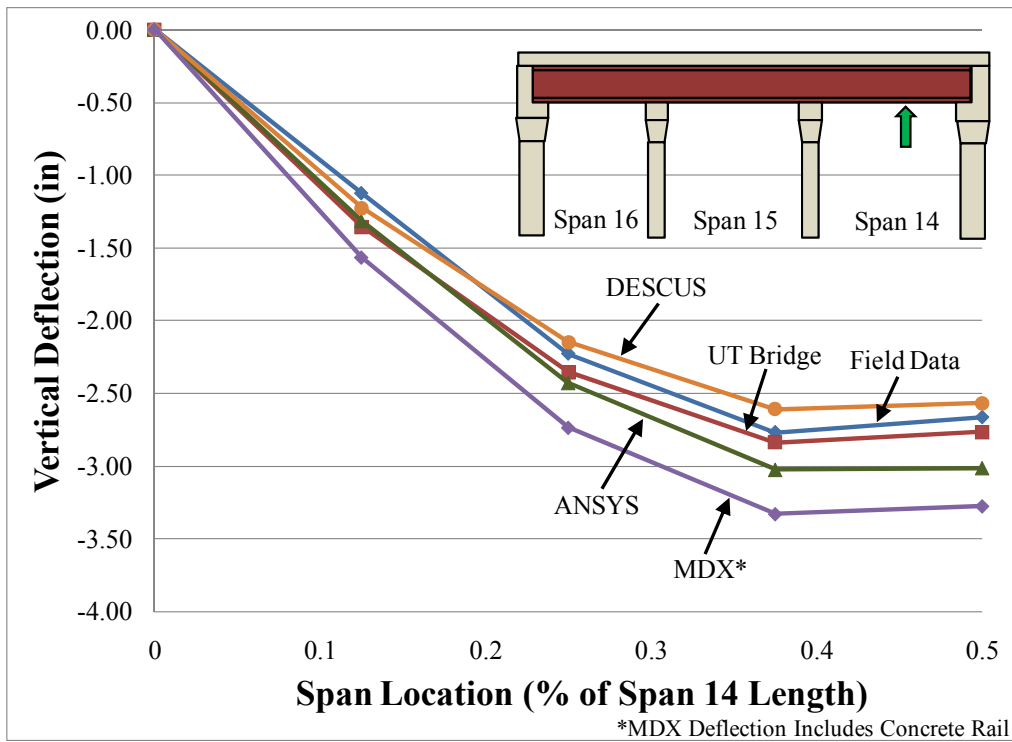
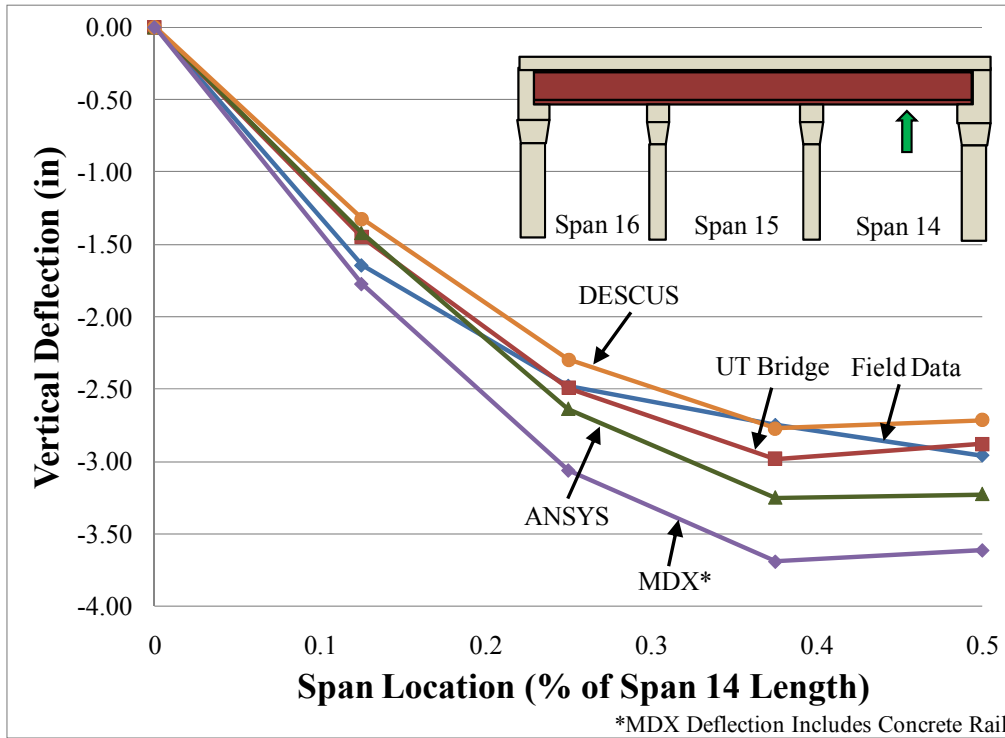


Figure 4.40: Girder 3 UT Bridge Comparison to Field Data and Commercial Programs



**Figure 4.41: Girder 4 UT Bridge Comparison to Field Data and Commercial Programs**

The second verification bridge presented here was built in Wichita Falls, Texas and analyzed independently by Dr. Quan Chen utilizing a three-dimensional finite element model in ANSYS. The original design of the bridge was carried out utilizing a grillage model that failed to predict excessive torsional flexibility in the bridge. As a result, the bridge experienced complications during the concrete placement. The subsequent ANSYS models were developed to identify the problem and to propose retrofits. The ANSYS models provided valuable validation data for UT Bridge. In addition, the Texas Department of Transportation also modeled the bridge as part of the design utilizing DESCUS. The results of the ANSYS and DESCUS models were compared to UT Bridge. There was a slight modification made to the UT Bridge program to account for the fact that the actual bridge had a point of tangency near the end of the bridge resulting in a slightly different span arrangement than a constant curvature modeled in UT Bridge. The last substructure unit was skewed 6 degrees to ensure the span lengths of all the girders matched the as-built condition in the field. Figure 4.42 – Figure 4.46 show the comparisons for all five girders along the length of the bridge for

the steel dead load only. The UT Bridge results had reasonable agreement with the ANSYS solution. The grillage model for the bridge overestimated the stiffness of the structure relative to the three-dimensional models. Figure 4.47 – Figure 4.51 show similar comparisons—the vertical deflection for the bridge with the entire concrete deck placed. The significant torsion in the structural system can be observed by comparing the relative displacements of Girders 1 and 5, which are the girders at the two edges of the bridge.

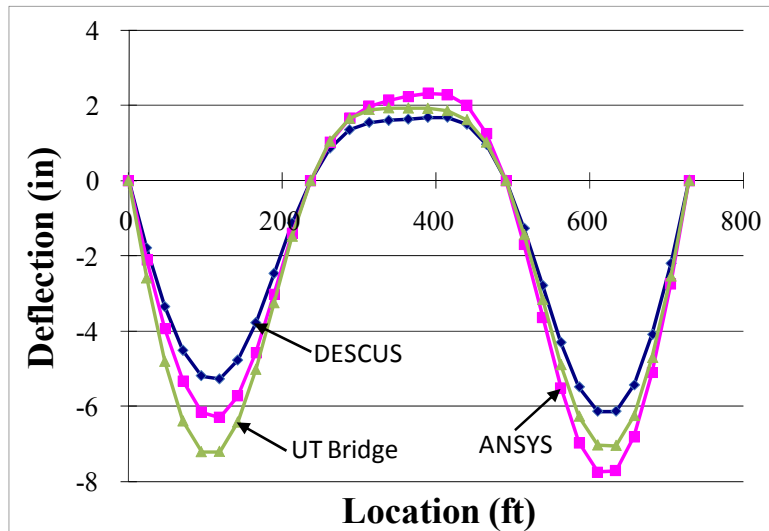


**Figure 4.42: Girder 1 Comparison for Steel Dead Load Only**

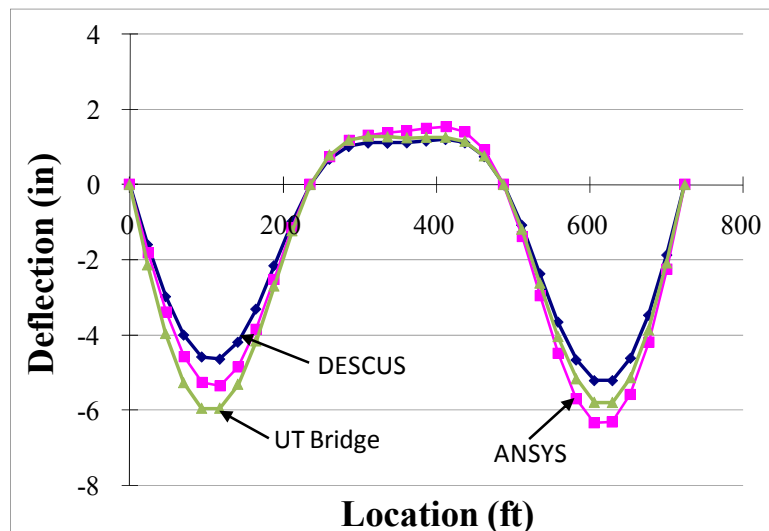


**Figure 4.43: Girder 2 Comparison for Steel Dead Load Only**

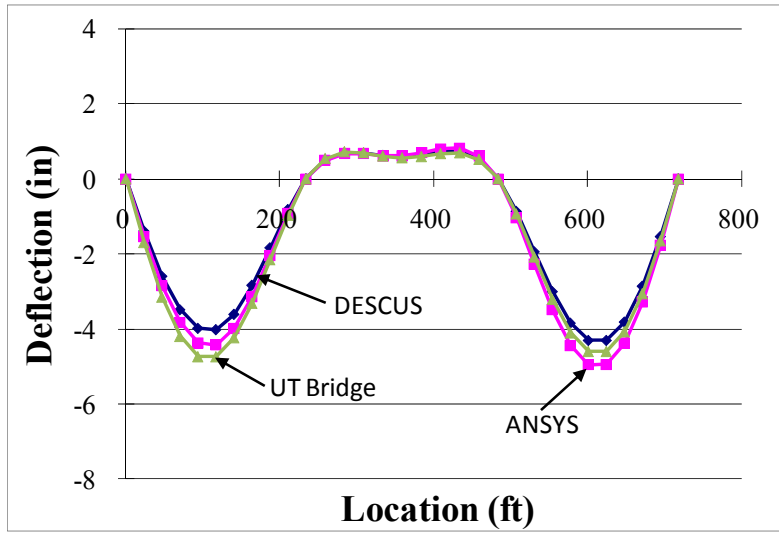


**Figure 4.44: Girder 3 Comparison for Steel Dead Load Only**

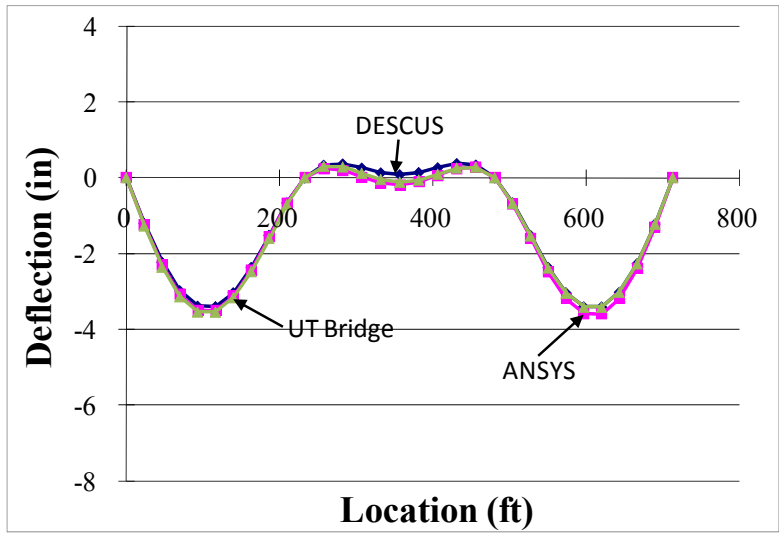


**Figure 4.45: Girder 4 Comparison for Steel Dead Load Only**



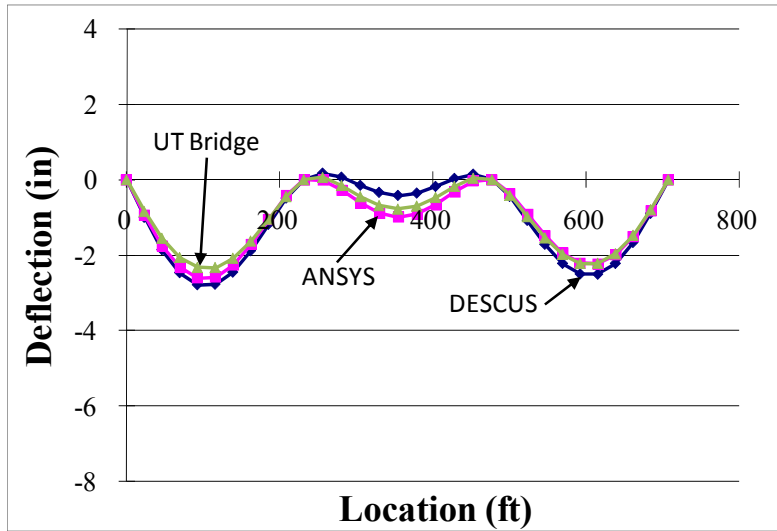


**Figure 4.46: Girder 5 Comparison for Steel Dead Load Only**

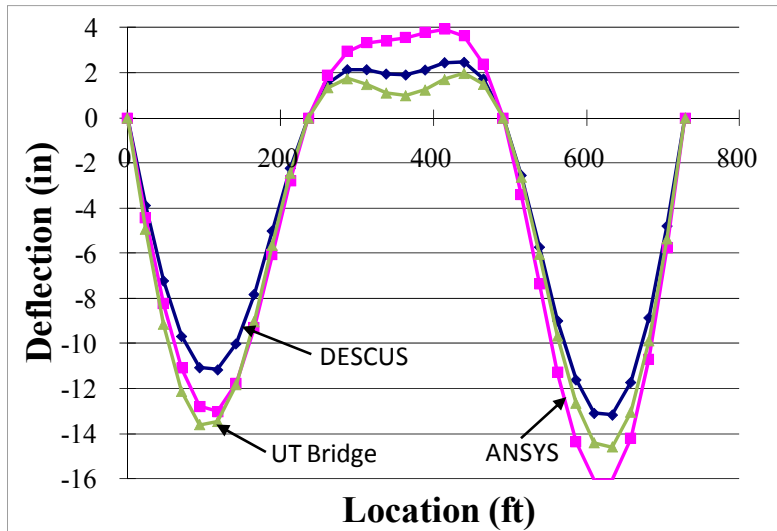


**Figure 4.47: Girder 1 Comparison for Steel and Concrete Slab Loading**

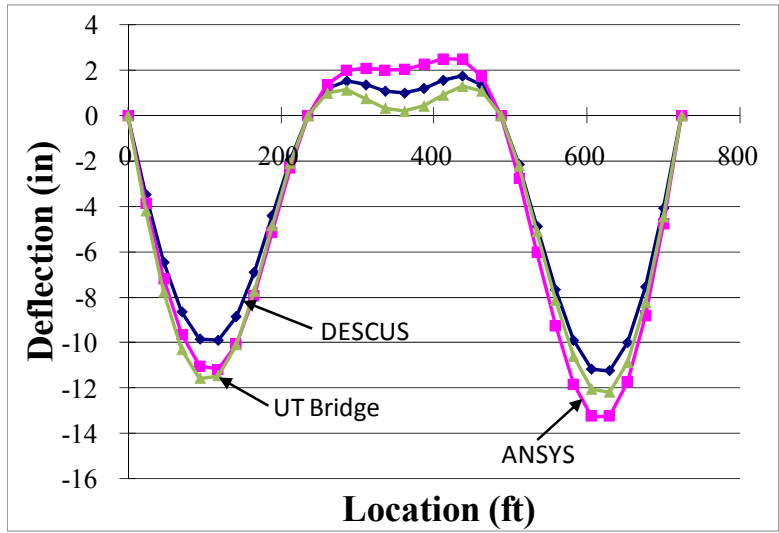


**Figure 4.48: Girder 2 Comparison for Steel and Concrete Slab Loading**

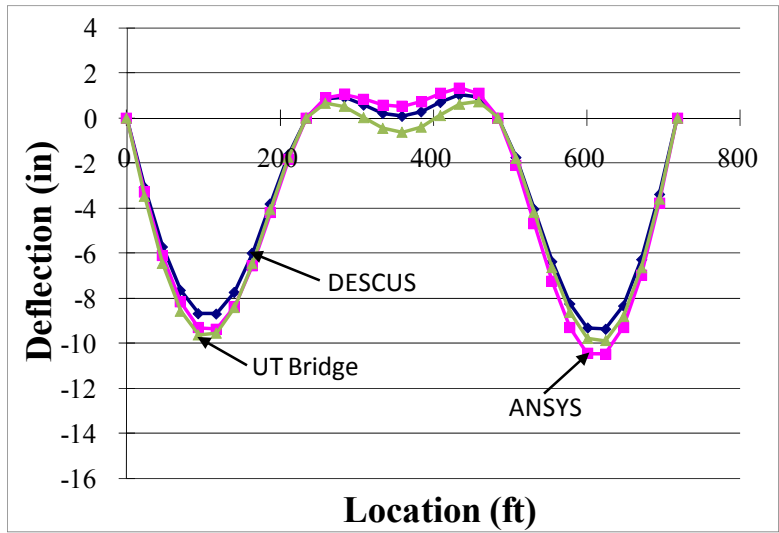


**Figure 4.49: Girder 3 Comparison for Steel and Concrete Slab Loading**

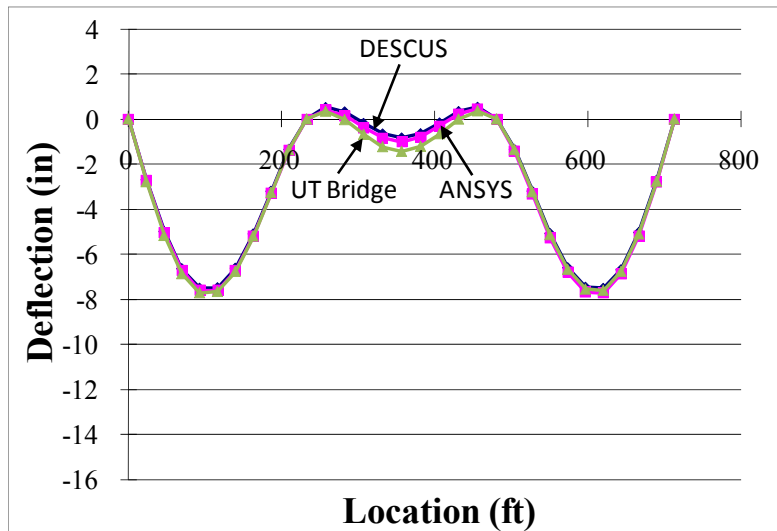


**Figure 4.50: Girder 4 Comparison for Steel and Concrete Slab Loading**

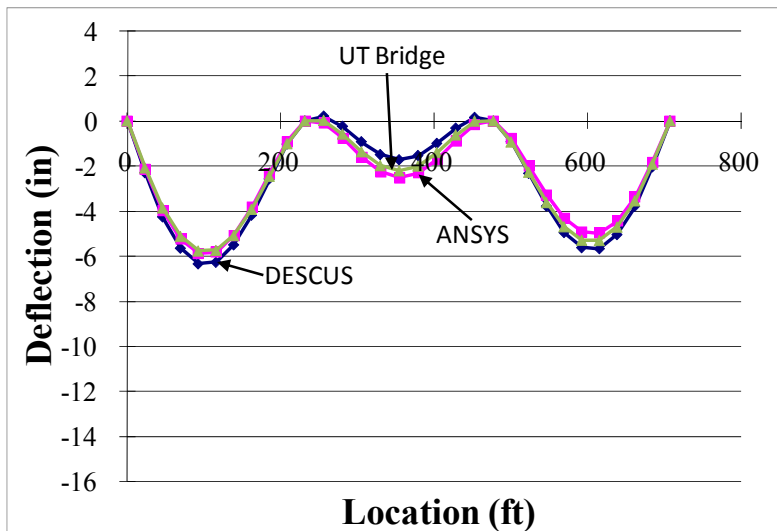


**Figure 4.51: Girder 5 Comparison for Steel and Concrete Slab Loading**

The final verification study that was completed was conducted to ensure the eigenvalue buckling analysis was accurate. A sampling of the results is given below. For the results shown, a prismatic simple span system with two girders was used. The boundary conditions were kept the same, but the loading was changed for each case. The first case simulated a constant axially loaded column providing a simple Euler buckling solution to compare the results of both UT Bridge and ANSYS. A schematic of case 1 is given in Figure 4.52. The second case simulated a beam with a constant moment that has a lateral torsional buckling solution given by Timoshenko that was compared to the UT Bridge and ANSYS solutions. A schematic of case 2 is given in Figure 4.53. The third

case simulated a beam with a point load at midspan. The theoretical solution for this structural system was a combination of the Timoshenko lateral torsional buckling solution and a  $C_b$  factor given by the Structural Stability Research Council (SSRC) to account for the moment gradient. A schematic of case 3 is given in Figure 4.54. Results for each case are given in Table 4.11 – Table 4.13. The results show good agreement with both theoretical and the commercially available finite element solutions over a range of loading and boundary conditions. It should be noted that modeling a three-dimensional beam supported at the bottom flange is not the most accurate model to comply with the assumptions made in the derivation of the theoretical solutions. Therefore, it should be known that the ANSYS results also have some slightly difference boundary conditions than UT Bridge and should not be interpreted as the baseline value, and difference between UT Bridge and ANSYS should not necessarily be interpreted as a problem with UT Bridge.

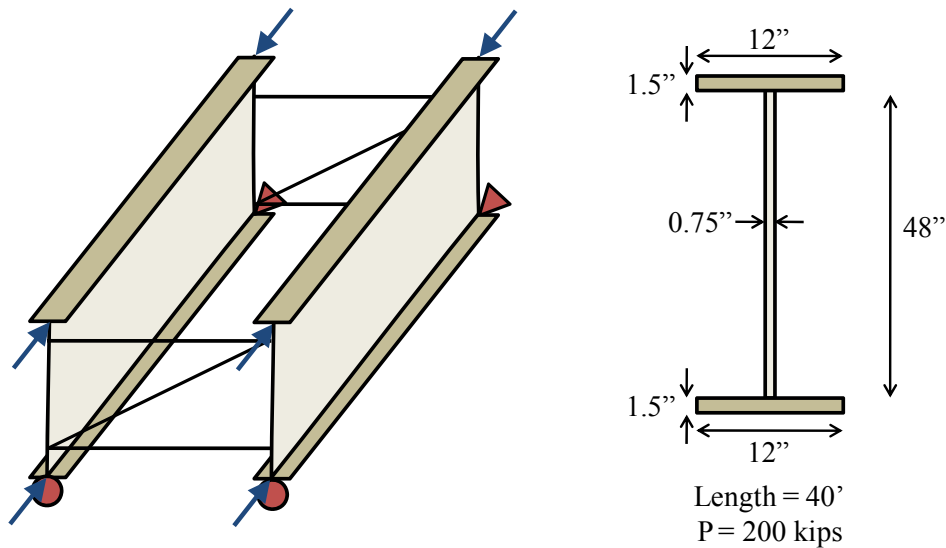


**Figure 4.52: Schematic of 1<sup>st</sup> Eigenvalue Buckling Check Constant Axial Load**

**Table 4.11: 1<sup>st</sup> Eigenvalue Buckling Check Results**

|           | Eigenvalue | % Difference |
|-----------|------------|--------------|
| Theory    | 2.699      | -            |
| UT Bridge | 2.6919     | 0.263        |
| ANSYS     | 2.687      | 0.445        |

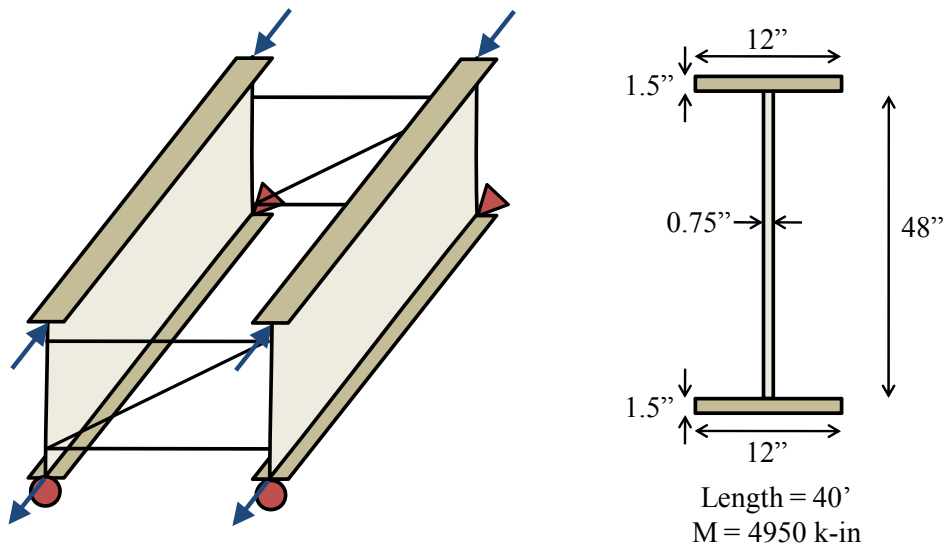


Figure 4.53: Schematic of 2<sup>nd</sup> Eigenvalue Buckling Check Constant Moment

Table 4.12: 2<sup>nd</sup> Eigenvalue Buckling Check Results

|           | Eigenvalue | % Difference |
|-----------|------------|--------------|
| Theory    | 3.8693     | -            |
| UT Bridge | 3.975      | -2.742       |
| ANSYS     | 3.753      | 3.006        |

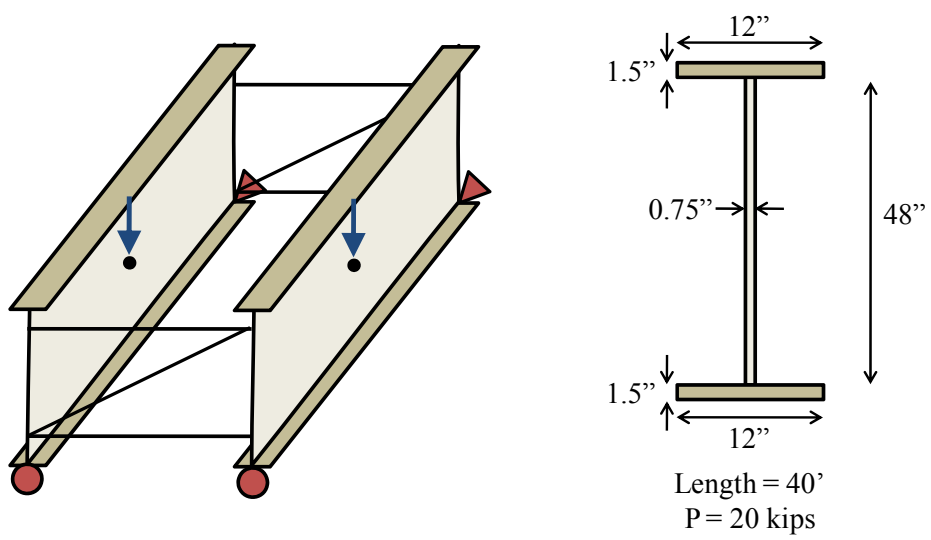


Figure 4.54: Schematic of 2<sup>nd</sup> Eigenvalue Buckling Check Point Load at Midspan

**Table 4.13: 3<sup>rd</sup> Eigenvalue Buckling Check Results**

|                | Eigenvalue | % Difference |
|----------------|------------|--------------|
| $M_{cr} * C_b$ | 10.501     | -            |
| UT Bridge      | 10.914     | -3.938       |
| ANSYS          | 9.721      | 7.424        |

#### 4.8 THE EFFECT OF UTILIZING COMPOSITE ACTION IN UT BRIDGE

One of the most useful aspects of UT Bridge is the ability to specify the concrete deck placement sequence and account for the level of composite action that is obtained during the hardening of early age concrete. Utilizing the linear incremental analysis discussed previously the total deflections and state of stress can be accurately predicted. To demonstrate the significance of such an analysis a theoretical bridge was developed in UT Bridge consisting of 2-200 ft. spans and four girders spaced at eight ft. The cross-section was simplified to only three different cross-sections with a depth of 84 in. The concrete deck placement sequence consisted of three different placements: 1) the positive moment region of span 1 (150 ft.), 2) the positive moment region of span 2 (150 ft.), and 3) the negative moment region of the bridge (100 ft.). This sequence can be seen in the UT Bridge screen shots given Figure 4.55 – Figure 4.57.

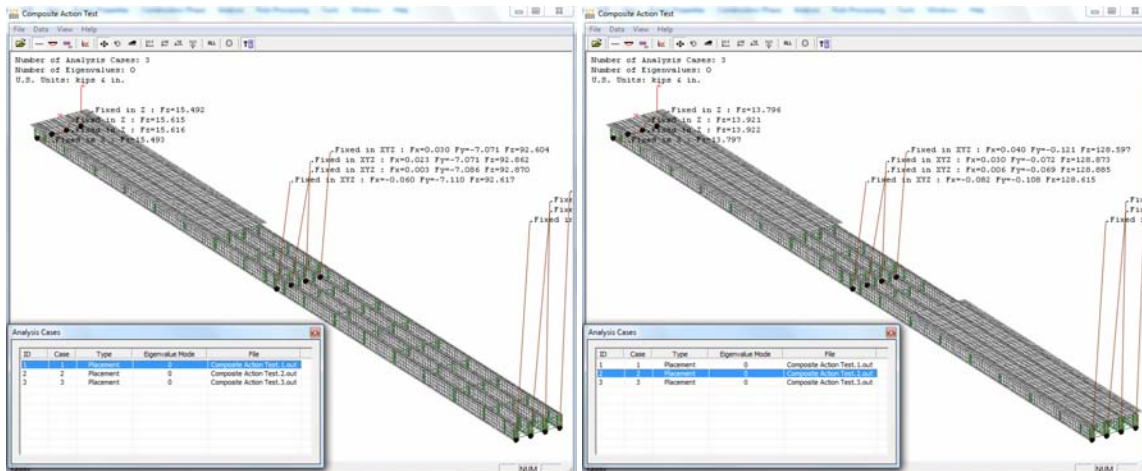


**Figure 4.55: Placement of Positive Moment Region of Span 1**

**Figure 4.56: Placement of Positive Moment Region of Span 2**

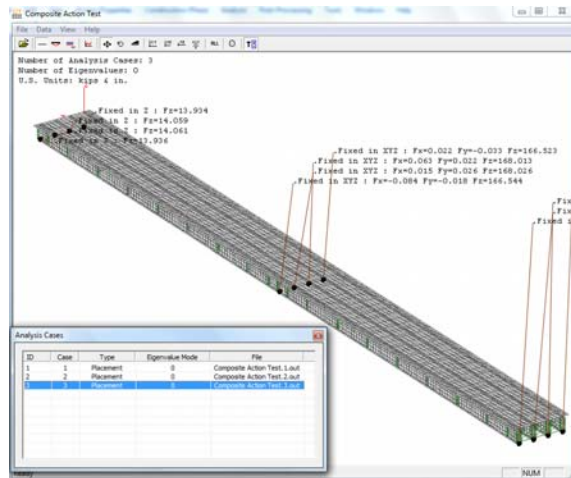


**Figure 4.57: Placement of Negative Moment Region of the Bridge**

To evaluate the effect of the composite action three analyses were performed. The first considered noncomposite action for the bridge and assumed the concrete was only a dead load applied to the structure. The second analysis assumed the concrete was partially composite and placed in the positive moment region first with span 1 completed 4 hours prior to the completion of span 2. Then the negative moment region was placed after the positive moment region was fully hardened. Finally, the third analysis assumed that each concrete region was placed separately with the previous section completely hardened prior the placement of the next section of deck. This was considered the fully composite analysis. Due to the straight bridge and even loading of the girders the deflected shape of each girder was essentially the same and only Girder 1 is reported here. Figure 4.58 is a graph showing the deflection of Girder 1 at the tenth points along the length of the girder.

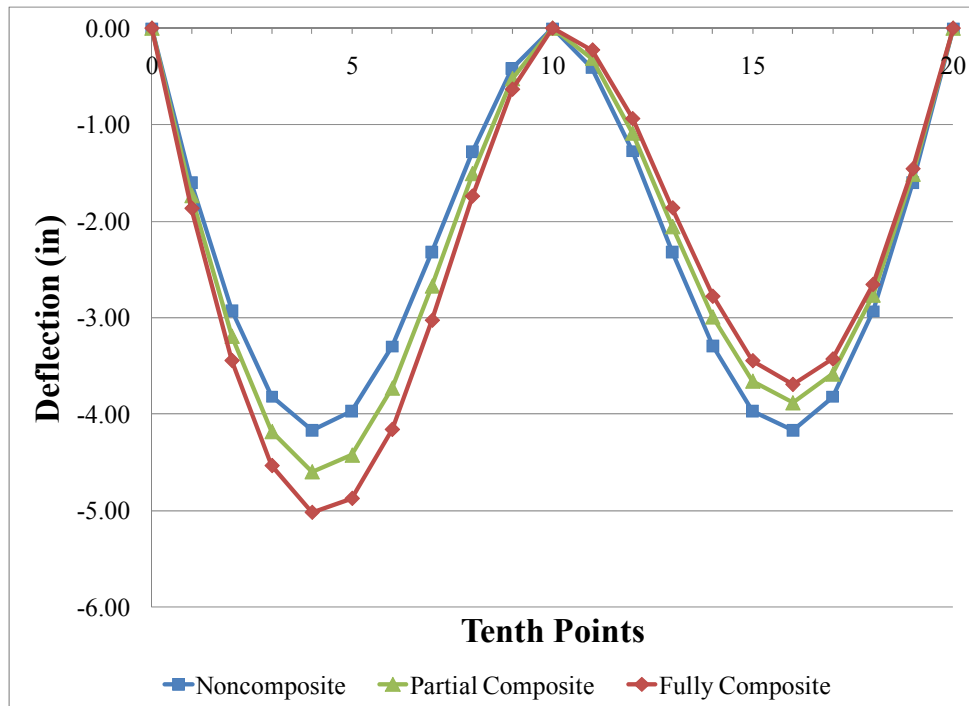


**Figure 4.58: Effect of Accounting for Composite Action in Deck Placement Analysis**

From the graph it can be shown that for a noncomposite bridge the deflections are symmetric as expected with a maximum deflection of 4.17 in. However, once the composite action is taken into account the final predicted deflections are not symmetric. The maximum deflection for the fully composite section is 5.02 in. or 20.4% higher than the noncomposite analysis. The partially composite section with span 1 positive moment region achieving 4 hours of normal curing resulted in the maximum deflection of 4.59 in. or a 10.1% increase. The reductions in the deflection at span two are smaller than the increase in span 1, but for the fully composite analysis the span 2 maximum deflection is 3.69 in. or a 11.5% decrease.

The conclusion from these analysis shows than predicting the total dead load deflections is extremely difficult especially when the design has little control over the placement timing. Unforeseen delays in the deck placement could have dramatic effects on the final girder geometry. It is important to note that while the technology available to perform detailed analysis improves, the full control of the variables that dictate the final performance of the bridge may lie outside the control of the structural engineer.



#### **4.9 UT BRIDGE CONCLUSIONS**

The UT Bridge program is a PC-based three-dimensional finite element software that includes a pre- and post-processor. The pre-processor consists of a set of user-friendly input forms that prompt the user for information on the structural system so that a three-dimensional model of the bridge can be generated. Once the basic geometry of the structural system has been defined, the user can define the erection sequence and check the behavior on a step-by-step basis.

The processor of the program is a robust finite element program that quickly discretizes the bridge, assembles the element stiffness matrices, and solves the subsequent set of linear equations. The program allows for both curved and straight I-girder bridges with any number of girders or spans. Skewed supports are allowed. Various loading types are available to the user including self weight, wind and point loads as well as additional temporary supports. A linear elastic or eigenvalue buckling analysis can be performed. The post-processor, UT Viewer, provides a three-dimensional graphical output that ensures correct geometry was modeled and allows for visualization of displacements, stresses, and rotations. Separate two-dimensional graphs are also available for displacements, stresses, and rotations evaluated at the tenth points of each span. The output data can be given in tabular form that can be copied to other programs. Cross-frame forces and reactions are also provided graphically or in tabular form. The program has been verified throughout its development at the element level, girder level, and system level. Verification of the program was completed by comparisons with field data, commercially available grillage programs, and three-dimensional finite element models in ANSYS. Some differences in the results should be expected relative to the field equipment accuracy, variations in the field conditions, and differences in the modeling assumptions. The availability of UT Bridge to engineers should provide a powerful tool for the evaluation of I-girder bridges during construction, offering a sector of the engineering community with an analysis tool that accurately and efficiently models existing conditions.

# **CHAPTER 5:**

## **CONCLUSIONS AND RECOMMENDATIONS**

---

### **5.1 INTRODUCTION**

Horizontally curved steel I-girder bridges play an important role in meeting the design challenges commonly encountered on highway interchanges in confined urban areas. This research project has provided insight into the behavior of these systems during construction and resulted in the development of computational tools that are capable of providing engineers and erectors accurate and intuitive methods to ensure safe and economic structures. The research has included a literature review of past research, field tests of actual bridges with realistic boundary conditions, finite element parametric studies, and program development. The following sections provide a summary of the conclusions from each phase of the research as well as a set of design recommendations and a list of potential future research topics in the area of curved I-girder erection and construction. The conclusions presented are based upon work documented in this dissertation as well as additional results from the research study that were presented by Schuh (2008), Farris (2008), and Petruzzi (2010).

### **5.2 LITERATURE REVIEW SUMMARY**

- There is a general lack of information about curved I-girders during the construction process, particularly in the area of field measurements of actual structures. Field measurements on actual structures provide valuable data on systems with as-built boundary conditions. Without this data, performing realistic laboratory tests or computational studies is difficult.
- The complicated behavior of the open cross section I-girder, specifically the warping torsional behavior, is difficult to accurately model utilizing a two-dimensional grillage computer program. The global torsional stiffness of a bridge is often not calculated correctly with traditional two-dimensional

models. Three-dimensional finite element models provide better accuracy for predicting structural response.

- The author is unaware of past studies focused on the stability requirements of steel girders during lifting.

### **5.3 RESULTS FROM FIELD TESTS**

- Measured stresses during lifting and erection were well below yield, with the highest relative changes occurring during girder fit-up and with crane release.
- Measured stresses during concrete deck placement were larger than the stresses experienced from the lifting and erection, but well below yielding.
- To obtain stresses during erection, well defined pre-lift boundary conditions are necessary so that the boundary conditions used in computer models correlate well with the actual conditions.
- Curved girders rotate when lifted. The rotation is due to two aspects: 1) rigid body rotation of the girder and 2) cross sectional twist due to torsion.
- Rigid body rotation is sensitive to the girder geometry and the locations of the lift points. If the center of gravity of the girder is not co-linear with the line of support defined by the lift points, the girder will rotate in a rigid body motion about the line of support. This rotation is not a function of the girder stiffness.
- Cross sectional twist is a result of the torque acting on the girder due to its self weight. The amount of twist is a function of the torque due to self weight, the support conditions, and the torsional stiffness of the girder.
- For some lifting scenarios, the warping stress can be as large as the bending stress.
- The concrete deck placement results in significant stress changes. The stresses are generally most critical for the top flange of an unsymmetric girder prior to hardening of the concrete since these girders are often designed for composite action resulting in a smaller top flange than the bottom flange. Girder deflection data recorded during placement of the concrete deck

provided validation data for use with the different software packages that were evaluated.

#### **5.4 THREE DIMENSIONAL FINITE ELEMENT MODELING**

- The three-dimensional finite element program ANSYS was used for parametric studies as well as comparisons with the UT Lift and UT Bridge programs.
- ANSYS was a good choice for this research project because it allows the creation of an input file with ANSYS's user defined parametric language. Thus, a single validated file could be altered to test a range of parameters providing valuable information about the behavior of curved I-girders during lifting, erection, and concrete deck placement.
- The dominate failure mode for straight I-girders during lifting is lateral-torsional buckling of the girder. During lifting, the buckling stress for straight girders segments with practical lengths was well below the 50 ksi material yield stress that is commonly used in bridge construction.
- Eigenvalue buckling analyses were compared with large displacement analyses to determine the accuracy of the buckling predictions. For girders with significant horizontal curvature, the eigenvalue was unconservative compared to the load levels that resulted in deformations deemed excessive by a survey of construction professionals. The eigenvalue buckling analysis accurately predicted the buckling behavior of relatively straight girders
- Eigenvalue buckling analyses on girders during lifting resulted in the development of moment gradient factors,  $C_b$ , to be used with the lateral-torsional buckling equation to account for the moment gradient caused by the lifting locations.
- The dominate failure mode for curved I-girders during lifting was excessive deformations from combined rotation and lateral bending of the cross section. An analysis of girder response should include stresses due to strong-axis

bending, lateral bending, and torsional warping stresses. For most curved girders with self weight loading during lifting, the maximum stresses were below yield stress. The maximum stress for horizontally curved girders was significantly higher when compared to a similar straight girders.

- Full geometric nonlinear analyses were required to accurately capture the behavior of curved I-girders during lifting.
- The boundary conditions and effects of temporary supports had a significant impact on partially constructed bridges. The details that were used for the temporary supports had a significant impact on the buckling behavior. Shore towers typically support the girder from the bottom flange and provide restraint from lateral movement, while a holding crane typically supports the girder from the top flange and does not provide significant lateral restraint.
- From a stability perspective, holding cranes tended to provide improved stability compared to shore towers due to the location of the support on the cross section. The effect of the support position on the cross section is similar to the effects of load position on the cross section.

## **5.5 DESIGN TOOL DEVELOPMENT**

- Two design tools were created during this research: 1) UT Lift and 2) UT Bridge
- UT Lift is a macro-enabled Microsoft Excel spreadsheet that utilizes the equations developed in the research and discussed in Chapter 3 of this dissertation to analyze curved I-girders during lifting.
- UT Lift allows for a girder of any radius of curvature with up to eight different cross sections and eighteen cross frames.
- UT Lift will calculate the center of gravity of the girder and the optimum location to lift the girder to prevent rigid body rotation.

- UT Lift allows for two lift points at any location along the girder and calculates the total rotation at the ends and middle location of the girder including both rigid body rotation and cross sectional twist.
- UT Lift also calculates the stresses at the lift points and middle location of the girder including strong-axis bending, weak-axis bending, and warping normal stresses.
- UT Lift should be used for curved I-girders lifted with a single crane and spreader bar or two cranes.
- UT Bridge is a user-friendly 3-D finite element analysis program that was discussed in Chapter 4 of this dissertation.
- UT Bridge allows for straight or curved bridges with any number of girders, spans, or skew angle of the substructure.
- UT Bridge performs either a sequenced erection analysis or a concrete deck placement analysis.
- UT Bridge is composed of a pre-processor developed using visual basic, a processor developed in Fortran, and a post-processor developed in C++.
- UT Bridge's post-processor, UT Viewer, reads the output files from the processor and displays a three-dimensional graphical representation of the bridge with scaled deflections or stress contours. Additionally, two-dimensional tenth-point graphs of the deflections, stresses, or rotations for each girder are available.
- UT Bridge has been verified throughout its development at the element, girder, and system levels. Field data from bridges during construction were used to verify predictions from commercially available grillage programs, and full three-dimensional finite element models in ANSYS.
- UT Bridge provides engineers with a powerful tool for the evaluation of I-girder bridge behavior during construction, offering a sector of the engineering community with an analysis tool that more accurately models the in-situ bridge system than is currently available.

## 5.6 FUTURE RESEARCH

Significant progress has been made during this research study toward understanding the behavior of curved I-girders during the entire construction process, from lifting of individual girder segments through concrete deck placement. However, much work is still needed in this area of research. Additional understanding of the behavior can be made with field measurements of the displacements of bridges during erection and construction. The displacement-based information obtained from an accurate field survey of the girders would allow good correlation to displacement-based finite element programs whose primary variable is displacement and secondary variable is stress. Verification of models with stress is necessary and reasonable, but the displacement information provides a more direct comparison for typical finite element analyses. Another area that was not studied in this research is the effect of skewed supports on curved girders. This additional complication needs to be captured in the field to ensure proper modeling on a computer. These additional tests should also focus on the bridge support systems to determine the effect of boundary conditions. The modeling method of the bridge bearings affects the calculated response, and the most appropriate method for modeling the girder supports should be studied further.

Two design tools were developed in this research: UT Lift and UT Bridge. These tools have limitations, and further research to increase their flexibility would be beneficial. For example, increasing the number of lift points possible in UT Lift would be helpful. UT Bridge has geometric limitations that could be expanded on, allowing the program to handle point-of-tangencies and point-of-curvatures along the length of a bridge or variable girder spacing. UT Bridge could be expanded to include various types of cross frames other than the typical X-type currently available. The erection sequence is specified from one end of the bridge to another, and the method for specifying the erection sequence could be made more general. The ability to carry out a full geometric nonlinear analysis would also improve the capabilities of UT Bridge. Another area of expansion would include additional loading patterns and additional flexibility in applying loads.

*Many studies, features, and topics are mentioned here due to goals yet unachieved. Yet, it is only a matter of time and will before these mysteries are unlocked and the boundary of human knowledge is expanded once again. The purpose of this project was to take a specific area of knowledge (the behavior of curved I-girder during construction) that was of particular interest to the individuals involved and shine some light of truth on the subject for others to walk in brighter understand of the topic rather than the twilight of rules of thumb and guessimation. However, as is often the case as we learn more, we find out how much more there is to be known.*



**APPENDIX A:**  
**UT BRIDGE PROCESSOR FLOW CHART**

---

The following flow chart contains the file names, subroutines, and major variable arrays used in the UT Bridge processor.

## **APPENDIX B:**

### **BRIDGE 88 BRIDGE PLANS**

---

The following set of bridge plans was used during the planning of the field studies, verification of the ANSYS bridge model, and verification of UT Bridge. Permission to publish these plans was obtained from the Texas Department of Transportation Bridge Division. Also included is a typed copy of the quality assurance bridge deck inspection sheet for the deck placement which includes the deck thickness variations.

| SH 130 Turnpike Project   |                  |           |       |             |                   |         |                  |           |       |             |                   |
|---|------------------|-----------|-------|-------------|-------------------|---------|------------------|-----------|-------|-------------|-------------------|
| QA Inspection Bridge Deck   |                  |           |       |             |                   |         |                  |           |       |             |                   |
| QA Inspection Report: 6045 08 04 16 01<br>Date: April 16, 2008    |                  |           |       |             |                   |         |                  |           |       |             |                   |
| Depth Checks Required by TXDOT Guide Schedule: Spans 14, 15, & 16 |                  |           |       |             |                   |         |                  |           |       |             |                   |
| Bridge 88 Area of Placement                                       |                  |           |       |             |                   |         |                  |           |       |             |                   |
| Length (ft) x Width (ft) / 9 = 2342.77 Total s.y.                 |                  |           |       |             |                   |         |                  |           |       |             |                   |
| Depth of Slab and Cover   |                  |           |       |             |                   |         |                  |           |       |             |                   |
|   | Location in Slab |           |       | Clear Cover | Depth of Concrete |         | Location in Slab |           |       | Clear Cover | Depth of Concrete |
|   | Station          | (1/4) Pt. | Bay # | (in)        | (in)              |         | Station          | (1/4) Pt. | Bay # | (in)        | (in)              |
| SPAN 16   | 11208+80         | 1st       | 1     | 2.5         | 9.625             | SPAN 14 | 11205+10         | 1st       | 1     | 2.625       | 10                |
|   | 11208+80         | 1st       | 2     | 2.5         | 9.75              |         | 11205+10         | 1st       | 2     | 2.5         | 10.125            |
|   | 11208+80         | 1st       | 3     | 2.375       | 9.375             |         | 11205+10         | 1st       | 3     | 2.5         | 9.625             |
|   | 11208+40         | 2nd       | 1     | 2.5         | 9.25              |         | 11204+64         | 2nd       | 1     | 2.75        | 10.125            |
|   | 11208+40         | 2nd       | 2     | 2.5         | 9.375             |         | 11204+64         | 2nd       | 2     | 2.5         | 10                |
|   | 11208+40         | 2nd       | 3     | 2.375       | 8.5               |         | 11204+64         | 2nd       | 3     | 2.25        | 9.875             |
|   | 11208+01         | 3rd       | 1     | 2.375       | 9.625             |         | 11204+17         | 3rd       | 1     | 2.5         | 9.5               |
|   | 11208+01         | 3rd       | 2     | 2.375       | 9.375             |         | 11204+17         | 3rd       | 2     | 2.5         | 10.125            |
|   | 11208+01         | 3rd       | 3     | 2.25        | 9.25              |         | 11204+17         | 3rd       | 3     | 2.25        | 9.625             |
| BENT 16   | 11207+61         | 4th       | 1     | 2.375       | 9.5               |         |                  |           |       |             |                   |
|   | 11207+61         | 4th       | 2     | 2.5         | 9.25              |         |                  |           |       |             |                   |
|   | 11207+61         | 4th       | 3     | 2.5         | 9.375             |         |                  |           |       |             |                   |
| SPAN 15   | 11207+10         | 1st       | 1     | 2.5         | 9.375             |         |                  |           |       |             |                   |
|   | 11207+10         | 1st       | 2     | 2.625       | 9.75              |         |                  |           |       |             |                   |
|   | 11207+10         | 1st       | 3     | 2.5         | 9.25              |         |                  |           |       |             |                   |
|   | 11206+59         | 2nd       | 1     | 2.625       | 9.875             |         |                  |           |       |             |                   |
|   | 11206+59         | 2nd       | 2     | 2.375       | 10                |         |                  |           |       |             |                   |
|   | 11206+59         | 2nd       | 3     | 2.25        | 9.75              |         |                  |           |       |             |                   |
|   | 11206+07         | 3rd       | 1     | 2.625       | 10.25             |         |                  |           |       |             |                   |
|   | 11206+07         | 3rd       | 2     | 2.625       | 10.125            |         |                  |           |       |             |                   |
| BENT 15   | 11206+07         | 3rd       | 3     | 2.5         | 9.5               |         |                  |           |       |             |                   |
|   | 11205+56         | 4th       | 1     | 2.5         | 9.25              |         |                  |           |       |             |                   |
|   | 11205+56         | 4th       | 2     | 2.5         | 9.25              |         |                  |           |       |             |                   |
|   | 11205+56         | 4th       | 3     | 2.5         | 9.375             |         |                  |           |       |             |                   |
| Inspector: Chris Tanner   |                  |           |       |             |                   |         |                  |           |       |             |                   |

**APPENDIX C:**  
**WICHITA FALLS ALIGNMENT “T” BRIDGE PLANS**

---

The following set of bridge plans was used in the verification of an ANSYS bridge model and UT Bridge. Permission to publish these plans was obtained from the Texas Department of Transportation Bridge Division.

**APPENDIX D:**  
**UT BRIDGE VERIFICATION: TXDOT DIRECT**  
**CONNECTOR 2-SPAN 469' DIRECT CONNECTOR**

---

The following set of bridge plans was a trial design considered by TxDOT, but altered before the final design was completed. They were modeled in ANSYS and used in the verification of UT Bridge. Permission to publish these plans was obtained from the Texas Department of Transportation Bridge Division.

## D.1 INTRODUCTION

In February 2010, several employees from the Texas Department of Transportation (TxDOT) approached the research team with a trial bridge design that show deviation between the deflection calculations from a 2-D grillage model developed in DESCUS and UT Bridge. To substantiate the accuracy of UT Bridge a pair of 3-D finite element analysis models were created in ANSYS to compare to the previously calculated information. The following appendix is a summary of the results of these analyses. Two important feature of the bridge should be noted: 1) the curved bridge has a narrow cross-section and 2) the bridge has an odd span arrangement with the shorter span 70% of the longer span.

## D.2 2-SPAN 469' DIRECT CONNECTOR BRIDGE PLANS

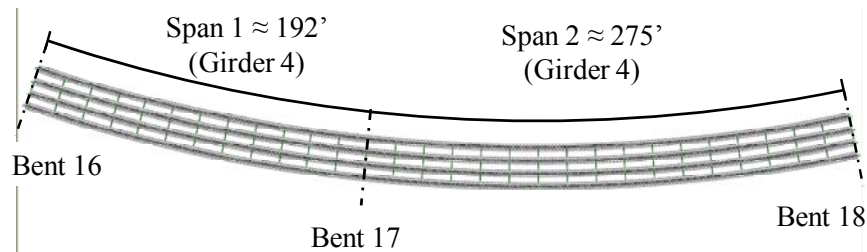


**Figure D.1: UT Bridge Screen Shot of Plan View of 469' Bridge**

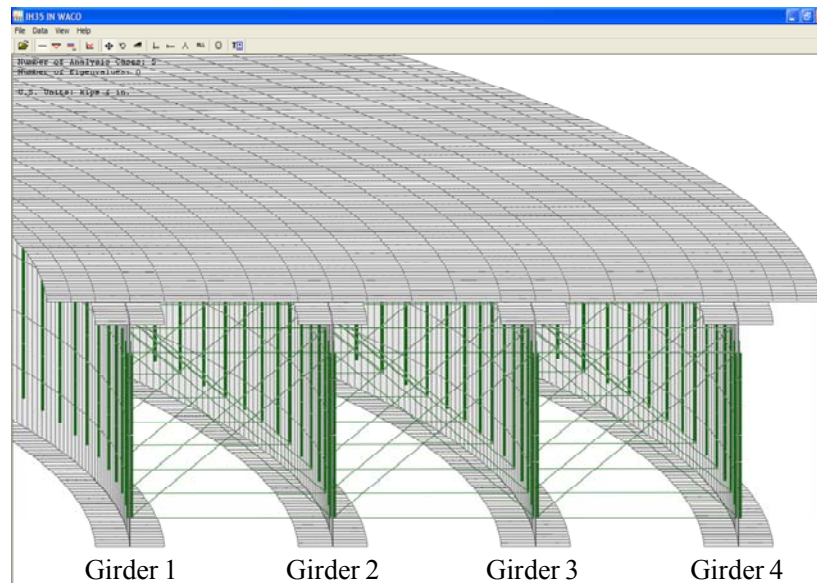
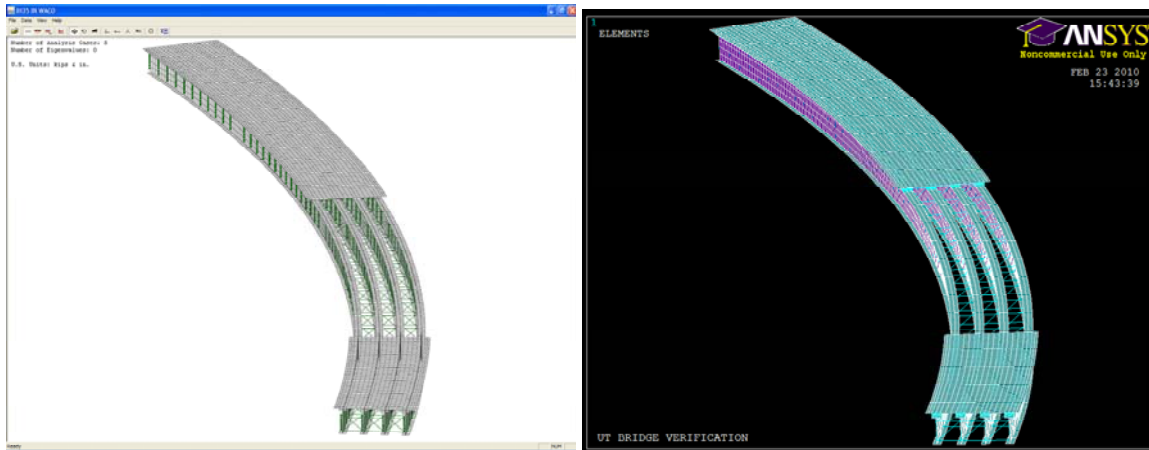


**Figure D.2: UT Bridge Screen Shot of 469' Bridge**

### **D.3 COMPARISON OF VERTICAL DEFLECTIONS**

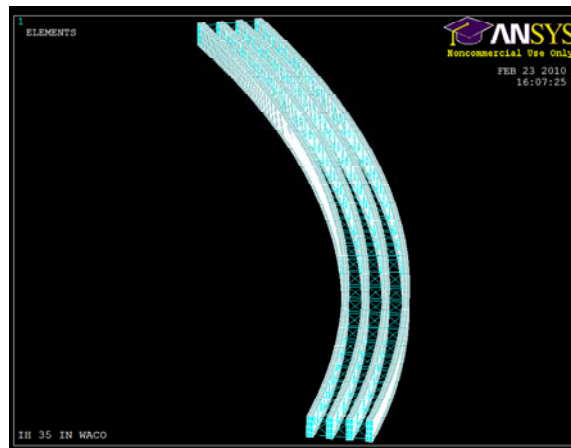
UT Bridge was compared to the 2-D grillage program (DESCUS) provided by the camber diagram developed by TxDOT. Additionally, two 3-D finite element models were created in ANSYS to compare to the results. The first (ANSYS 1) model utilized the geometry and meshing generated by UT Bridge, but analysis with ANSYS' 8-node shell elements (SHELL93), 2-node beam elements (BEAM4), and 2-node truss elements (LINK8). The deck was modeled with shell elements and flexible springs to simulate the noncomposite action. The second (ANSYS 2) model utilized an independent node generation algorithm and generator. The same 8-node shell elements (SHELL93) were used for both the girder and the stiffeners, while 2-node truss elements (LINK8) were used for the cross frames. The deck was not explicitly modeled with shell elements, but rather it was modeled as a distributed load along the top flange of each girder. All models were assumed to behave noncompositely to facilitate an accurate comparison due to DESCUS's inability to perform a composite analysis and limitations of the ANSYS 2 model. As a result the model assumes the deck was fully placed instantaneously on steel bridge for this set of analyses. Figure D.3 and Figure D.4 are a set of screen shots from each of the three models created to compare with TxDOT's DESCUS model. Figure D.5 through Figure D.8 are a set of graphs with the tenth point deflections calculated by UT Bridge, DESCUS, the first ANSYS model (ANSYS 1), and the second ANSYS model (ANSYS 2).



(a) UT Bridge

(b) ANSYS 1

Figure D.3: UT Bridge, ANSYS1 Screen Shot of 469' Direct Connector



ANSYS 2

Figure D.4: ANSYS2 Screen Shot of 469' Direct Connector

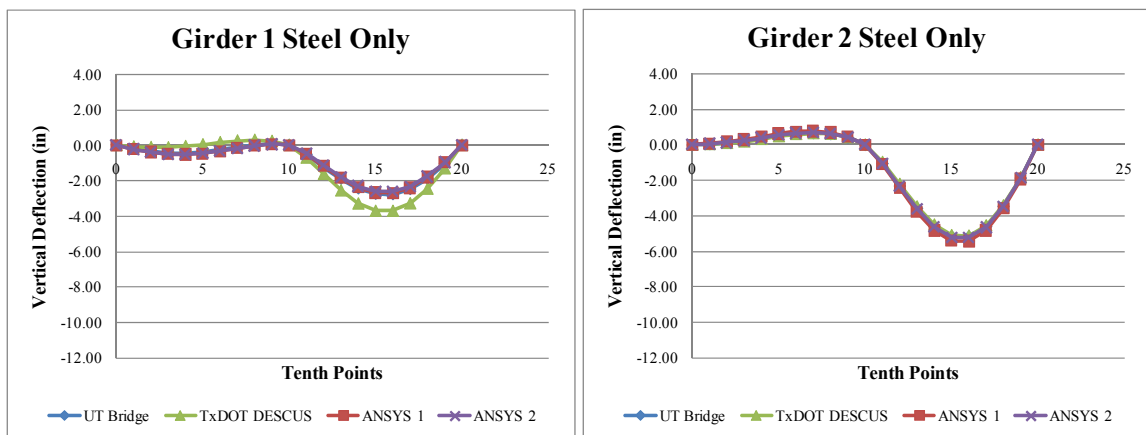
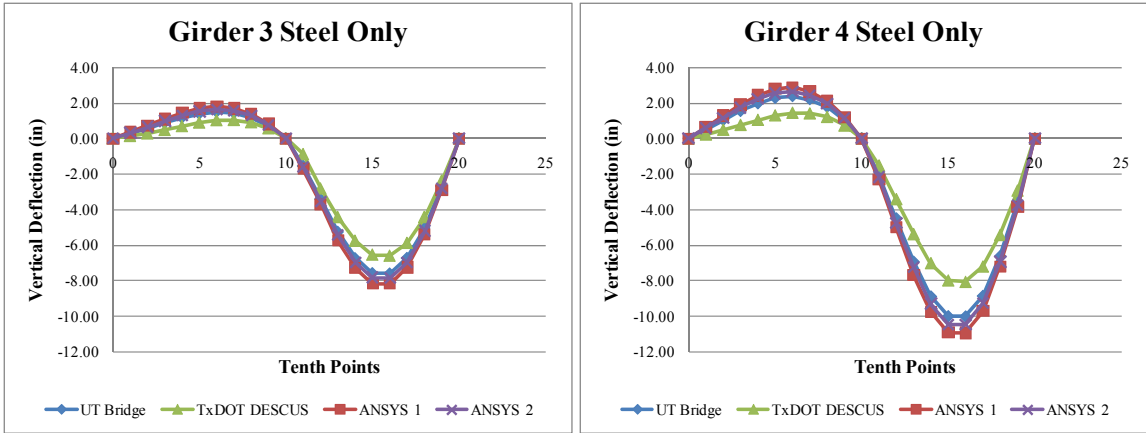
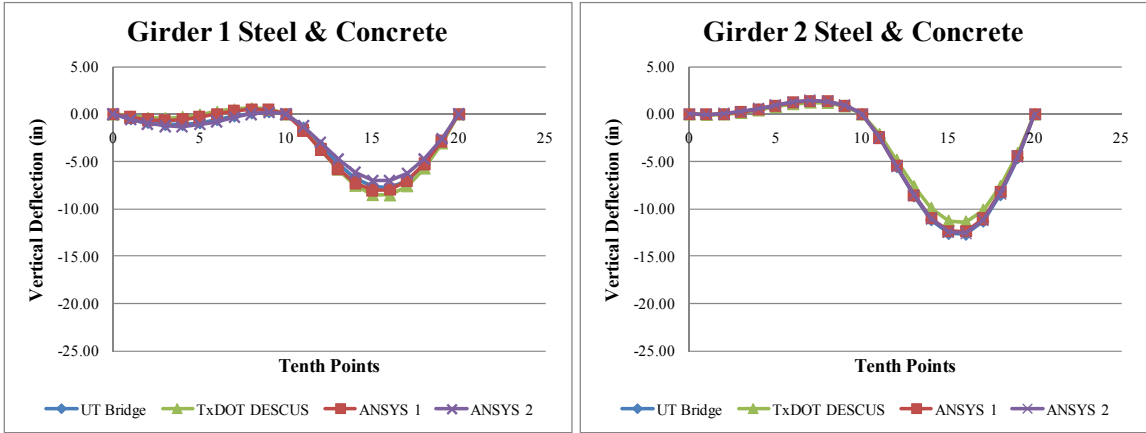


Figure D.5: Steel Dead Load Program Comparison for Girder 1 and 2





**Figure D.6: Steel Dead Load Program Comparison for Girder 3 and 4**



**Figure D.7: Steel & Concrete Deck Dead Load Program Comparison for Girder 1 & 2**

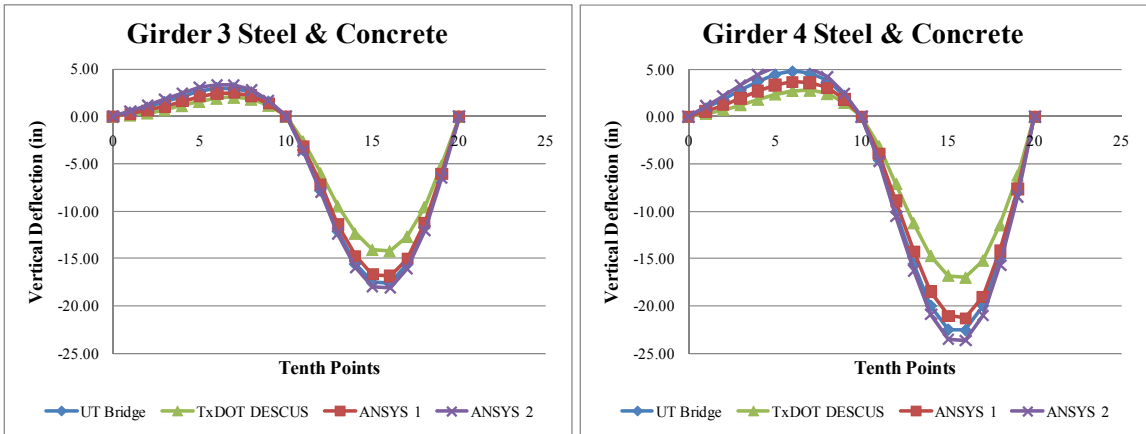


**Figure D.8: Steel & Concrete Deck Dead Load Program Comparison for Girder 3 & 4**

#### D.4 CONCLUSION FROM MODEL COMPARISON

As a result of the analyses, UT Bridge was validated for this bridge and compared well with both the ANSYS 1 and ANSYS 2 models. DESCUS overpredicted the global torsional stiffness of the bridge. This results in less global twist as shown by larger deflections for the interior girder (Girder 1) and smaller deflections for the exterior girder (Girder 4). It should be noted that all the models predicted between 1 ½ ft. to 2 ft. of vertical deflection for Girder 4. This indicates a relatively flexible bridge and a potential fabrication, erection, and construction problem. Thus alternative were investigated to reduce the total predicted deflection.

#### D.5 ALTERNATE 1: CONCRETE PLACEMENT VARIATION

A benefit of UT Bridge is the ability to specify the concrete placement stages. This allows for composite action of the bridge to be taken into account. Thus the follow plan was assumed for the concrete placement sequence.

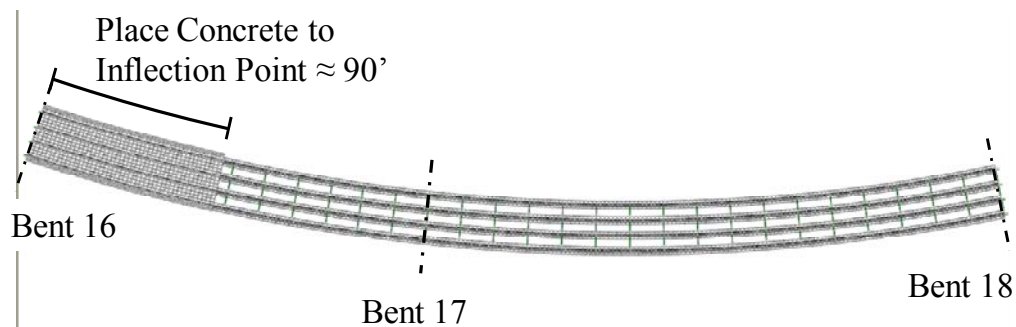


*Figure D.9: Step 1 Composite Deck Stiffening*

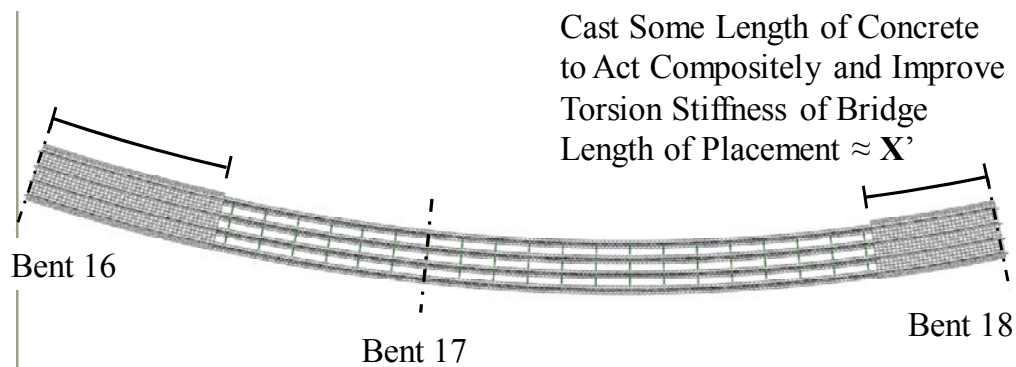


*Figure D.10: Step 2 Composite Deck Stiffening*

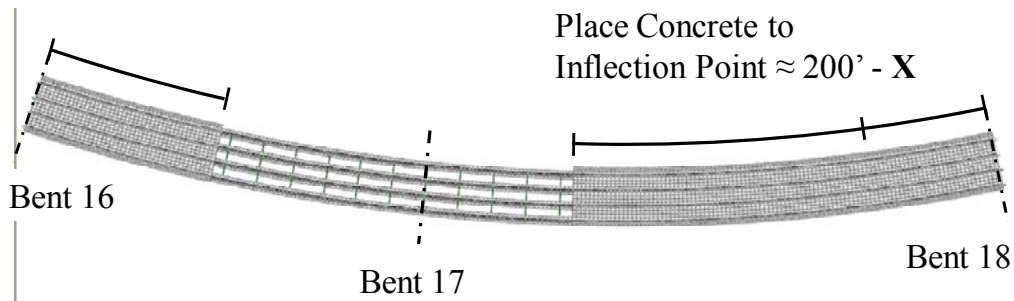


**Figure D.11: Step 3 Composite Deck Stiffening**

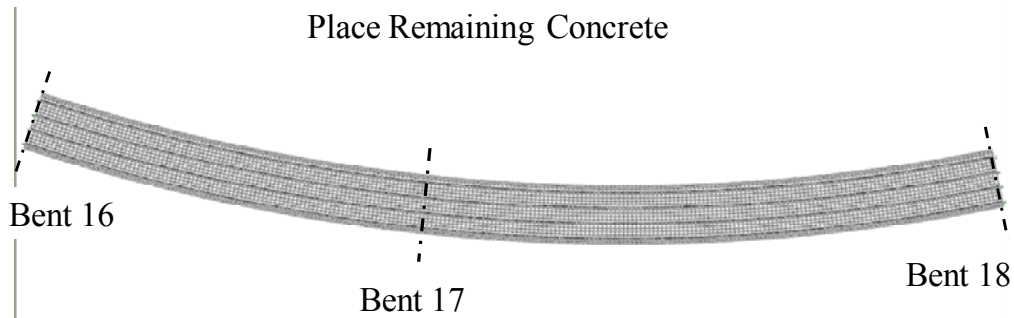


**Figure D.12: Step 4 Composite Deck Stiffening**

As a result the length of deck casted and allowed to harden in step 2 was vary as a distance from Bent 18. Then the total deflection was graphed. The follow figures show the deflection at the 15<sup>th</sup> tenth point or the middle of Span 2. The results indicate that when 60 ft. of deck is cast in the second step the deflections were minimized. This reduced the predicted maximum deflection from 22.5 in. to 16.3 in, an approximately 27.5% reduction in the maximum deflections.



**Figure D.13: Total Deflected with Varied Deck Placement Sequence for Girders 1 & 2**

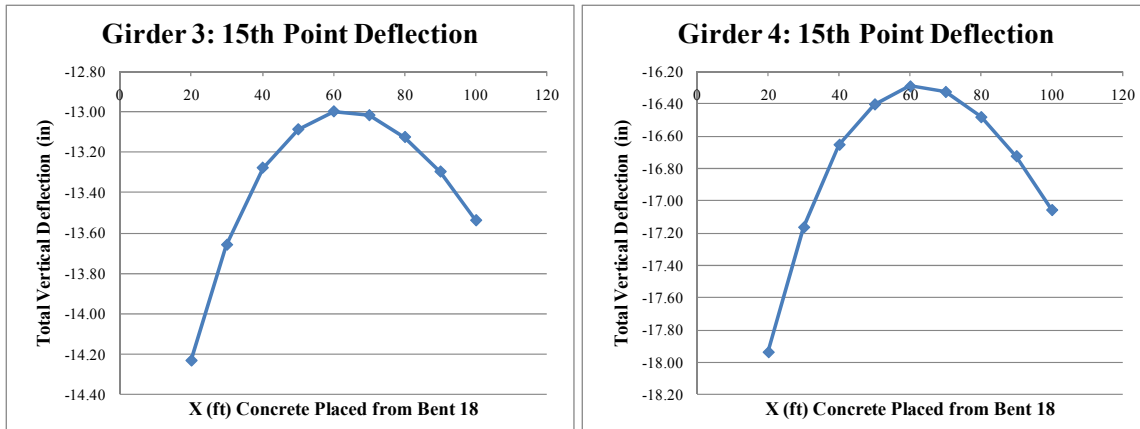


**Figure D.14: Total Deflected with Varied Deck Placement Sequence for Girders 3 & 4**

### D.6 ALTERNATE 2: INCREASE GIRDER DEPTH

Another option considered was to increase the depth of the girders. According to AASHTO LRFD 4<sup>th</sup> edition (2007) section 2.5.2.6.3 *Optional Criteria for Span-to-Depth Ratios*:

*“... For curved steel girder systems, the span-to-depth ratio,  $L_{as}/D$ , of each steel girder should not exceed 25 when the specified minimum yield strength of the girder in regions of positive flexure is 50 ksi or less.”*

Thus, it can be concluded that since the girders were dimensioned as 8 ft. deep and the length of Span 2 is 275 ft. then the span-to-depth ratio is approximately 34, which is well above the suggested limit of 25. To comply with this span-to-depth ratio the girder would need to be 11 ft. deep. This was not possible due to clearance issues and roadway geometric constraints provided by the transportation engineer.

### D.7 ALTERNATE 3: TORSIONAL STIFFENING TRUSS

A final scenario that was analyzed to reduce the torsional flexibility of the bridge and provide minimal deflections. A torsional stiffening bottom chord truss could be installed on the bridge after erection and prior to concrete deck placement. The truss would minimize rotations, but would add additional cost to the construction of the bridge. The truss was extended two panel points at each support as shown by Figure D.15 and

Figure D.16. Figure D.17 and Figure D.18 show a set of graphs with the comparisons of the total dead load deflections with the results from the bottom chord truss analysis included.

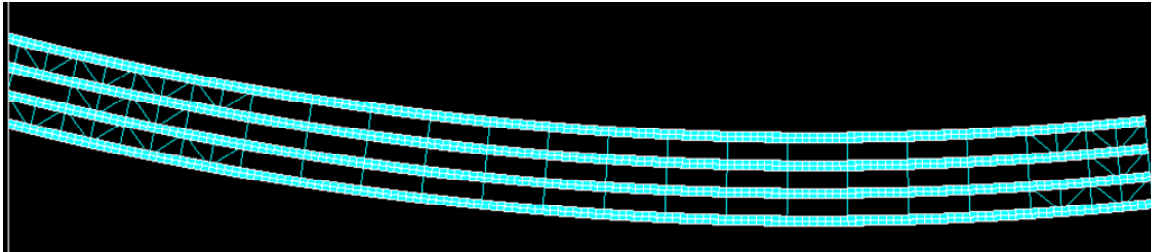


**Figure D.15: ANSYS Plan View of Span 2 with Bottom Chord Truss**

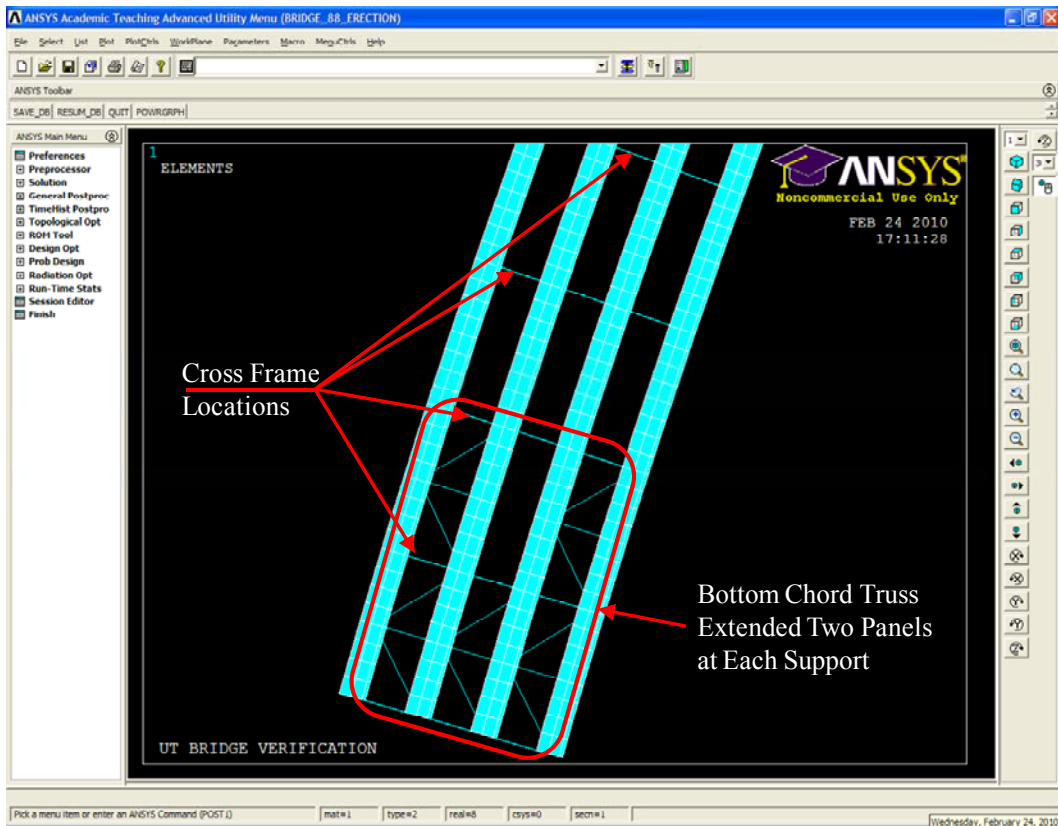


**Figure D.16: ANSYS Plan View of Bent 18 with Bottom Chord Truss**

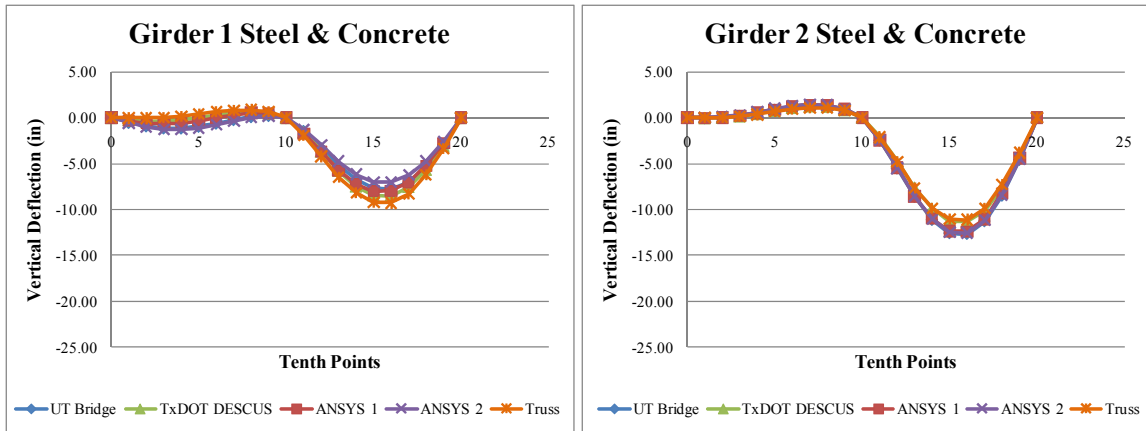


**Figure D.17: Total Dead Load Deflections Including Model with Bottom Chord Truss**

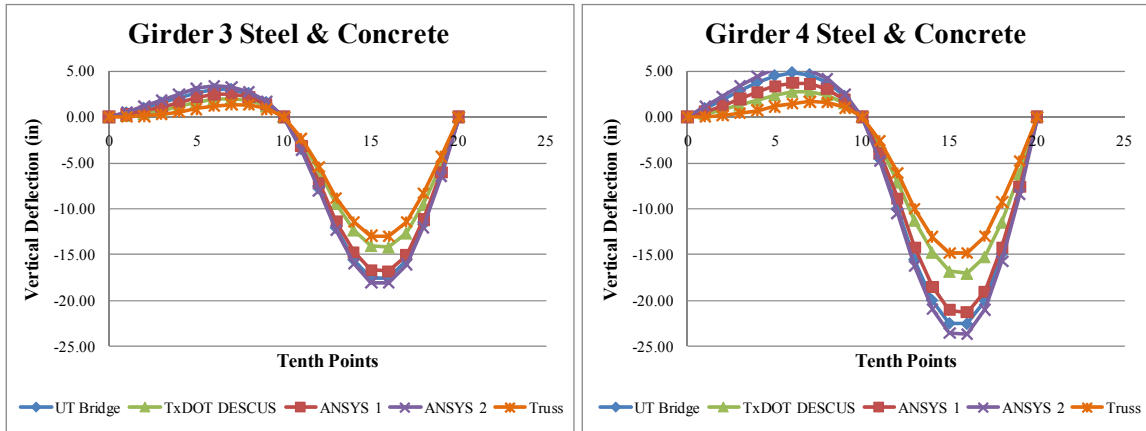


**Figure D.18: Total Dead Load Deflections Including Model with Bottom Chord Truss**

Thus for the model with the bottom chord truss the global torsional stiffness was increase resulting in an increase in the maximum deflection of Girder 1 from 7.8 in. to 9.2 in. or a 18% increase while the maximum deflection of Girder 4 decreased from 22.5 in. to 14.8 in. or a 34% decrease.

## D.8 CONCLUSIONS

After presenting the options and alternatives a decision was made to consider reconfiguring the span arrangements and possibly add a third span to provide additional symmetry. However several lessons can be garnished from the series of analysis.

- 1) Cross-sectionally narrow bridges can have torsional flexibility issues even if the radius of curvature is relatively large, in this case approximately 900 ft.

- 2) Bridges with odd span arrangement magnify potential problems through the continuity of the girder system
- 3) Bridges with span-to-depth ratios larger than the AASHTO recommendations can have insufficient stiffness resulting in excessive deformations.
- 4) According for the composite action of the deck decreased the maximum deformation by 27.5%.
- 5) Adding a bottom chord truss to the two panel points at each support reduced the maximum deformation by 34%.
- 6) A good rule of thumb for engineers is to assume that the actual bridge deformations are within 10% of their computationally predicted values from a good bridge analysis model.

**APPENDIX E:**  
**UT BRIDGE VERIFICATION: TXDOT DIRECT**  
**CONNECTOR 2-SPAN 428' DIRECT CONNECTOR**

---

The following set of bridge plans was a trial design considered by TxDOT, but altered before the final design was completed. They were modeled in ANSYS and used in the verification of UT Bridge. Permission to publish these plans was obtained from the Texas Department of Transportation Bridge Division.



## E.1 INTRODUCTION

In February 2010, several employees from the Texas Department of Transportation (TxDOT) approached the research team with a trial bridge design that show deviation between the deflection calculations from a 2-D grillage model developed in DESCUS and UT Bridge. To substantiate the accuracy of UT Bridge a pair of 3-D finite element analysis models were created in ANSYS to compare to the previously calculated information. The following appendix is a summary of the results of these analyses. Two important feature of the bridge should be noted: 1) the curved bridge has a narrow cross-section and 2) the bridge has an odd span arrangement with the shorter span 70% of the longer span.

## E.2 2-SPAN 469' DIRECT CONNECTOR BRIDGE PLANS

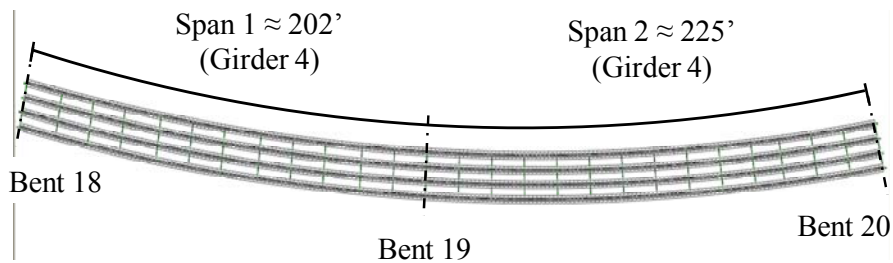


**Figure E.1: UT Bridge Screen Shot of Plan View of 428' Bridge**

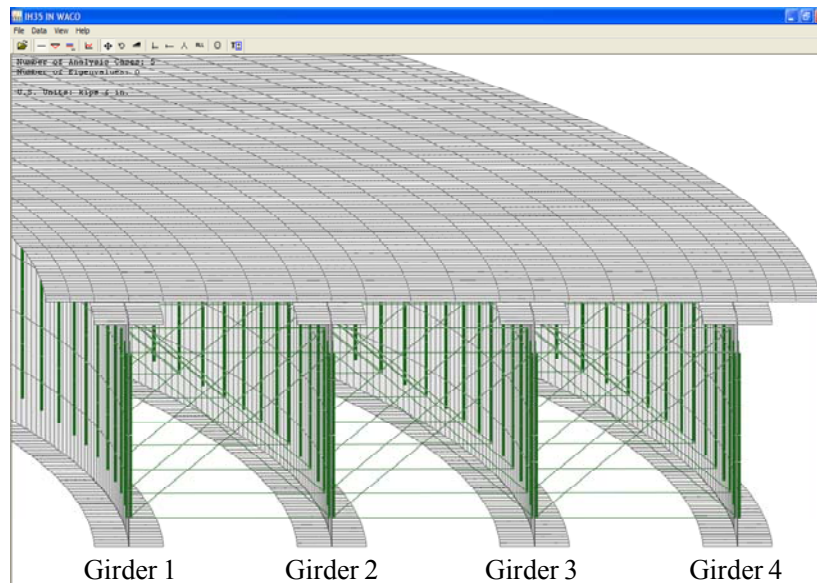


**Figure E.2: UT Bridge Screen Shot of 428' Bridge**

### E.3 COMPARISON OF VERTICAL DEFLECTIONS

UT Bridge was compared to the 2-D grillage program (DESCUS) provided by the camber diagram developed by TxDOT. Additionally, two 3-D finite element models were created in ANSYS to compare to the results. The first (ANSYS 1) model utilized the geometry and meshing generated by UT Bridge, but analysis with ANSYS' 8-node shell elements (SHELL93), 2-node beam elements (BEAM4), and 2-node truss elements (LINK8). The deck was modeled with shell elements and flexible springs to simulate the noncomposite action. The second (ANSYS 2) model utilized an independent node generation algorithm and generator. The same 8-node shell elements (SHELL93) were used for both the girder and the stiffeners, while 2-node truss elements (LINK8) were used for the cross frames. The deck was not explicitly modeled with shell elements, but rather it was modeled as a distributed load along the top flange of each girder. All models were assumed to behave noncompositely to facilitate an accurate comparison due to DESCUS's inability to perform a composite analysis and limitations of the ANSYS 2 model. As a result the model assumes the deck was fully placed instantaneously on steel bridge for this set of analyses. Figure D.5 through Figure D.8 are a set of graphs with the tenth point deflections calculated by UT Bridge, DESCUS, the first ANSYS model (ANSYS 1), and the second ANSYS model (ANSYS 2). The horizontal geometry for this 428' direct connector was not singularly curved, but included a 119' tangent portion between two sections of equal radius of curvature. While UT Bridge does not explicitly model this geometry, the ability to skew the substructure allows the program the ability to match the span lengths for each girder. UT Bridge assumes a right forward skew and the necessary skews are given in Table E.1.

***Table E.1: UT Bridge Specified Substructure Skew***

| Substructure 1<br>(Bent 18) | Substructure 2<br>(Bent 19) | Substructure 3<br>(Bent 20) |
|-----------------------------|-----------------------------|-----------------------------|
| 6.22°                       | 0.07°                       | -1.02°                      |

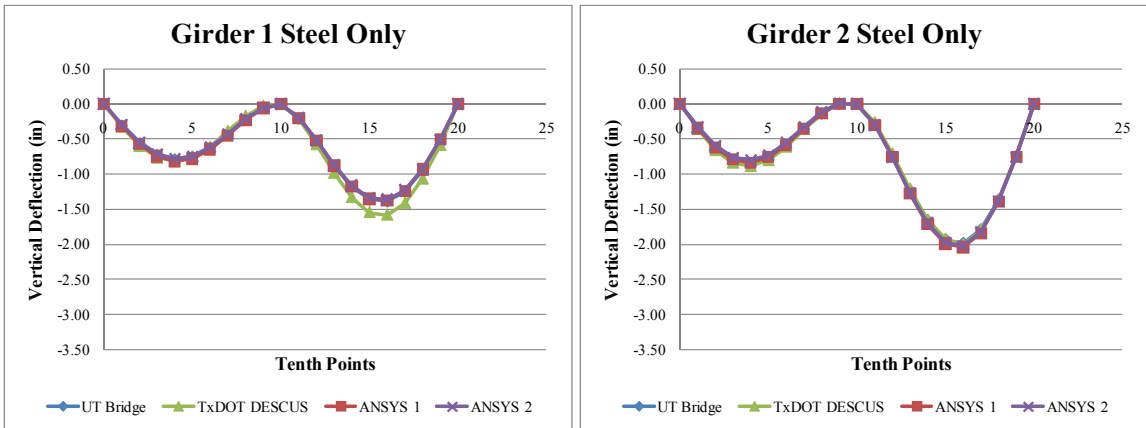


**Figure E.3: Steel Dead Load Program Comparison for Girder 1 and 2**

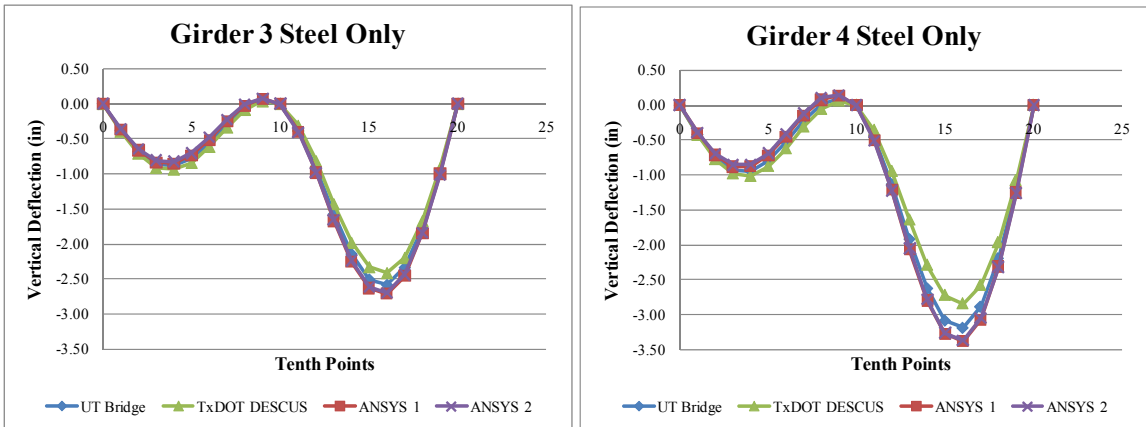


**Figure E.4: Steel Dead Load Program Comparison for Girder 3 and 4**

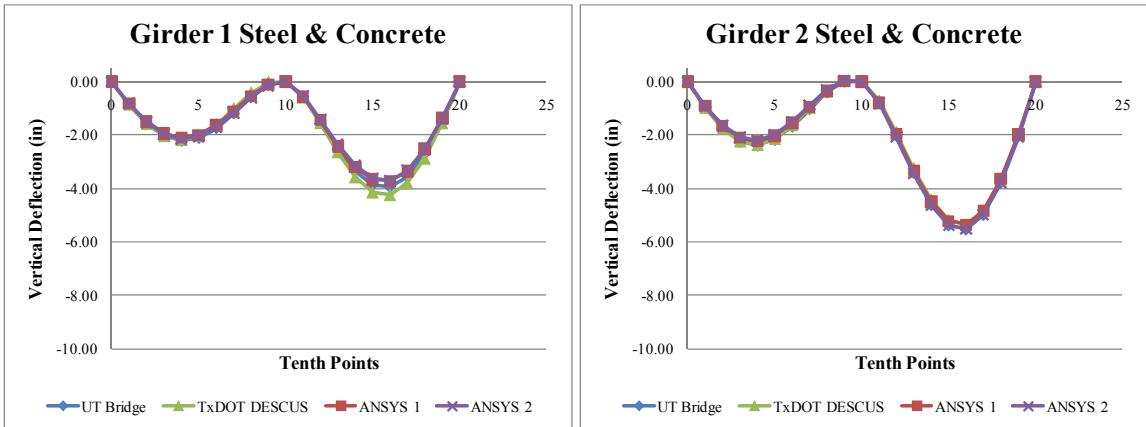


**Figure E.5: Steel & Concrete Deck Dead Load Program Comparison for Girder 1 & 2**

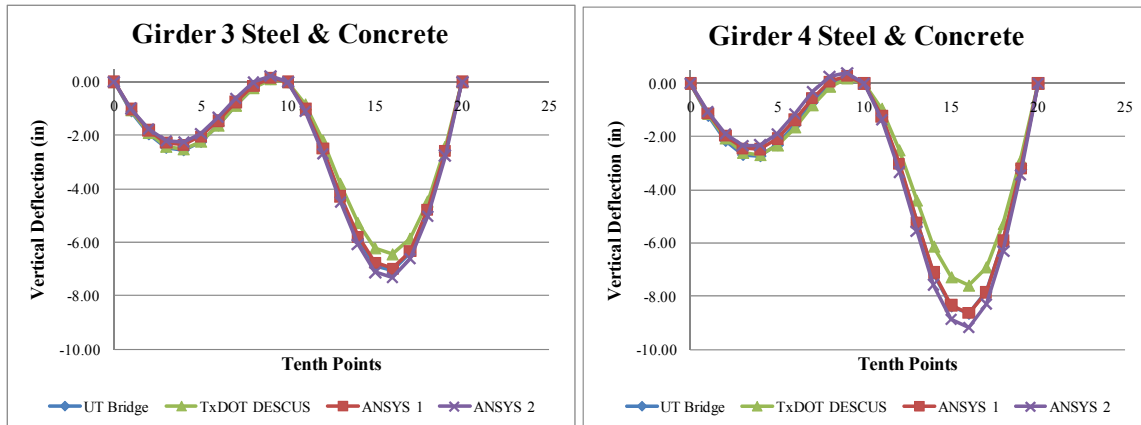


**Figure E.6: Steel & Concrete Deck Dead Load Program Comparison for Girder 3 & 4**

#### **E.4 CONCLUSION FROM MODEL COMPARISON**

The analyses showed a good correlation of the ANSYS models to UT Bridge. DESCUS overpredicted the global torsional stiffness of the bridge. This results in less global twist as shown by larger deflections for the interior girder (Girder 1) and smaller deflections for the exterior girder (Girder 4). It should be noted that the current bridge performed significantly better than 469' direct connector presented in Appendix D. This is due to two major differences, 1) relatively similar span length results in more symmetric bridge and 2) a shorter maximum span length of 225 ft. compared to the 275 ft. span in the Appendix D bridge.

**APPENDIX F:**  
**UT BRIDGE VERIFICATION: SPUR 366 EXTENSION**  
**CONNECTOR F**

---

The following set of bridge plans was designed by Huitt-Zollars, Inc. for the extension of US 366 Spur. A 2-D grillage model in MDX was completed as part of the design and the results were compared to UT Bridge as verification of the programs accuracy. Permission to publish these plans was obtained from the Charlie Quade of Huitt-Zollars, Inc.

## F.1 COMPARISON OF VERTICAL DEFLECTIONS

UT Bridge was compared to the 2-D grillage program (MDX) provided by the camber diagram developed by Huitt-Zollars, Inc. Both models were assumed to behave noncompositely to facilitate an accurate comparison due to MDX's inability to perform a composite analysis. As a result the model assumes the deck was fully placed instantaneously on steel bridge for this set of analyses. Figure F.1 and Figure F.2 are a set of graphs with the tenth point deflections calculated by UT Bridge and MDX. The analysis shows good correlation between MDX and UT Bridge.

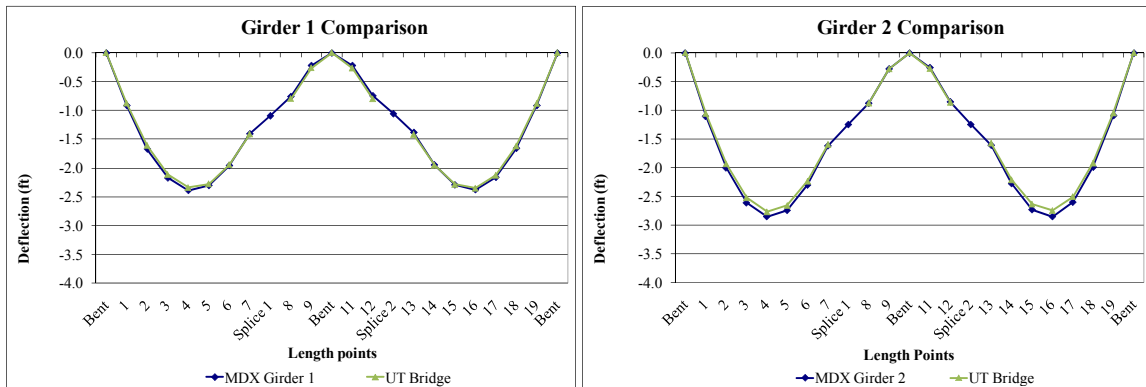


**Figure F.1: Steel & Concrete Deck Dead Load Program Comparison for Girder 1 & 2**

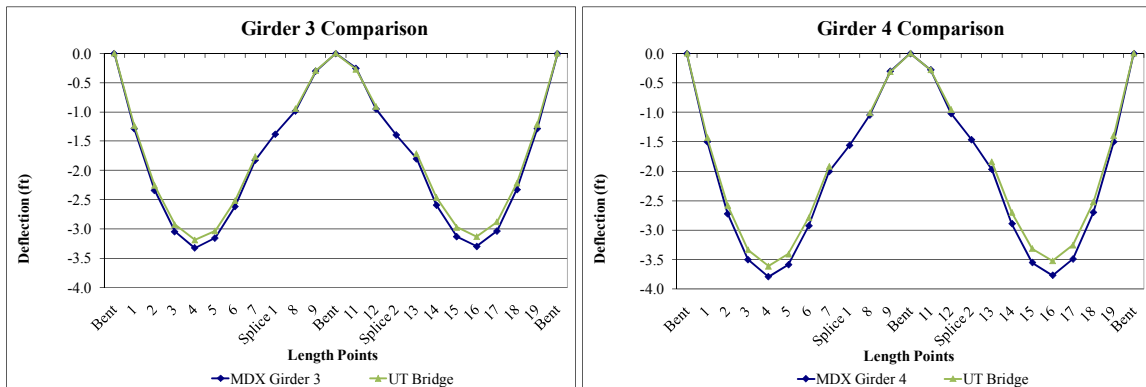


**Figure F.2 Steel & Concrete Deck Dead Load Program Comparison for Girder 3 & 4**

## REFERENCES

---

- AASHTO/NSBA Steel Bridge Collaboration (2007) *Steel Bridge Erection Guide Specification*, Washington, D.C.
- ABAQUS Version 6.9 (2010) Dassault Systèmes Providence, RI
- ADINA Structures (2010) ADINA R&D Inc. Watertown, MA
- American Association of State Highway and Transportation Officials (AASHTO). (1980). *Guide specifications for horizontally curved bridges*, Washington, D.C.
- American Association of State Highway and Transportation Officials (AASHTO). (1993). *Guide specifications for horizontally curved bridges*, Washington, D.C.
- American Association of State Highway and Transportation Officials (AASHTO). (2003). *Guide specifications for horizontally curved bridges*, Washington, D.C.
- American Association of State Highway and Transportation Officials (AASHTO). (2007) *AASHTO LRFD Bridge Design Specifications*, 4<sup>th</sup> Edition, Washington, D.C.
- American Association of State Highway and Transportation Officials (AASHTO). (2008) *AASHTO LRFD Bridge Construction Specifications*, 2<sup>nd</sup> Edition, 2008 Interim Revisions, Washington, D.C.
- AASHTO/AWS (2008) *D1.5 Bridge Welding Codes*, American Welding Society, 5<sup>th</sup> Edition.
- American Institute of Steel Construction (AISC). (2005) *Steel Construction Manual*, 13<sup>th</sup> Edition.
- ANSYS, Finite element program users' manual, Version 11.0. (2007). ANSYS, Inc.
- Bathe, Klaus- Jürgen (1996). Finite Element Procedures Prentice-Hall, Englewood Cliffs, NJ.
- Beal, D. B., and Kissane, R. J. (1971a). *First Interim Report on Research Project 42-1*, New York State Department of Transportation, Engineering Research and Development Bureau, Albany, New York.
- Beal, D. B., and Kissane, R. J. (1971b). *Second Interim Report on Research Project 42-1*, New York State Department of Transportation, Engineering Research and Development Bureau, Albany, New York.

- Beal, D. B., and Kissane, R. J. (1972). *Third Interim Report on Research Project 42-1*, New York State Department of Transportation, Engineering Research and Development Bureau, Albany, New York.
- Bell, Bradley J. (2004). *Effects of Erection Procedures on the Response of a Horizontally Curved I-girder Bridge*. Master's Thesis, The University of Pennsylvania State University, University Park, PA.
- Bishara, Alfred G. and Elmir, Wassef E. (1990). "Interaction Between Cross Frames and Girders," *Journal of Structural Engineering*, Vol. 116, No. 5, May Pg 1319-1333.
- Brennan, P.J. (1970). "Horizontally curved bridges first annual report: Analysis of horizontally curved bridges through three-dimensional mathematical model and small scale structural testing." *Syracuse Univ., First Annual Rep., Research Project HPR-2(111)*, Syracuse, N.Y.
- Brennan, P.J. (1971). "Horizontally curved bridges second annual report: Analysis of Seekonk River Bridge small scale structure through three-dimensional mathematical model and small scale structural testing." *Syracuse Univ., Second Annual Rep., Research Project HPR-2(111)*, Syracuse, N.Y.
- Brennan, P.J. (1974). "Analysis and structural testing of a multiple configuration small scale horizontally curved highway bridge." *Syracuse Univ., Research Project HPR-2(111)*, Syracuse, N.Y.
- "Bretschneider's Formula," <http://mathworld.wolfram.com/BretschneidersFormula.html>, Access July 9, 2008.
- Brogan, D. K. (1974). "Bending behavior of cylindrical web panels." M.Sc. Thesis, Carnegie Mellon University, Pittsburgh, PA.
- BSDI (2010) Bridge Software Development International Ltd. Coopersburg, PA
- Canadian Institute of Steel Construction (CISC), (2002). Torsional Sections Properties of Steel Sections.
- Chapelle, Dominique & Bathe, Klaus-Jürgen (2003). The Finite Element Analysis of Shells: Fundamentals 1<sup>st</sup> Edition, Springer.
- "Chapter 1: V-load analysis, an approximate procedure, simplified and extended for determining moments and shears in designing horizontally-curved open-frame highway bridges." (1984). *U.S.S. highway structures design handbook*, Vol. 1, United States Steel Corp., Pittsburgh, Pa.



- Chavel, Brandon William (2008). *Construction and Detailing Methods of Horizontally Curved Steel I-girder Bridges*, PhD Dissertation, University of Pittsburgh, Pittsburgh, PA.
- Chavel, B. W., and Earls, C. J. (2006). "Construction of a horizontally curved steel I-girder bridge: Erection sequence." *Journal of Bridge Engineering*, Vol. 11, No. 1, pp. 81-90.
- Chavel, B. W., and Earls, C. J. (2006). "Construction of a horizontally curved steel I-girder bridge: Inconsistent detailing." *Journal of Bridge Engineering*, Vol. 11, No. 1, pp. 91-98.
- Chen, Q. (2008). *Effects of Thermal Loads on Texas Steel Bridges*. PhD dissertation, University of Texas.
- Clough, R. W., (1960). "The Finite Element Method in Plane Stress Analysis", Proc. 2nd ASCE Conf. On Electronic Computation, Pittsburg, Pa. Sept. 1960.
- Coletti, Domenic and Yadlosky, John (2008). "Analysis of Steel Girder Bridges New Challenges." *Transportation Research Record: Journal of the Transportation Research Board*, No. 2050, Transportation Research Board of the National Academies, Washington, D.C., 2008, pp. 67-77.
- Consortium of University Research Teams (1975). "Tentative design specifications for horizontally curved highway bridges." *Part of Final Rep., Research Project HPR2-(111)*.
- Courant, R. (1943). "Variational Methods for the Solutions of Problems of Equilibrium and Vibrations," *Bull. Am. Math. Soc.*, Vol. 49, pp. 1-23.
- Culver, C. G. (1972). "Design recommendations for curved highway bridges." *Final Rep. for Research Project 68-32*, Pennsylvania Department of Transportation, Harrisburg, Pa.
- Culver, C. G., and Frampton, R. E. (1970). "Local instability of horizontally curved members." *Journal of the Structural Division, ASCE*, Vol. 96, No. 2, pp. 245-265.
- Culver, C. G., and Nasir, N. (1971). "Inelastic flange buckling of curved plate girders." *Journal of the Structural Division, ASCE*, Vol. 97, No. 4, pp.1239-1257.
- Culver, C. G., Dym, C. L., and Brogan, D. K. (1972). "Bending behavior of cylindrical web panels." *Journal of the Structural Division, ASCE*, Vol. 98, No. 10, pp. 2291-2308.

- Culver, C. G., Dym, C. L., and Uddin, T. (1973). “Web slenderness requirements for curved girders.” *Journal of the Structural Division, ASCE*, Vol. 99, No. 3, pp. 417–430.
- CXML (2001) Compaq Extended Math Library Reference Guide Compaq Computer Corporation, Houston, TX
- Davidson, J. S., and Yoo, C. H. (1996). “Local buckling of curved I-girder flanges.” *Journal of Structural Engineering*, ASCE, Vol. 122, No. 8, pp. 936-947.
- Davidson, J. S., and Yoo, C. H. (2000). “Evaluation of strength formulations for horizontally curved flexural members.” *Journal of Bridge Engineering*, Vol. 5, No. 3, pp. 200-207.
- Davidson, J. S., Keller, M. A., and Yoo, C. H. (1996). “Cross-frame spacing and parametric effects in horizontally curved I-girder bridges.” *Journal of Structural Engineering*, ASCE, Vol. 122, No. 9, pp. 1089-1096.
- DESCUS I Version 10.2 (2008) BEST Center Bridge Engineering Software & Technology Center, College Park, MD
- Fan, Z. (1999). *Field and Computational Studies of Steel Trapezoidal Box Girder Bridges*. PhD dissertation, University of Houston.
- Farris, Jamie F. (2008) *Behavior of Horizontally Curved Steel I-girders During Construction* Master’s Thesis, University of Texas at Austin, Austin, TX.
- Fasl, J. D. (2008). *The Influence of Overhang Construction on Girder Design*. Master’s Thesis, University of Texas.
- Felippa, Carlos A. “Introduction to Finite Element Methods”, Textbook for Introduction to Finite Element Methods (ASEN 5007), University of Colorado at Boulder, 2004. Web accessed June 5, 2009. <http://www.colorado.edu/engineering/CAS/courses.d/IFEM.d/>
- Fiechtl, A. L., Fenves, G. L., and Frank, K. H. (1987). “Approximate Analysis of Horizontally Curved Girder Bridges.” *Final Rep. No. FHWA-TX-91-360-2F*, Center for Transportation Research, University of Texas at Austin, Austin, TX.
- Galambos, T. V., Hajjar, J. F., Huang, W., Pulver, B. E., Leon, R. T., and Rudie, B. J. (2000). “Comparison of measured and computed stresses in a steel curved girder bridge.” *Journal of Bridge Engineering*, Vol. 5, No. 3, pp. 191-199.
- Hartmann, Joseph L. (2005) *An Experimental Investigation of the Flexural Resistance of Horizontally Curved Steel I-Girder Systems*, PhD Dissertation, University of Maryland, College Park, MD.

- Heins, C. P. (1972). "Design data for curved bridges." *Rep. No. 47*, summary report for Maryland Department of Transportation and Federal Highway Administration, Washington, D.C.
- Helwig, Todd A., Frank, Karl H., Yura, Joseph A. (1997). "Lateral-torsional buckling of singly symmetric I-beams." *Journal of Structural Engineering*, Vol. 123, No.9, pp. 1172-1179.
- Huang, W. H. (1996). *Curved I-girder systems* PhD Dissertation, Department of Civil Engineering, University of Minnesota.
- Jung, S., and White, D. (2005). "Shear strength of horizontally curved steel I-girders – finite element analysis studies." *Journal of Constructional Steel Research*, 62, pp. 329-342.
- Kassimali, Aslam (1999). Matrix Analysis of Structures Brooks/Cole, Pacific Grove, CA.
- Kuo, J. T. C. and Heins Jr., C. P. (1971). "Behavior of Composite Beams Subjected to Torsion", University of Maryland Civil Engineering Research Report #39. College Park, MD.
- KWH Constructors. (n.d.). *Project Galleries-Bridge Construction-William R Bennett Bridge*. Retrieved October 26, 2009, from KWH Constructors: [http://www.kwhconstructors.com/img/gallery/williamr.bennettbridge/wrb\\_bridge\\_5.JPG](http://www.kwhconstructors.com/img/gallery/williamr.bennettbridge/wrb_bridge_5.JPG)
- Lehoucq, R.B., Sorensen, D.C., and Yang, C. (1998). *ARPACK User's Guide Solution of Large Scale Eigenvalue Problems with Implicitly Restarted Arnoldi Method*. SIAM, Philadelphia.
- Linzell, D. G. (1999). "Studies of a Full-Scale Horizontally Curved Steel I-Girder Bridge System Under Self-Weight", Ph.D Dissertation, Georgia Institute of Technology, July 1999.
- Linzell, D., Leon, R. T., and Zureick, A. (2004). "Experimental and analytical studies of horizontally curved steel I-girder bridge during erection." *Journal Bridge Engineering*, Vol. 9, No. 6, pp. 521-530.
- LUSAS Bridge Version 14 (2010) Finite Element Analysis Ltd. Surrey, UK
- Mast, Robert F. (1989) "Lateral Stability of Long Prestressed Concrete Beams Part 1" *PCI Journal*, Vol. 34, No. 1, pp 34-53.
- McGuire, William, Gallagher, Richard H., Ziemian, Ronald D. (2000) Matrix Structural Analysis 2<sup>nd</sup> Edition, John Wiley & Sons, Inc. New York, NY.

- McManus, P.F., Nasir, G.A., and Culver, C.G. (1969) “ Horizontally curved girders – state of the art.” *Journal of the Structural Division*, ASCE, Vol. 97, No. 10, pp. 2459-2580.
- McManus, P.F. (1971). *Lateral buckling of curved plate girders*, Ph.D. Dissertation, Carnegie-Mellon University, Pittsburgh, PA.
- MDX Version 6.5 (2009) Curved & Straight Steel Bridge Design & Rating. MDX Software, Inc.
- Mohareb, M. and Nowzartash, F. (2003). “Exact Finite Element for Nonuniform Torsion of Open Sections” *Journal of Structural Engineering*, Vol. 129, No. 2, February, pp. 215-223.
- Mondkar, D. P., and Powell, G. H. (1974). “CURVBRG—A computer program for analysis of curved open girder bridges.” *UC-SESM Rep. No. 74-17*, Univ. of California, College of Engineering, Berkeley, Calif.
- Mozer, J., and Culver, C. (1970). “Horizontally curved highway bridges – stability of curved plate girders.” *Rep. No. P1, Research Project HPR-2(111)*, Carnegie Mellon University, Pittsburgh.
- Mozer, J., Ohlson, R., and Culver, C. (1971). “Horizontally curved highway bridges – stability of curved plate girders.” *Rep. No. P2, Research Project HPR-2(111)*, Carnegie Mellon University, Pittsburgh.
- Mozer, J., Cook, J., and Culver, C. (1973). “Horizontally curved highway bridges – stability of curved plate girders.” *Rep. No. P3, Research Project HPR-2(111)*, Carnegie Mellon University, Pittsburgh.
- Nakai, H., Kitada, T., and Ohminami, R. (1985). “Proposition for Designing Intermediate Transverse Stiffeners in Web Plate of Horizontally Curved Girders.” *JSCE*, no. 362/I-4 October, pp. 249-257 (in Japanese).
- Nakai, H., Kitada, T., Ohminami, R. and Kawai, T. (1986). “A study on Analysis and Design of Web Plate in Curved Girder Bridges Subjected to Bending.” *JSCE*, No. 368/I-5 April, pp. 235-244 (in Japanese)
- Nasir, G. A. (1970). *Buckling of stiffened and unstiffened curved plate elements*, Ph.D. Dissertation, Carnegie-Mellon Univ., Pittsburgh.
- National Transportation Safety Board (2006). Highway Accident Brief, Accident No. HWY-04-MH-023, May 31, 2006, Washington, D.C.

- Nevling, D., Linzell, D., and Laman, J. (2006). "Examination of Analysis Accuracy for Curved I-Girder Bridges through Comparisons to Field Data." *Journal of Bridge Engineering*, Vol. 11 No. 2, March 1, pp. 160-168.
- NCHRP Synthesis 345. (2005) *Steel Bridge Erection Practices, A Synthesis of Highway Practice*, Transportation Research Board of the National Academies, Washington, D.C.
- "Numerical Differentiation," [http://en.wikipedia.org/wiki/Numerical\\_differentiation](http://en.wikipedia.org/wiki/Numerical_differentiation), Access December 18, 2008.
- Ozgun, Cagri, White, Donald W. and Leon, Robert T. (2009) "Behavior of Curved and Skewed I-girder Bridge Systems During Construction and Recommendations for Practice." Structural Stability Research Council Annual Stability Conference Proceedings, Phoenix, AZ, April 1-4, pp. 431-450.
- Petruzzi, Brian J. (2010) *Stabilizing Techniques for Curved Steel I-girders during Construction* Master's Thesis, University of Texas at Austin, Austin, TX.
- "Point Line Distance," <http://mathworld.wolfram.com/Point-LineDistance2-Dimensional.html>, Access February 9, 2009.
- Popp, Daniel (2004). *U-TrAp 2.0: Linearized Buckling Analysis of Steel Trapezoidal Girders*, Master's Thesis, The University of Texas at Austin, Austin, TX.
- Reddy, J.N. (2006). An Introduction to the Finite Element Method 3<sup>rd</sup> Edition, McGraw-Hill, New York, NY.
- Richardson, Gordon, and Associates, Consulting Engineers (1963). "Analysis and Design of Horizontally Curved Steel Bridge Girders," United States Steel Structural Report, ADUSS 88-600301.
- Saint-Venant, B (1843). "Memoire sur le calcul de la resistance et de la flexion des pieces solides a simple ou a double courbure, en prenant simultanement en consideration les divers efforts auxquels elles peuvent entre soumises dans tous les sens." *Compt-Rendus*, Vol. 27, l'Academic des Sciences de Paris, Paris, France 942, 1020-1031 (in French).
- Salmon, Charles G, Johnson, John E., Malhas, Faris A. (2009) Steel Structures Design and Behavior, 5<sup>th</sup> Edition, Pearson Education, Inc., Upper Saddle River, NJ.
- Schelling, D. Namini, Ahmad H., and Fu, Chung C. (1989). " Construction Effects on Bracing on Curved I-Girders," *ASCE Journal of Structural Engineering*, Vol. 115, No. 9, September, pp. 2145-2165.

- Schuh, Andrew C. (2008) *Behavior of Horizontally Curved Steel I-girders During Lifting* Master's Thesis, University of Texas at Austin, Austin, TX.
- Seaburg, Paul A. and Carter, Charles J. (1997). "Torsional Analysis of Structural Steel Members," *Steel Design Guide Series 9*, American Institute of Steel Construction (AISC), Chicago, IL.
- Stegmann, T. H., and Galambos, T. V. (1976). "Load factor design criteria for curved steel girders of open cross section." *Washington Univ. Research Rep. No. 43*, Washington Univ., St. Louis.
- Stith, J. C., Schuh, A. C., Farris, J. F., Petruzzi, B. J., Helwig, T. A., Williamson, E. B., Frank, K. H., Engelhardt, M. D. (2009). "Guidance for Erection and Construction of Curved I-girder Bridges." *Final Rep. No. FHWA-TX-09/0-5574*, Center for Transportation Research, University of Texas at Austin, Austin, TX.
- Structural Stability Research Council (SSRC) (1998) Guide to Stability Design Criteria for Metal Structures, 5<sup>th</sup> Edition T. V. Galambos, ed., John Wiley & Sons, Inc., New York, N.Y.
- Structural Stability Research Council (SSRC) Task Group 14. (1991). "A look to the future." *Rep. of workshop on horizontally curved girders*, Chicago, 1-18.
- Texas Steel Quality Council. (2007) *Preferred Practices for Steel Bridge Design, Fabrication, and Erection*, Texas Department of Transportation, Austin, TX.
- Timoshenko, Stephen P. and Woinowsky-Krieger, S. (1959). Theory of Plates and Shells 2<sup>nd</sup> Edition, McGraw-Hill College.
- Timoshenko, Stephen P. and Gere, J. (1961). Theory of Elastic Stability 2<sup>nd</sup> Edition, McGraw-Hill College, New York, NY.
- Topkaya, Cem. (2002). *Behavior of Curved Steel Trapezoidal Box Girders During Construction*, Ph.D. Dissertation, University of Texas at Austin, Austin, TX, August.
- Topkaya, Cem, Yura, Joseph A., and Williamson, Eric B. (2004). "Composite Shear Stud Strength at Early Concrete Ages" *Journal of Structural Engineering* June, pg. 952-960.
- Tung, David H. and Fountain, Richard S. (1970) "Approximate Torsional Analysis of Curved Box Girders by the M/R-Method." *Engineering Journal*, American Institute of Steel Construction, Volume 7, No. 3, July, pp. 65-74.

- Turco, Greg “Field Retrofitting a Curved Girder Bridge to Increase Torsional Stiffness.” Proceeding of National Steel Bridge Alliance 2009 World Steel Bridge Symposium, San Antonio, Texas, November 17 – 20, 2009.
- Turner, M. J., Clough, R. W., Martin, H. C. and Topp, L. J. (1956). “Stiffness and Deflection Analysis of Complex Structures”, *J. Aeronautical Science* 23 (9), Sept. pp. 805-823.
- Yoo, C. H. and Carbine, R. L. (1985). “ Experimental Investigation of Horizontally Curved Steel Wide Flange Beams Analysis.” *Proc., Structural Stability Research Council Annual Technical Session: Stability Aspects of Industrial Buildings*, 183-191.
- Yoo, C. H. and Choi, B. H. (2000). “Literature Search–Horizontally Curved Steel Girder Bridges,” NCHRP 12-52 Quarterly Report, submitted to the Transportation Research Board, Washington, D.C., March 2000.
- Yoo, C. H. and Davidson, J. S. (1997). “Yield interaction equations for nominal bending strength of curved I-girders.” *Journal of Bridge Engineering*, Vol. 2 No. 2, pp. 37-44.
- Yoo, C. H. and Littrell, P. C. (1986). “ Cross-Bracing effects in Curved Stringer Bridges.” ASCE, *Journal of Structural Engineering*, Vol. 112, No. 9, September, pp. 2127-2140.
- Zienkiewicz, O.C. (1977). The Finite Element Method 3<sup>rd</sup> Edition. McGraw-Hill, London.
- Zureick, A., and Naquib, R. (1999). “Horizontally curved steel I-girders state-of-the-art analysis methods.” *Journal of Bridge Engineering*, Vol. 4, No. 1, pp. 38-47.
- Zureick, A., Linzell, D., Leon, R. T., and Burrell, J. (2000). “Curved steel I-girder bridges: experimental and analytical studies.” *Engineering Structures*, Vol. 22, No. 2, pp. 180-190.

## VITA

---

Jason Clarence Stith was born on January 21, 1982 in Elizabethtown, Kentucky to Richard and Veronica Stith. After graduating from Central Hardin High School in Cecilia, Kentucky in 2000, he enrolled in the University of Kentucky. During the Spring Semester of 2002 he attended the University of New South Wales in Sydney, Australia as a study abroad student. He graduated with a Bachelor of Science in Civil Engineering in 2004 from the University of Kentucky. He spent the Summer Semester of 2004 on an Institute for Shipboard Education Semester at Sea program which is academically run through the University of Pittsburgh. In May of 2005 he received a Master's of Science in Civil Engineering and in December of 2005 a Master's in Business Administration both from the University of Kentucky. He entered the doctoral program in the Civil Engineering department at the University of Texas at Austin in August of 2006. On December 29, 2004 he married Samantha Lea Bell of Upton, Kentucky.

Permanent Address:

480 Salt River Road

Vine Grove, KY 40175

This manuscript was typed by the author.